Designing of Chitosan and metal/metal oxide nanoparticle based nanocomposites for tissue engineering and drug delivery applications

A THESIS SUBMITTED TO THE

UNIVERSITY OF PUNE

FOR THE DEGREE OF

DOCTOR OF PHILOSOPHY

IN

CHEMISTRY

BY

SANGEETA KUMARI

RESEARCH SUPERVISOR

Dr. R. P. SINGH

RESEARCH CO-GUIDE

Dr. N. N. CHAVAN

POLYMER SCIENCE AND ENGINEERING DIVISION
CSIR - NATIONAL CHEMICAL LABORATORY

PUNE 411008

July 2013

राष्ट्रीय रासायनिक प्रयोगशाला
(वैज्ञानिक तथा औद्योगिक अनुसंधान परिषद)
डॉ. होमी भाभा मार्ग पुणे - 411 008. भारत
NATIONAL CHEMICAL LABORATORY
(Council of Scientific & Industrial Research)
Dr. Homi Bhabha Road, Pune - 411 008. India.

CERTIFICATE

This is to certify that the work presented in the thesis entitled **"Designing of Chitosan and metal/metal oxide nanoparticle based nanocomposites for tissue engineering and drug delivery applications"**, which is being submitted by **Miss Sangeeta Kumari**, was carried out by the candidate at CSIR-National Chemical Laboratory, Pune, under our supervision. Such materials as obtained from other sources have been duly acknowledged in the thesis.

17-7-2013

Dr. R. P. Singh
Research Supervisor (Retired)
Polymer Science and Engineering Division
CSIR-National Chemical Laboratory
Pune 411 008, INDIA.

Dr. N. N. Chavan
Research Co-Guide
Polymer Science and Engineering Division
CSIR-National Chemical Laboratory
Pune 411 008, INDIA

DECLARATION BY RESEARCH SCHOLAR

I, **Miss Sangeeta Kumari**, hereby declare that the thesis entitled **"Designing of Chitosan and metal/metal oxide nanoparticle based nanocomposites for tissue engineering and drug delivery applications",** which is being submitted for the degree of Doctor of Philosophy to the University of Pune, has been carried out by me at Polymer Science and Engineering Division, CSIR-National Chemical Laboratory, Pune 411 008, India under the supervision of **Dr. R. P. Singh** and co-guidance **of Dr. N. N. Chavan**.

The work is original and has not been submitted to in part or full by me for any other degree or diploma to this or any other university.

Kumari

(SANGEETA KUMARI)
Research Scholar

Dedicated to My Family

ACKNOWLEDGEMENTS

I would like to express my sincere gratitude to Dr. R.P. Singh for his invaluable guidance. I sincerely thank him for teaching me the skills of presenting and writing the technical matters. He has not just guided me in the scientific problems, but has always taken extra efforts to shape my approach towards research. He has always been a perfectionist and a good critic to bring this thesis in its present form. I learnt a great deal from interacting with him. I would also like to express my gratitude to Dr. N. N. Chavan for his invaluable guidance. I would like to express my sincere gratitude towards Mrs. Durgesh Singh.

I am grateful to Dr. Saurav Pal, the Director, CSIR-NCL, Pune, for providing the infrastructure and facilities for my research work. I am very much grateful to Dr. A. J. Verma, Head, PSE division, for providing me access to the facilities in the division. I am also very thankful to other scientists in the division namely, Dr C. Ramesh, Dr. C. V. Avadhani, Mr. K.G. Raut, Dr. K. Guruswamy, Dr. A.K. Lele, Dr. B. B Idage, Mr. S. K. Menon, Mrs. D. A. Dhoble, Mr. Saroj jha, Mrs. S. Poorvi and Mrs. Pooja muddellu for their timely help, fruitful discussions and support. I also acknowledge CSIR, New Delhi for financial assistance for my research work and granting Junior and Senior Research Fellowship. How can I forget my colleagues! Without their support, cooperation, discussions and timely help, my research work could not have matured enough. I also express my sincere thanks to my divisional colleague. I am again thankful to Dr. M. Patole (NCCS, Pune University) for his cooperation in my research work. I am also thankful to Mr. A.B. Gaikwad, Mr. Gholap (CMC) for SEM and TEM facilities.

I would like to express thanks to my NCL friends for their moral support and love. Apart from this I am thankful to the GJ Hostel mess-workers including Chakru, Mani and others for preparing yummy food.

I am indebted and place on record my deep sense of gratitude to my parents (Mr. Chandrajit Ram and Mrs Prabhavati Devi), My Bhaiya- bhabhi (Avinash Kumar and Rita Devi), my sister (Kavita Goel) and brother in law (Ratnesh Goel), my younger brother (Arun Kumar, Rinku), my sweet niece (Jyoti, Khushi, Anurag and Aditya) and my best friend Pankaj Kumar, for their unconditional love, support and encouragement which helped me reach this far. I do not think I can ever repay them. I am grateful to God, for giving me such loving family life.

Finally, I express my prayers and gratitude to my grandparents (Late Sri Kashi Ram and Late Smt Somari Devi) and Almighty (Unified force) for the lead.

(Sangeeta Kumari)

CONTENTS

Chapter 1: Introduction

Chapter 2: Scope and Objectives

Chapter 3 A: Preparation and Characterization of Glycolic Acid-g-Chitosan-Gold Nanoflower Based Nanocomposite Scaffolds for Drug Delivery and Tissue Engineering Applications

Chapter 3 B: Preparation and Characterization of Glycolic Acid-g-Chitosan-Gold Nanoparticles Based Nanocomposite Films

Chapter 4 A: Preparation and Characterization of Glycolic Acid-g-Chitosan- Au-Fe_3O_4 Hybrid Nanoparticles Based Nanocomposite Scaffolds for Drug Delivery and Tissue Engineering Applications

Chapter 4 B: Preparation and Characterization of Glycolic Acid-g-Chitosan-Au-Fe_3O_4 Hybrid Nanoparticles Based Nanocomposite Films

Chapter 5 A: Preparation of Glycolic Acid-g-Chitosan-Pt-Fe_3O_4 Hybrid Nanoparticles Based Nanohybrid Scaffolds for Tissue Engineering and Drug Delivery Applications

Chapter 5 B: Preparation and Characterization of Glycolic Acid-g-Chitosan-Pt-Fe_3O_4 Hybrid Nanoparticles Based Nanocomposite Films

Chapter 6 A: Preparation and Characterization of Glycolic Acid-g-Chitosan-Co_3O_4 Nanoparticles Based Nanohybrid Scaffolds for Drug-Delivery and Tissue Engineering Applications

Chapter 6 B: Preparation and Characterization of Glycolic acid-g-Chitosan-Co_3O_4 Nanoparticles Based nanocomposite Films

Chapter 7 A: Preparation of Glycolic Acid-g-Chitosan-Co_3O_4-Fe_3O_4 Hybrid Nanoparticles Based Nanohybrid Scaffolds for Drug-Delivery and Tissue Engineering

Chapter 7 B: Preparation and Characterization of Chitosan-g-Glycolic Acid-Co_3O_4-Fe_3O_4 Hybrid Nanoparticles Based Nanocomposite Film

Chapter 8: Conclusions

ABSTRACT

Title of the Thesis

Designing of Chitosan and metal/metal oxide nanoparticle based nanocomposites for tissue engineering and drug delivery applications

Chitosan is a nontoxic, biodegradable, and biocompatible polysaccharide of β(1-4)-linked D-glucosamine and N-acetyl-D-glucosamine. This derivative of natural chitin presents remarkable properties that have paved the way for the introduction of chitosan in the biomedical and pharmaceutical fields. Nevertheless, the properties of chitosan, such as its poor solubility in water or in organic solvents, can limit its utilization for a specific application. An elegant way to improve or to impart new properties to chitosan is the chemical modification of the chain, generally by grafting of functional groups, without modification of the initial skeleton in order to conserve the original properties. The fuctionalization is carried out on the primary amine group, generally by quarterisation, or on the hydroxyl group. The nanocomposites of inorganic materials in polymer matrices have attracted a great deal of attention because of their wide area of applications including biosensors. Different approaches have been developed for the synthesis of nanocomposites such as incorporation of premade nanoparticles into the polymer matrix. This can be achieved with the use of a common blending solvent or by reduction of metal salt dispersed in polymer matrix using an external reducing agent. The Metallic and metal oxide nanoparticles have become an area of growing interest of fundamental studies and technological applications, due to their unique mechanical, chemical and magnetic properties. The metal nanoparticle embedded polymer film can show enhanced mechanical properties.

Thus, the present research work is aimed to refocus on the possibilities of utilization of CS and metal/metal oxide nanoparticle based nanocomposites for various applications esp. as a drug carrier for sustained release and as a scaffold in tissue engineering and other biomedical applications. ***Chapter 1*** gives an **introduction** and literature background on this area. ***Chapter 2*** reveals the **scope, objectives, and approaches** of the present study.

Chapter 3 focus on the **preparation and characterization of Glycolic acid-g-chitosan-gold nanoflower nanocomposite *scaffolds* for drug delivery and tissue engineering**. The gold nanoflower (three dimensional branched nanoparticle) with >30 tips, under controlled temperature condition. The drug loaded novel nanohybrid scaffold is prepared by freeze drying of grafted polymer solution. Grafting of glycolic acid to the chitosan and incorporation of drug to it were evaluated by Fourier transform infrared spectroscopy (FTIR). The nanohybrid scaffolds were found to be stable towards the pH of the medium. The cell viability study shows that prepared nanohybrid scaffolds are biocompatible. The next part of this chapter focus on **preparation and characterization of glycolic acid-g-chitosan-gold nanoparticle based nanohybrid films.** These nanocomposite films was characterised by conventional technique. An enhancement in mechanical and tensile properties of nanocomposites than pure chitosan was observed. The water absorption behavior of the nanocomposites was evaluated by measuring swelling degree. These nanocomposites could be applied in the field of biomedical.

Chapter 4 focuses on **preparation and characterization of glycolic acid-g-chitosan- Au-Fe_3O_4 hybrid nanoparticle based novel nanohybrid scaffolds for drug delivery and tissue engineering application.** The Au-Fe_3O_4 hybrid nanoparticles were prepared and characterised. The chitosan-g-glycolic acid and Au-Fe_3O_4 hybrid nanoparticles based nanohybrid scaffold was prepared freeze drying. Grafting of glycolic acid and drug loading in

porous scaffold was characterized by Fourier transform infrared spectroscopy. The nanohybrid scaffolds were found to be stable regardless of pH of the medium and play a key role in cell adhesion, proliferation and migration. Au-Fe_3O_4 hybrid nanoparticles reinforcement was found to control the drug (Cyclophosphamide) release rate in phosphate buffer saline solution (pH 7.4). The next part of this chapter focus on **preparation and characterization of glycolic acid-g-chitosan- Au-Fe_3O_4 hybrid nanoparticles based nanohybrid films.** These nanocomposite films was characterised by conventional technique. An enhancement in mechanical and tensile properties of nanocomposites than pure chitosan was observed.

Chapter 5 focuses on **preparation and characterization of glycolic acid-g-chitosan- Pt-Fe_3O_4 hybrid nanoparticle based novel nanohybrid scaffolds for drug delivery and tissue engineering application.** The Pt-Fe_3O_4 hybrid nanoparticles were prepared and characterised. The chitosan-g-glycolic acid and Pt-Fe_3O_4 hybrid nanoparticles based nanohybrid scaffold was prepared freeze drying. The nanohybrid scaffolds were found to be stable regardless of pH of the medium and play a key role in cell adhesion, proliferation and migration. The next part of this chapter focus on **preparation and characterization of glycolic acid-g-chitosan- Pt-Fe_3O_4 hybrid nanoparticles based nanohybrid films.** These nanocomposite films was characterised by conventional technique. An enhancement in mechanical, tensile and water absorption properties of nanocomposites than pure chitosan was observed.

Chapter 6 focuses on **preparation and characterization of glycolic acid-g-chitosan-Co_3O_4 hybrid nanoparticle based novel nanohybrid scaffolds for drug delivery and tissue engineering application.** The Co_3O_4 hybrid nanoparticles were prepared by

hydrothermal process and characterised. The chitosan-g-glycolic acid and Co_3O_4 hybrid nanoparticles based nanohybrid scaffold was prepared freeze drying. The nanohybrid scaffolds were found to be stable regardless of pH of the medium and play a key role in cell adhesion, proliferation and migration. The next part of this chapter focus on **preparation and characterization of glycolic acid-g-chitosan- Co_3O_4 hybrid nanoparticles based nanohybrid films.** An enhancement in mechanical and tensile properties of nanocomposites than pure chitosan was observed.

Chapter 7 focuses on **preparation and characterization of glycolic acid-g-chitosan-Co_3O_4-Fe_3O_4 hybrid nanoparticle based novel nanohybrid scaffolds for drug delivery and tissue engineering application.** The Co_3O_4-Fe_3O_4 hybrid nanoparticles were prepared and characterised. The chitosan-g-glycolic acid and Co_3O_4-Fe_3O_4 hybrid nanoparticles based nanohybrid scaffold was prepared by freeze drying. Grafting of glycolic acid and drug loading in porous scaffold was characterized by Fourier transform infrared spectroscopy. The nanohybrid scaffolds were found to be stable regardless of pH of the medium and play a key role in cell adhesion, proliferation and migration. The next part of this chapter focus on **preparation and characterization of glycolic acid-g-chitosan-Co_3O_4-Fe_3O_4 hybrid nanoparticles based nanohybrid films.** These nanocomposite films was characterised by conventional technique. An enhancement in mechanical and tensile properties of nanocomposites than pure chitosan was observed. The water absorption behavior of the nanocomposites was evaluated by measuring swelling degree. These nanocomposites could be useful in the field of biomedical.

Chapter 8 This chapter summarizes the results and describes the salient conclusions of the study. Future perspectives for further research are also expressed.

Abbreviations

Å	Angstrom
λ	Wave length
nm	Nanometre
μm	Micrometre
cm^{-1}	Wavenumber
AFM	Atomic Force Microscopy
ATR-FTIR	Attenuated Total Reflectance Fourier Transform
CPA	Cyclophosphamide
DMA	Dynamic Mechanical Analysis
DSC	Differential Scanning Calorimetry
EDAX	Energy-Dispersive Absorption X-Ray
FTIR	Fourier Transform Infra Red
PPMS	Physical Property Measuring System
SAED	Selected Area Diffraction Pattern
SEM	Scanning Electron Microscopy
Tg	Glass Transition Temperature
TEM	Transmission Electron Microscopy
TST	Tensile Strength Testing
UV	Ultraviolet
XRD	X-Ray Diffraction
XPS	X-Ray Photo Electron Spectroscopy

List of Tables

List of Figures

List of schemes

CHAPTER 1

Introduction

A biomaterial is any material, natural or man-made, that comprises whole or part of a living substrate or biomedical device which performs, augments or replaces a natural function.

1.1 INTRODUCTION

Biomaterials are materials intended to interface with biological systems to evaluate, treat, augment or replace any tissue, organ or function of the body[1]. This definition is somewhat restrictive, because it excludes materials used for devices such as surgical or dental instruments. Exposure to body fluids usually implies that the biomaterial is placed within the interior of the body and this places several strict restrictions on materials that can be used as a biomaterial[2]. Biomaterials have many important functions, such as it can be used for a heart valve or may be bioactive and used for a more interactive purpose such as hydroxy-apatite coated hip implants[3-6]. Biomaterials are also used in drug delivery (a construct with impregnated pharmaceutical products that can be placed into the body, which permits the prolonged release of a drug over an extended period of time) [7-11], dental applications and surgery.

1.2 EVOLUTIONS OF BIOMATERIALS

Recently, tissue engineering combines the principles and methods of the life sciences with those of engineering to elucidate fundamental understanding of structure-function relationships in normal and diseased tissues, to develop materials and methods to repair damaged or diseased tissues and to create entire tissue replacement[12]. Tissue engineering thus spans from controlling cellular responses to material implants, manipulating the healing environment to control the structure of the regenerated tissue, producing cells and tissues for transplantation into the body and developing a quantitative understanding of many biological equilibrium and rate processes. Biomaterials play an important role in many of these activities[13], for example serving as matrices to guide tissue regeneration, releasing polypeptide growth factors to stimulate as vascularisation response to a composite cell polymer implant and blocking antibody permeation into transplant of cells from another

species. To initiate the natural developmental events, it requires functional cells that constitute the target tissue, a matrix or scaffold supporting those cells, bioactive molecules regulating cellular behavior and the compatible integration of this composite in the damaged tissue[14]. An implant composed of a biodegradable and biocompatible scaffolds, the reservoir own cells and biomolecule that modulate the cells to form the neotissues would be the foundation for the future generation of biomedical engineering[15, 16].

This implant creates a local environment for pre-loaded cell proliferation and differentiation in the targeted tissue and also interacts with the host's tissue and integrates into it. Only foreign part left is scaffold, which will be degraded and excreted from the human body. In this manner the implant eventually transforms itself into the patient's own body. The biomolecules and the cells together with the intrinsic properties of the chosen biomaterials determine the biocompatibility and longevity of the implants. Though this strategy is still in its infancy, diverse knowledge has been accumulated toward addressing its key elements including scaffold structure, bimolecular recognition, cell sources, and material properties [17-21].

1.3 PROPERTIES OF BIOMATERIALS FOR TISSUE ENGINEERING:

The main functions of tissue engineering scaffolds are:

1. *It should be biocompatible*
2. *It should provide temporary mechanical support.*
3. *It should guide tissue regeneration and organization.*
4. *It should promote tissue formation and subsequent regeneration*

The scaffold or matrix for bone repair must be optimized for biocompatibility, biodegradability and biomedical properties:

1. **Biocompatibility:** The most important property of a biomaterial is that, it must be immune acceptable. The host immune system should recognize the implant as part of the host and not reject it. Biocompatibility depends on the biological environment and the way it exists with respect to tissue reaction. The biomaterial should minimize an inflammatory response[22].

2. **Biodegradability:** The implanted biomaterial should be degraded and expelled from the host's physiological system. Ideally, the entire scaffold would be degraded when the damaged tissue is totally regenerated[23].

3. Biomechanical properties: The implanted biomaterials must have certain mechanical strength to maintain tissue growth and integration or at least survive the hydrostatic pressure and other mechanical conditions at the damaged tissue site[24]. A successfully designed device has to fill the mechanical requirements of the implant location.

4. Micro topography: It plays an important role in the cellular and adhesion[25]. On rougher surfaces, the cells appear to form local contacts that allow the cells to span across the space between surfaces. In contrast, on smooth surfaces, the cells are able to spread, perhaps forming greater number of hemi-desmosomes as anchors to the substrate.

5. Porosity: Scaffolds should be highly porous with interconnected pore network. The large void volume in scaffold facilitates anchorage-dependent cell seeding; maximize attachment, migration and growth, extracellular matrix production, fluid circulation and vascularisation within the pore space throughout the scaffold structure[26].

6. Surface Chemistry: The surface chemistry plays an important role in cell adhesion[27]. Cellular adhesion at the cell-material interface is mediated by proteins adsorbed from the surrounding medium onto the substratum[28,29]. The material ions modify the adsorption and orientation of proteins on the surface and thus affect the subsequent cell binding. However, a highly adhesive surface allowing for a strong cell adhesion may also result in cell

immobilization[30]. The polymeric scaffolds have great advantages in terms of their degradability and other properties, they lack desirable surface properties.

Various Examples of medical and dental materials and their applications is shown in **Table 1.1.**

Table 1.1 Examples of medical and dental materials and their applications

Material	**Principal applications**
Ceramics and glasses	
Alumina	Joint replacement, dental implants
zirconia	Joint replacement
Calcium phosphates	Bone repair and augmentation, surface coatings on metals
Bioactive glasses	Bone replacement
Porcelain	Dental restorations
Carbons	Heart valves, percutaneous devices, dental implants
Polymers	
Polyethylene	Joint replacement
Polypropylene	Sutures
Polyamides	Sutures
PTFE	Soft-tissue augmentation, vascular prostheses
Polyesters	Vascular prostheses, drug delivery systems
Polyurethanes	Blood-contacting devices
PVC	Tubing
PMMA	Dental restorations, intraocularlenses, joint replacement(bone cements)

Silicones	Soft-tissue replacement, ophthalmology
Hydrogels	Ophthalmology, drug-delivery systems
Composites	Dental restorations
BIS-GMA-quartz/silica filler	Dental restorations (dental cements)
PMMA-glass fillers	
Metals and alloys	Fracture fixation, stents, surgical
316L stainless steel	Instruments
CP-Ti, Ti-Al-V, Ti-Al-Nb, Ti-13Nb-13Zr, Ti-Mo-Zr-Fe	Bone and joint replacement, fracture fixation, dental implants, pacemaker encapsulation
Co-Cr-Mo, Cr-Ni-Cr-Mo	Bone and joint replacement, dental implants, dental restorations, heart valves
Ni-Ti	Bone plates, stents, orthodontic wires
Gold alloys	Dental restorations
Silver products	Antibacterial agents
Platinum and Pt-Ir	Electrodes
Hg-Ag-Sn amalgam	Dental restorations

Abbreviations: *CP-Ti, commercially pure titanium; PET, polyethylene terephthalates (Dacron, E.I. DuPont de Nemours & Co.); PTFE, polytetra fluoroethylenes (Teflon, E.I. DuPont de Nemours & Co.); PVC, polyvinyl chlorides; PMMA, polymethyl methacrylate; BIS-GMA, bisphenol A-glycidyl. Source: Adapted from Ref 3*

1.4 PROPERTIES OF BIOMATERIALS FOR DRUG DELIVERY:

There are two way in which drug is given to a patient:

1. Single dose drug release system

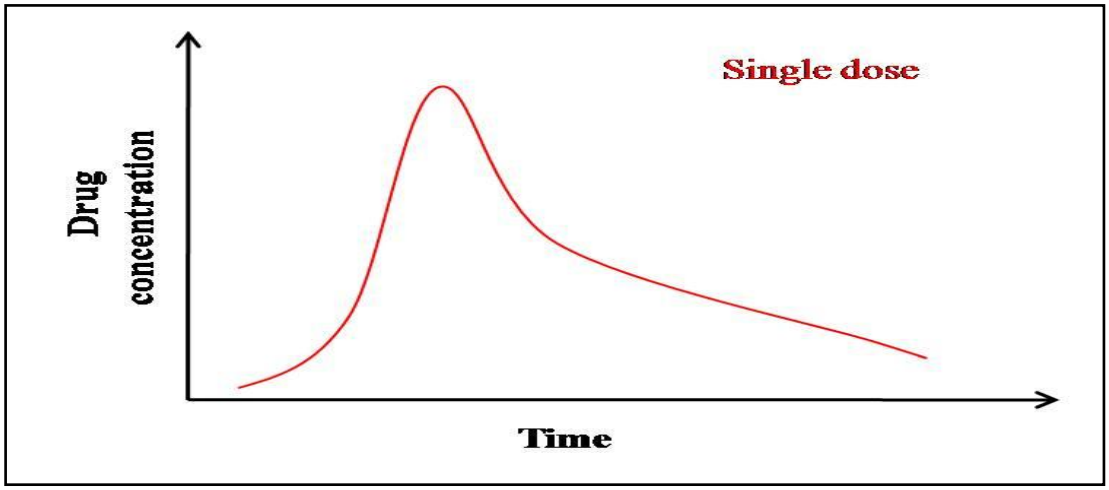

Figure 1.1 *Illustrates single dose drug release system*

2. Multi dose drug release system

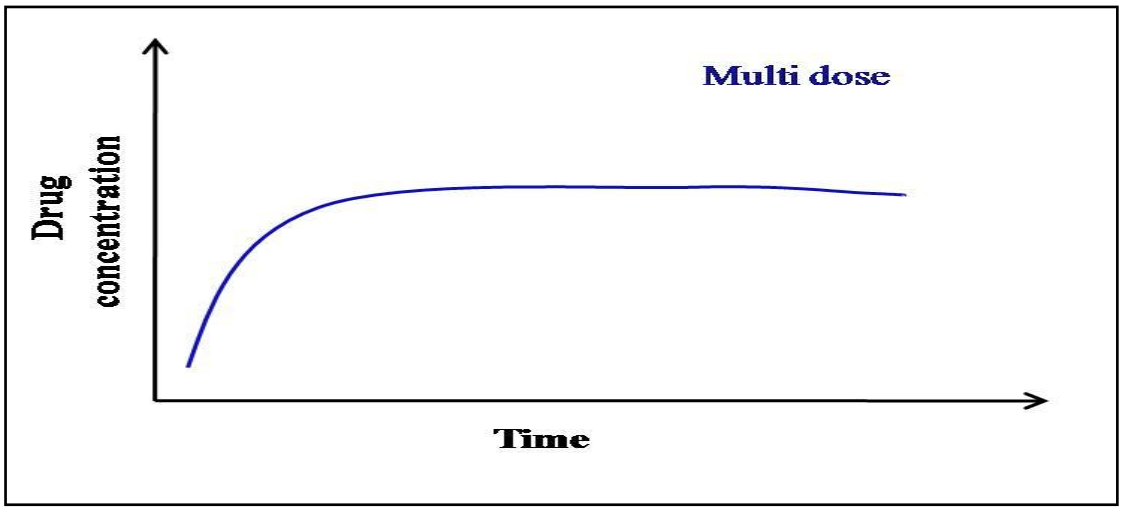

Figure 1.2 *Illustrates multi dose drug release system*

In a single dose drug release system, when a patient takes single dose of drug its concentration in his blood increases rapidly but very fast decrease in the drug concentration is also observed (**Figure 1.1**). To maintain an effective concentration of drug in the blood, the patient must take other dose at different interval (**Figure 1.2**).

The aim of a controlled drug delivery system is to maintain the concentration of drug in the blood within several days with a single dose. So the goal of the controlled drug release device is to maintain a constant amount of drug with just a single dose and this kind of delivery preserves medications that are rapidly destroyed by the body and improve patient comfort.

1.5 CLASSIFICATION OF DRUG DELIVERY SYSTEM

Drug delivery system is classified on the basis of mechanism that controls the drug release as:

- ***By Reservoir device***: It is the device, in which the drug forms a reservoir surrounded by a diffusion barrier; it consists of membranes, capsules and liposomes.

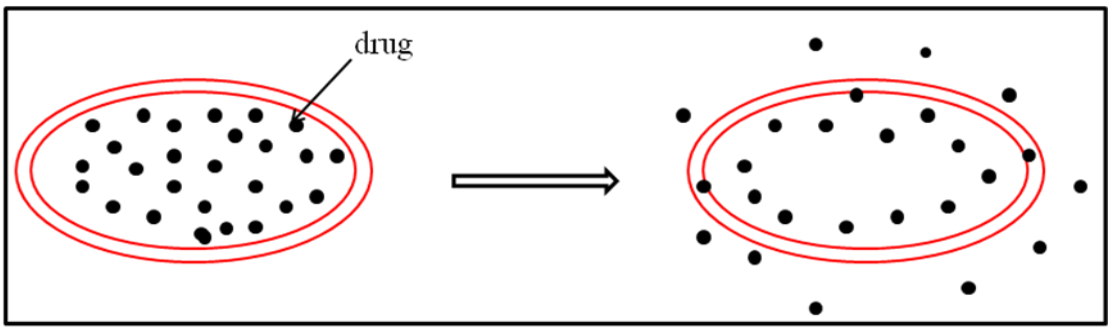

Reservoir device

- ***By Monolithic device:*** It is the device, in which the drug is dispersed or dissolved in a polymer. The release is directly linked to the choice of polymer and its properties

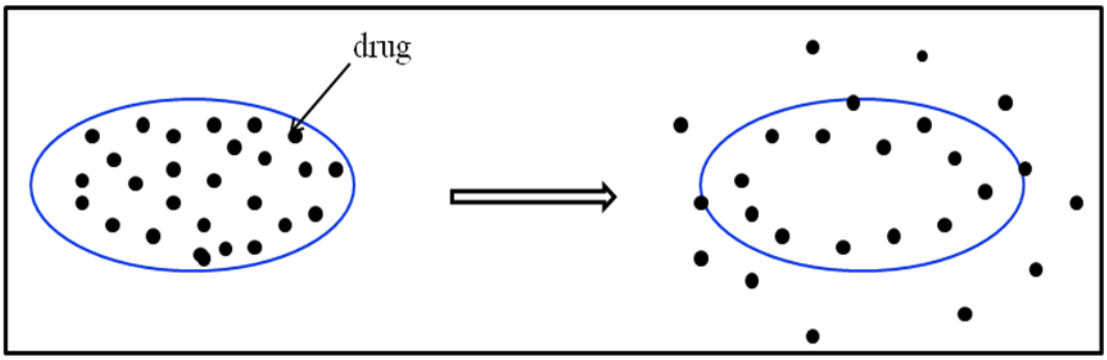

Monolithic device

- ***By Biodegradable delivery system:*** It is a drug delivery system in which drug is dispersed in a biodegradable polymer and this polymer is degraded which allows drug

to be released.

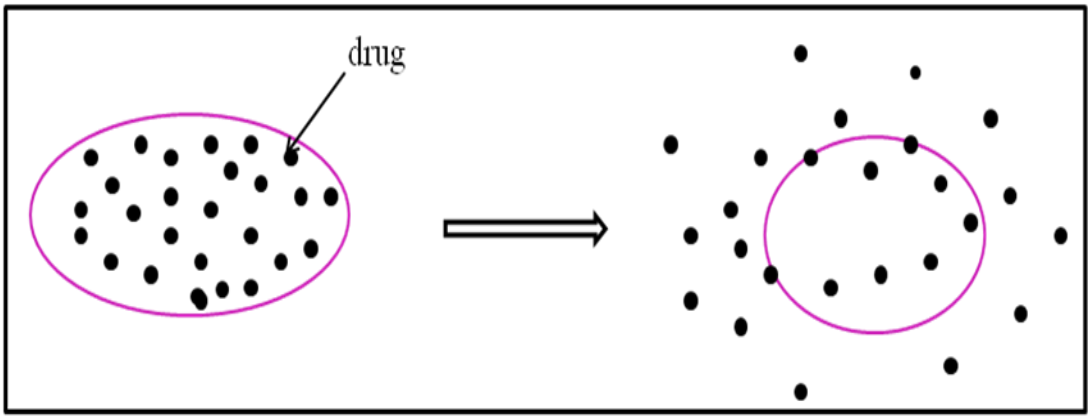

Biodegradable delivery system

- **By *pendant chains drug delivery system:*** In this system, drug is bound to polymer by covalent bonds which are destroyed by a chemical mechanism.
- ***By solvent controlled system:*** In this system, drug is dispersed in a polymer that swell in the fluid where it is used, thus the glass transition of polymer is decreased and drug can diffuse in the polymer and be released.

1.6 THE GOALS OF DRUG DELIVERY

There are two main goals of drug delivery:

- *To overcome the inherent limitations associated with biomacromolecular therapeutics, which include a short plasma half-life, poor stability and potential immunogenicity.*
- *To maximize the therapeutic activity while minimizing the toxic side effects of drugs.*

The current drug-delivery systems are effective at releasing drugs in a controlled fashion to produce a high local concentration. Smaller particles have greater surface area-to-volume ratios, which increase the particle's dissolution rate, enabling them to overcome solubility-limited bioavailability. The nano-scale drug-delivery systems (nano-scaled materials (10^{-9} to 10^{-7} m) can be manufactured to combine desirable modules, both biological and synthetic,

for various applications. Many properties of nano-scale drug-delivery systems can be tailored for specific applications: solubility (inherent hydrophilicity of the material, addition of solubilizing moiety), biodistribution (molecular weight, addition of targeting group), biocompatibility (electrical charge, addition of bioinert functionality), biodegradability (backbone, spacer), drug release (physical interaction between drug and carrier, chemical cleavage of covalent spacer), drug encapsulation (physical interaction between drug and carrier) and shape (materials and chemistry employed). Drug is covalently conjugated to the matrix of the scaffold. In multiple drug release different drugs are encapsulated within one particulate system[31]. Temporal control of drug release to specific site is important, either the prepared substrate should deliver drugs in a pulsatile manner or release of drugs at different times. This could be achieved in a number of ways. For example, drugs could be entrapped within separate populations of particles with differing release kinetics. They could be entrapped within or beneath polymer layers of differing thicknesses or with differing degradation rates. Drugs could be contained within chip-like implantable devices that are programmed to release defined payloads in response to electrical stimuli or polymer degradation[32,33].

1.7 CONTROLLED-RELEASE DRUG DELIVERY SYSTEMS:

Controlled-release drug delivery system covers wide range of products:

- **Delayed release system:** Systems are those in which drug release is delayed for a finite "lag time", after which release is unhindered (e.g. enteric coated oral tablets).
- **Extended release system:** Extended-release (or prolonged-release) dosage forms include any system in which the drug is made available over an extended period of time after administration.

- **Site-specific targeting system & Receptor targeting system:** are those that deliver the active substance at the desired biological site, e.g. the diseased organ or tissue (site-specific targeting) or the particular drug receptor within an organ or tissue (receptor targeting).
- **Controlled release system:** Systems providing some actual therapeutic temporal and/or spatial controls of drug. According to the classification proposed by Chien and Lin[34], the Controlled-release drug delivery systems are summarized in **Table 1.2.**

Table 1.2 Types of Controlled-Release Drug Delivery systems.

Group	Drug Delivery System	Drug Release Control Mechanism	Example
Rate-programmed systems	Polymer Membranes, Permeation systems, Polymer Matrix/Hybrid Systems. Micro-reservoir partition systems.	Diffusion	Ocusert, Transderm-Nitro, Norplant Nitrodisc, Syncromate-C.
Activation-Modulated Systems	Osmotic-Hydrodynamic Pressure, Vapor-pressure activated systems Mechanical-force activated systems Hydration-activated systems Magnetic, Sonophoresis, pH, Ion, Hydrolytic, Temperature, Enzyme.	Modulation of the activation input	Alzet osmotic pump, Acutrim tablet, Infusaid, Nasal metered dose nebulisers. Syncro-Male-B, Valrelease tablet, Lapron-Depot, Zoladex.
Feed-back regulated systems	Bio-erosion and Bio-responsive regulated systems, Self-Regulating systems.	Concentration of the activating substance in the body.	

1.8 SCAFFOLDS

In tissue engineering cells are often implanted or 'seeded' into an artificial structure capable of supporting three-dimensional tissue formation. These structures are typically known as scaffolds.

1.8.1 Classification of scaffold materials

- **Synthetic organic materials:** It mainly involve polyester family eg. poly (α-hydroxyl acids) such as polylactide (PLA), polyglycolide (PGA) and their co-polymer (PLGA).
- **Organic materials of natural origin:** collagen, alginate, fibrin glue; and chitosan.
- **Synthetic inorganic materials:** mainly hydroxyapatite, tricalcium phosphate, glass ceramics and metal/ metal oxide based nanoparticles.

1.8.1.1 ORGANIC MATERIALS

Due to their availability in large variety of compositions and forms, organic materials are widely used in several different applications (solids, films, gels, etc.). All the polymers of synthetic and natural origin that have been investigated for use as scaffolds in tissue engineering are biodegradable and biocompatible, also having their own distinctive characteristics[35]. It is well known that synthetic and natural biopolymers are mechanically weak, do not have good bioactivity, degrade too fast in physiological media losing their mechanical properties and sterilization processes (autoclave, ethylene oxide and irradiation) and may alter polymer properties[36].

1.8.1.2 POLYMER USED FOR BIOMATERIALS

1.8.1.2.1 Synthetic polymers

Synthetic polymers can be produced in large quantities and their synthesis allows for direct control over chemical composition[37]. Synthetic biomaterials are generally biologically inert, have more predictable properties and unique advantage of tailored property profiles for specific applications, devoid of many of the disadvantages of natural polymers. As compared to enzymatically degradable polymers, hydrolytically degradable polymers are generally preferred as implants due to their minimal site-to-site and patient-to-patient variations. In late 1960s, first successful performance of synthetic poly (glycolic acid) based suture system led to the design and development of a new array of biodegradable polymers as transient implants for orthopaedic and related medical applications. A vast majority of the research has focus on the synthetic polymers that already have the advantage of food and drug administration approval as sutures[38]. These belong to the aliphatic polyester family e.g. poly (α-hydroxyl acids), mainly PLA, PGA and their copolymer. Biodegradable polyesters (synthetic polymers) have succeeded to some degree in tissue engineering applications but despite their attractive properties, they are limited by some drawbacks[39]. The main drawbacks of these polymers are: low biocompatibility, generation of acidic degradation by-products, processing difficulties and loss, that is too rapid of mechanical integrity while degrading[40].

1.8.1.2.2 Natural polymers

Natural polymers can be considered as the first biodegradable biomaterials used clinically. These polymers may be much more similar to the native cellular milieu that has been optimized through evolution. Scaffolding applications requires such natural materials, which are expected to have a higher biocompatibility and have demonstrated a better and faster healing process[41]. Natural polymers possess several inherent advantages such as bioactivity, the ability to present receptor-binding ligands to cells, susceptibility to cell-triggered

proteolytic degradation and natural remodelling. One of the most important example of natural polymer is chitosan.

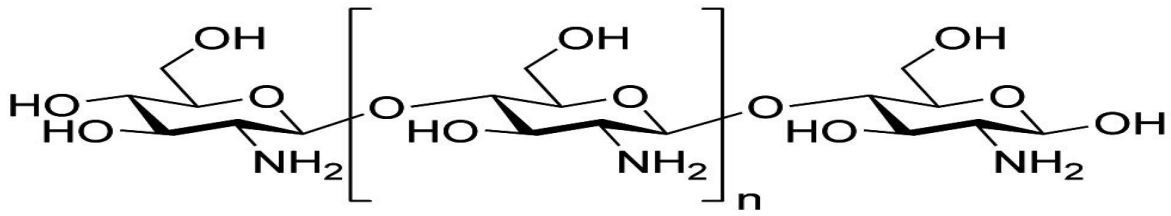

STRUCTURE OF CHITOSAN

Chitosan is derived from partial deacetylation of chitin, which is most abundant natural polysaccharide[42] known after cellulose. Several million tons of chitin is harvested worldwide from the shell of shrimp, lobster, crab or krill[43] every year. Due to its chemical nature and biological properties, chitosan biomaterial is highly versatile (**Figure 1.3**)[44]. First, it is biocompatible, biodegradable, bioresorbable and has a hydrophilic surface, which facilitates cell adhesion, proliferation and differentiation[45]. Second, with its cationic nature in physiological pH, chitosan mediates non-specific binding interactions with various proteins. Soluble proteins, most of which are negatively charge, may also be expected to have varying binding affinities to chitosan based material[46].

Chitosan is a linear polysaccharide composed of randomly distributed (β-1, 4)-linked D-glucosamine (deacetylated unit) and N-acetyl-D-glucosamine (acetylated unit). It has been widely used in food industry, for making biosensors[47] and drug delivery due to its biocompatibility, film forming properties[47, 48] and polycationic nature. Chitosan is selected in the present work because it easily forms stable film on the solid support, which has been used in the development of biosensors[47,49,50]. Chitosan is hydrophilic and compatible with nanoparticle and has better processability due to the presence of amino group (pKa value is 6.2) in the chain. Chitosan also possesses hydroxyl functional group which acts as potential

site for altering the polymers functionality[51,52,53]. The grafting of side glycolic acid leads to marked changes in the chitosan structure[54, 55].

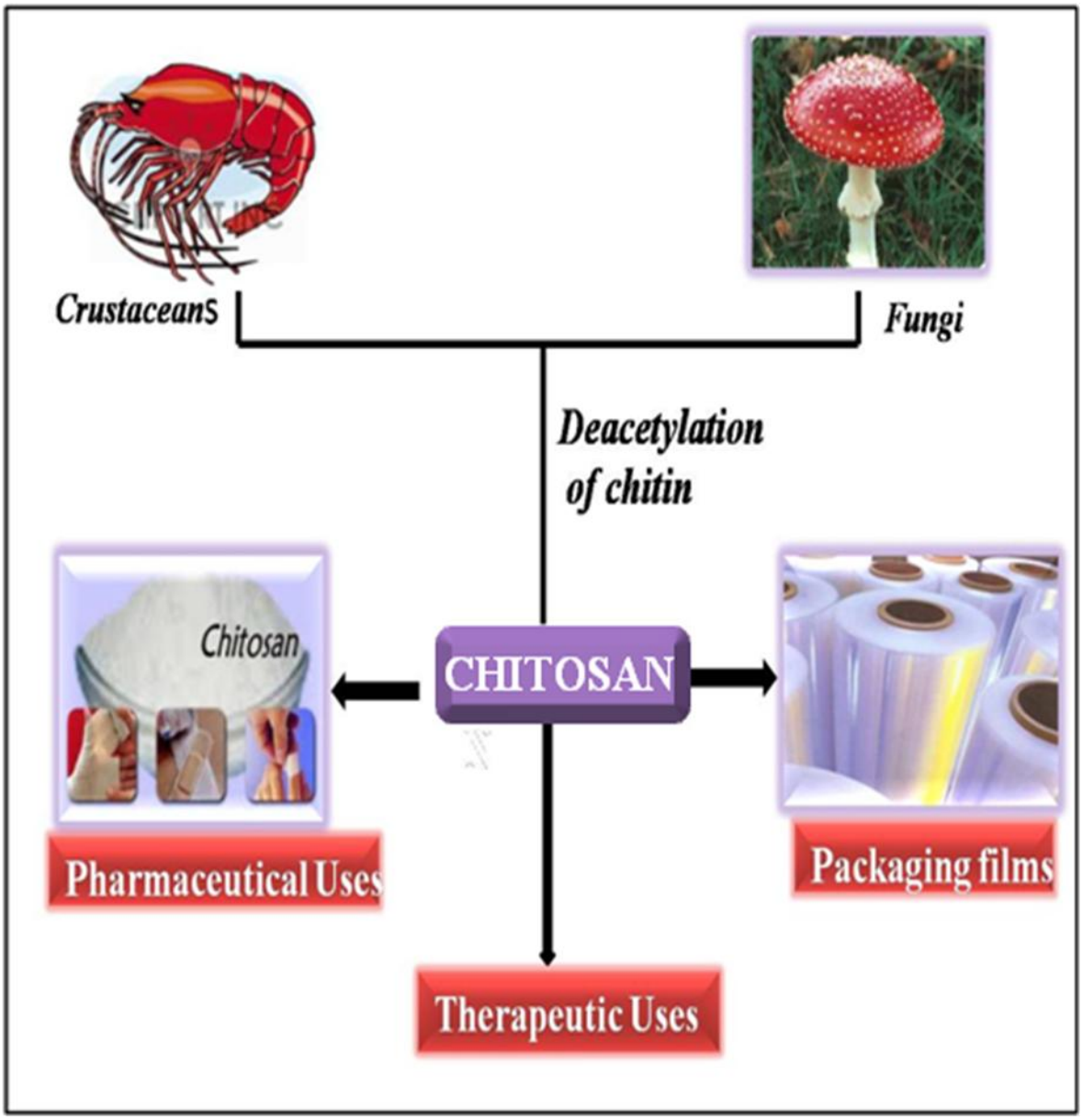

Figure 1.3 *Production and various applications of chitosan*

Chitosan has a number of other desirable properties for a tissue scaffold: it has anticoagulant properties, antibacterial and antifungal action[56]. Moreover, chitosan has an excellent ability to be processed into porous structures and smooth films for use in cell transplantation and in tissue regeneration[57]. Chitosan properties have only been thoroughly

studied in the last few decades[58], starting approximately when the scientific principles for use of the monomer N- acetyl glucosamine in enhancing wound healing process were reported in 1960[59]. In the 1970s, the role of chitosan in potentiating wound healing was documented for various animal models[60]. **Table 1.3** shows the various forms, applications and properties of chitosan.

Table 1.3 Various forms, applications and properties of chitosan.

Form	**Application**	**Route of delivery/properties**
Beads	Drug Delivery	Oral
Microspheres	Enzyme Immobilization	Oral, Implantable, Injectable
Coatings	Surface Modification, Textile Finishes	Chitosan increases mucoadhesiveness of Alginate capsules
Fibers	Medical Textiles, Sutures	Biodegradable
Nanofibers	Guided Bone Generation,	
Films	Wound Care, Dialysis Membranes	
Powder	Adsorbent for pharmaceutical and medical devices, Surgical glove powder,	
Sponge	Mucosomal Hemostatic dressing, Wound Dressing, Enzyme Entrapment	
Shaped Objects	Orthopedics, Contact Lenses	
Solutions	Cosmetics, Bacteriostaic Agents, Hemostatic agents, Anticoagulant, Anti-tumor agent.	Moisture Holding, Oral, Nasal Complex Formation-Gene Delivery
Gels	Delivery Vehicle, Implants, Coatings,	
Tablets	Compressed Diluents, Disintegrating Agents	Oral, Buccal
Capsules	Delivery Vehicle	

Since then, chitosan material has been widely investigated in a number of biomedical applications[61-66], from wound dressings, drug or gene delivery systems and nerve regeneration to space filling implant. The utility of chitosan as a scaffolding material to support cell growth and proliferation has also been reported[67-69].

However, pure chitosan has very attractive properties, it lacks bioactivity and is mechanically weak[70]. These drawbacks limit its biomedical applications. For these reasons, it is highly desirable to develop a hybrid material made of chitosan and appropriate inorganic filler, hoping that it can combine the favorable properties of the materials, and further enhance tissue regenerative efficacy. **Table 1.4** Shows the general chemical and biological properties of chitosan.

Table 1.4 Gives the general chemical and biological properties of chitosan

Chemical Properties	**Biological Properties**
Cationic Polyamine	Naturally Occurring Polymer
High charge density	Biodegradable
Adheres to negatively charged surfaces	Biocompatible
High Molecular weight polyelectrolyte	Safe and non-toxic
Reactive –NH2 and –OH group	Anti-carcinogen

Figure 1.4 explains the various applications of chitosan. Chitosan is much easier to process than chitin, but the stability of chitosan materials is generally lower, owing to their more hydrophilic character and, especially, pH sensitivity. The advantage of chitosan is not only its biodegradability and its antibacterial activity but also the hydrophilicity introduced by addition of the polar groups able to form secondary interactions (–OH and –NH_2 groups involved in H bonds with other polymers).

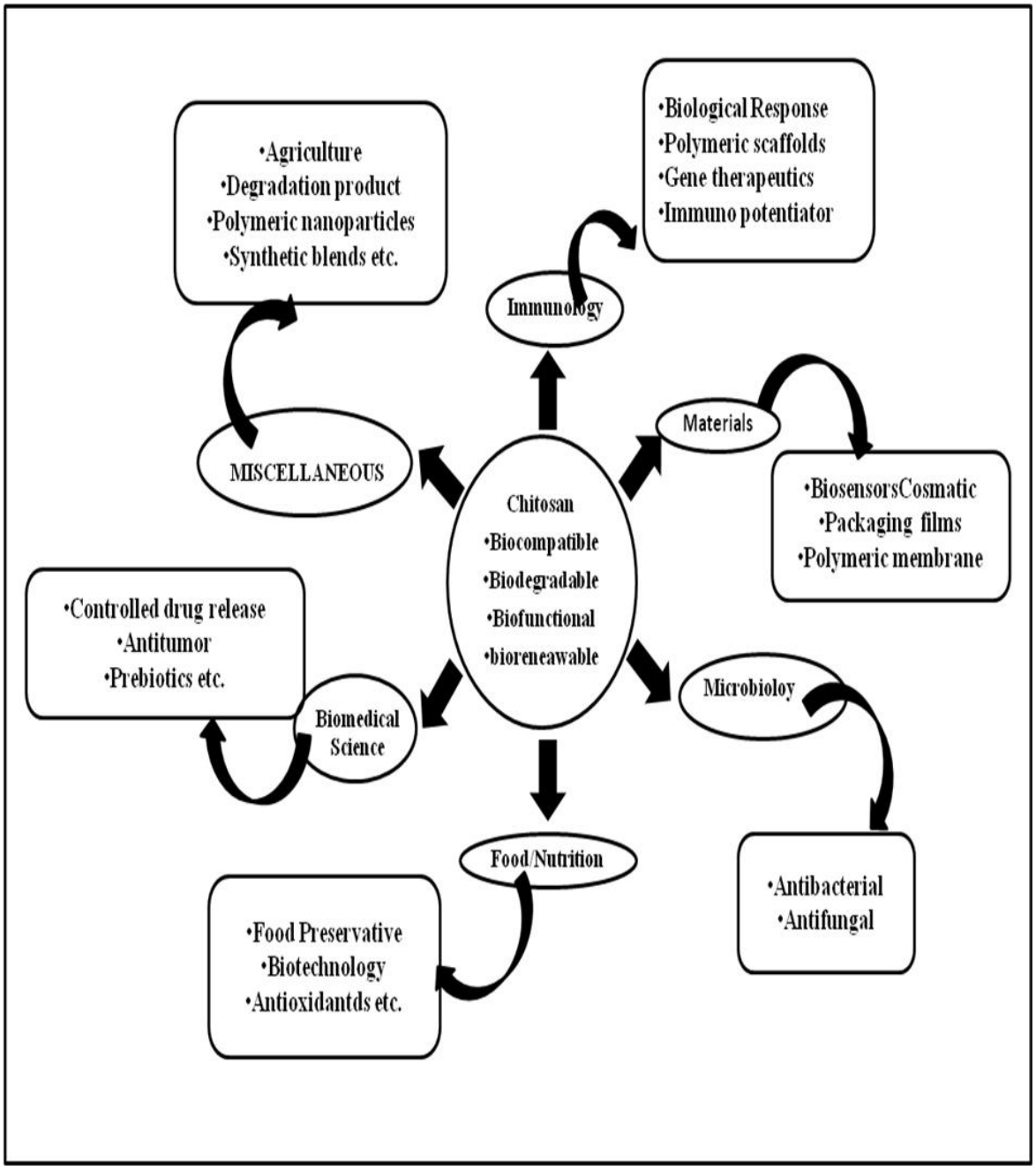

Figure 1.4 *Explains the various applications of chitosan.*

1.9 CHEMICAL MODIFICATION OF CHITOSAN BY GRAFT COPOLYMERIZATION

In a structure of chitosan as mentioned in many literature[71-73], one can differentiate specific reactions involving the $–NH_2$ group at the C-2 position or nonspecific reactions of –OH groups at the C-3 and C-6 positions (especially esterification and etherification)[74]. The important point of

difference between the chitosan and cellulose is $–NH_2$ in the C-2 position, where three –OH groups of nearly equal reactivity are available. These groups have been proposed to introduce different functional groups on chitosan using acryl reagents in an aqueous medium; introduction of N-cyano-ethyl groups is said to produce some cross-linking through a reaction between the nitrile group and the amine group[75]. Various chemical modification reactions of chitosan is shown in **Figure 1.5.**

Figure 1.5 Gives the various chemical modification reactions of chitosan

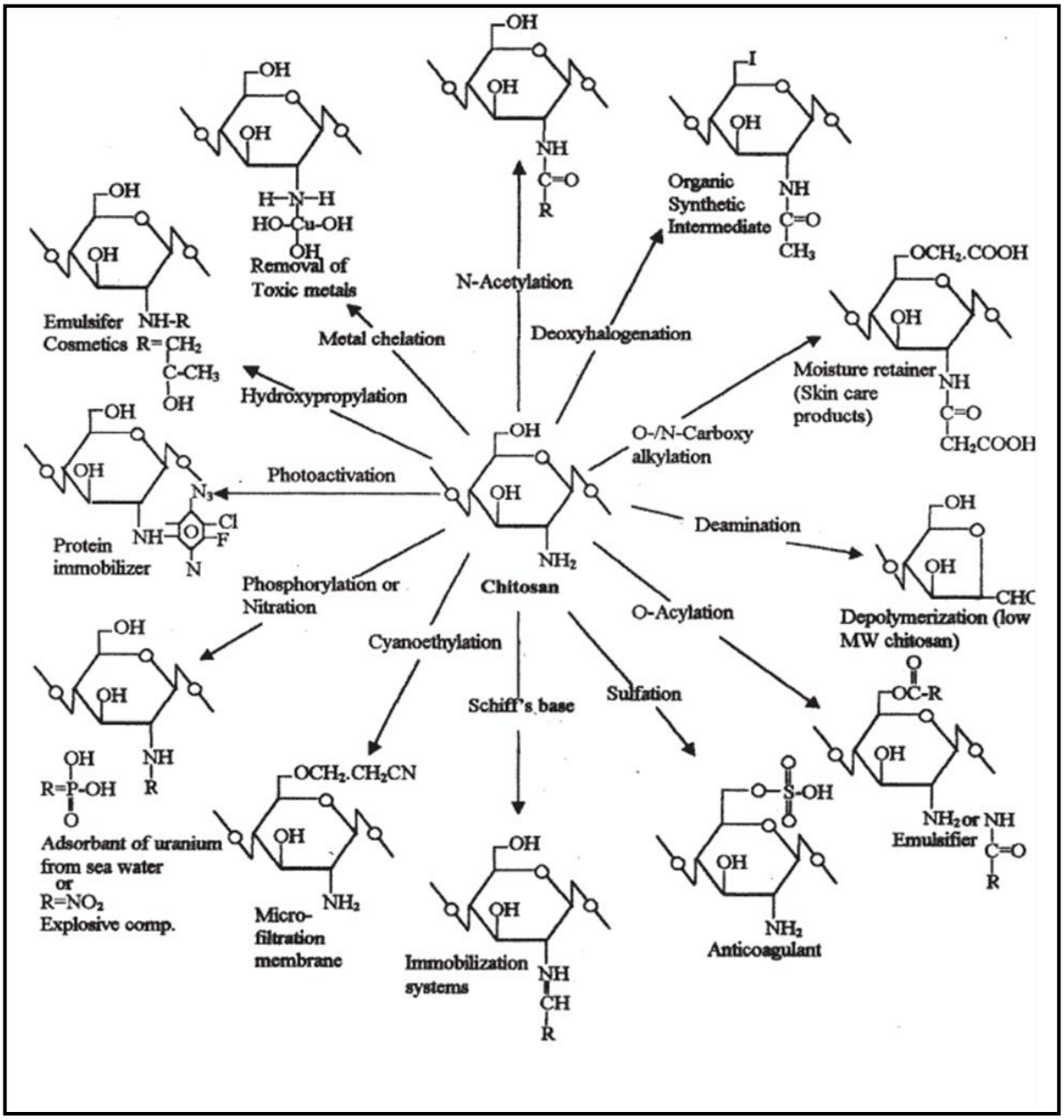

1.9.1 GRAFT COPOLYMERIZATION

Graft copolymerization reaction introduces side chains and makes various molecular designs possible, thus affording novel types of tailored hybrid materials composed of natural polysaccharides and synthetic polymers. The properties of the graft copolymers may be controlled by molecular structure, length and number of side chains attached. It is thus one of the most attractive approaches towards constructing versatile molecular environments. Several types of chitosan-graft-copolymers with acrylic, vinyl, non-vinyl, etc. have been prepared for use as flocculants, paper binder-strengthener, slow-release drug carrier, etc. Graft copolymerization onto chitosan has been attempted by various methods but it is performed typically with 2, 2-azo bisisobutyronitrile, Ce(IV) or a redox system.

1.10 BIO-NANOCOMPOSITE SCAFFOLD

1.10.1 NANOHYBRID SCAFFOLDS BASED ON CHITOSAN AND INORGANIC FILLERS

Bionanocomposites form a fascinating interdisciplinary area that brings together biology, materials science and nanotechnology. New bionanocomposites are impacting diverse areas, in particular, biomedical science. Generally, polymer nanocomposites are the result of the combination of polymers and inorganic/organic fillers at the nanometer scale. Existing biopolymers include, but are not limited to, polysaccharides, aliphatic polyesters, polypeptides and proteins and polynucleic acids, whereas fillers include clays, hydroxyapatite and metal nanoparticles[76]. The interaction between filler components of nanocomposites at the nanometer scale enables them to act as molecular bridges in the polymer matrix. This is the basis for enhanced mechanical properties of the nanocomposite as compared to conventional microcomposites[77]. Bionanocomposites add a new dimension to these enhanced properties in that they are biocompatible and/or biodegradable materials. The biodegradable

materials can be described as materials degraded and gradually absorbed and/or eliminated by the body, whether degradation is caused mainly by hydrolysis or mediated by metabolic processes[78]. Therefore, these nanocomposites are of immense interest to biomedical technologies such as tissue engineering, bone replacement/ repair, dental applications and controlled drug delivery.

A great deal of research is focused on polymer-inorganic nanocomposites (PINCs) over the last two decade. As a result of the development in nanotechnology, inorganic nanomaterials have been designed /discovered and fabricated with important cooperative physical phenomena, such as superparamagnetism, size-dependent band-gap, ferromagnetism, electron and phonon transport. Yet, they typically suffer from high manufacture expense and the shaping and further processing of these materials is often difficult and demanding or impossible[79]. Polymers, on the other hand, are flexible light weight materials and can be produced at a low cost. They are also known to allow easy processing and can be shaped into thin films by various techniques such as dip-coating, spin-coating, film-casting and printing generated to the PINCs. Therefore, the drawbacks of using inorganic nanostructured materials can be overcome by employing a polymer matrix to embed a relatively small content of inorganic nanoparticles. The integration of inorganic nanoparticles into a polymer matrix allows both properties from inorganic nanoparticles and polymer to be combined enhanced and thus, advanced new functions can be generated to the PINCs. In this way, the inorganic nanoparticles are acting like 'additives' to enhance polymer performance and thus are also termed 'nano-fillers' or 'nano-inclusions' [80,81].

Frequently employed inorganic nano-fillers include metals and metal alloys (e.g. Au, Pt, Fe and CoPt), oxides (e.g. ferric oxide). For a breakthrough in utilization, graft copolymerization onto chitosan will be a key point, which will introduce desired properties and enlarge the

field of the potential applications of chitosan by choosing various types of side chains. Chemical modification of chitosan is useful for the association of bioactive molecules to polymer and controlling the drug release profile. These properties make chitosan a good candidate for the development of conventional and novel drug delivery systems.

1.11 CHARACTERIZATION TECHNIQUES OF NANOHYBRIDS

1.11.1 Transmission Electron Microscopy (TEM)

A transmission electron microscope (TEM) is used to observe the fine scale structure. A TEM functions exactly as its optical counterpart except that it uses a focused beam of electrons instead of visible light to "image" the specimen and gain insight about the structure and composition. The four basic operations involved are: 1) A stream of electrons is formed and accelerated towards the specimen using a positive electrical potential, 2) This stream is confined and focused using a metal aperture and magnetic lenses into a thin, monochromatic beam, (magnetic lenses are circular electro-magnets capable of projecting a precise circular magnetic field in a specified region) 3) The focused beam is impinged on the sample by a magnetic lens, 4) The energetic electrons then interact with the irradiated sample. These interactions and effects are detected and transformed into an image.

1.11.2 Atomic Force Microscopy (AFM)

The AFM works by measuring a local property-such as height, with a probe or tip placed very close to the sample. The small probe-sample separation makes it possible to take measurements over a small area. To acquire an image the microscope scans the probe over the sample while measuring the local property in question. The resulting image resembles an image that both consist of many rows or lines of information placed one above the other.

AFM operates by measuring attractive or repulsive forces between a tip and the sample. In its repulsive contact mode, the instrument lightly touches a tip at the end of a leaf spring or cantilever to the sample. As a raster-scan drags the tip over the sample, some sort of the detection

apparatus measure the vertical deflection of the cantilever, which indicates the local sample height. In non contact mode, the AFM devices topographic images from measurements of attractive forces, the tip does not touch the sample.

1.11.3 Scanning Electron Microscopy (SEM)

This technique is essentially employed when high resolution three- dimensional images of the surface morphology are desired. When an electron beam impinges on a sample, back scattered electrons and X-rays are produced**.** A scintillation detector detects secondary electron**s,** which are emitted from a surface with low energy 50 eV.

1.11.4 Fourier Transform Infra-Red (FT-IR) Spectroscopy

In FT-IR spectroscopy, IR radiation is passed through the sample. Some of the IR radiations are absorbed by the sample and some are passed through it (transmitted). The resulting spectrum represents the molecular absorption and transmission, creating the molecular fingerprint of the sample.

1.11.5 X-ray Diffraction (XRD)

X-ray diffraction (XRD) is a non-destructive analytical technique for identification and quantitative determination of long-range order in various crystalline compounds. XRD uses the "fingerprint" of crystalline material to allow identification and quantification of unknown phases in a mixture. X-rays are electromagnetic radiation generated when an electron beam is accelerated through a high voltage field and hits a metal, which acts as an anode. The wavelength of x-ray is comparable to the size of atoms; therefore, they can be effectively used to measure the structural arrangement of atoms in materials. X-rays diffracted from different atoms interfere with each other. If the atoms are arranged in a periodic fashion, as in the case of crystals, the peaks in the interference pattern will correspond to the distribution of atoms. The peaks in an x-ray diffraction pattern are directly related to the atomic distances by Bragg's law:

$n \lambda = 2d \sin \theta$

where, λ is the wavelength of x-ray, is the inter-planar distance, dθ is the scattering angle and n an integer representing the order of the diffraction peak.

1.11.6 Ultraviolet–visible spectroscopy

The absorption or reflectance in the visible range directly affects the perceived color of the chemicals involved. This technique is complementary to fluorescence spectroscopy, in that fluorescence deals with transitions from the excited state to the ground state, while absorption measures transitions from the ground state to the excited state. Molecules containing π-electrons or non-bonding electrons (n-electrons) can absorb the energy in the form of ultraviolet or visible light to excite these electrons to higher anti-bonding molecular orbitals. The more easily excited the electrons (i.e. lower energy gap between the HOMO and the LUMO), the longer the wavelength of light it can absorb.

1.11.7 Dynamic mechanical analysis

This technique is used to study and characterize materials. It is most useful for studying the viscoelastic behavior of polymers. A sinusoidal stress is applied and the strain in the material is measured, allowing one to determine the complex modulus. The temperature of the sample or the frequency of the stress are often varied, leading to variations in the complex modulus; this approach can be used to locate the glass transition temperature of the material, as well as to identify transitions corresponding to other molecular motions. Polymers composed of long molecular chains have unique viscoelastic properties, which combine the characteristics of elastic solids and Newtonian fluids. The classical theory of elasticity describes the mechanical properties of elastic solids where stress is proportional to strain in small deformations.

1.11.8 Thermogravimetric analysis

It is a testing performed on samples that determine changes in weight in relation to a temperature program in a controlled atmosphere. Such analysis relies on a high degree of

precision in three measurements: weight, temperature and temperature change. As many weight loss curves look similar, the weight loss curve may require transformation before results may be interpreted. A derivative weight loss curve can identify the point where weight loss is most apparent.

1.12 Conclusion

The biomaterial, which has been implanted in the body, should be compatible with the existing tissue while performing its function i.e., the body receiving the implant should not reject it physiologically. The implanted material should have appropriate mechanical properties for the location in which it is implanted. Sometimes empirical evidence through simple burst or biaxial tests is all that is needed for confirmation. Other times, it is necessary and convenient to find the natural biomaterial's properties and model using finite element analysis**,** expanding the limits of what experiments and conditions can be tested. Just as a structural engineer is able to determine if a high rise building will withstand the forces of strong winds when it is full erected before construction ever begins, a biomedical engineer can use these data to determine if an implant will fail mechanically when subjected to the wear and tear of daily living inside a person.

Further understanding of the natural tissues and advancement of the composite science are necessary in order to achieve this goal. Experimental and clinical studies are needed to test new candidate materials or composites having the required qualities for biomaterial. We have come a long way from the beginnings of natural biomaterial implantation and we are at a point when the available technology intersects with the desire for knowledge. All of today's available tools can yield valuable and accurate information. It only depends on the researcher to choose how much information they need and how best to use it.

The work underlying this thesis is to answer the fundamental questions:

- Chitosan can be modified to obtain better thermal and mechanical properties and the formulation with Au nanoparticle could be useful for a controlled drug release carrier. **(*Chapter 3*)**.
- Chitosan can be modified to obtain better thermal and mechanical properties and the formulation with Au-Fe_3O_4 hybrid nanoparticle could be useful for a controlled drug release carrier. **(*Chapter 4*)**.
- Chitosan can be modified to obtain better thermal and mechanical properties and the formulation with Pt-Fe_3O_4 hybrid nanoparticle could be useful for a controlled drug release carrier. **(*Chapter 5*)**.
- Chitosan can be modified to obtain better thermal and mechanical properties and the formulation with Co_3O_4 hybrid nanoparticle could be useful for a controlled drug release carrier. **(*Chapter 6*)**.
- Chitosan can be modified to obtain better thermal and mechanical properties and the formulation with Co_3O_4-Fe_3O_4 hybrid nanoparticle could be useful for a controlled drug release carrier. **(*Chapter 7*)**.

1.13 REFERENCES

1. D. F. Williams, *The Williams Dictionary of Biomaterials. Liverpool University Press,* Liverpool (1999).
2. C. M. Agrawal, *JOM,* 31 (1998).
3. J. Karp and R. Langer, *Curr. Opin. Biotech*., **18**, 454 (2007).
4. G. Balssundaram and T.J. Webster, *Nanomed*., **1**, 169 (2006).
5. L.S. Nair and C.T. Laurencin, *Adv. In Biochem. Eng*., **102**, 47 (2006).
6. R. Langer, *MRS Bull*., **31**, 477 (2006).
7. C. Du and J. Moradian-Oldak, *Biomed. Mater*., **1**, R10 (2006).

8. B. Baroli, *J. Chem. Technol. Biotechnol*., **81**, 491 (2005).

9. T. Hadlock and C. Sundback, *Exp. Opi. Biol. Therap*., **6**, 1105 (2006).

10. E. Anitua, M. Sanchez, G. Orive and I. Andia, *Trends Pharmacolog. Sci*., **29**, 37 (2008).

11. L. De-Laporte and L.D. Shea, *Adv. Drug Del. Rev*., **59**, 292 (2007).

12. R. Langer and J.P. vacanti, *science.*, **260,** 920 (1993).

13. N. A. Peppas and R. Langer, *Science.*, **263,** 1715 (1994).

14. V. M. Goldberg, and A. J. Caplan, *Orhopedic tissue engineering, Eds Goldberg and Caplan, Marcell Dekker,* Inc., New York, **1**, (2004).

15. S. MacNeil, *Mater. Today*, **11**, 26 (2008).

16. 15. P.X. Ma, *Adv. Drug. Del. Rev*., **60**, 184 (2008).

17. K.J.C. Burg, S. Porter and J.F. Kellan, *Biomater*., **21**, 2347 (2000).

18. A.J. Salgado, O.P. Coutinho and R.L. Reis, *Macromol. Biosci.*, **4**, 743 (2004).

19. M. C. Kruyt et al, *Biomater*., **25**, 1463 (2004).

20. J. Sun, S.Y. Wu and F. Lin, *Biomater*., **26**, 3953 (2005).

21. H. Hu, C. Lin, P.P. Lui and Y. Leng. *J. Biomed. Mater. Res., A*, **65**, 24 (2003).

22. D.W. Hutmacher, *Biomater*., **21**, 2529 (2000).

23. T. Tateishi, G. Chen and T. Ushida, *J. Art. Organs*, **5**, 77 (2002).

24. A.J. Salgado, O.P. Cautinho and R.L. Reis, *Macromol. Biosci*., **4**, 743 (2004).

25. E.K.F. Yim, K.W. Leong, *Nanomed. Nanotechnol. Biol. Med.*, **1**, 10 (2005).

26. J.W. Wang and M.H. Hon, *J. Biomed. Mater. Res.*, **64**, 262 (2003).

27. A.J. Gracia, *Adv. Polym. Sci*., **203**, 171 (2006).

28. Y.P. Jiao and F.Z. Cui, *Biomed. Mater.*, **2**, R24 (2007).

29. C.J. Wilson, R.E. Clegg, D.I. Leavesley and M.J. Pearcy, *Tissue Eng*., **11**, 1 (2005).

30. M.C. Durrieu, *ITBM-RBM*, **26**, 229 (2006).

31. C.P. Reis, R.J. Wenfeld, A.J. Ribeiro and F. Veiga, *Nanomed. Nanotechnol. Biol. Med.*, **2**, 53 (2006).

32. R.V. Kulkarni and S. Biswanath, *J. Appl. Biomater. Biomech.*, **5**, 125 (2007).

33. S. Murdan, *J. Control. Rel.*, **92**, 1 (2003).

34. Y.W. Chien and S. Lin, II Edn., *Encyclp. Pharma. Technol.*, Vol I, Marcel-Dekker Inc, Basel(CH), 811 (2002).

35. P.A. Gunatillake and R. Adhikari, *Eur. Cell Mater.*, **5**, 1 (2003).

36. Y. Zhang and M. Zhang, *J. Biomed. Mater. Res.*, **61**, 1 (2002).

37. S. Ramakrishna, J. Mayer, E. Wintermantel and K.W. Leong, *Compost. Sci. Technol.*, **61**, 1189 (2001).

38. J.L. Ifkovits and J.A. Burdick, *Tissue Eng.*, **13**, 2369 (2007)

39. D.W. Hutmacher, J.C. Goh and S.H. Teoh, *Ann. Acad. Med. Singapore*, **30**, 183 (2001).

40. M. Jobmann and G. Rafler, *Internat. J. Pharmaceut.*, **242**, 213 (2002).

41. J.P. Vacanti, R. Langer, J. Upton and J.J. Marler, *Adv. Drug Del. Rev.*, **3**, 165 (1998).

42. E. Khor and L.Y. Lim, *Biomater.*, **24**, 2339 (2003).

43. R. Hejazi and M. Amizi, *In Polymeric Biomaterials, Marcel Dekker, NY*, **213** (2001).

44. (a) M.N.V. Ravi Kumar, *Reac. Funct. Polym.*, **46**, 1 (2000), (b) K.V. Harish Prashanth and R.N. Tharantharan, *Trends Food Sci. Technol.*, **18,** 117 (2007).

45. J.K. Suh and H.W. Matthew, *Biomater.*, **24**, 2589 (2000).

46. A. Domard and M. Domard, *In Polymeric Biomaterials, Marcel Dekker, NY*, **187** (2001).

47. W. Wang and H. Cui, *J. Phys. Chem. C.*, **112,** 10759 (2008) .

48. Shan and H. Tenhu, *Chem. Commun.*, 44**,** 4580 (2007).

49. M. H. Xue, Q. Xu, M. Zhou and J. J. Zhu, *Electrochem. Commun.*, **8,** 1468 (2006).

50. Y. Du, X. L. Luo, J. J. Xu and H. Y. Chen, *Bioeletrochemistry.*, **70,** 342 (2007).

51. Jr. David S dos Santos, P. J. G. Goulet, N. P. W. Pieczonka, Jr ONOliveira and R. F. Aroca, *Langmuir.,* **20,** 1027 (2004).

52. K. Kurita, *Prog. Polym. Sci.,* **26,** 1921 (2001).

53. R.L. Hong and J.Y. Yu, *J. Biomed. Mater: Appl. Biomater.,* **71B,** 52 (2004).

54. M. Xie, H. H. Liu, P. Chen, Z. L. Zhang, X. H. Wang, Z. X. Xie, Y. M. Du, B.Q. Pand and D. W. Pang, *Chem. Commun.,* 5518 (2005).

55. J.Xie, Q. Zhang, J. Y. Lee and D. I. C. Wang, *ACS Nano.,* **2,** 2473 (2008).

56. Y. Hamilton, Y. Yuan, D.A. Rigney, B.M. Chesnutt, A.D. Puckett, J.L. Ong, Y. Yang and J.D. Bumgardner, *Polym. Int*., **56**, 641 (2007).

57. M. Ishihara, K. Obara, S. Nakamura, M. Fujita, K. Masuoka, Y. Kanatani, B. Takase and M. Kikuchi, *J. Artif. Org*., **9**, 8 (2006).

58. Z. Liu, Y. Jiao, Z. Zhang and C. Zhou, *J. Biomed. Mater. Res*., **83 A**, 1110 (2007).

59. K. Song, P. Wen and T. Liu, *Key Eng. Mater*., **373**, 722 (2008).

60. P.R. Klokkevold, L. Vandemark, E.B. Kenney and G.W. Bernard, *J. Periodontol*., **67**, 1170 (1996).

61. (a) B.L. Reynolds, *Am. J. Surg*., **26**, 113 (1960), (b) R.N. Tharantharan and F.S. Kittur, *Critical Rev. Food Sci. Nutri.,* **43,** 61 (2003).

62. J.F. Prudden, P. Migel, P. Hanson, L. Friedrich and L. Balassa, *Am. J. Surg*., **119**, 560 (1970).

63. (a) W. Liu, S.J. Sun, X. Zhang and D. Yao, *J. Biomater. Sci. Polym. Edn.,* **14**, 851 (2003), (b) M. Rinaudo, *Polym. Int.,* **57,** 397 (2008).

64. H. Yi, L-Q. Wu, W.E. Bentley, R. Ghadssi, G.W. Rubloff and J.N. Culver, *Biomacromol.*, **6**, 2881 (2005).

65. Z. Li, H.R. Ramay, K.D. Hauch, D. Xiao and M. Zhang, *Biomater*., **26**, 3919 (2005).

66. L. Wang, E. Khor, A. Wee and L.Y. Lim, *J. Biomed. Mater. Res.*, **63**, 610 (2002).

67. T.H. Kim, J.W. Nah, M.H. Cho, T.G. Park and C.S. Cho, *J. Nanosci. Nanotechnol.*, **6**, 2796 (2006).

68. Z. Ding, J. Chen, S. Gao, J. Chang and E.T. Kang, *Biomater.*, **25**, 1059 (2004).

69. I. Adekogbe and A. Ghanem, *Biomater.*, **26**, 7241 (2005).

70. A.D. Metcalfe and M.W. Ferguson, *J.R. Soc. Interface*., **4**, 413 (2007).

71. T.H.M. Abou-Aiad, K.N. Abd-El-Nour, I.K. Hakim and M.Z. Elsabee, *Polym.*, **47**, 379 (2005).

72. S.F. Wang, L. Shen, W.D. Zhang and Y.J. Tong, *Biomacromol.*, **6**, 3067 (2005).

73. M. Morimoto, H. Saimoto and Y. Shigemasa, *Trends Glycosci. Glycotech.*, **14**, 205 (2002).

74. B. Liao, R. Liu and Y. Huang, *Polym. J.*, **39**, 1071 (2007).

75. B. Liao, R. Liu and Y. Huang, *Polym. J.*, **39**, 1071 (2007).

76. E. Ruiz-Hitzky, M. Darder and P. Aranda, *J. Mater.Chem.*, **15**, 3650 (2005).

77. A.P. Alivisatos, *Science.*, **271**, 933 (1996).

78. A.U. Daniels, M.K.O. Chang and K.P. Andriano, *J. Appl. Biomater.*, **1**, 57 (1990).

79. H. A. Henle and J. Kaskel, *Chem. Soc. Rev.*, **36,** 1454 (2007)

80. T. Ramanathan, S. Stankovich, D. A. Dikin, H. Liu, H. Shen and S. T. Nguyen. et al. *J. Polymer. Sci. B. Polymer. Phys.*, **45,** 2097 (2007).

81. L. Vaisman, E. Wachtel, H. D. Wagner and G. Marom, *Polymer.*, **48,** 6843 (2007).

CHAPTER 2

Scope and Objectives

2.1 INTRODUCTION AND OBJECTIVES

Bionanocomposites have established themselves as a promising class of hybrid materials derived from natural synthetic biodegradable polymers and organic/inorganic fillers. In the last few years, the exploration on these bio-materials has received very important attention from researchers with expertise in diverse areas of nanotechnology[1,2], biomedical engineering[3] and material science.

The nanotechnology field is one of the interesting areas for current research and development in all technical disciplines. The nanocomposites of inorganic materials in polymer matrices have attracted a great deal of attention because of their wide area of applications including biosensors[4]. Different approaches have been developed for the synthesis of nanocomposites such as incorporation of premade nanoparticles into the polymer matrix. This can be achieved with the use of a common blending solvent or by reduction of metal salt dispersed in polymer matrix using an external reducing agent[5]. The metallic and metal oxide nanoparticles have become an area of growing interest of fundamental studies and technological applications, due to their unique mechanical, chemical and magnetic properties[6]. The metal nanoparticle embedded polymer film can show enhanced mechanical and biomedical properties.

Chitosan is non-toxic, biocompatible, biodegradable and polar biopolymer[7,8]. Due to its biodegradability, biocompatibility and avirulence, Chitosan has been used in many biomedical applications. The properties of high mechanical strength, hydrophillicity, good adhesion and non-toxicity of chitosan offer it as food additive, anticoagulant and wound healing accelerator. Though chitosan has the ability to form films, the tensile properties of pristine chitosan film are poor (due to its crystallinity). Thus, the modification of chitosan has gained its importance for tailoring the desired mechanical properties[9–11]. Since chitosan is alkaline in nature, by combining it (as graft copolymer or blend) with the biodegradable

polymers like polylactic acid, polyglycolic acid which generate acidic biproducts, the local toxicity at the implant site can be reduced[12–14].

Chitosan has been widely used in tissue engineering as a scaffold[15], orthopedic implants[16] and in drug delivery applications[17]. Generally, drug release kinetics of polymeric drug delivery systems is usually characterized by membrane permeability and diffusion coefficient, which are employed to describe the release behavior of the membrane reservoir system and the diffusion mechanism of the release system[18]. Furthermore, both indexes in polymer-based materials are strongly dependent on crystallinity, plasticization and swelling behavior of the biopolymer drug delivery vehicle, which are also affected by the type and presence of the nanofillers[19-21]. So, the secondary objective of the proposed work is to evaluate the effect of the nanofillers on the controlled drug release from the nanohybrids.

2.2 APPROACHES

2.2.1 Glycolic acid grafted chitosan and gold nanoparticles based nanocomposite

2.2.1.1 Grafting of chitosan with glycolic acid

2.2.1.2 Preparation of grafted chitosan and gold nanoparticles based nanocomposite films and porous scaffolds

2.2.1.3 Structural analysis by XRD, FTIR, UV, TEM, SEM, DMA, TST, TGA and AFM techniques.

2.2.1.4 Loading of cyclophosphamide drug and controlled release studies.

2.2.1.5 Biocompatibility studies by *in-vitro* cell-culture testing.

2.2.2 Glycolic acid grafted chitosan and Au-Fe_3O_4 hybrid nanoparticle based nanocomposite

2.2.2.1 Grafting of chitosan with glycolic acid

2.2.2.2 Preparation of grafted chitosan and Au-Fe_3O_4 hybrid nanoparticles based nanocomposite films and porous scaffolds

2.2.2.3 Structural analysis by XRD, FTIR, UV, TEM, SEM, PPMS, DMA, TST, TGA and AFM techniques.

2.2.2.4 Loading of cyclophosphamide drug and controlled release studies.

2.2.2.5 Biocompatibility studies by *in-vitro* cell-culture testing.

2.2.3 Glycolic acid grafted chitosan and Pt-Fe_3O_4 hybrid nanoparticle based nanocomposite

2.2.3.1 Grafting of chitosan with glycolic acid

2.2.3.2 Preparation of grafted chitosan and Pt-Fe_3O_4 hybrid nanoparticles based nanocomposite films and porous scaffolds

2.2.3.3 Structural analysis by XRD, FTIR, UV, TEM, SEM, PPMS, DMA, TST, TGA and AFM techniques.

2.2.3.4 Loading of cyclophosphamide drug and controlled release studies.

2.2.3.5 Biocompatibility studies by *in-vitro* cell-culture testing.

2.2.4 Glycolic acid grafted chitosan and Co_3O_4 hybrid nanoparticle based nanocomposite

2.2.4.1 Grafting of chitosan with glycolic acid

2.2.4.2 Preparation of grafted chitosan and Co_3O_4 hybrid nanoparticles based nanocomposite films and porous scaffolds

2.2.4.3 Structural analysis by XRD, FTIR, UV, TEM, XPS, SEM, PPMS, DMA, TST, TGA and AFM techniques.

2.2.4.4 Loading of cyclophosphamide drug and controlled release studies.

2.2.4.5 Biocompatibility studies by *in-vitro* cell-culture testing.

2.2.5 Glycolic acid grafted chitosan and Co_3O_4-Fe_3O_4 hybrid nanoparticle based nanocomposite

2.2.5.1 Grafting of chitosan with glycolic acid

2.2.5.2 Preparation of grafted chitosan and Co_3O_4 -Fe_3O_4 hybrid nanoparticles based nanocomposite films and porous scaffolds

2.2.5.3 Structural analysis by XRD, FTIR, UV, TEM, SEM, PPMS, XPS, DMA, TST, TGA and AFM techniques.

2.2.5.4 Loading of cyclophosphamide drug and controlled release studies.

2.2.5.5 Biocompatibility studies by *in-vitro* cell-culture testing.

2.3 REFERENCES

1. R.A. Hule and D.J. Pochan, *MRS Bull.,* **32**, 354 (2007).
2. I.K. Tonle, T. Diaco, E. Ngameni and C. Detellier, *Chem. Mater.,* **19**, 6629 (2007).
3. M.T. Sulak, O. Gokdogan, A. Gulce and H. Gulce: *Bioelectro.,* 2**1,** 1719 (2006).
4. J.H. Park, Y.T. Lim, O.O. Park, J.K. Kim, J.W. Yu and Y.C. Kim, *Chem. Mater.,* **16,** 688 (2004).
5. A.S. Edelstein and R.C. Cammarata, *Nanomaterials: Synthesis, Properties and Application*, Institute of Physics Publishing: London, (1996)
6. P.J. VandeVord, H.W.T. Matthew, S.P. DeSilva, L. Mayton, B. Wu and P.H. Wooley*: J. Biomed. Mater. Res.,* **59,** (2002), p. 585.
7. S. Kim, Y. Jeon, H. Byun and P. Park: *Subacute oral toxicity of chitosan oligosaccharide on Sprague Dawley rats, Proceedings of the 8th International Chitin and Chitosan Conference and 4th Asia Pacific Chitin and Chitosan Symposium*; Tokyo, Kodansha Scientific Ltd., (2001).
8. N. Kubota and K. Ogha, *J. Appl. Polym. Sci.,* **42,** 495 (1991).

9. S. V. Madihally and H. W. Matthew, *Biomaterials.*, **20,** 1133 (1999).

10. D. Depan, B. Kumar and R. P. Singh, *J Biomed Mater Res: Appl. Biomater.*, **84B,** 184 (2008).

11. Q. Xin and A. Anders Wirsen, *J. Appl. Polym. Sci.*; **74,** 3193 (1999).

12. K. Y. Lee, W. S. Ha and W. H. Park, *Biomaterials.*, **16,** 1211 (1995).

13. S. Miyazaki and H. Yamaguchi, *Acta. Pharm. Nord.*, **2,** 401 (1990).

14. D. Depan, A. P. Kumar and R. P. Singh, *Journal of Biomedical Materials Research Part A.*, 372 (2006).

15. H. Liu, H. Fan, Y. Cui, Y. Chen, K. Yao and J.C.H. Goh, *Biomacromol*., **8**, 1446 (2007).

16. A. Di-Martino, M. Sittinger and M.V. Risbud, *Biomater*., **26**, 5983 (2005).

17. X. Wang, Y. Du, J. Luo, B. Lin and J.F. Kennedy, *Carbohyd. Polym.*, **69**, 41 (2007).

18. R. Langer, *Chem. Eng. Commun*., **6**, 1 (1980).

19. L.H. Sperling, *Intro. to Phys. Polym. Sci., John Wiley and Sons*, New York, **148** (1992).

20. K. Kesenci, L. Fambri, C. Migliaresi and E. Piskin, *J. Biomater. Sci. Polym. Ed.*, **11**, 617 (2000).

21. V. Arrighi, J.J. McEwen, H. Qian and M.B. Serrano Prieto, *Polym*, **44**, 6259 (2003).

CHAPTER 3

A: Preparation and Characterization of Glycolic Acid-g-Chitosan-Gold Nanoflower Based Nanocomposite Scaffolds for Drug Delivery and Tissue Engineering Applications

3.1 INTRODUCTION

In the recent years, synthesis and shape dependent properties of anisotropic gold nanostructures[1] such as nanoflower, nanocone, nanorod and nanopolygon were intensly studied[2-10]. Gold nanomaterials are of wide interest for fundamental research[11, 12], biological sensing and catalytic[13] applications. They possess excellent biocompatibility, low toxicity and relatively low reactivity, thus providing benefits to the living system. Several physical and chemical methods have been employed to fabricate gold nanoparticles[14, 15], producing a wide variety of shapes. Morphology and size greatly influence the optical properties and surface reactivity of the gold nanomaterials[16-18]. Typically, during the synthesis of nanoparticle, they tend to aggregate resulting in the different nanoforms like flowers, rods and prism[11, 19]. Nanoflowers have tremendous applications as sensors, optoelectronic devices, for making solar cell, in the field of drug delivery and tissue engineering. The most common method in tissue engineering is to construct a porous 3D structure onto which cells can attach and proliferate, commonly referred to as a tissue scaffold[20].

The properties such as inherent biodegradability, biocompatibility and mechanical properties are essential for the scaffolds in tissue engineering applications. The scaffolds should also be durable, stress resistant, flexible, pliable and elastic with reasonable tensile properties, which could bear the stresses exerted by different parts of the body having varying contours. According to Peppas et. al.[21], the increase in flexibility of the scaffolds could improve the contact between the scaffold material and the tissue; hence it promotes the penetration of the polymeric chains into the tissue to form strong adhesion. The surface morphology and structural integrity of the scaffolds should also allow the cells to attach and proliferate. In therapeutic applications, the efficiency of a drug lies in targeting specific body parts and maintaining a desired concentration level for longer period of time. However, its

use is limited due to side effects of gastrointestinal tract, central nervous system, and other ulcerogenic effects, which are often consequences of high plasma levels following the administration of conventional formulations[22].

Chitosan is a linear polysaccharide composed of randomly distributed (β-1, 4)-linked D-glucosamine (deacetylated unit) and N-acetyl-D-glucosamine (acetylated unit). It has been widely used in food industry, for making biosensors[1] and drug delivery due to its biocompatibility, film forming properties[23] and polycationic nature. Chitosan is selected in the present work because it easily forms stable film on the solid support, which has been used in the development of biosensors[24-26]. Chitosan is hydrophilic and compatible with nanoparticle and has better processability due to the presence of amino group (pKa value is 6.2) in the chain. Chitosan also possesses hydroxyl functional groups which act as potential site for altering the polymers functionality[27, 28]. Chitosan is modified by chemical reactions, which involves the reactive hydroxyl and amino groups of the polymer chain. The grafting of side glycolic acid leads to marked changes in the chitosan structure[29, 30].

3.2 EXPERIMENTAL

3.2.1 Materials

Low molecular weight chitosan (Mv 1.5×10^5, degree of deacetylation was 85%), cyclophosphamide (drug) and glycolic acid (99% purity) were obtained from Sigma Aldrich. Gold chloride ($HAuCl_4$) and sodium borohydride ($NaBH_4$) were obtained from M/s Sisco Research Laboratories, Mumbai. All the glass wares were cleaned thoroughly using chromic acid, detergent and finally rinsed with acetone. Ultra pure water was prepared by a Milli-Q system and it is used throughout.

3.2.2 Synthesis of gold nanoflower

The current method of synthesis of Au nanoflower is different from other reported methods[29]. Gold nanoflowers (AuNF, 10^{-4} M) were obtained by reducing the $HAuCl_4$ precursor with 0.1 M $NaBH_4$. Upon addition of the reducing agent to the solution of $HAuCl_4$, immediately a ruby red colour appeared. The resulting solution was sonicated for 30 sec under controlled temperature condition, which results in the formation of gold nanoflowers.

3.2.3 Preparation of drug loaded scaffold of glycolic acid grafted chitosan and gold nanoflower nanocomposites.

Preparation involves aqueous dispersion of gold nanoflowers, suspension of chitosan in glycolic acid, mixing them, drying and dehydration. Chitosan was dispersed in glycolic acid and gold nanoparticle in deionised water (50ml) overnight at room temperature. The resulting solution was heated up to 80 ^{0}C with continuous degassing for 30-40 min. After degassing, solution was cooled and followed by drug addition, which was stirred for 5 h so that drug completely mixes with the solution. The solution is then poured in tissue culture plates (20 × 20 mm diameter) and it is quenched in liquid nitrogen and the sample is then freeze dried by lyophilisation at -100 ^{0}C for 6 h.

Table 3.1 Formulation of Cyclophosphamide (CPA)-loaded nanohybrid of chitosan-g-glycolic acid and Au nanoflower

S.No	Chitosan (g)	Glycolic acid (g)	AuNF (ml)	CPA (%)	Drying Process	Sample code
1	1	1	_	_	Vacuum	CGAu-1
2	1	1	50	_	Vacuum	CGAu-2
3	1	1	50	10	Freeze	CGAu (SD)

The water molecules were removed by freezing and subsequent sublimation of ice crystals, which leads to the formation of pores. On the other hand, the polymer-rich phase consists mostly of the polymer solution and forms the cell walls around the pores[28]. The formulations are given in **Table 3.1**.

3.3 CHARACTERIZATION OF NANOHYBRID

3.3.1 Scanning electron microscopy (SEM)

Scanning Electron Microscpy (SEM) (Model: JOEL Stereoscan 440, Cambridge) was used to analyse the surface morphology of the samples. Prior to the observation, specimens were fixed on the copper grid.

3.3.2 Transmission electron microscopy (TEM)

The Particle size, morphology and selected area electron diffraction pattern of gold nanoflower were analysed with High Resolution Transmission Electron Microscpy (HR-TEM model Technai TF30, 300KV FEG).

3.3.3 Fourier transform infrared spectroscopy (FT-IR)

Perkin-Elmer Spectrum GX is used to compare the Fourier transform infrared spectroscopy (FT-IR) of neat chitosan (CS), glycolic acid grafted chitosan (CGAu-1) and drug loaded scaffold CGAu (SD) at wavenumber ranging from 4000 to 400 cm^{-1} with resolution of 4.0 cm^{-1}.

3.3.4 X-ray diffraction (XRD)

XRD patterns of the samples were recorded on X-ray Diffractometer (WAXRD – Rigaku (Japan)) with Cu-kα radiation at a voltage of 50 KV. The scanning rate was 4^0/min and the scanning scope of 2θ was from 2^0 to 80^0 at room temperature.

3.3.5 Swelling behaviour

The swelling behaviour of porous scaffold was determined by exposing them to media of different pH: 1N HCl, 1N NaOH and simulated body fluid (SBF, pH 7.4) solutions. Shape retention of the porous scaffold was determined by measuring the change in the diameter as a function of time in the media.

3.3.6 Cell viability

Cell viability study was performed on SP2/0 mouse myeloma cell line as direct contact test. For this, after every fixed interval of time, 100µl of the cell culture was incubated for MTT assay and the absorbance is taken in spectrophotometer plate reader. The relative cell growth was compared to control cell, which exhibit cell culture medium without chitosan. It was calculated by using the given eq. (1)

$$\% \text{ Live cell} = 100 - \left[\frac{(C - T)}{(C - B)} \times 100 \right] \quad (1)$$

C = OD of control

T = OD of test sample

B = OD of blank

OD = Optical density

3.3.7 In vitro drug release

The drug loaded nanohybrid scaffold (CGAu (SD)) were immersed in 10 ml of aliquots of 0.1 M phosphate buffer (pH 7.4) and incubated at 37 ^{0}C. After specific interval 3 ml aliquot of the specimen were withdrawn and immediately fresh medium is added to it. Drug content in the each aliquot was quantitatively analysed by UV-vis spectrophotometer (UV-NIR- PL Lamda 950) at 180 nm.

3.4 RESULTS AND DISCUSSION

Scheme 3.1 *Schematic illustration of grafting of glycolic acid on chitosan, formation of CS-g-glycolic acid and gold nanoflower nanohybrid scaffold and interaction between chitosan-g-glycolic acid, drug and Au nanoflowers*

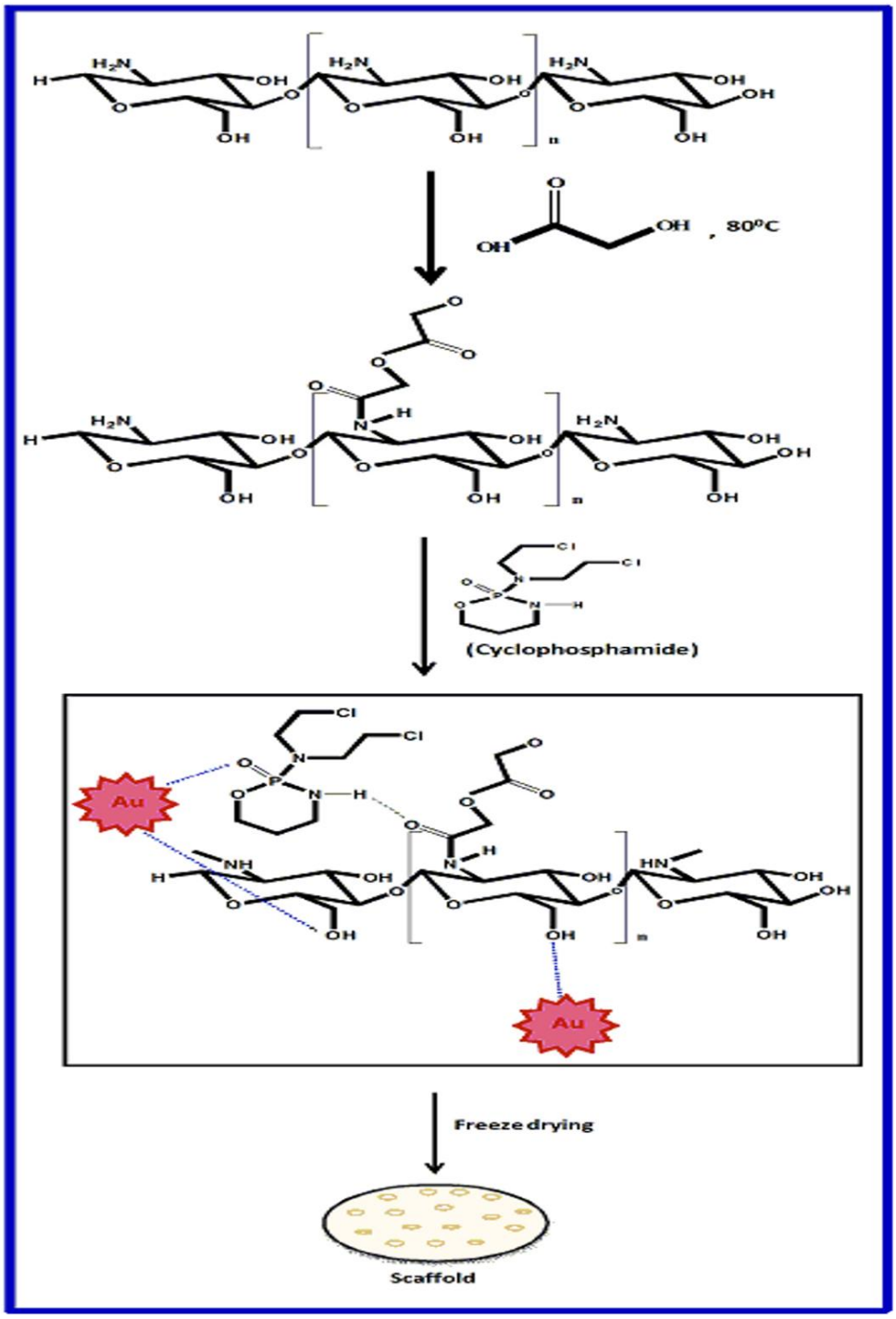

3.4.1 SEM analysis of gold nanoflowers

Figure 3.1 (a) and (b) shows typical SEM image of gold nanoflower synthesised by reducing 10^{-4} M $HAuCl_4$. The synthesised nanocrystals are quasi spherical in shape with irregular, short protrusion like tips (>30 in numbers). The overall dimensions of these nanoflowers are 82 ± 5 nm (see inset in **Figure 3.1** (a) for histogram of size distribution).

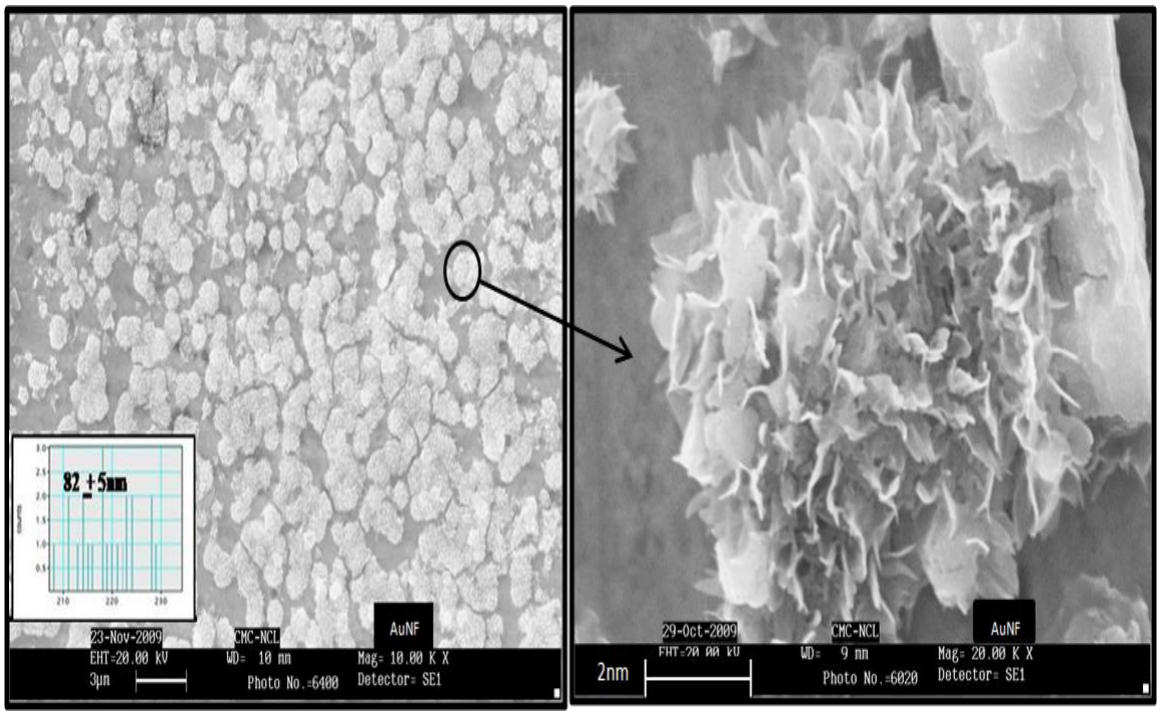

Figure 3.1 *(a, b) SEM image of Au nanoflower formed after the sonication of reduced solution of $HAuCl_4$ under controlled temperature condition.*

3.4.2 TEM analysis of gold nanoflowers

The TEM image **Figure 3.2** (a) of nanoflowers exhibit region of varying contrast. **Figure 3.2** (b) shows the high resolution TEM image of single crystalline protrusion from the core of the Au nanoflower, which are crystalline and randomly oriented as shown in selected area diffraction (SAED) pattern **Figure 3.2** (c). The electron diffraction pattern can be determined by face centred cubic (fcc) structure of gold. Morphologically nanoflowers are regarded as spheres and branch particles[31-33]. These gold nanoflowers posses more surface area due to the

protrusion like tips, therefore, interaction of these nanoflower with the grafted chitosan biopolymer is more efficient in comparison to smooth surface gold nanoparticle.

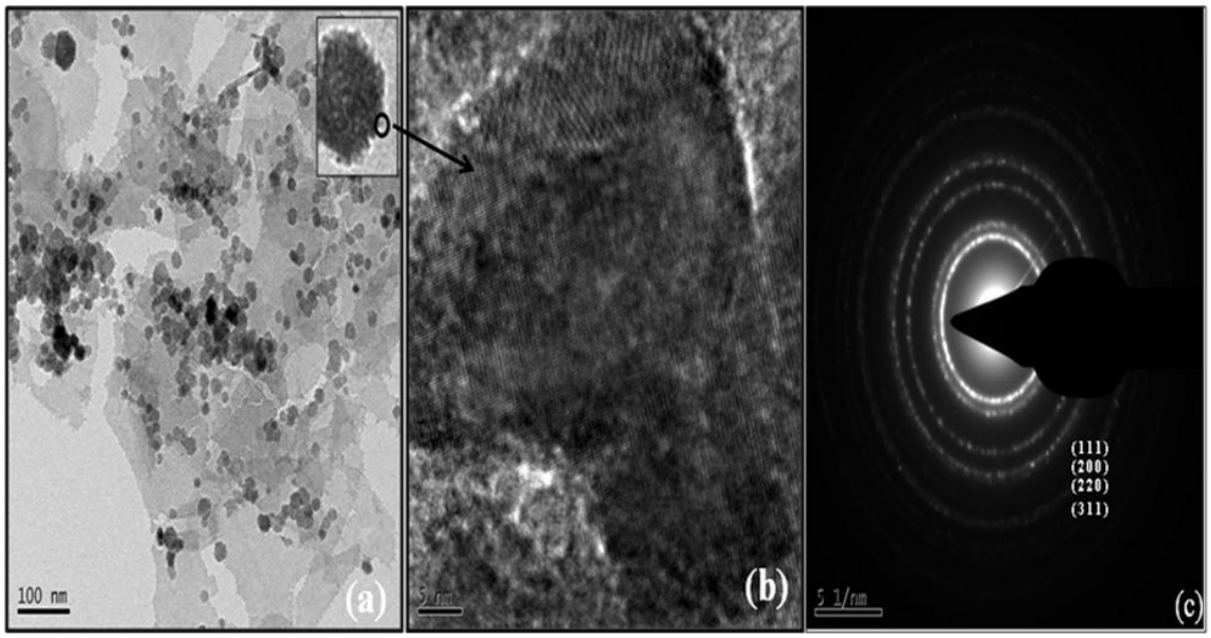

Figure 3.2 *(a) TEM image of Au nanoflower, (b) HRTEM image of Au nanoflower, (c) SAED Pattern of Au nanoflower.*

3.4.3 FTIR analysis

FT-IR was used to analyse the structure of neat chitosan (CS), glycolic acid grafted chitosan (CGAu-1) and drug loaded scaffolds (CGAu (SD)) (**Figure 3.3**). In the spectrum of neat chitosan, peak at 1633 cm^{-1} is attributed to –N-H bending vibration of amine group and a broad band at 3500 cm^{-1} corresponds to –OH stretching band. In grafted chitosan (CGAu-1), –N-H bending vibration shifted towards the lower frequency (1574 cm^{-1}) confirming the interaction of glycolic acid onto NH_3^+ group. Appearance of a new peak at 1725 cm^{-1} is attributed to the υ_{co} stretching. These two peaks confirm the conversion of amine (NH_2) to amide (–NH-C=O). The drug (cyclophosphamide) possesses secondary amine in the molecule, which shows –N-H bending at 1648 cm^{-1}. The P=O group in the drug molecule shows υ_{PO} stretching band at 1237 cm^{-1}. In the FTIR spectrum of scaffold (CGAu (SD)), N-H

bending vibration of drug molecule and the υ_{CO} stretching band of glycolic acid is observed to be shifted towards lower frequency region, indicating the interaction of N-H group of drug with C=O group of glycolic acid through H-bonding. The P=O stretching band of drug and –OH stretching band of the grafted chitosan is shifted towards the lower frequency region in CGAu (SD) confirming the interaction of gold nanoflower with drug molecule and chitosan chain through metallic bond.

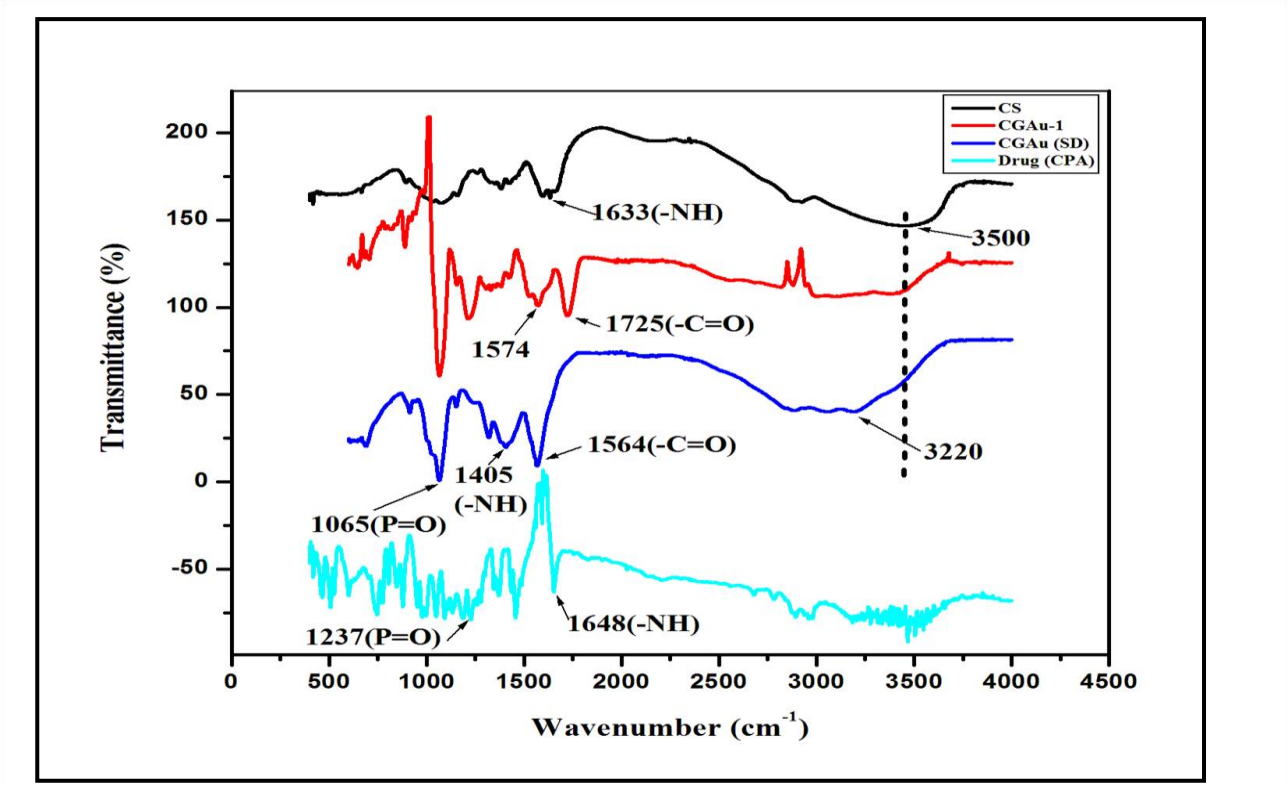

Figure 3.3 *FTIR spectra of neat chitosan (CS), grafted chitosan (CGAu-1), grafted chitosan and AuNF nanohybrid scaffold (CGAU (SD)) and drug Cyclophosphamide (CPA).*

3.4.4 XRD analysis

Figure 3.4 (a) Illustrates the X- ray diffraction pattern of neat chitosan (CS) and glycolic acid grafted chitosan (CGAu-1). It was observed that neat chitosan (CS) shows the characteristic peak at 10.9^{o} and 19.8^{o}, which correspond to a hydrated crystalline structure and an amorphous structure of chitosan, respectively[34-36]. Grafting of chitosan with glycolic acid (CGAu-1) resulted in a shift of peak from 10.9^{o} to 10.2^{o} and 19.8^{o} to 20.7^{o} which

confirms the interaction of chitosan with glycolic acid. These peaks were shifted from 10.2^{o} to 8.6^{o} and 20.7^{o} to 21.7^{o}, showing the interaction of gold nanoflower with the grafted chitosan (CGAu-2) as shown in **Figure 3.4** (b).

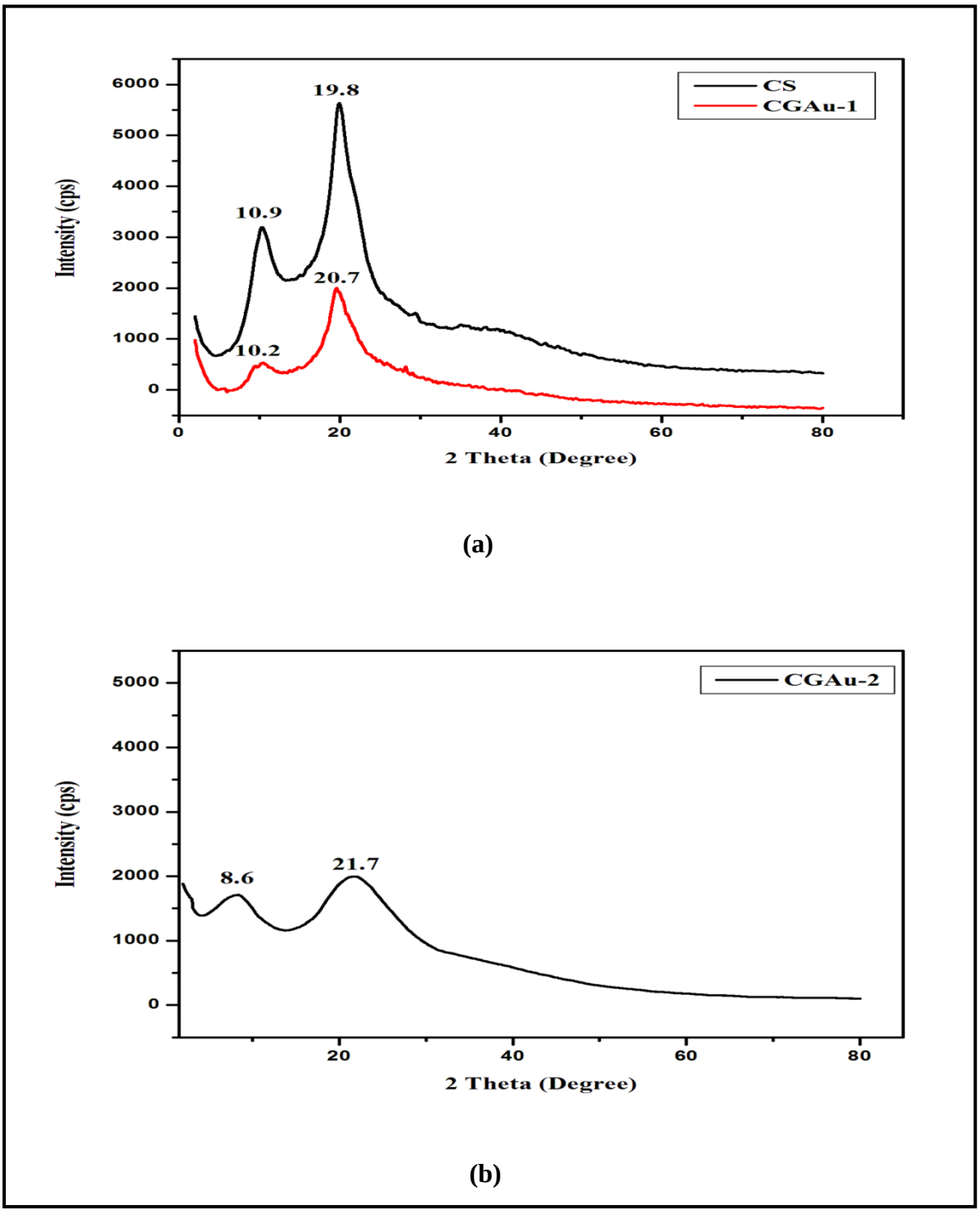

Figure 3.4 *(a) X-ray diffraction spectra of neat chitosan and grafted chitosan. (b) X-ray diffraction spectra of CS-g-glycolic acid and AuNF nanohybrid scaffold.*

3.4.5 Morphological study of scaffold

Morphology of porous scaffold is examined by SEM. **Figure 3.5** (a), (b) and (c) show SEM images of grafted chitosan scaffold, grafted chitosan and Au nanoflower nanohybrid scaffold with and without drug. It is observed that upon drug loading, pore size of scaffold decreases.

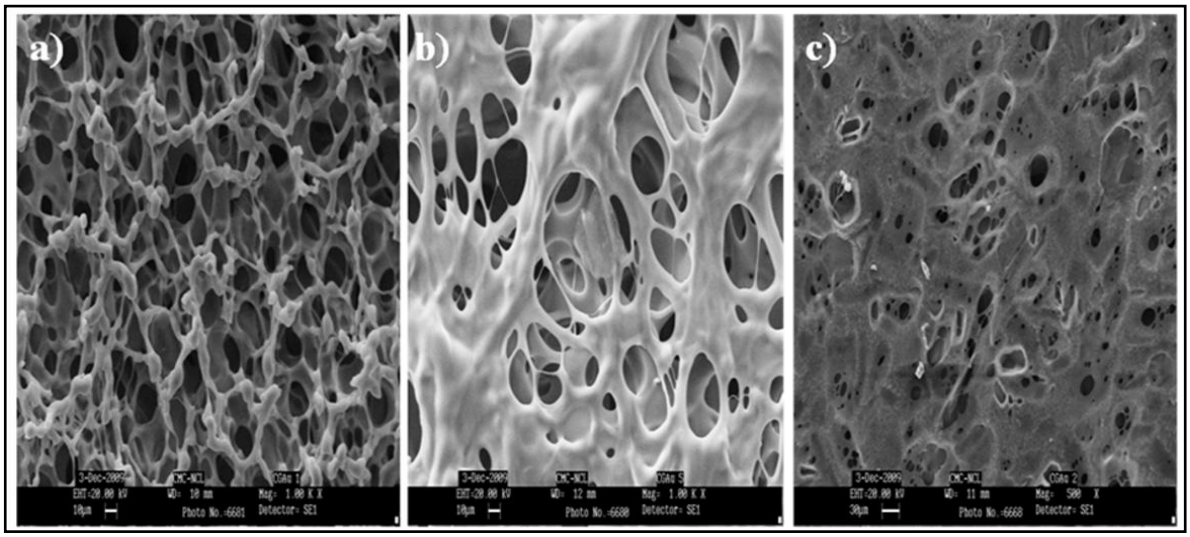

Figure 3.5 *SEM image of (a) grafted chitosan scaffold, (b) grafted chitosan and AuNF nanohybrid scaffold without drug, (c) grafted chitosan and AuNF nanohybrid scaffold with drug.*

3.4.6 Swelling behaviour

Swelling behaviour of scaffold was investigated by exposing it to media at different pH: 1 N HCl, 1 N NaOH and simulated body fluid (SBF, pH 7.4) solutions. Shape retention was studied by measuring the change in the diameter as a function of immersion time in the media[37]. Swelling behaviour and structural stability of scaffolds strongly depend upon the pH of the implantation site for their practical use in tissue engineering. The in vitro cell culture studies indicate that initial swelling is desirable[21, 38], but continuous swelling reduces the mechanical integrity and leads to the generation of compressive stress to the surrounding

tissue. The scaffolds were subjected to SBF (pH 7.4), HCl (pH 1.2) and NaOH (pH 14) for 24 h. **Figure 3.6** illustrates that in an acidic medium, and swelling of scaffold is higher than that of the SBF (Simulated body fluid) and alkaline solution. Scaffold "CGAu-1" was found to dissolve completely in the HCl solution within 3 h of immersion, whereas rate of swelling is very low in NaOH and reached the plateau level around 3 h of immersion but increase in size of scaffold is observed within 4 h in SBF solution. In the case of AuNF loaded scaffold "CGAu (SD)", its complete dissolution was observed in HCl solution within 2 h of immersion, whereas slight swelling was observed in SBF within 2.5 h. This reveals that the nanohybrid scaffold is stable towards the SBF and higher pH solution. Generally, swelling of chitosan involves the protonation of amino/imine groups and the mechanical relaxation of coiled chitosan chain[39, 40].

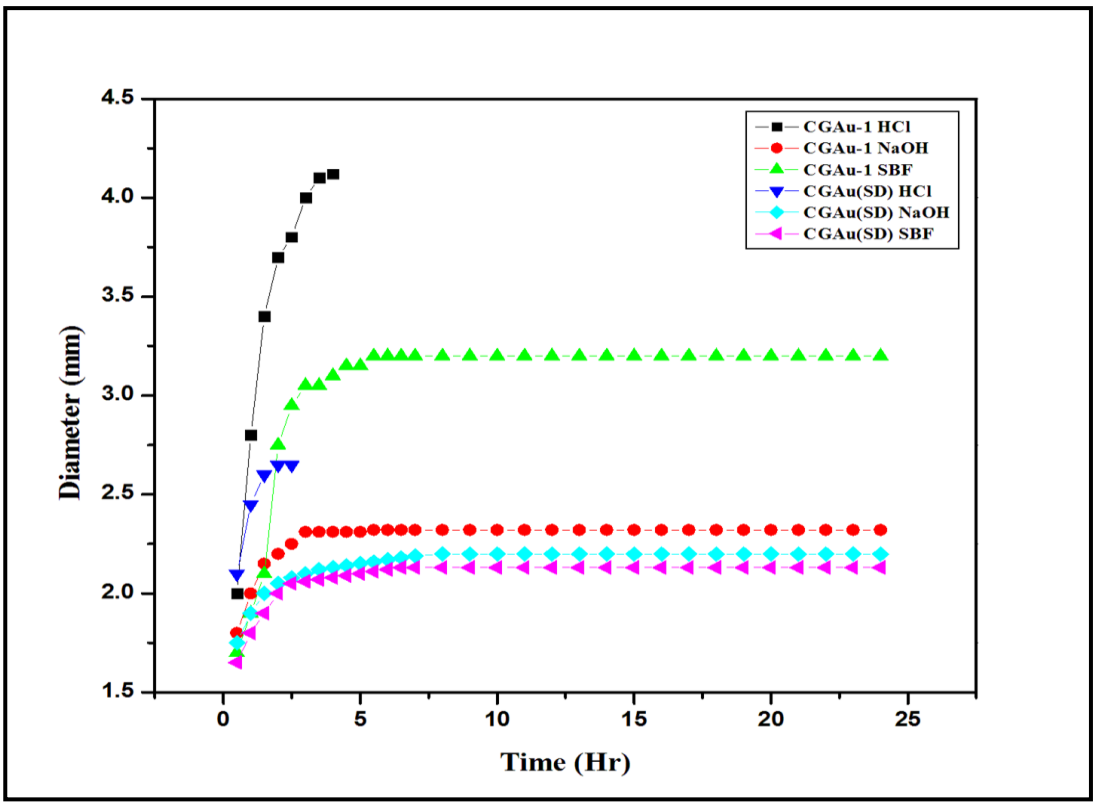

Figure 3.6 *Shape retention of scaffolds prepared from grafted chitosan and AuNF nanohybrid.*

3.4.7 Cell viability study

Cell viability Study is done with SP2/0 mouse myeloma cell to examine the biocompatibility of the scaffold. Cell viability was measured by MTT assay (**Figure 3.7**) and is cultured on "CGAu (SD)" specimen (at 250µg ml^{-1}). Growth of the cells cultured on the scaffold was higher during the first 2 h but slight decrease in the cell number was observed in next 4 h. This may be because during proliferation, cells have occupied all the available space on the scaffold. Present study implies that the cell proliferation is not affected by the incorporation of gold nanoflower (AuNF) into glycolic acid grafted chitosan[36]. This may be due to the enhanced interaction between AuNF and growing cells on the biopolymer matrix. AuNF may develop London- van der Waals forces with cells. These gold nanoflower can act as adhesive between biopolymer and cells.

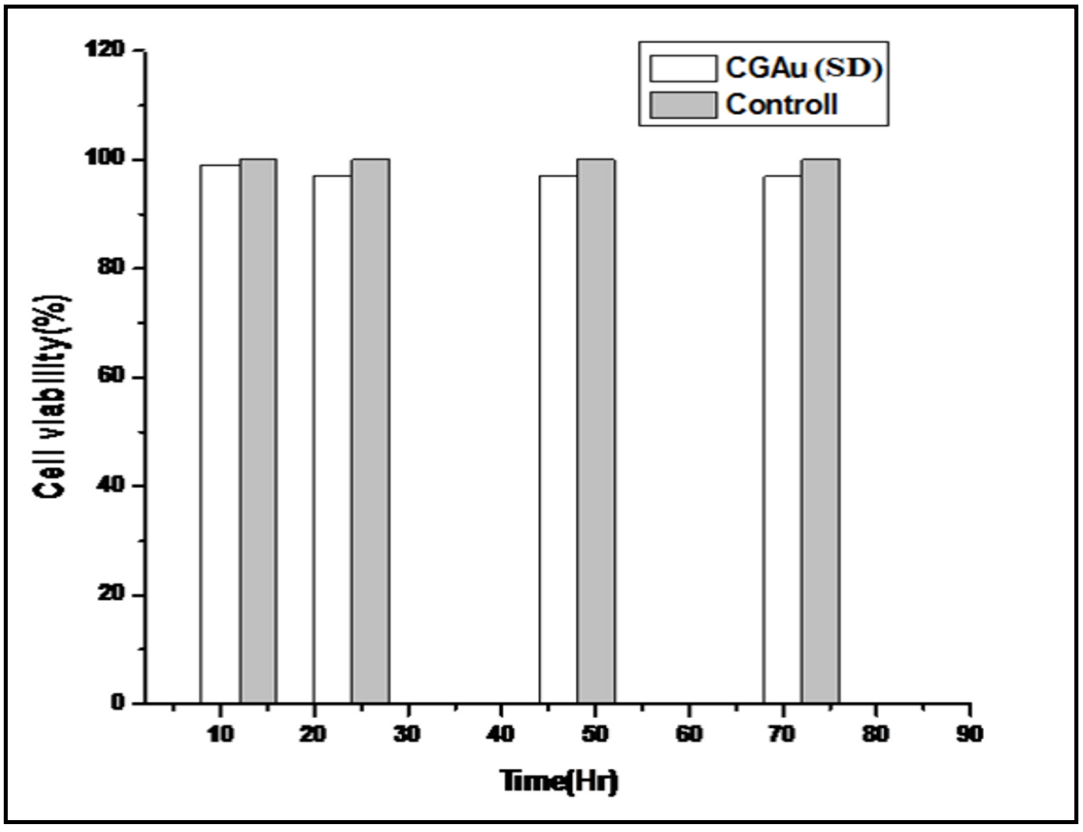

Figure 3.7 *Cell viability study done with MTT assay of cultured cells.*

3.4.8 In vitro drug release

In vitro drug release was examined with SBF (pH 7.4) and release media was quantified by UV-visible spectral absorbance values. **Figure 3.8** shows UV-vis spectra of in vitro drug release study illustrating variation in the absorbance of the drug in the scaffold with respect to time. It is observed that initially the release of drug was high and decreases with the time. This is because the drug which is at the surface of scaffold is released much faster than the drug incorporated deeply into the pores of the scaffold. The effect of incorporation of gold nanoflower layers can be significantly observed as reduced rate of release at initial stage of immersion (up to 150 min). Initially, the specimen is solvated, which facilitates the lateral diffusion of drugs[41] after 200 min, the rate of release decreases over the time.

This may be due to the interactions of gold nanoparticle layers and grafted glycolic acid chains with the loaded drug[36]. In FTIR spectra of drug (cyclophosphamide), the band at 3459 cm^{-1} corresponds to υ_{NH} stretching of drug molecule and that of CGAu (SD), shifting of υ_{co} stretching band towards the lower frequency region indicates the interaction of NH group of drug (cyclophosphamide) with C=O group of amide via H-bonding. The υ_{NH} stretching band of drug is observed to shift towards the lower frequency region in the CGAu (SD) specimen. Thus, it confirms the interaction between drug (cyclophosphamide) and scaffold surface via (N-H----O=C-) H-bond. In addition, the hydrogen bonding between carbonyl oxygen of glycolic acid grafted upon chitosan and H of secondary amine of drug (cyclophosphamide) can also assist in controlling the delivery of drug molecule as shown in the **Scheme 3.1**.

From the present study, we observed that by grafting bio polymeric chains onto chitosan and incorporating gold nanoflower, the desired properties (physical and swelling behaviour) can be tailored. Addition of gold nanoflower into biopolymers may be used for the sustained delivery of drug[42].

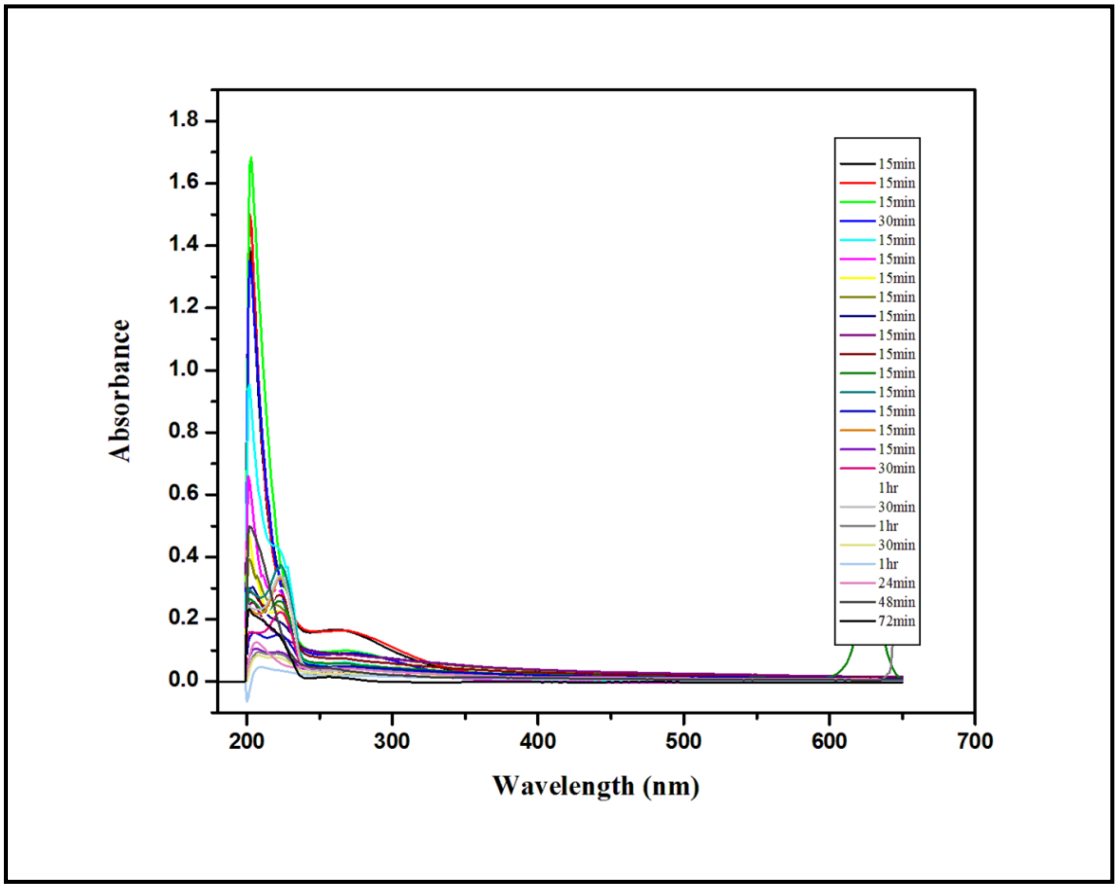

Figure 3.8 *Drug release profile from the prepared nanohybrid scaffold (CGAu (SD))*

3.5 CONCLUSIONS

The present study examined the potential use of 'hybrids' of CS-g-glycolic acid and gold nanoflower as biomaterial. The nanohybrid scaffold exhibited porous morphology which is attributed to phase separation. The scaffolds of nanohybrid are stable towards the SBF and alkaline pH value of the solution over time. In vitro drug release study of this nanohybrid scaffold is performed; it is observed that initially there is higher and faster release of drug, which decreases with time. The incorporation of gold nanoparticle was observed to control the initial release of drug. We concluded that a combination of glycolic acid grafted chitosan biopolymer chains and gold nanoflower can be envisaged in the field of drug delivery and biomaterials.

3.6 REFERENCES

1. W. Wang and H. Cui, *J. Phys. Chem. C.*, **112**, 10759 (2008).
2. S. E. Skrabalak, J. Chen, L. Au, X. Lu, X. Li and Y. Xia, *Adv. Mater.*, **19,** 3177 (2007).
3. B. I. Kharisov, *Recent patents on nanotechnology.*, **2,** 190 (2008).
4. X. Zhang, M. Tsuji, S. Lim, N. Miyamae, M. Nishio, S. Hikino and M. Umezu, *Langmuir.*, **23**, 6372 (2007).
5. H. Yuan, W. Ma, C. Chen, J. Zhao, J. Liu, H. Zhu and X. Gao, *Chem. Mater.*, **19,** 159 (2007).
6. A. M. Schwartzberg, T. Y. Olson, C. E. Talley and J. Z. Zhang, *J. Phys. Chem. B.*, **110** 19935 (2006).
7. A. Sanchez-Iglesias, I. Pastoriza-Santos, J. Perez-Juste, B. Rodriguez-Gonzalez, F. J. Gd. Abajo and L. M. Liz-Marzan, *Adv. Mater.*, **18**, 2529 (2006).
8. C. L. Nehl, H. Liao and J. H. Hafner, *Nano Lett.*, **6,** 683 (2006).
9. E. Hao, R. C. Bailey, G. C. Schatz, J. T. Hupp and S. Li, *Nano Lett.*, **4,** 327(2004).
10. J. Thaddeus, J. Norman, C. D. Grant, D. Magana, J. Z. Zhang, J. Liu, D. Cao, F. Bridges and A. V. Buuren, *J.Phys. Chem. B.*, **106,** 7005(2002).
11. Jr. David S dos Santos, P. J. G. Goulet, N. P. W. Pieczonka, Jr ONOliveira and R. F. Aroca, *Langmuir.*, **20,** 1027 (2004).
12. M. C. Daniel and D. Astruc, *Chem. Rev.*, **104,** 293 (2004).
13. Y. W. C. Cao, R. Jin and C. A. Mirkin, *Science.*, **297,** 1536 (2002).
14. C. Shan, F. Li1, F. Yuan, G. Yang, L. Niu and Q. Zhang, *Nanotechnology.*, **19,** 285601 (2008).
15. S. D. Bunge, T. J. Boyle and T. J Headley, *Nano Lett.*, **3,** 901 (2003).
16. S. K. Ghosh and T. Pal, *Chem. Rev.*, **107,** 4797 (2007).

17. M. P. Pileni, *J. Phys. Chem. C.*, **111,** 9019 (2007).

18. S. Eustis and M. A. El-Sayed, *Chem. Soc. Rev.*, **35,** 209 (2006).

19. L. M. Liz-Marzan, *Mater. Today.*, **7,** 26 (2004) -31.

20. X. B. Jin, Y. S. Sun, K. Zhang, J. Wang, X. D. Ju and S. Q. Lou, *Acta Pharmacol Sin.*, **28,** 663(2007).

21. A. Peppas, and S.R. Lustig, *Ann. of the New York Acad. of Sci.*, **446,** 26 (1985).

22. H. Suleyman, B. Demircan, and Y. Karagoz, *Pharmocol. Res.*, **59,** 247 (2007).

23. J. Shan and H. Tenhu, *Chem. Commun.*, **44,** 4580 (2007).

24. M. H. Xue, Q. Xu, M. Zhou and J. J. Zhu, *Electrochem. Commun.*, **8**, 1468 (2006).

25. T. Tangkuaram, C. Ponchio, T. Kangkasomboon, P. Katikawong and W. Veerasai, *Biosens. Bioelectron.*, **22,** 2071(2007).

26. Y. Du, X. L. Luo, J. J. Xu and H. Y. Chen, *Bioeletrochemistry.*, 70, 342 (2007).

27. K. Kurita, *Prog. Polym. Sci.*, **26,** 1921 (2001).

28. R.L. Hong and J.Y. Yu, *J. Biomed. Mater: Appl. Biomater.*, **71B,** 52 (2004).

29. M. Xie, H. H. Liu, P. Chen, Z. L. Zhang, X. H. Wang, Z. X. Xie, Y. M. Du, B.Q. Pand and D. W. Pang, *Chem. Commun.*, **44,** 5518 (2005).

30. J. Xie, Q. Zhang, J. Y. Lee and D. I. C. Wang, *ACS Nano.*, **2,** 2473 (2008).

31. J. Xie, J. Y. Lee and D. I. C. Wang, Chem. Mater., **19,** 2823 (2007).

32. L. Zhong, X. Zhai, X. Zhu, P. Yao and M. Liu, *Langmuir.*, **26,** 5876 (2010).

33. W. E. Doering, M. E. Piotti, M. J. Natan and R. G. Freeman, *Adv. Mater.*, **19,** 3100(2007).

34. J. W. Rhim, I. N. Hong Seok, H. M. Park and K. W. N. G Perry, *J. Agric. Food Chem.*, **54,** 5814 (2006).

35. Y. Mei and Y. J. Zhao, *Agric. Food Chem.*, **51,** 1914 (2003).

36. S. I. Park and Y. Zhao, *J. Agric. Food Chem.*, **52,** 1933 (2004).

37. D. Depan, A. P. Kumar and R. P. Singh, *Acta Biomaterialia.*, **5,** 93(2009).

38. N. Shanmugasundram, P. Ravichandaran, P. N. Reddy, N. Ramamurth, S. Pal and K. P. Rao, *Biomaterials.,* **22,** 1943(2001).

39. L.Vachoud, N. Zydowicz and A. Domard, *Carbohydrate Res.,* **326,** 295(2000).

40. Y. Zhang, C. Xue, Z. Li, Y. Zhang and X. Fu, *Carbohydrate Polymers.,* **65** 229(2006).

41. T. Takahashi, Y. Yamada, K. Kataoka and Y. Nagasaki, *Journal of Controlled Release.,* **107** 408(2005).

42. L. G. Griffth and G. Naughton, *Science.*, **295,** 1009(2002).

CHAPTER 3

B: Preparation and Characterization of Glycolic Acid-g-Chitosan-Gold Nanoparticles Based Nanocomposite Films

3.2.1 INTRODUCTION

A wide range of materials, including inorganic, organic and biological, are now used in the synthesis, fabrication and processing of nanostructures with unique physical properties.[1] This approach is illustrative of the expansion of nanoscience, driven by potential applications in fundamental research and nanotechnology. Gold nanoparticles have found widespread use in fundamental research [2] as well as in sensing, biological[3] and catalytic[4] applications.[5, 6] Gold nanoparticles can produce wide variety of shapes including prisms,[7] rods, wires,[8] and spheres by several chemical and physical methods, which have been employed to fabricate gold nanoparticles.[9,10] Polymers also offer control over the rate of the reduction process and thus enable the production of nanoparticles of different shapes and sizes.[11] The stabilization of gold nanoparticles with chitosan has been extensively reported.[12, 13] Biopolymer based on chitosan is the N-deacetylated form of chitin derived by deacetylation of chitin. Chitosan is highly basic polysaccharides, it has primary amino groups that have pKa values of about 6.3.[14]

Chitosan is modified by chemical reaction, which involves the reactive amino and hydroxyl groups of the polymer chain. The grafting of glycolic acid on chitosan leads to marked changes in its structure. [15, 16] Due to this unique property many potential products using chitosan have been developed, including chelating agents for removal of traces of heavy metals from aqueous solutions, flocculating agents for water and waste water treatment, wet strength additives for paper, adhesives, photographic and printing applications etc.

The objective of this work is therefore, to determine the effects of glycolic acid grafted chitosan and gold nanoparticles concentrations on the barrier, mechanical and thermal properties of glycolic acid grafted chitosan films containing nanoparticles in view of their possible use in the field of biomedical.

3.2.2 EXPERIMENTAL

3.2.2.1 Materials

Chitosan of low molecular weight ($Mv=1.5\times10^5$, degree of deacetylation was 85%), glycolic acid (99% purity) was obtained from Sigma Aldrich. Gold chloride ($HAuCl_4$) and Sodium borohydride ($NaBH_4$) were obtained from Sisco Research Laboratories, Mumbai. Ultra pure water was prepared by a Milli-Q system and it is used throughout.

3.2.2.2 Synthesis of gold nanoparticles

Gold nanoparticles (AuNP) of 10^{-4} M were obtained by reducing the $HAuCl_4$ precursor with 0.1 M $NaBH_4$. Upon addition of reducing agent to the solution of $HAuCl_4$, immediately a ruby red colour appeared which results in the formation of gold nanoparticles.

3.2.2.3 Synthesis of glycolic acid grafted chitosan

In a round bottom flask containing chitosan and glycolic acid in 1:1 ratio. To it pyridine (Py), lithium chloride (LiCl), Tri-phenyl phosphate (TPP) was added in 1:1:1 ratio. To the reaction mixture 12 ml of N-methyl pyrilidone (NMP) was added. The reaction mixture was stirred and refluxed for 8 h at 120^0. After 8 h, the viscous reaction mixture was cooled to room and precipitated with methanol. The precipitate was dried at 70 ^{0}C for 10 h under reduced pressure.

3.2.2.4 Preparation of glycolic acid –g-chitosan and Au nanoparticle nanocomposite film

The grafted chitosan was dispersed in deionised water for 1 h with constant stirring at room temperature. After 1 h, AuNP were added to the resulting solution and stirred overnight at room temperature. The resulting solution was heated up to 80 ^{0}C with continuous degassing for 45 min. The solution was casted on a glass plate and dried at 60 ^{0}C in vacuum for 8 h.

Table 3.2.1 The formulation of chitosan-g-glycolic acid and Au nanoparticle

S. No	Chitosan (g)	Glycolic acid (g)	AuNP (ml)	Sample code
1	1	0	0	CS
2	1	1	0	CGA-1
3	1	1	50	CGA-2
4	1	1	100	CGA-3

Samples were extracted with methanol in soxhlet apparatus for 48 h, to remove the oligomers of glycolic acid and unreacted glycolic acid. The formulation of chitosan and nanoparticle (AuNP) are given in Table **3.2.1**.

3.2.3 CHARACTERIZATION OF NANOCOMPOSITE FILM

3.2.3.1 Transmission electron microscopy (TEM)

The particle size, morphology and Selected Area Diffraction pattern (SAED) of Au nanoparticles were analysed with High Resolution Transmission electron microscopy (HR-TEM model Technai TF30, 300KV FEG).

3.2.3.2 Fourier transform infrared spectroscopy (FT-IR)

The Nicolet Nexus 870 attenuated total reflectance Fourier transform infrared (ATR-FTIR) spectrometer equipped with a smart endurance diamond accessory (64 scans, 4 cm^{-1} resolution, wave number range 4000-550 cm^{-1}) was used to analyse neat chitosan (CS), chitosan grafted glycolic acid (CGAu-1) and grafted chitosan nanocomposite with gold nanoparticles (CGAu-2).

3.2.3.3 X-ray diffraction (XRD)

XRD patterns of the samples were recorded on X-ray Diffractometer (WAXRD – Rigaku (Japan)) with Cu-kα radiation at a voltage of 50 KV. The scanning rate was 4^0/min and the scanning scope of 2θ was from $2^0$to 80^0 at room temperature.

3.2.3.4 Atomic force microscopy (AFM)

The surface morphology of nanohybrid film were investigated by atomic force microscopy (AFM) (Model: Nanoscope IV) under contact mode.

3.2.3.5 Dynamic mechanical analysis (DMA)

Mechanical strength of prepared films were investigated with a dynamic mechanical thermal analyser (DMTA RSA3, TA instrument) in tensile mode at a frequency of 1Hz with heating rate of 5 ^{0}C/min in the temperature range from -10 ^{0}C to 200 ^{0}C.

3.2.3.6 Tensile strength testing (TST)

The tensile stress testing of film was determined by Linkam TST 350. A dumb bell strip was cut from each membrane and strained to break at a constant crosshead speed of 10 mm/min. The break stress and strain was calculated with the associated software (Linkam).

3.2.3.7 Thermogravimetric analysis (TGA)

TGA Q5000 instrument were used to conduct the thermogravimetric analysis (TGA) of the sample. Temperature ranges from 50 ^{0}C to 900 ^{0}C with the heating rate of 10 ^{0}C/min under nitrogen with flow rate 20 ml/min.

3.2.4 RESULTS AND DISCUSSION

3.2.4.1 TEM analysis of gold nanoparticles

Figure 3.2.1 (a, b) shows TEM image of Au nanoparticles exhibits spherical morphology and same overall size.[17] The high resolution image of Au nanoparticles (**Figure 3.2.1** (c)) shows that the distance between the two adjacent lattice planes in Au domain is 2.34 Å,

which is consistent with the literature value of 2.35 Å for (1 1 1) plane. The selected area diffraction pattern (**Figure 3.2.1** (d)) (SAED) also shows crystallinity of Au nanoparticle.

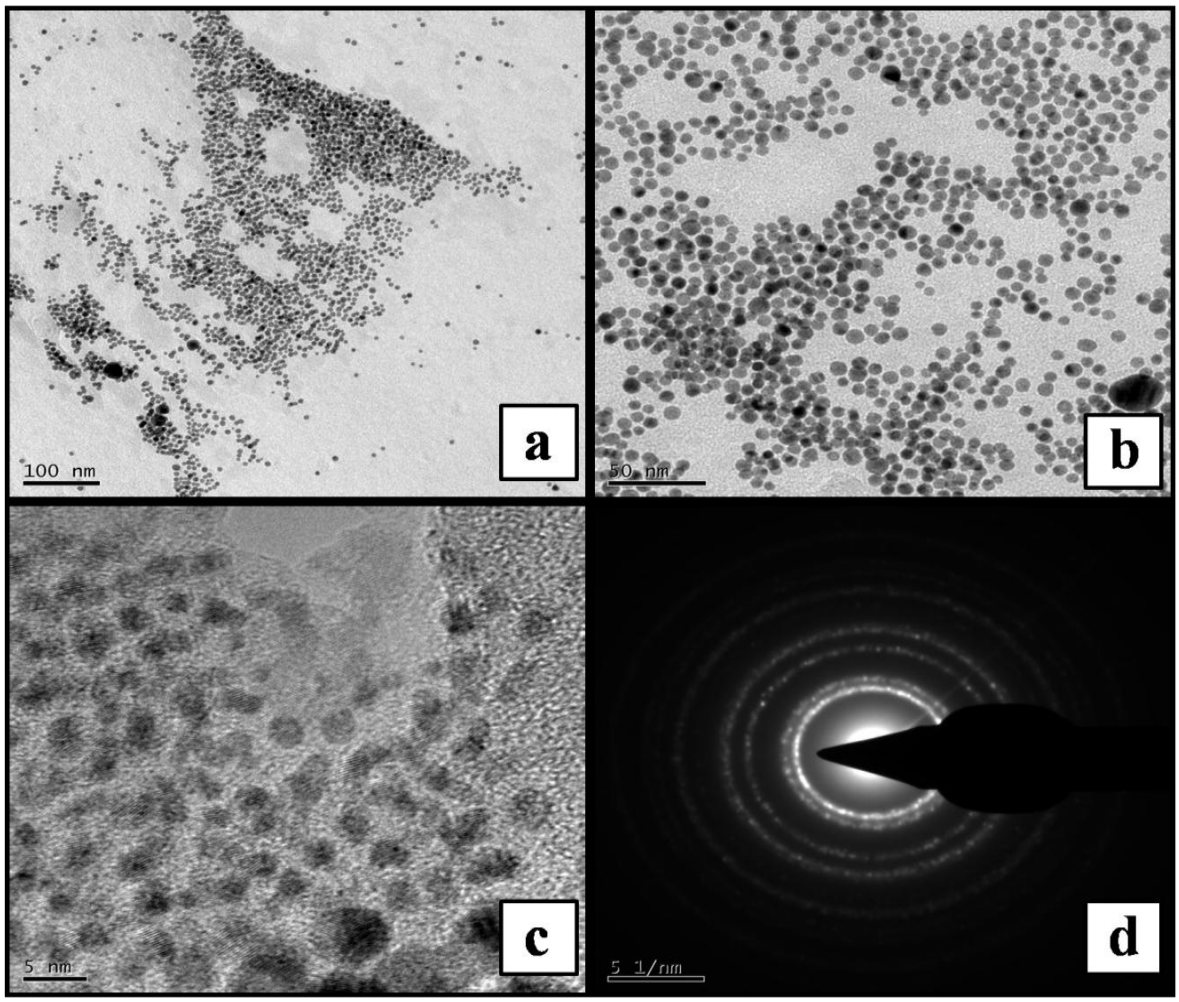

Figure 3.2.1 *(a, b) TEM image Au nanoparticles (c) HRTEM image of Au nanoparticles (d) SAED pattern of Au nanoparticles.*

3.2.4.2 FTIR analysis

Fourier transform infrared (FT-IR) spectra were used to investigate the structural information about neat chitosan (CS), glycolic acid grafted chitosan (CGA-1) and its nanocomposite with Au nanoparticle (CGA-2) (**Figure 3.2.2**). The In the spectrum of neat chitosan, peak at 1637 cm^{-1} is attributed to the –N-H stretching vibration of amine ($–NH_2$) group and 3500cm^{-1} (-OH stretching). a new peak (CGA-1)appear at 1730 cm^{-1} corresponds

to υ_{co} stretching and shifting of peak (-NH stretching) towards the lower frequency region (1564 cm^{-1}) confirms the interaction of glycolic acid with NH_2 group of chitosan. These two peaks confirms the conversion of amine (NH_2) to amide (–NH-C=O). In the FTIR spectrum of CGA-2 include shift in peak to 1723 cm^{-1} (-C=O stretching) and 3401 cm^{-1} (-OH stretching) it may due to the interaction of Au nanoparticles with –C=O group of glycolic acid and –OH group of chitosan via metallic bond.

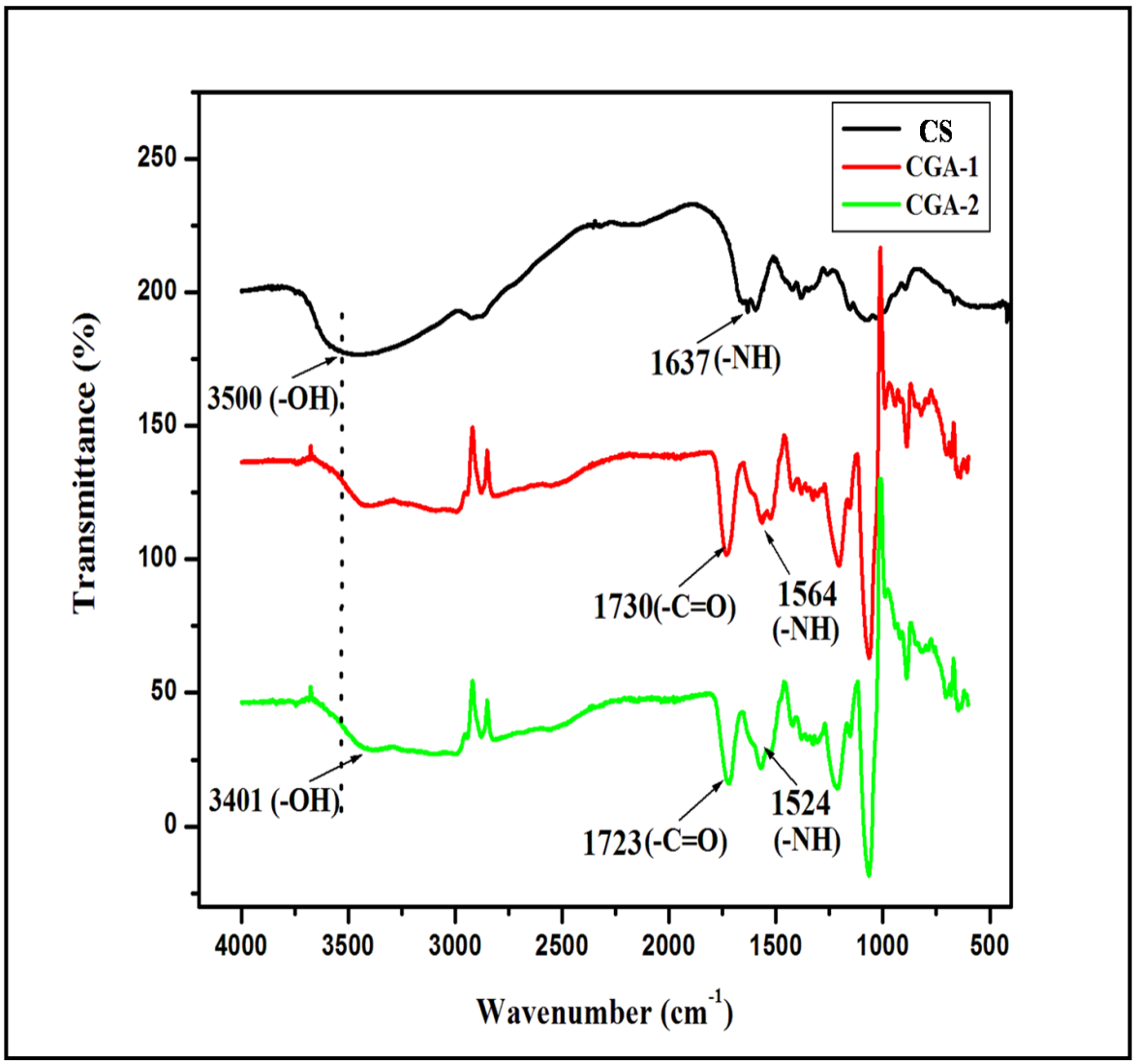

Figure 3.2.2 *FTIR spectra of neat chitosan (CS), grafted chitosan (CGA-1) and grafted chitosan-Au nanoparticle nanocomposite film.*

3.2.4.3 XRD analysis

Figure 3.2.3 (a) and (b) illustrates the XRD pattern of pure chitosan (CS), glycolic acid grafted chitosan (CGA-1) and CGA-1 with Au nanoparticle (CGA-2) nanocomposite films. It was observed that neat chitosan (CS) shows the characteristic peak at 10.9^{o} and 19.8^{o}, which correspond to a hydrated crystalline structure and a slightly less crystalline structure of chitosan, respectively.[18-20] In grafted chitosan (CGA-1) film, XRD peaks were shifted from 10.9^{0} to 10.1^{0} and 19.8^{0} to 20.6^{0} confirming the interaction of glycolic acid with chitosan. These peaks were shifted from 10.1^{o} to 8.5^{o} and 20.6^{o} to 21.6^{o}, showing the interaction of gold nanoflower with the grafted chitosan (CGA-2).

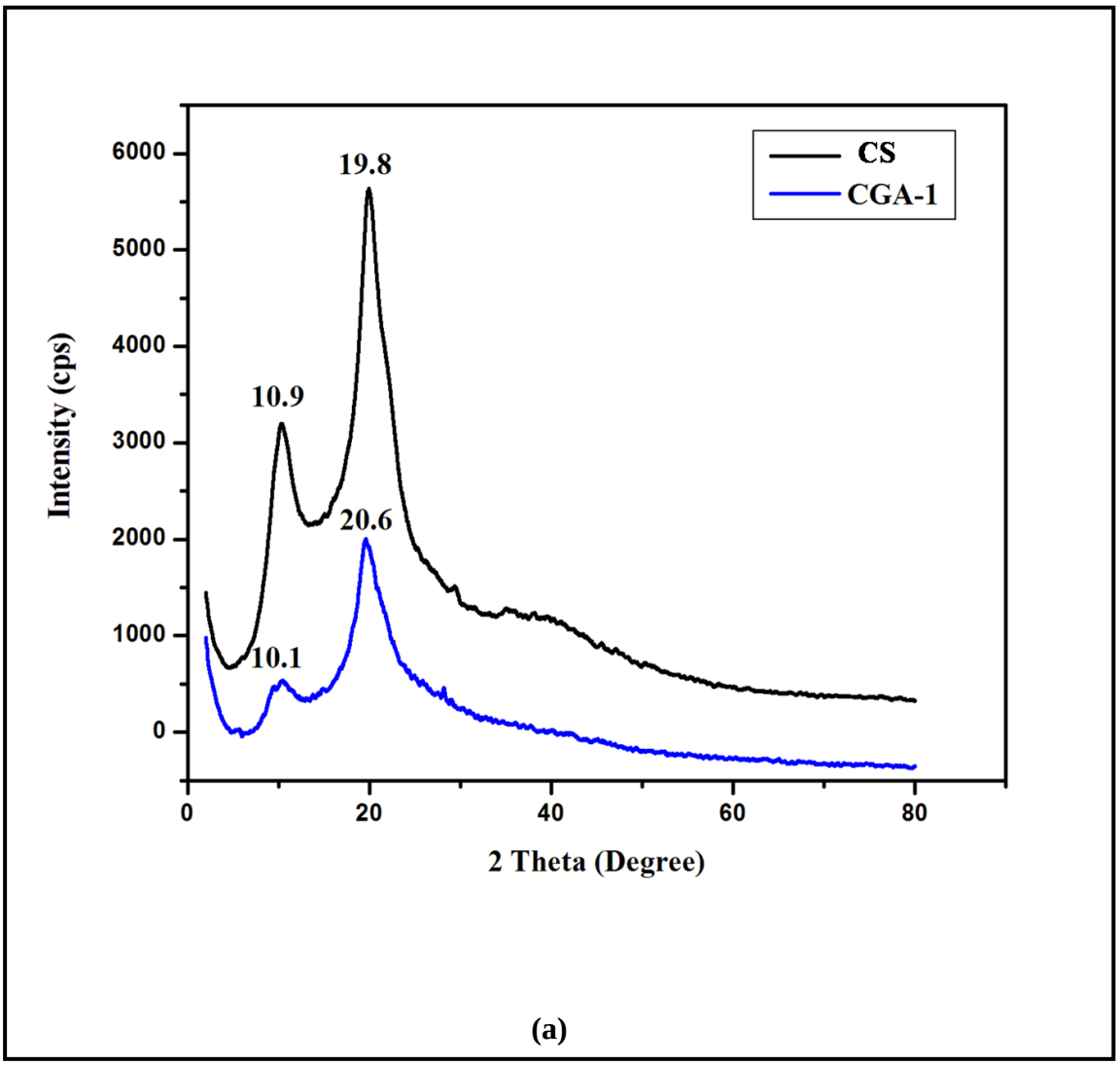

(a)

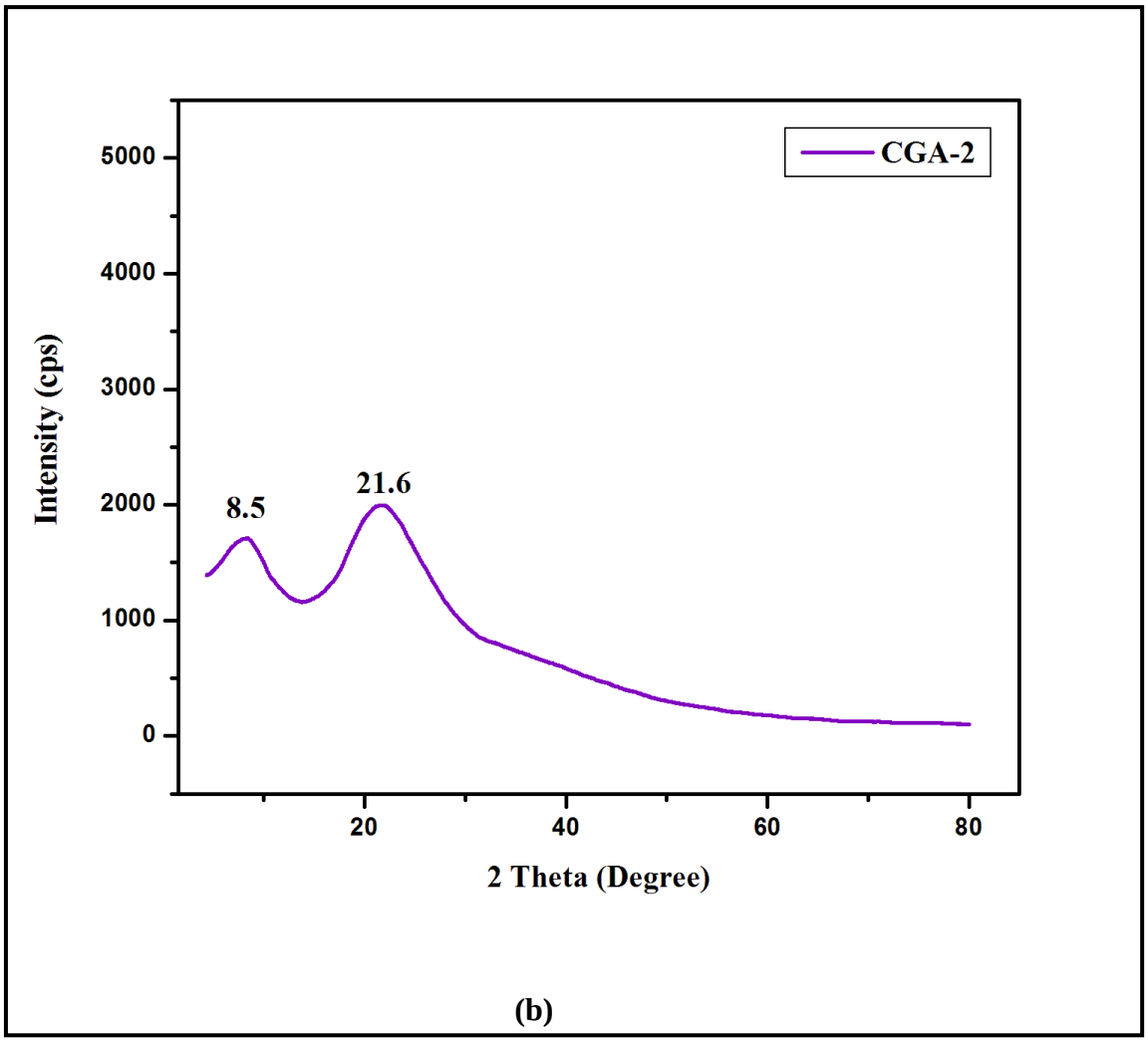

Figure 3.2.3 *(a) X-ray diffraction spectra of neat chitosan, grafted chitosan; (b) X-ray diffraction spectrum of grafted chitosan/ Au nanoparticle nanocomposite films.*

3.2.4.4 Morphological analysis

Atomic Force Microscopy (AFM) was used to investigate the surface topography of neat chitosan (CS), grafted chitosan (CGA-1) and grafted chitosan with Au nanoparticle nanocomposite (CGA-2) film. **Figure 3.2.4** (a) shows the AFM image of chitosan film with smooth surface. Upon grafting the chitosan, roughness and height of the film surface were also increased (**Figure 3.2.4** (b)). The incorporation of Au nanoparticle in the matrix of chitosan film is shown in **Figure 3.2.4** (c, d).

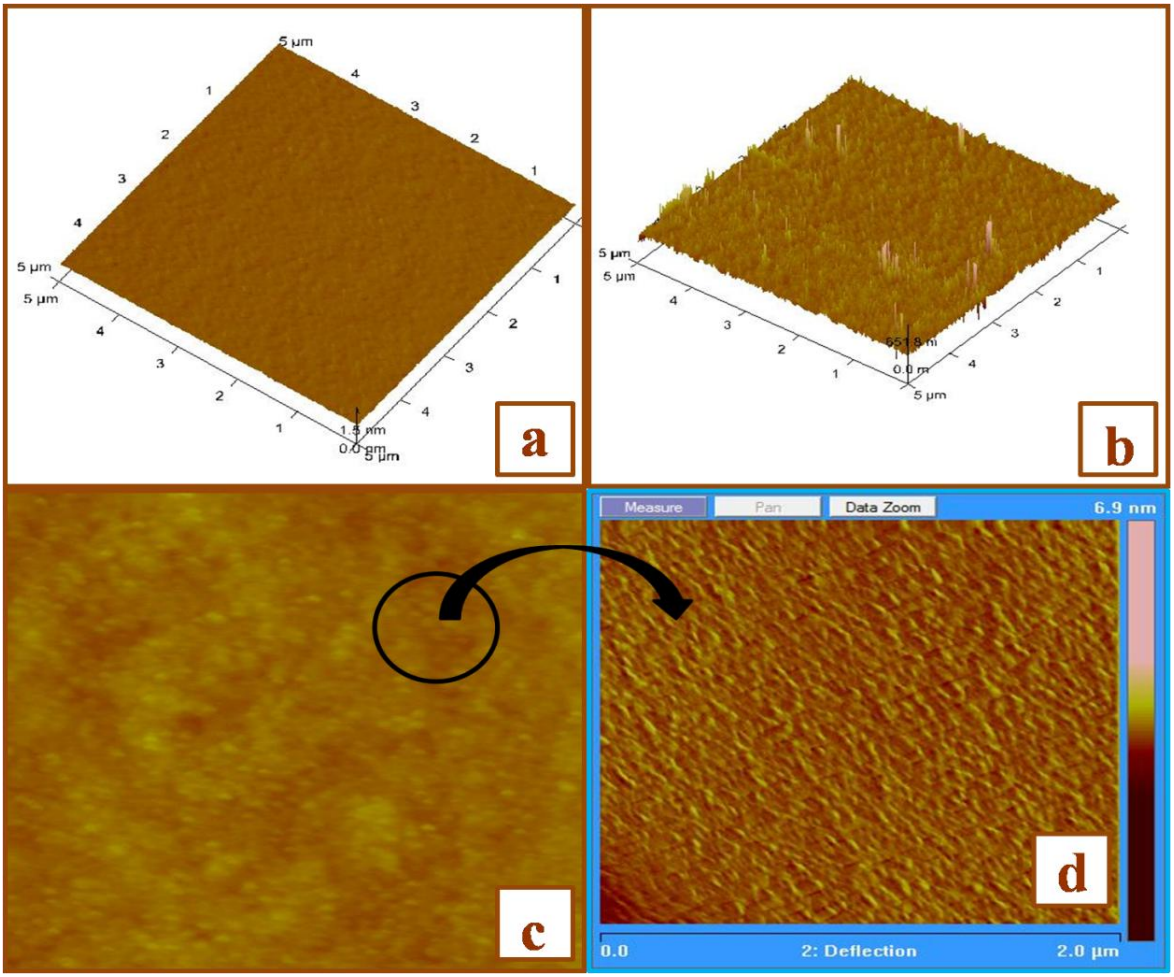

Figure 3.2.4 *(a) AFM image of pure chitosan film; (b) AFM image of grafted chitosan film. (c, d) AFM image of grafted chitosan/Au nanoparticle nanocomposite films.*

3.2.4.5 Dynamic mechanical analysis

Figure 3.2.5 (a), (b), (c), (d) shows the variation in dynamic mechanical thermal property of CS-g-GA/Au nanoparticle nanocomposite, which determines the stability, viscoelastic property and glass transition temperature of the polymer.[21] The storage modulus [E'] of neat chitosan film is 1.59×10^8 [Pa] and it decreases to 1.57×10^8 [Pa] for grafted polymer film. The storage modulus of nanocomposite film increases with the increase in nanoparticle content. Upon increasing the temperature segmental motion of the polymer increases and sharp increase in tanδ is observed which corresponds to α relaxation temperature associated with

the glass transition temperature T_g. The pure chitosan film shows T_g at 153.86 ^{0}C and due to increase in the mobility of the polymer chains, decrease in T_g of grafted film is observed. The addition of Au nanoparticle restricts the mobility of the chains and causes the increase in the storage modulus and improves the mechanical strength polymer film (**Table 3.2.2**).

Table 3.2.2 Viscoelastic properties of grafted chitosan-Au nanoparticle nanocomposites

Sample Code	Pt-Fe_3O_4 (ml)	Storage modulus (Pa) at 84 ^{0}C	Tan delta (δ)
CS	0	1.59×10^8	0.42
CGA-1	0	1.57×10^8	0.59
CGA-2	50	2.487×10^6	0.49
CGA-3	100	8.18×10^6	0.51

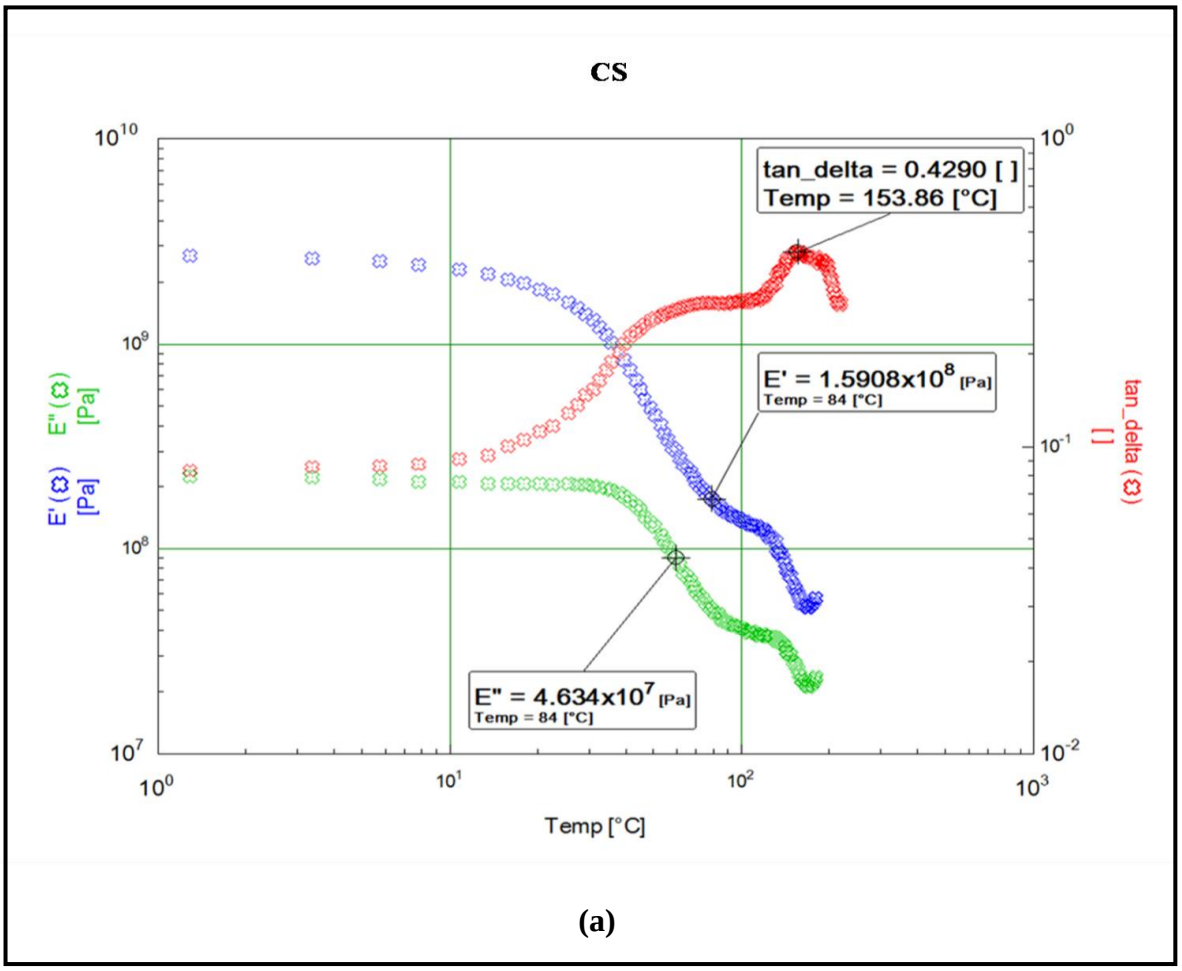

(a)

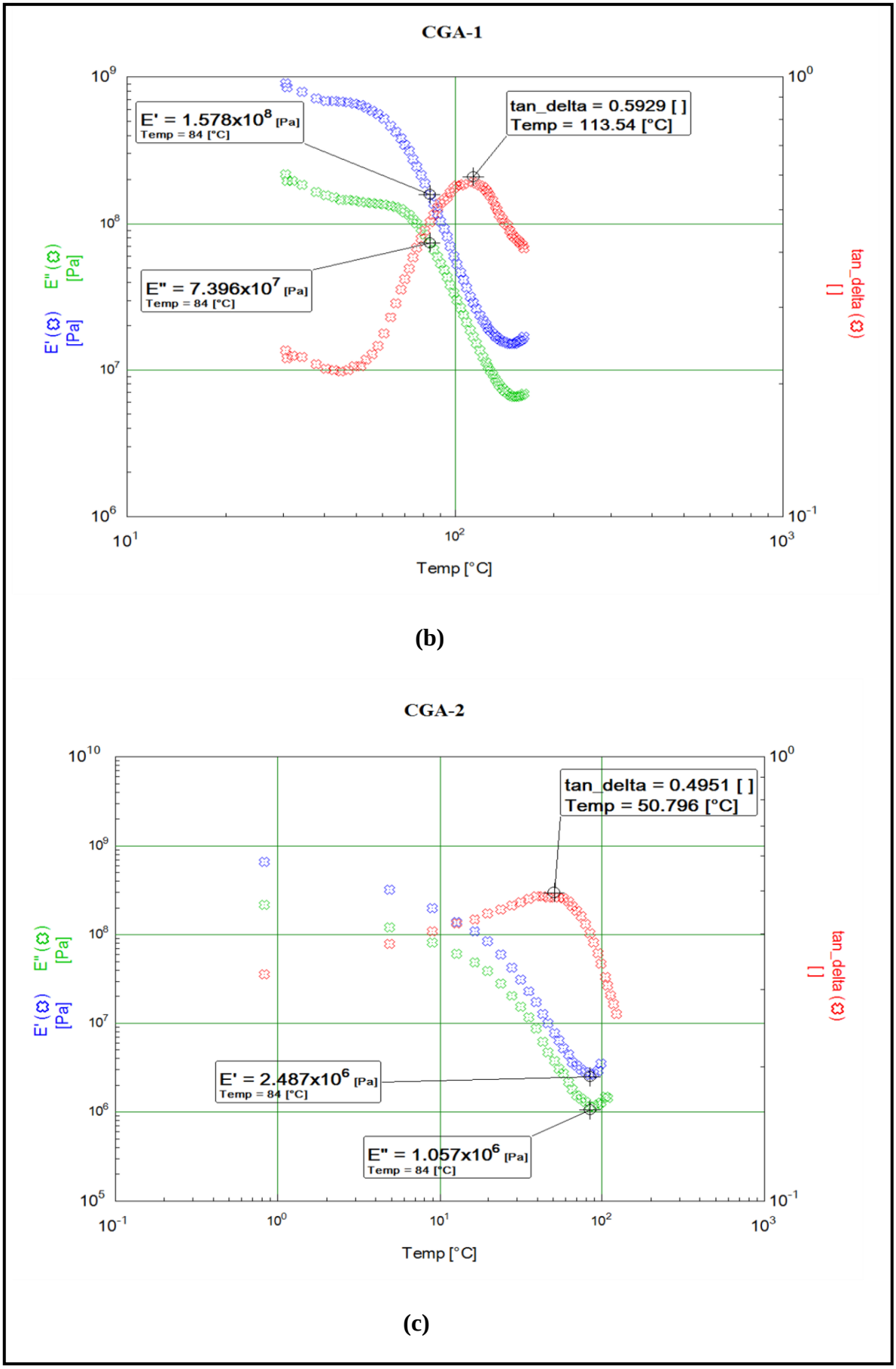
CGA-1
E' = 1.578x10^8 [Pa]
Temp = 84 [°C]
tan_delta = 0.5929 [ ]
Temp = 113.54 [°C]
E" = 7.396x10^7 [Pa]
Temp = 84 [°C]
E'(ω) E"(ω) [Pa]
tan_delta (ω) [ ]
Temp [°C]
(b)
CGA-2
tan_delta = 0.4951 [ ]
Temp = 50.796 [°C]
E' = 2.487x10^6 [Pa]
Temp = 84 [°C]
E" = 1.057x10^6 [Pa]
Temp = 84 [°C]
E'(ω) E"(ω) [Pa]
tan_delta (ω) [ ]
Temp [°C]
(c)

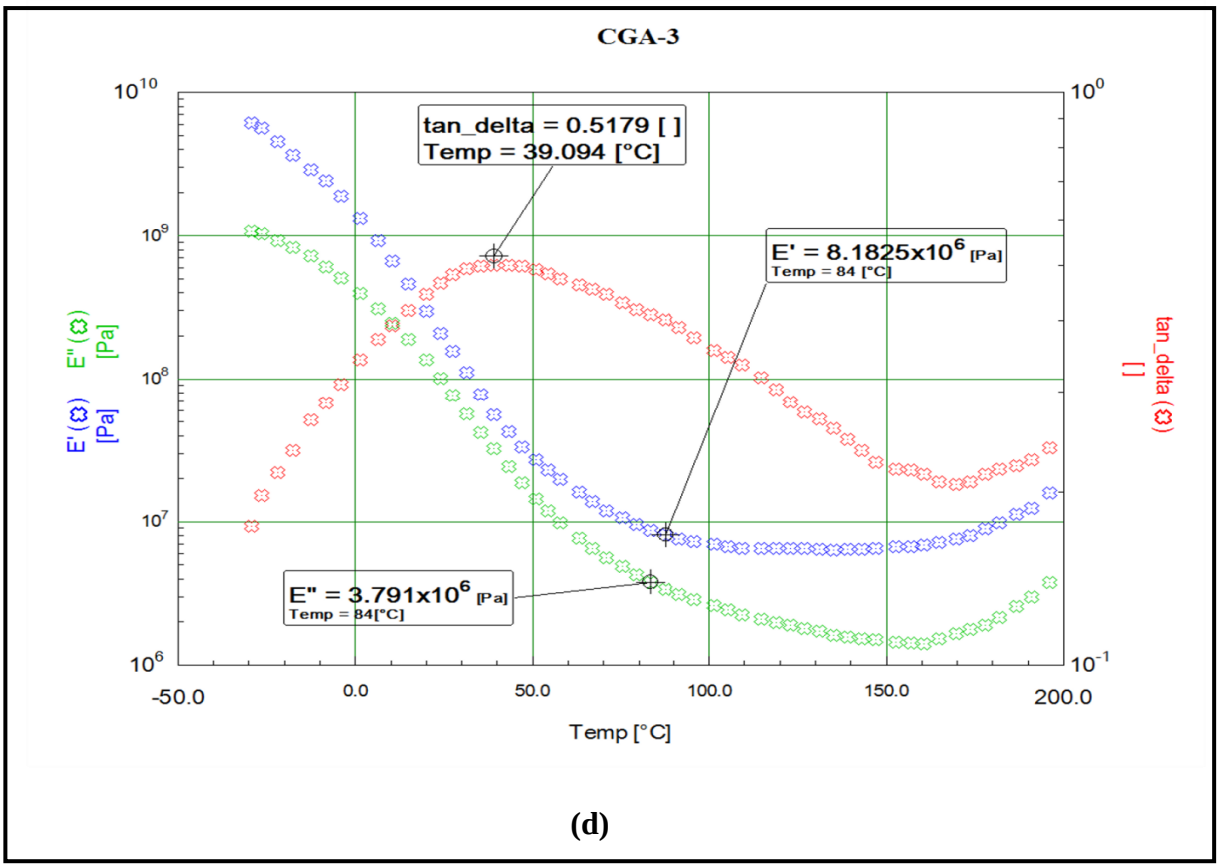

(d)

Figure 3.2.5 *Temperature variation of tanδ, glass transition temperature, storage modulus [E'] and loss modulus [E''] (a) Pure chitosan film (b) Grafted chitosan film (c) Grafted chitosan/Au nanoparticle nanocomposite films (d) Grafted chitosan/Au nanoparticle nanocomposite films*

3.2.4.6 Tensile stress testing

Figure 3.2.6 (a) shows the tensile properties of neat chitosan (CS), grafted chitosan (CGA-1) and CS-g-GA/Au nanoparticle nanocomposite (CGA-2) film. All the membranes were semi-transparent and had uniform thickness of 0.19 mm. Crosshead speed used while testing is 10 mm/min at 27 ^{0}C. The pure chitosan film exhibits a break stress as 25- 26 %. The neat chitosan film shows elastic modulus of 0.9855 MPa.)). The grafted chitosan shows a decrease in elastic modulus. Increase in elastic modulus was observed upon incorporation of

nanoparticle in polymer matrix (**Table 3.2.3**). Nanoparticles improve the tensile strength of the polymer film (**Figure 3.2.6** (b)).

Table 3.2.3 Tensile strength and testing of chitosan and nanocomposites

Sample Code	Elastic modulus (MPa)	Stress (%)	Strain (%)
CS	0.9855	47.97	25.83
CGA-1	0.9556	6.38	83.29
CGA-2	0.9776	6.07	69.16

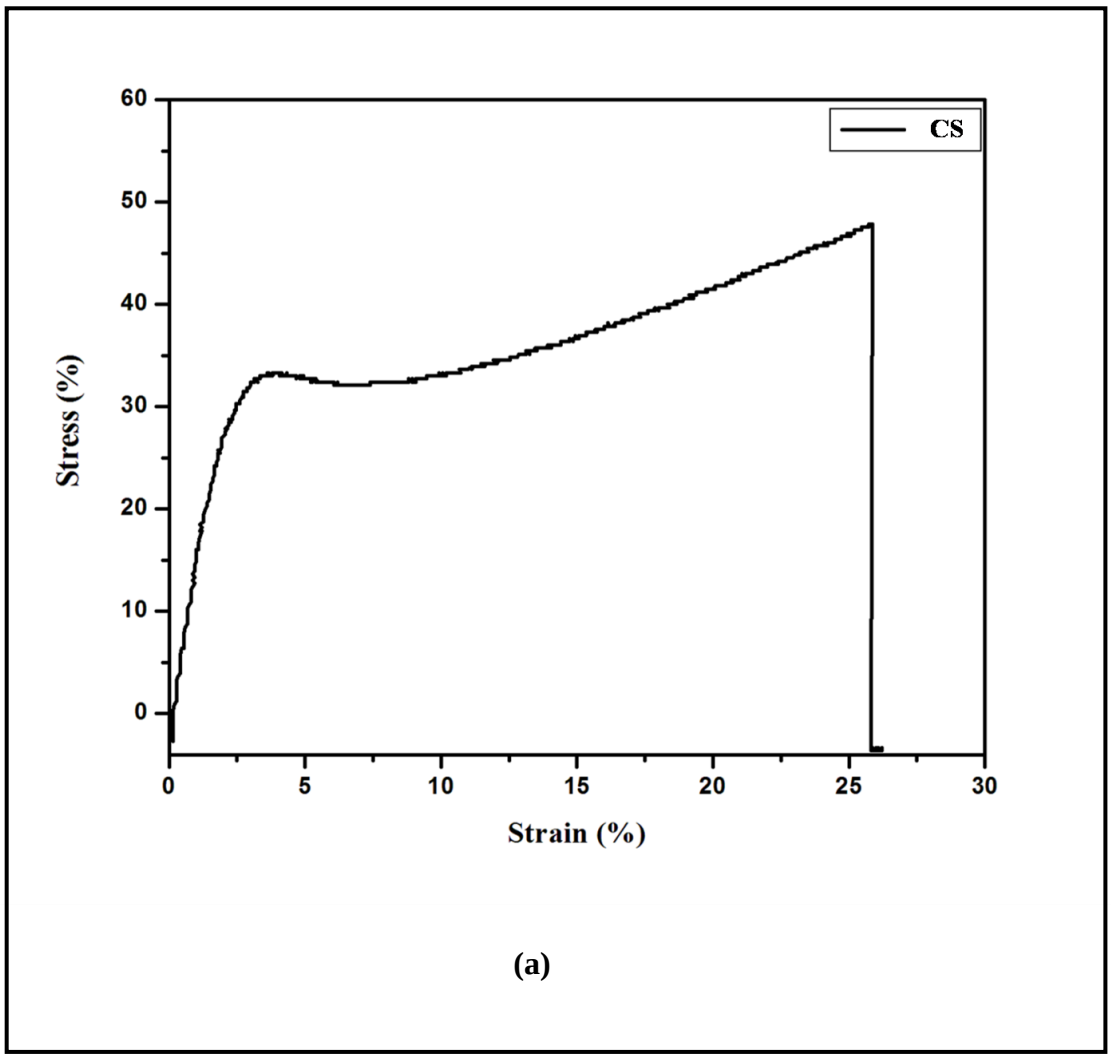

(a)

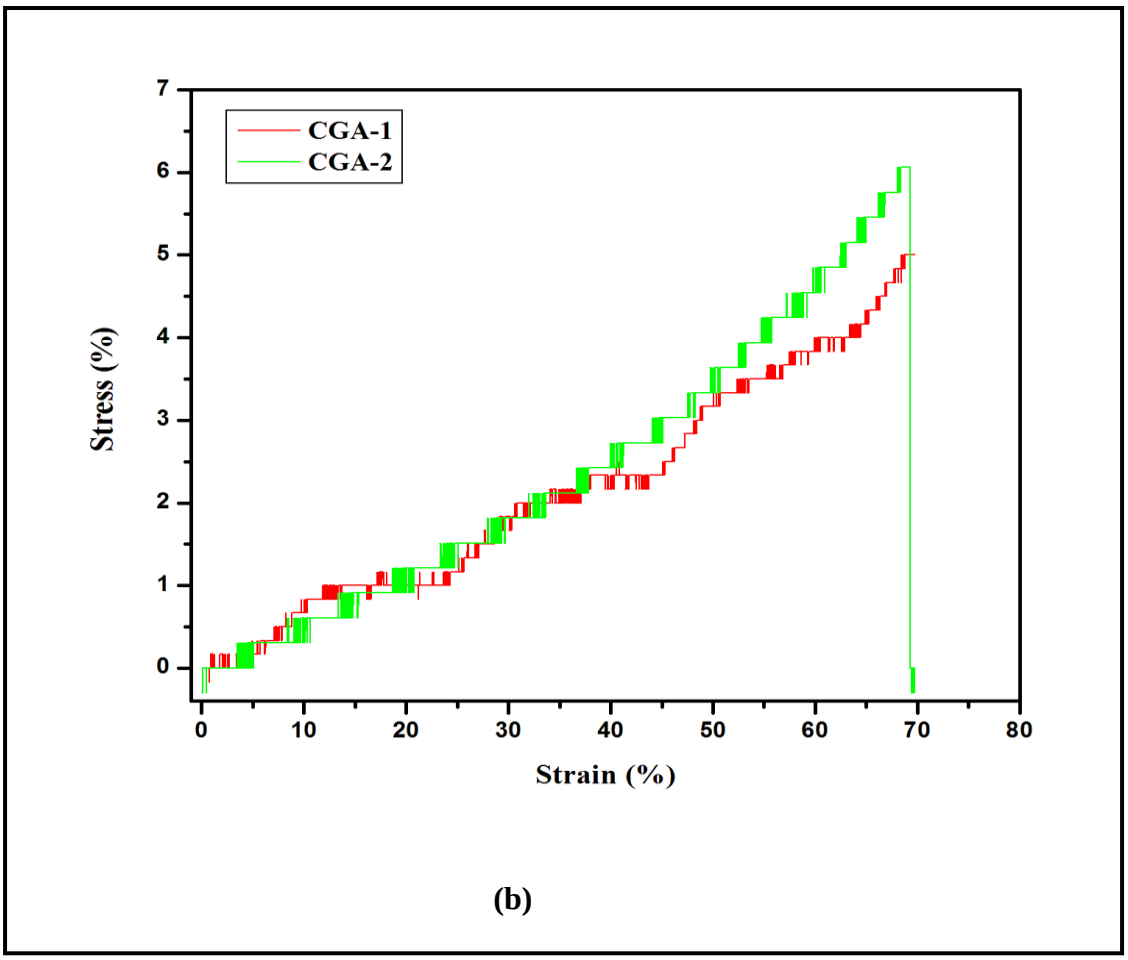

Figure 3.2.6 *(a) Stress strain behavior of pure chitosan membranes (b) Effect of grafting and nanoparticle stress strain behavior of grafted and nanocomposite chitosan membranes.*

3.2.4.7 Thermogravimetric analysis

Figure 3.2.7 shows the thermal degradation of chitosan and nanocomposite with various components under nitrogen flow. Two steps of non-oxidative degradation were observed. The weight loss at 50-150 ^{0}C is attributed to the water absorbed in chitosan. However the weight loss in the temperature range of 200-350 ^{0}C corresponds to the degradation and deacetylation of chitosan.[22] The thermal stability of chitosan decreases; this is due to the poor heat barrier properties of nanoparticle for polymer matrix during the formation of chars.[23] Decrease in char residue is observed upon addition of nanoparticles (**Table 3.2.4**).

Table 3.2.4 TGA results for chitosan and its nanocomposites

Sample Code	Temperature at 20% loss (^{0}C)	char at 900 ^{0}C (wt %)
CS	310	27.1
CGA-1	246	27.7
CGA-2	266	26.2

This result indicates the significant effect of combination of glycolic acid and nanoparticles on the thermal properties of chitosan. The amount of weight loss at this temperature range decreases with the addition of nanoparticles in polymer matrix. This confirms that due the grafted chitosan-Au nanoparticles bonding water absorbability that is hydrophillicity of the films decreases.

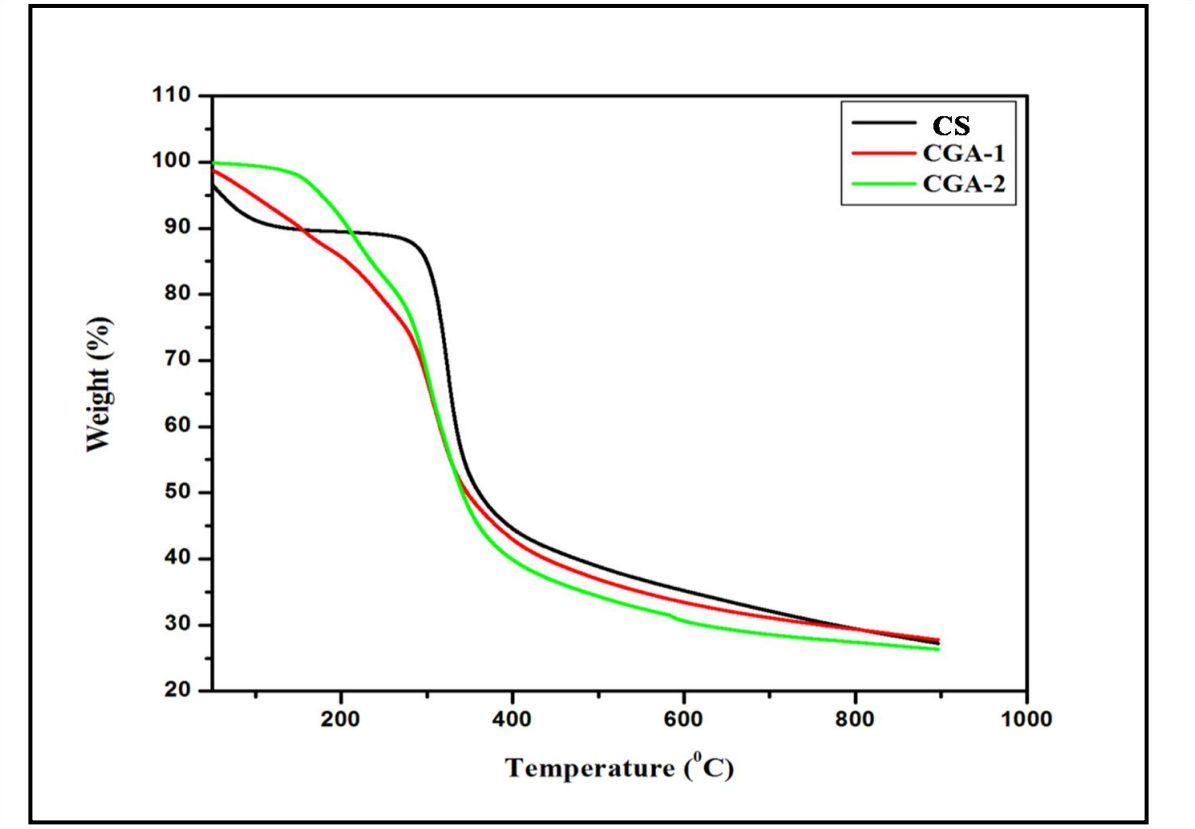

Figure 3.2.7 *Thermogravimetric curves of prepared nanocomposites.*

3.2.4.8 Water absorption behavior of film

The behavior of water absorption of CS-*g*-GA/ Au nanoparticle composites was investigated and results were shown in **Table 3.2.5**. The water absorption of composite films decreases with an increase of nanoparticle with chitosan matrix. This is probably due to the formation of a barrier in the form of cross-linking points, which prevents water permeation into CS. Pure CS is hydrophilic, but it doesn't absorb much water. There are many –OH and –NH groups in CS, which cause strong intermolecular and intramolecular hydrogen bonds; thus the infiltration and diffusion of water, are restrained. The water absorption of glycolic acid grafted CS is higher than neat CS. It can be attributed to the fact that the integrity of molecular structure is broken in grafted CS, which can expose more functional groups for water absorption. This swelling extent will depend on the osmotic pressure and charge repulsion, the degree of ionization and grafting extent also[24]. In comparison of grafted CS, samples of nanocomposites have shown lower water absorption and it decreases with increasing content of nanoparticle. Upon increasing content of nanoparticle reduces the exposure of more functional group towards the water, thus the hydrophobicity of the nanocomposite film increases.

The increasing content of nanoparticle increases the immobilized phase throughout the matrix. The interaction between the mobilized and immobilized phases has shown to reduce the water absorption[25] and have already been demonstrated.[26]

Table 3.2.5 Sorption behavior of the nanocomposites

Sample Code	Water Absorption (%)
CS	54
CGA-1	77.7
CGA-2	34.48
CGA-3	28.55

3.2.5 CONCLUSIONS

In the present study, inorganic-organic hybrids were prepared from biopolymer and hybrid nanoparticles. The glycolic acid grafted chitosan-Au nanoparticles based nanocomposites were prepared by film casting method. The grafted glycolic acid chains were acting as plasticizer to give flexible films. The interaction of cationic chitosan with Au nanoparticles is through metallic bond, which results in enhancement in structural and functional properties. The dynamic mechanical thermal analysis (DMTA) measures the shift in the glass transition temperature (Tg) of the composites from the maxima of the α transition curves. The tensile strength of nanocomposite increases with increasing content of nanoparticles. The increasing content of nanoparticles decreases the water absorption, which imparts little branched crystalline structure in the film. The results showed that increasing content of nanoparticles reduces hydrophillicity of the nanocomposite film. The longer water retention and swelling behavior properties were discussed, which could be applied in the field of biomedical.

3.2.6 REFERENCES

1. A. N. Shipway, E. Katz and I. Willner, *Chem. Phys. Chem.*, **1,** 18(2000).
2. M. C. Daniel and D. Astruc, *Chem. Rev.*, **104,** 293(2004).
3. D. C. Hone, P. I. Walker, R. Evans-Gowing, S. FitzGerald, A. Beeby and I. Chambrier, et al., *Langmuir.*, **18,** 2985(2002).
4. C. Mohr, H. Hofmeister, J. Radnik and P. Claus, *J. Am. Chem. Soc.,* **125,** 1905 (2003).
5. Y. W. C. Cao, R. Jin and C. A. Mirkin, *Sci.,* **297,** 1536 (2002).
6. M. J. Natan, L. A. Lyon, D. L. Feldheim and A. F. Jr. Colby, *In Metal Nanoparticles: Synthesis, Characterization and Application.* New York, (2002).

7. L. M. Liz-Marzan, *Mat. Tod.,* **7,** 26 (2004).
8. T. Hassenkam, K. Norsgaard, L. Iversen, C. Kiely, M. Brust and T. Bjornholm, *Adv. Mat.* **14,** 1126 (2002).
9. G. Frens, *Nat. Phys. Sci.* **241,** 20 (1973).
10. S. D. Bunge, T. J. Boyle and T. J. Headley, *Nano. Let.* **3,** 901 (2003).
11. N. Toshima and T. Yonezawa, *J. Chem.* **22,** 1179 (1998).
12. D. S. Jr. Dos Santos, P. J. G. Goulet, N. P. W. Pieczonka, O. N. Jr. Oliveira and R. F. Aroca, Langmuir., **20,** 10273 (2004).
13. K. Esumi, N. Takei and T. Yoshimura, *Colloids Surf.* B., **32,** 117 (2003).
14. P. Sorlier, A. Denuzière, C. Viton and A. Domard. *Biomacromolecules.,* **2,** 765 (2001).
15. M. Xie, H. H. Liu, P. Chen, Z. L. Zhang, X. H. Wang, Z. X. Xie, Y. M. Du, B. Q. Pand and D. W. Pang, Chem. Commun. **44,** 5518 (2005).
16. J. Xie, Q. Zhang, J. Y. Lee and D. I. C. Wang, *ACS Nano.* **2,** 2473 (2008).
17. J. Rodriguez-Fernandez, J. Perez-Juste, F. J. G. Abajo and L. M. Liz- Marzan, *Langmuir.,* **22,** 7007(2006).
18. J. W. Rhim, I. N. Hong Seok, H. M. Park and K. W. N. G. Perry, *J. Agric. Food. Chem.,* **54,** 5814(2006).
19. Y. Mei and Y. J. Zhao, *Agric. Food. Chem.*, **51**, 1914(2003).
20. S. I. Park and Y. Zhao, *J. Agric. Food. Chem.* **52,** 1933(2004).
21. F. Al-Sagheer and S. Muslim, *J. Nanomaterials.,* **2010,** 1(2009) -7.
22. S. F. Wang, L. Chen and Y. J. Tong, *J. Polym. Sci. Part. A. Polym. Chem.* **44,** 686(2006).
23. S. F. Wang, L. Shen, Y. J. Tong, L. chen, I. Y. Phang and T. X. Liu, *Polym. Degrad. Stab.,* **90,** 123(2005).

24. P. Seong and Y. Jin, P. Ham, *Biomaterials.,* **22,** 323(2000).

25. A. P. Kumar and R. P. Singh, Novel Hybrid of Clay, Cellulose, Thermoplastics. *I. J. Appl. Polym. Sci.,* **104,** 2672 (2007).

26. G. Tsagaroulos and A. Eisenberg, *Macromol.,* **28,** 6067(1995).

CHAPTER 4

A: Preparation and Characterization of Glycolic Acid-g-Chitosan-Au-Fe_3O_4 Hybrid Nanoparticles Based Nanocomposite Scaffolds for Drug Delivery and Tissue Engineering Applications

4.1 INTRODUCTION

Advances in nanotechnology play an important role in designing nanomaterials with specific functional properties that can address the shortcomings in the area of diagnostics and therapeutics. The advantages of the nanoparticles are mainly due to their nanoscale size and large surface area with the ability to get functionalized with therapeutic moieties, bio-molecules[1] and targeting ligands. The potential of nanomaterials has sparked enormous interest in the drug industries and has envisaged several applications, as can be evidenced by the exponential growth of activities in this field. The nanoparticles can easily gain access to various areas of the body without interfering into normal functions and has the requisite potential for therapeutic and diagnostic applications[2]. Due to this reason "hybrid" nanostructures can be obtained or it may be embedded in biocompatible materials to impart new functionalities. The hybrid nanostructures are desirable for many application like sustained drug delivery[3], hyperthermia[4, 5], diagnosis[6-11] and biological and chemical sensing. The nanostructure mediated drug delivery is a key technology for the realization of nano-medicine and plays an important role in improving the properties of already existing therapeutic and diagnostic modalities. The nanoscale drug delivery system also helps in stabilizing drug molecules[12,13].

A wide range of materials have been employed as drug carriers such as lipids, surfactant, dendrimers and natural or synthetic polymers[14-17]. Among these, polysaccharides have received increasing interest because of their outstanding physical and biological properties[18]. This cationic polysaccharide has drawn increasing attention within biomedical applications, owing to its abundant availability, unique muco-adhesive, and inherent pharmacological and biological properties such as biocompatibility, biodegradability, non-toxicity and low-

immunogenicity[19–21]. The grafting of glycolic acid on chitosan leads to marked changes in its structure[22, 23].

4.2 Experimental

4.2.1 Materials

Chitosan (M_w = 1.5×10^5) 85% degree of deacetylation, glycolic acid (99% purity), oleic acid (OA), oleylamine (OAM), 1-octadecene iron (0) pentacarbonyl ($Fe(CO)_5$), 1, 2-tetradecanediol and cyclophosphamide (CPA) drug was obtained from Sigma Aldrich. Gold chloride ($HAuCl_4$), 3-(4,5-dimethylthiazol-2-yl)-2,5-diphenyltetrazolium bromide (MTT) and Phenyl ether was obtained from Sisco Research Laboratories.

4.2.2 Synthesis of Au-Fe_3O_4 hybrid nanoparticles (AFNP)

Au-Fe_3O_4 hybrid nanoparticles were synthesized in this work with reference to the literature[24]. First AFNP was prepared by the thermal decomposition of $HAuCl_4$ at high temperature. 1mmol of $HAuCl_4$ and 9mmol OAM were added to 20 ml phenyl ether. It is followed by the addition of 4mmol of 1, 2-tetradecanediol. The reaction mixture was heated slowly upto 185 ^{0}C for 1.5 h under inert atmosphere. The reaction mixture was then cooled down to room temperature and precipitated with ethanol. After centrifugation, precipitate was dried and redispersed in 20 ml of hexane containing 10 mM OAM. In the step, OA, OAM and 1-octadecene were heated 100 ^{0}C under argon atmosphere. The AFNP dispersed in hexane was injected at this temperature, followed by flushing with argon (to remove hexane) and then heated to 120 ^{0}C, at which $Fe(CO)_5$ was injected. The reaction mixture was slowly heated to reflux (1^{0}C min^{-1}) for 4.5 h. After cooling to room temperature, the reaction mixture was stirred for 1 h, followed by precipitation with acetone and then dried in air **(Scheme 4.1)**.

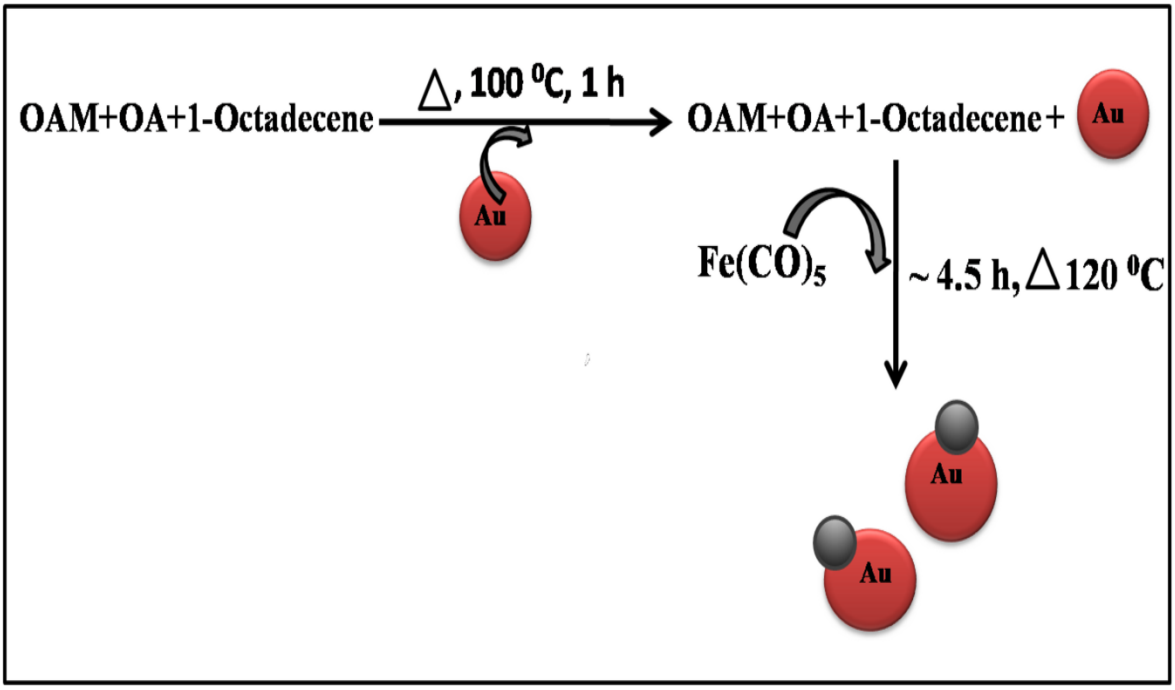

Scheme 4.1 *Synthesis of Au/Fe_3O_4 hybrid nanoparticles.*

4.2.3 Preparation of nanohybrid scaffolds and drug loading

Chitosan-g-glycolic acid and Au-Fe_3O_4 nanoparticle nanocomposite film was prepared by dispersing chitosan in deionised water for 1h with constant stirring at room temperature. Glycolic acid was added to the solution after 1h, which is allowed to stir for 12h. After 12h, Au-Fe_3O_4 hybrid nanoparticles were added to the resulting solution and stirred overnight at room temperature. The solution was heated upto 80 ^{0}C with continuous degassing for 45 min. The Solution was cooled to room temperature after degassing, which is followed by CPA addition 20 mg and stirred for 5 h, so that drug completely mixes with solution. After 5 h, solution was poured in tissue culture plates (50×50 mm diameter). The drug loaded solution was quenched in liquid nitrogen and freeze dried by lyophilisation under -100 ^{0}C temperature for 6 h **(Scheme 4.2)**. The formulations are shown in the **Table 4.1**. In lyophilisation water molecules were removed by freezing and sublimation of ice crystals, which lead to the formation of pores. The polymer-rich phase forms the cell walls around the pores[25].

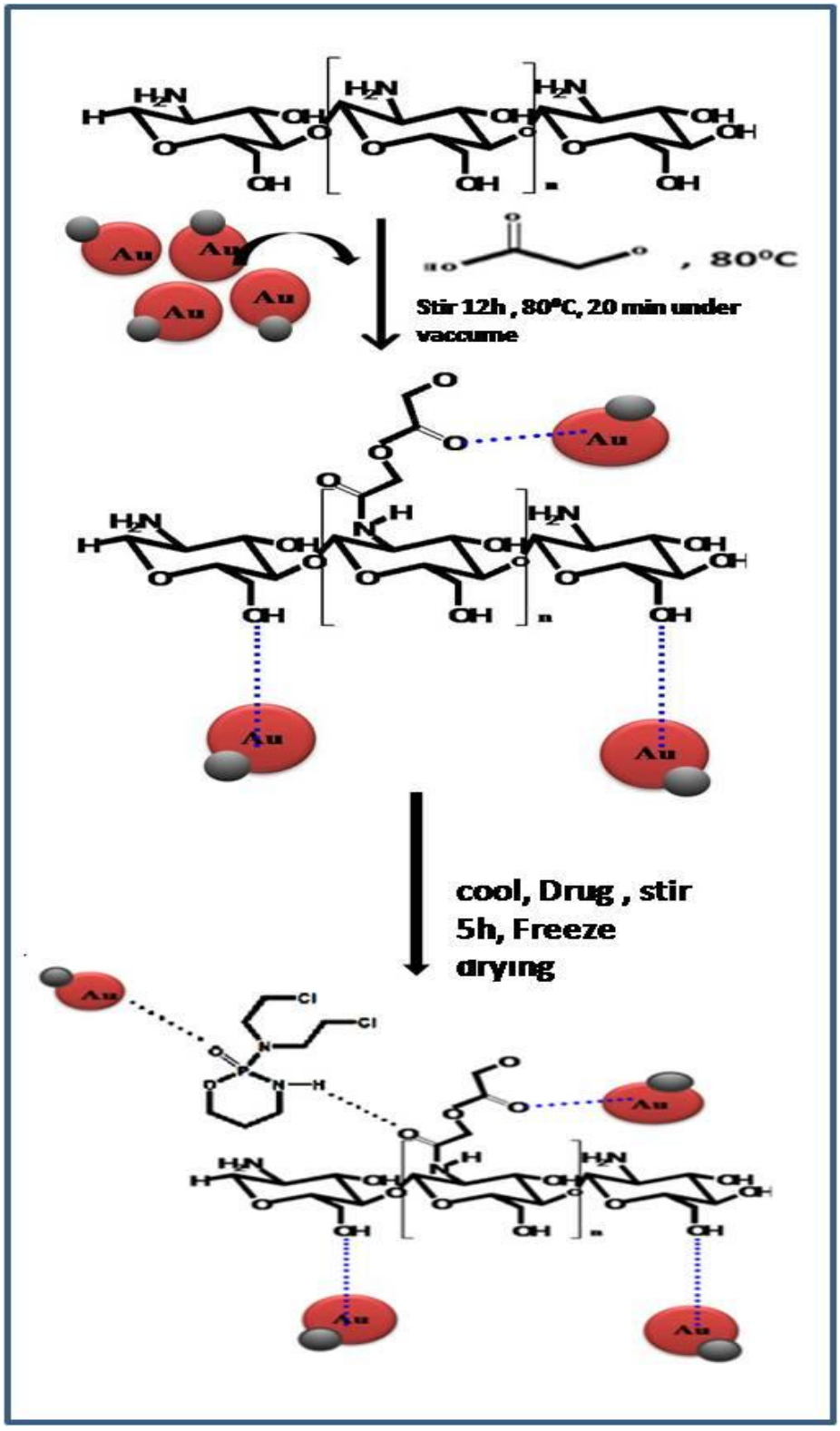

Scheme 4.2 *Schematic illustration of grafting of glycolic acid on chitosan, formation of Chitosan-g-glycolic acid-Au-Fe_3O_4 hybrid nanoparticles based nanohybrid scaffold and interaction between chitosan-g-glycolic acid, drug and Au nanoflowers*

Table 4.1 Formulation of cyclophosphamide (CPA)-loaded nanohybrid of chitosan-g-glycolic acid and Au-Fe_3O_4 hybrid nanoparticles

S.No	Chitosan (g)	Glycolic acid (g)	AFNP (mg)	CPA (mg)	Drying Process	Sample code
1	1	1	_	_	Vacuum	CGAF-1
2	1	1	50	_	Vacuum	CGAF-2
3	1	1	50	10	Freeze	CGAF-(D)

4.3 CHARACTERIZATION OF NANOHYBRID

4.3.1 Transmission electron microscopy (TEM)

The surface morphology, selected area diffraction pattern of Au-Fe_3O_4 hybrid nanoparticles can be investigated with High Resolution Transmission Electron Microscpy (HR-TEM model Technai TF30, 300KV FEG). The samples of Au-Fe_3O_4 hybrid nanoparticles for TEM studies were prepared by placing drop on carbon coated copper grids.

4.3.2 Physical property measuring system (PPMS)

The formation of Au-Fe_3O_4 hybrid nanoparticles was also determined by measuring hysteresis loops of the synthesised nanoparticles from physical property measuring system (PPMS) (quantum design Inc. San Diego, USA) equipped with 7T superconducting magnet and a vibrating sample magnetometer.

4.3.3 Fourier transform infrared spectroscopy (FT-IR)

ATR-FTIR spectroscopy of neat chitosan (CT), chitosan grafted glycolic acid (CGAF-1), nanohybrid scaffold (CGAF-(D)) and drug (CPA) were performed over a range of 4000-400 cm^{-1} at a resolution of 2 cm^{-1} using a Nicolet spectrometer system.

4.3.4 Scanning electron microscopy (SEM)

Surface morphology of the samples were analysed with Scanning Electron Microscpy (SEM) (Model: JOEL Stereoscan 440, Cambridge). Prior to the observation, specimens were fixed on the copper grid.

4.3.5 Swelling behaviour

The swelling behaviour of porous scaffold was determined by exposing them to media of different pH: 1N HCl, 1N NaOH and simulatedbody fluid (SBF, pH 7.4) solutions. Shape retention of the porous scaffold was determined by measuring the change in the diameter as a function of time in the media.

4.3.6 In vitro drug release

The drug loaded nanohybrid scaffold (CGAF-(D)) were immersed in 10 ml of aliquots of 0.1 M phosphate buffer (pH 7.4) and incubated at 37 ^{0}C. After specific interval, 3 ml aliquot of the specimen were withdrawn and immediately fresh medium is added to it. Drug content in each aliquot was quantitatively analysed by UV-vis spectrophotometer (UV-NIR- PL Lamda 950) at 180 nm.

4.3.7 In vitro cell culture study

In vitro cell culture was carried out using L929 cell. These cells are derived from an immortalized mouse fibroblast cell line, is internationally recognized cells that are routinely used in *in-vitro* cytotoxicity assessments. The scaffold was sterilised by putting it in 6 well tissue culture plate containing isopropanol (5 ml) and exposed to UV radiation for 4 h. L929 cells were further seeded on nanohybrid scaffold placed in 6-well plate at a density of 5×10^{3} cells/well and incubated at 37 °C, 5% CO2 and 95% humidity incubation conditions. The tissue culture plate containing only cells were used as control.

4.3.8 Cell proliferation assay

To study the cell proliferation on different substrates, cell proliferation was determined by the colorimetric MTT assay. MTT assay is based on the reduction of yellow 3-(4,5

dimethylthiazol-2-yl)-2,5-diphenyltetrazolium bromide (MTT) salt in MTT to form purple formazan by dehydrogenase enzymes secreted from the mitochondria of metabolically active cells. The amount of formazan formed is directly proportional to the number of viable cells. After 2 h, 4 h, 6 h, 24 h, 48 h, 72 h, the cells solution (100 µl) was transferred to an ELISA micro-plate and optical density (OD) was measured at 540 nm using the spectroscopic method[26]. The relative cell growth was compared to control cell, which exhibit cell culture medium (isopropanol and L929 cells) without chitosan. It was calculated by using the given eq. (1)

$$\% \text{ Live cell} = 100 - \left[\frac{(C - T)}{(C - B)} \times 100 \right] \quad (1)$$

C = OD of control

T = OD of test sample

B = OD of blank

OD = Optical density

All the in vitro tests were done in triplicate and results were reported as an average value.

4.4 RESULTS AND DISCUSSION

4.4.1 Morphological study of Au-Fe_3O_4 hybrid nanoparticles

The TEM image of Au-Fe_3O_4 hybrid nanoparticle (**Figure 4.1**(a)) exhibit spherical morphology. **Figure 4.1** (b) shows the high resolution image of Au-Fe_3O_4 hybrid nanoparticles, which confirms that the two lattices are indeed commensurate. The distance between the two adjacent lattice planes in Au domain is 2.35Å, consistent with the reported value of 2.35Å for (1 1 1) plane and that in Fe_3O_4 domains 4.88Å, consistent with the literature value of 4.88Å for (1 1 1) faces. Selected area diffraction pattern (SAED) also shows crystallinity of hybrid nanoparticle (**Figure 4.1** (c)). **Figure 4.1** (d) shows TEM-

EDAX of hybrid nanoparticle, which confirms the formation of Au-Fe_3O_4 hybrid nanoparticles.

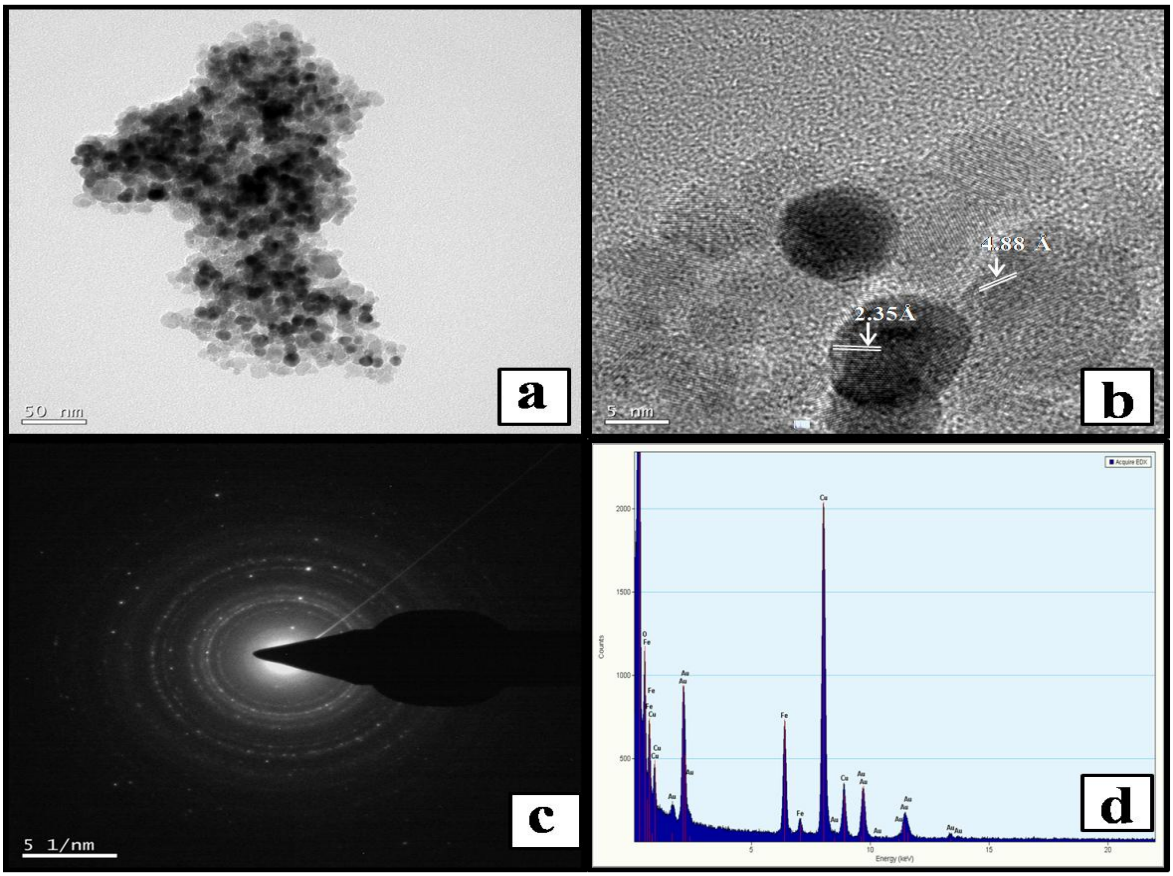

Figure 4.1 *(a) TEM image Au/Fe_3O_4 hybrid nanoparticles; (b) HRTEM image of Au-Fe_3O_4 hybrid nanoparticles (White line delineates distance between two lattice plane in Au domain and Fe_3O_4 domain); (c) SAED pattern of Au-Fe_3O_4 hybrid nanoparticles; (d) TEM-EDAX of Au-Fe_3O_4 hybrid nanoparticles.*

4.4.2 Physical property measurement system (PPMS) analysis

The magnetic properties of the hybrid nanoparticles were investigated to evaluate the influence of the diamagnetic Au on Fe_3O_4 domains. **Figure 4.2** shows magnetic hysteresis loops recorded at 300 k of Au-Fe_3O_4 hybrid nanoparticle with Fe_3O_4 nanoparticle of size 5-10nm. Hybrid nanoparticles are super paramagnetic, however, the saturation magnetization decreases with Au particles[27]. The decrease in the magnetization of Au-Fe_3O_4 hybrid nanoparticle confirms the formation of Au-Fe_3O_4 hybrid nanoparticles.

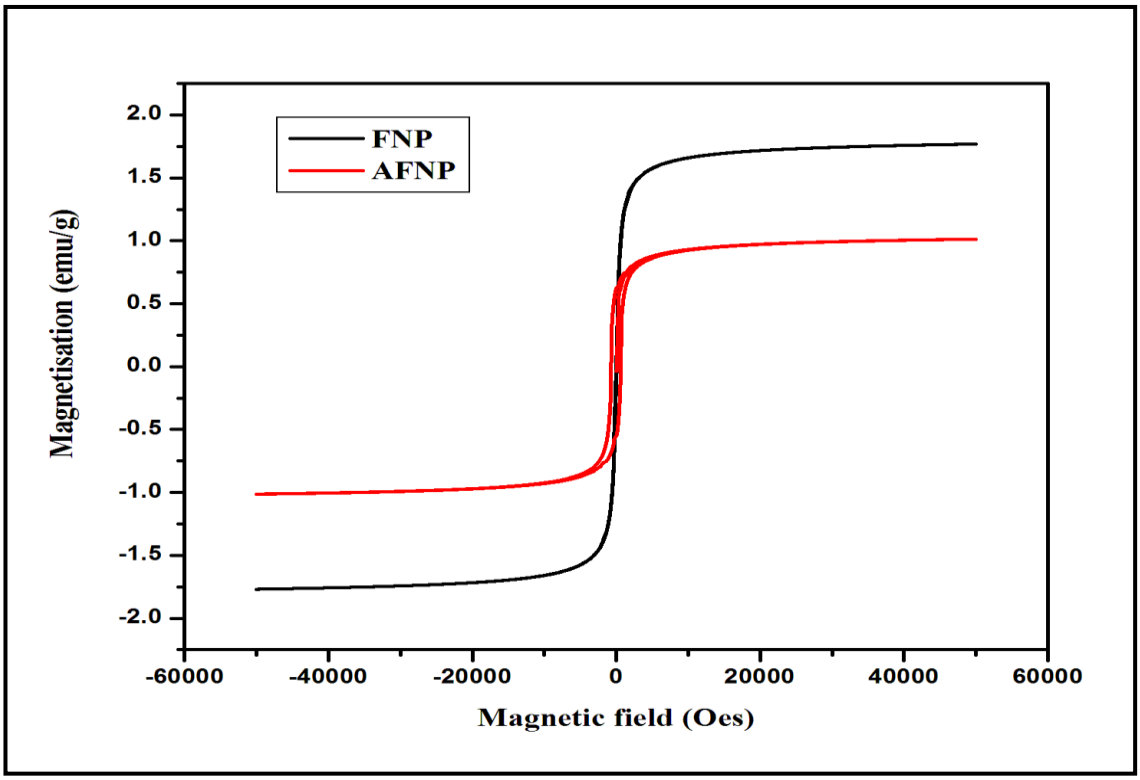

Figure 4.2 *Magnetic hysteresis curve recorded at 300k of Au-Fe_3O_4 hybrid nanoparticle (AFNP) with Fe_3O_4 nanoparticles (FNP).*

4.4.3 Fourier transform infrared (FT-IR) analysis

Figure 4.3 shows the FTIR spectra of CT, CGAF-1, CGAF-(D) and CPA. The characteristic peaks in the FTIR spectrum of CT indicate 1632 cm^{-1} (-NH stretching) and 3500cm^{-1} (-OH stretching). The presence of extra peak at 1734 cm^{-1} (-C=O stretching) and shifting of peak (-NH stretching) towards the lower frequency region (1572 cm^{-1}) confirms the interaction of glycolic acid with NH_2 group of chitosan. The grafting of glycolic acid on chitosan was confirmed by the formation of amide (–NH-C=O) linkage between amine (-NH_2) group of chitosan and –C=O group of glycolic acid. In the FTIR spectrum of CPA the peak at 1237 cm^{-1} (-P=O stretching) and 1654 cm^{-1} (-NH stretching) are observed. The FTIR spectrum of CGAF-(D) include shift in peak 1067 cm^{-1} (-P=O stretching) and 3190 cm^{-1} (-OH stretching) it may due to the interaction of Au-Fe_3O_4 hybrid nanoparticles with –P=O group of drug molecule and –OH group of chitosan via metallic bond. The peak at 1565 cm^{-1}

in CGAF-(D) is attributed to shift in –C=O stretching towards lower frequency region, it may be due to the interaction of CPA with –C=O group of grafted glycolic acid via H- bonding.

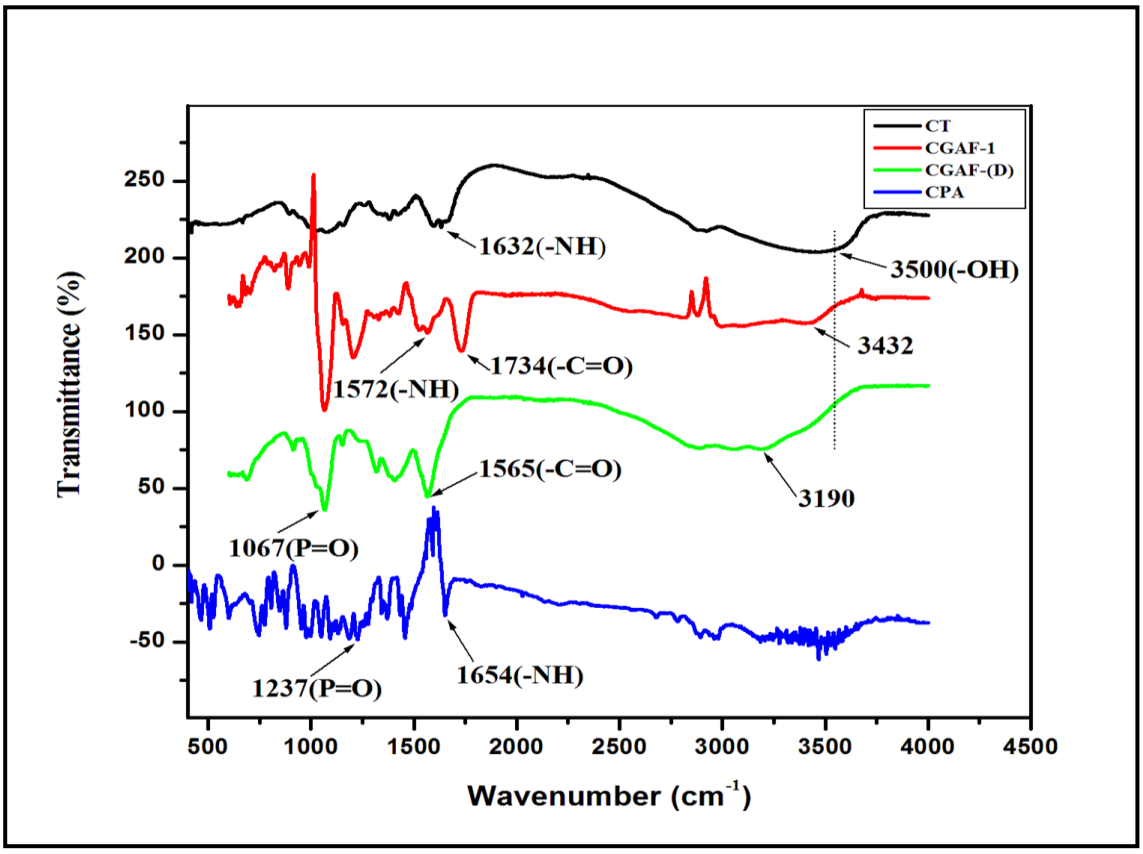

Figure 4.3 *FTIR spectra of neat chitosan (CT), grafted chitosan (CGAF-1), grafted chitosan and Au-Fe_3O_4 nanohybrid scaffold (CGAF-(D)) and drug Cyclophosphamide (CPA).*

4.4.4 SEM observation of scaffolds

Figure 4.4 shows SEM image of nanohybrid scaffolds before drug (**Figure 4.4** (a, b)) loading and after drug addition (**Figure 4.4** (c, d)). It is observed that pore size of scaffold before drug addition was ranging from 3.37 to 5.28 µm, but upon addition of drug pore size decreases and lies in the range of 3.4µm to 4.9 µm. The decrease in the pore size may be due to the incorporation of drug molecule in the pores of scaffold. **Figure 4.4** (e) SEM-EDAX of scaffold confirms the incorporation of Au-Fe_3O_4 hybrid nanoparticles in it.

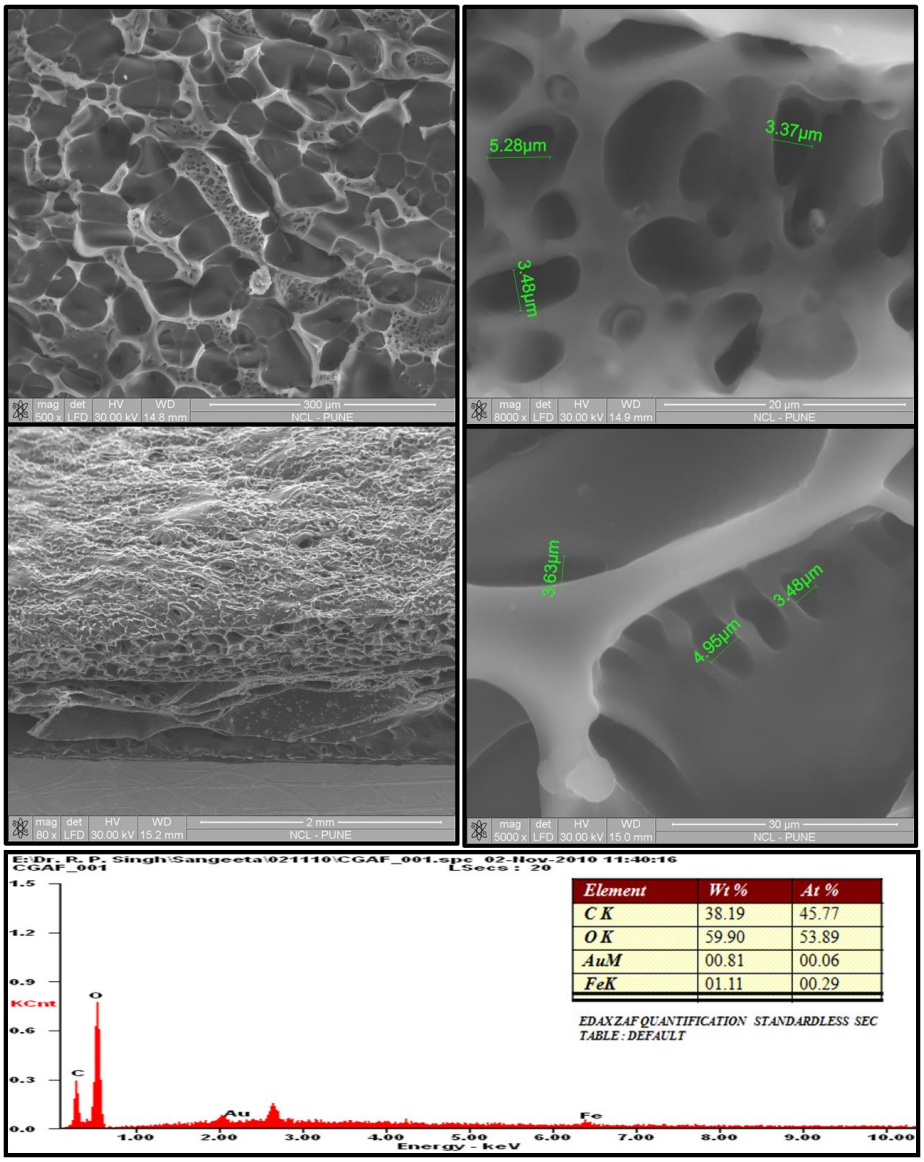

Figure 4.4 (a, b) SEM image of grafted chitosan and Au-Fe_3O_4 nanohybrid scaffold without drug; (c, d) SEM image of grafted chitosan and Au-Fe_3O_4 nanohybrid scaffold with drug; (e) EDAX of nanohybrid scaffold(CGAF- (D)).

4.4.5 Swelling behavior of scaffold

Structural stability and swelling behavior of scaffold strongly depends upon the pH of the implantation site for their practical use in tissue engineering. Swelling behavior of scaffold was investigated by exposing it to media at different pH: 1N HCl, 1N NaOH and simulated body fluid (SBF) (pH 7.4) solutions for 24 h.

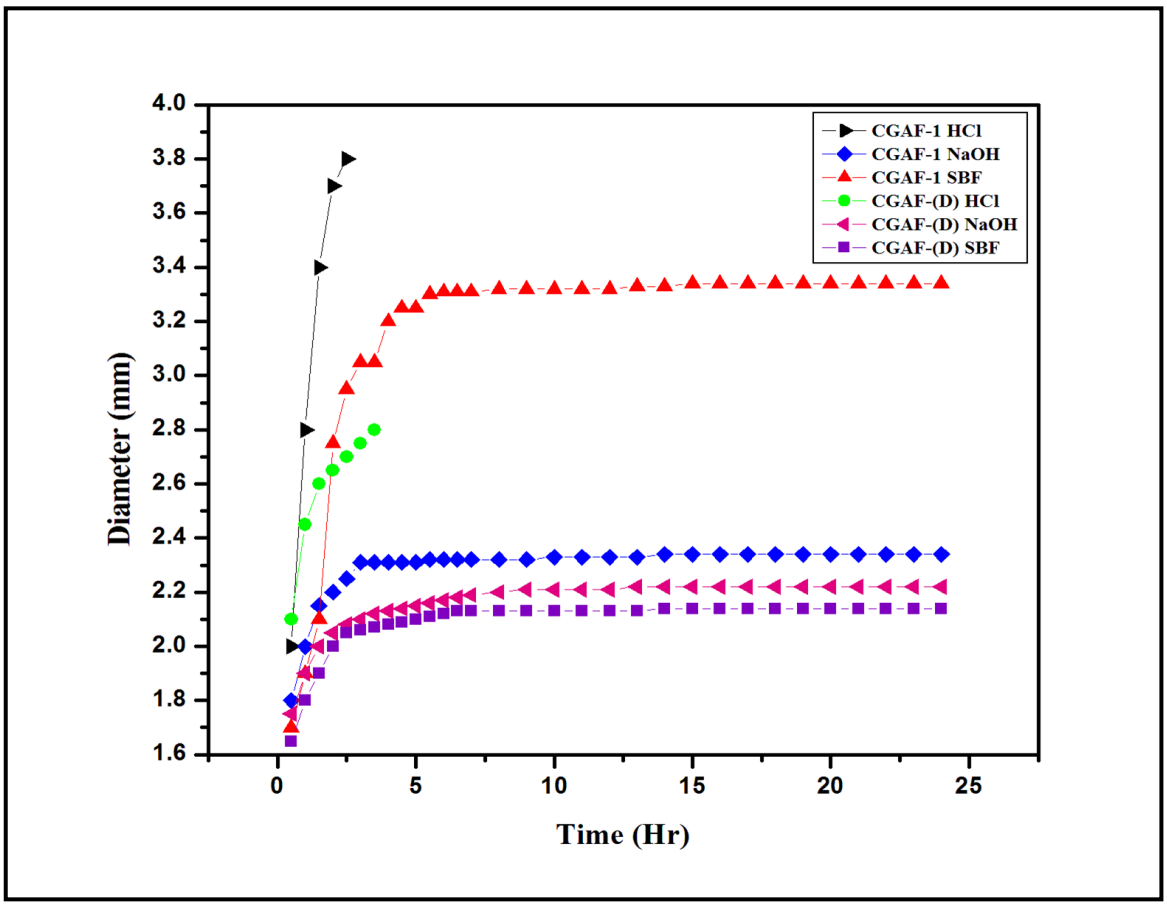

Figure 4.5 *Shape retention of scaffolds prepared from grafted chitosan and Au-Fe_3O_4 nanohybrid.*

The shape retention of scaffold was determined by measuring the change in the diameter as a function of immersion time in the media (**Figure 4.5**)[28]. Swelling of chitosan involves the protonation of amino/imine groups and the mechanical relaxation of coiled chitosan chain[29,30]. The in vitro cell culture studies indicate that initial swelling is desirable[31,32] but continuous swelling reduces the mechanical integrity and leads to the generation of compressive stress to the surrounding tissue. In acidic medium, scaffold (CGAF-1) are dissolved completely within 2.5 h of immersion, whereas in basic medium (NaOH) rate of swelling is very low and reach the plateau level around 3 h of immersion but size of scaffold is found to increase within 3.5 h in SBF solution, whereas nanohybrid scaffold (CGAF-(D)) dissolves completely in HCl within 3.5 h. Nanohybrid scaffold slight swelling was observed

in NaOH and SBF within 5 h. These results reveal that the nanohybrid scaffold (CGAF-(D)) is stable towards the SBF and higher pH solution.

4.4.6 Drug release study

Figure 4.6 illustrates the variation in absorbance of drug loaded scaffold with respect to time. In vitro drug release was investigated with SBF (pH 7.4) and release media was quantified by UV-visible spectral absorbance values. Initially the release of drug from freeze dried scaffold can be observed to be faster and higher and release of drug decreases with time.

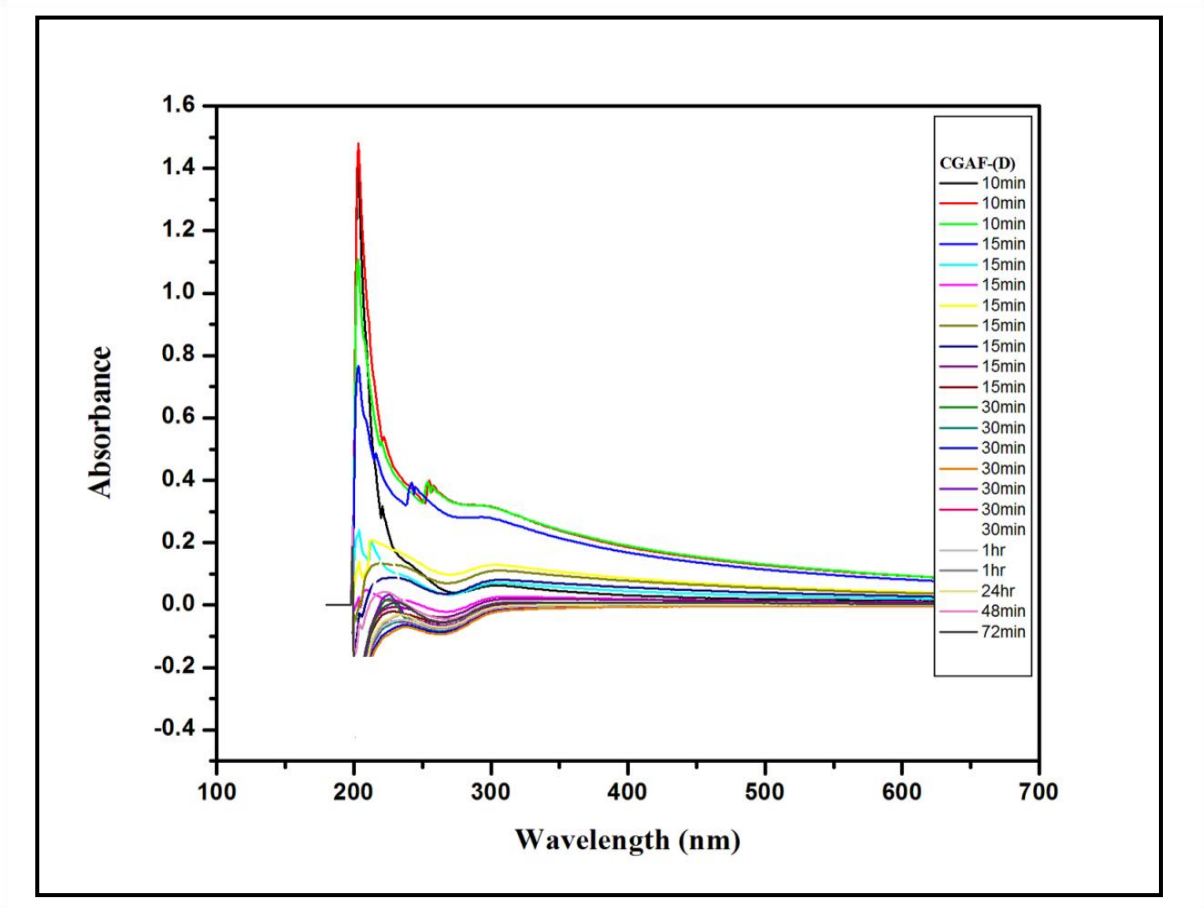

Figure 4.6 *Drug release profile from the prepared nanohybrid scaffold (CGAF- (D)).*

This is because the drug which is present on the surface of the scaffold is released much faster than the drug embedded deeply into the pores of scaffold. The incorporation of Au-Fe_3O_4 hybrid nanoparticle effect can be significantly observed as reduced rate of release at

initial stage of immersion (upto 200 min). The specimen is solvated initially, which facilitates the lateral diffusion of drug[33] after 250min, The rate of release of drug decrease over the time, it may be due to the interaction of Au-Fe_3O_4 hybrid nanoparticle and grafted glycolic acid chains with the loaded drug[34].

4.4.7 Cell viability study

MTT assay was carried out to evaluate the proliferation of L929 on (CGAF-(D)). The growth of the cells cultured on the scaffold was higher during the first 2 h but slight decrease in the cell number was observed in next 4 h.

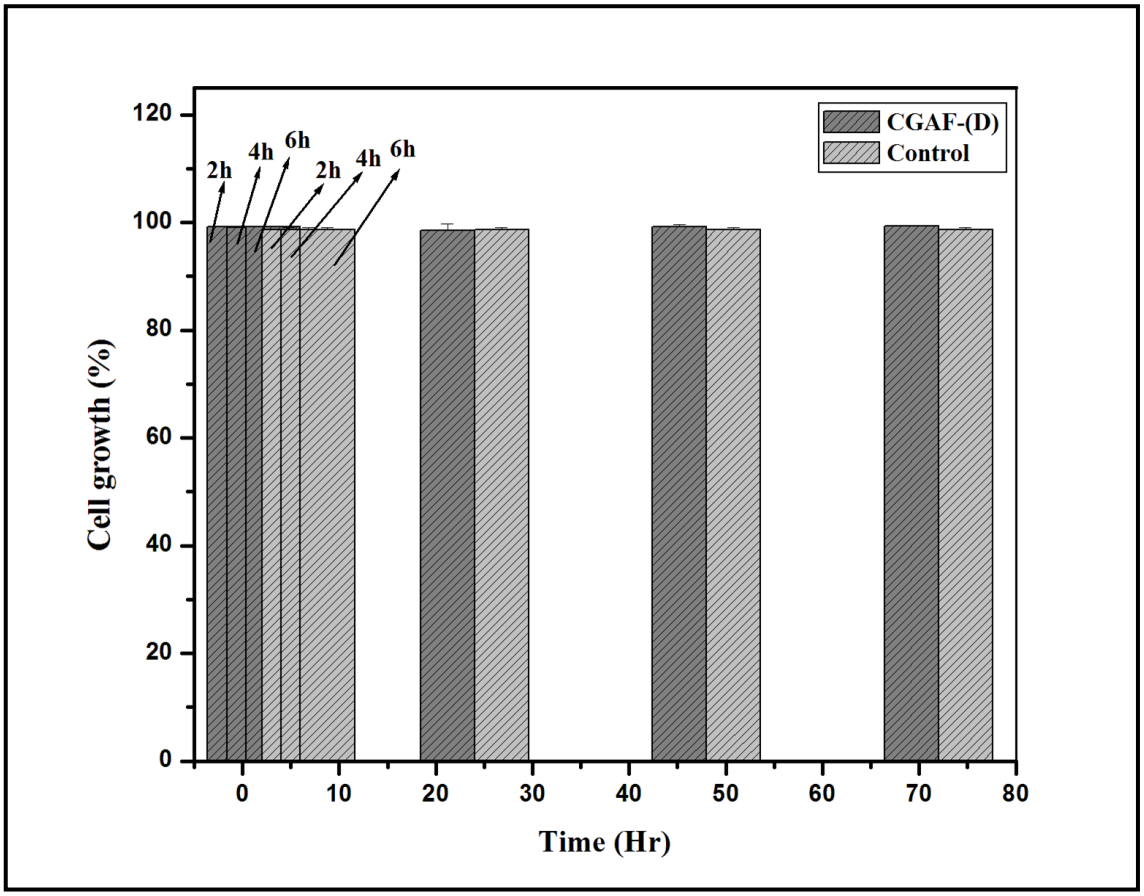

Figure 4.7 *Cell viability study done with MTT assay of cultured cells.*

This may be because during proliferation cells have occupied all the available spaces on the scaffold[34]. The present study implies that cell proliferation is not affected by the incorporation of Au-Fe_3O_4 nanoparticles into glycolic acid grafted chitosan[35]. This may be

due to the enhanced interaction between Au-Fe_3O_4 hybrid nanoparticles and growing cells on the biopolymer matrix (**Figure 4.7**). The results of improved cell adherence and proliferation on scaffold was mainly due to the presence of reactive groups on the polymer surface and improved hydrophillicity after hydrolysis, similar to those reported by other researchers[36]. The Au-Fe_3O_4 hybrid nanoparticles may develop London- van der Waals forces with cells. These Au-Fe_3O_4 hybrid nanoparticles can act as adhesive between biopolymer and cells.

4.5 CONCLUSION

In summary, glycolic acid functionalised chitosan- Au-Fe_3O_4 hybrid nanoparticle based novel nanohybrid scaffold was prepared. The FTIR confirmed the interaction of cationic chitosan with Au-Fe_3O_4 nanoparticles via metallic bond and linkage of drug with the polymer matrix via H-bond. The nanohybrid scaffold posses porous morphology. The nanohybrid scaffolds are stable regardless of pH of the medium. The porous nanohybrid scaffolds have shown faster and higher drug release. Our result demonstrated that glycolic acid functionalised chitosan-Au-Fe_3O_4 hybrid nanoparticle based novel nanohybrid scaffold has promising properties of cell proliferation stimulating ability, which are crucial for a tissue engineering applications.

4.6 REFERENCES

1. H. Maeda, J. Wu, T. Sawa, Y. Matsumura and K. Hori, *J. Control. Rel.*, **65,** 271 (2000).
2. J.H. Thrall, *Radiology.*, 230, 315(2004).
3. H. Cheng, C.J. Kastrup, R. Ramanathan, D.J. Siegwart, M. Ma, S.R. Bogatyrev, Q. Xu, K.A. Whitehead, R. Langer and D.G. Anderson, *ACS Nano.*, **4,** 625 (2010).
4. D. Bahadur and J. Giri, *Sadhana.*, **28,** 639 (2003).

5. P. Pradhan, J. Giri, R. Banerjee, J. Bellare and D. Bahadur, *J. Magn. Magn. Mater.* **311,** 208 (2007).
6. W.B. Tan, S. Jiang and Y. Zhang, *Biomaterials.*, **28,** 1565 (2007).
7. W. Jiang, B.Y. Kim, J.T. Rutka and W.C. Chan, *Nat. Nanotechnol.* **3,** 145 (2008).
8. V. Bagalkot, L. Zhang and E. Levy-Nissenbaum, *Nano Lett.* **7,** 3065 (2007).
9. D.A. LaVan, T. McGuire and R. Langer, Small-scale systems for in vivo drug delivery, *Nat. Biotechnol.*, **21,** 1184 (2003).
10. B. Reinhard, S. Sheikholeslami, A. Mastroianni, A.P. Alivisatos and J. Liphardt, *Proc. Natl. Acad. Sci. U.S.A.*, **104,** 2667 (2007).
11. N.L. Rosi and C.A. Mirkin, Nanostructures in biodiagnostics, *Chem. Rev.*, **105,** 1547 (2005).
12. D.A. LaVan, D.M. Lynn and R. Langer, *Nat. Rev. Drug Discovery* **1,** 77 (2002).
13. H.S. Panda, R. Srivastava and D. Bahadur, *J.Phys. Chem.* **B113,** 15090 (2009).
14. R. Duncan, *Nat. Rev. Drug Discov.* **2,** 347 (2003).
15. R. Duncan, *J. Drug Target* **14,** 333 (2006).
16. V. Torchilin, *Expert Opin. Drug Deliv.* **5,** 1003 (2008).
17. S.G. Sampathkumar and K.J. Yarema, *Chem. Biol.* **12,** 5 (2005).
18. Z. Liu, Y. Jiao, Y. Wang, C. Zhou and Z. Zhang, *Adv. Drug Deliv. Rev.* **60,** 1650 (2008).
19. M.N. Kumar, R.A. Muzzarelli, C. Muzzarelli, H. Sashiwa and A.J. Domb, *Chem. Rev.* **104,** 6017 (2004).
20. L. Illum, *Pharm. Res.* 15, 1326 (1998).
21. O. Felt, P. Buri and R. Gurny, *Drug. Dev. Ind. Pharm.* 24, 979 (1998).
22. M. Xie, H.H Liu, P. Chen, Z.L Zhang, X.H Wang, Z.X Xie, Y.M Du, B.Q Pand and D.W Pang, *Chem. Commun.* 44, 5518 (2005).

23. J. Xie, Q. Zhang, J.Y Lee and D.I.C Wang, *ACS Nano.*, 2, 2473 (2008).

24. Y. Wei, R. Klajn, A.O. Pinchuk and B.A. Grzybowski, *Smal.,l* 4, 1635 (2008).

25. R.L. Hong and J.Y. Yu, *Appl. Biomater.*, 71B (2004) 52-65.

26. T. Takahashi and M. Yamaguchi, *J. Colloid Interface Sci.*, **146,** 556 (1991).

27. T.D. Schladt, M.I. Shukoor, K. Schneider, M.N. Tahir, F. Natalio, I. Ament, J. Becker, F.D. Jochum, S. Weber, O. Köhler, P. Theato, L.M. Schreiber, C. Sönnichsen, C. Schröder, W.E.G. Müller and W. Tremel. *Angew Chem.*, **49,** 3976 (2010).

28. D. Depan, A.P. Kumar and R.P. Singh, *Acta Biomaterialia.*, **5,** 93 (2009).

29. L. Vachoud, N. Zydowicz and A. Domard, *Carbohydrate Res.* **326,** 295 (2000).

30. S. Aiba, *Int. J. Biol. Macromol,.* **13,** 40 (1991).

31. L.M. Liz-Marzan, *Mater Today.*, **7,** 26 (2004).

32. N. Shanmugasundram, P. Ravichandaran, P.N. Reddy, N. Ramamurth, S. Pal and K.P. Rao, *Biomaterials.*, **22,** 1943 (2001).

33. T. Takahashi and M. Yamaguchi, *J. Colloid Interface Sci.* **146,** 556 (1991).

34. S.I Park and Y. Zhao, *J. Agric. Food Chem.* **52,** 1933 (2004).

35. T. Takahashi and M. Yamaguchi, *J. Colloid Interface Sci.* **146,** 556 (1991).

36. F. Chen, C.N. Lee and S.H. Teoh, *Mater. Sci. Eng. C.*, **27,** 325 (2007).

CHAPTER 4

B: Preparation and Characterization of Glycolic Acid-g-Chitosan-Au-Fe_3O_4 Hybrid Nanoparticles Based Nanocomposite Films

4.2.1 INTRODUCTION

In the recent years, development of organic–inorganic hybrids has also been another field of research in preparing biocomposite/ biomimetic materials. The Metallic and metal oxide nanoparticles have become an area of growing interest for fundamental studies and technological applications, due to their unique mechanical, electronic, chemical, magnetic and optical properties[1-6]. Recently, polymer-nanoparticle composite and multifunctional hybrid materials[7] are finding increasing interest in biological system and material science, due to their synergistic and hybrid properties. These nanocomposites of inorganic materials in polymer matrices have wide area of applications such as micromechanical devices[8], optical device[9], catalytic, biosensors[10] and membrane[11]. Several methods for the preparation of multicomponent nanoparticles have been reported[12-20]. Thus, it will be worthwhile to develop a new biocomposite materials based on glycolic acid grafted onto chitosan with improved mechanical, thermal and tensile properties. Chitosan is a biodegradable, biocompatible and nontoxic biopolymer that exhibit excellent film forming ability[21, 22]. The physicochemical and biological properties of chitosan are greatly influenced by its molecular weight and degree of deacetylation. The grafting of glycolic acid on chitosan leads to marked changes in its structure[23, 24].

In this chapter, we are interested to prepare macromolecular organic–inorganic hybrids of Au/ Fe_3O_4 hybrid nanoparticles and chitosan grafted with glycolic acid. It involves grafting of glycolic acid on chitosan in the presence of Au/ Fe_3O_4 hybrid nanoparticles without using any catalyst and using water as solvent. It is also expected that grafted glycolic acid chains may act as internal plasticizers to reduce the brittleness of chitosan films to obtain more soft and elastic film and this will introduce side chains and thus make various molecular designs

possible, affording novel types of tailored hybrid materials composed of natural polysaccharide and grafted polymer.

4.2.2 EXPERIMENTAL

4.2.2.1 Materials

Chitosan of low molecular weight (Mw=1.5×10^5, degree of deacetylation was 85%), glycolic acid (99% pure), iron (0) pentacarbonyl (Fe $(CO)_5$), oleic acid (OA), oleylamine (OAM) and 1-octadecene was obtained from Sigma Aldrich. Phenyl ether and gold chloride ($HAuCl_4$) was obtained from M/s Sisco Research Laboratories. Deionised water was used throughout the work, which is obtained from a Milli-Q system.

4.2.2.2 Preparation of chitosan-g-glycolic acid and Au/ Fe_3O_4 hybrid nanoparticle nanocomposite film

Glycolic acid grafted chitosan (1g) (Discussed in **chapter 3B. section 3.2.2.3**) was dispersed in deionised water (50 ml) and stirred for 1 h with constant stirring at room temperature. After 1 h, Au/ Fe_3O_4 nanoparticles (50 mg) (Synthesis of Au/ Fe_3O_4 nanoparticles is discussed in **chapter 4A**. **section 4.2.2**) were added to the solution and stirred overnight at room temperature. The resulting solution was heated up to 80 ^{0}C with continuous degassing for 45 min. The solution was casted on a glass plate and dried at 60 ^{0}C for 8 h to promote dehydration of grafted chitosan copolymer with formation of the corresponding amide linkages. To remove the oligomers of glycolic acid and unreacted glycolic acid, the samples were extracted with methanol in soxhlet apparatus for 48 h.

Table 4.2.1 The formulation of chitosan-g-glycolic acid and Au/Fe_3O_4 hybrid nanocrystals

S. No	Chitosan (g)	Grafted Chitosan (g)	Au/Fe_3O_4 (mg)	Sample code
1	1	0	0	CS
2	0	1	0	CGAuF-1
3	0	1	40	CGAuF-2
4	0	1	80	CGAuF-3

The formulation of chitosan and nanoparticle (Au/ Fe_3O_4) are given in **Table 4.2.1.** The thickness of resulting films were measured and found to be about 0.19 mm.

4.2.3 CHARACTERIZATION OF NANOCOMPOSITE FILM

4.2.3.1 Fourier transform infrared spectroscopy

Nicolet Nexus 870 attenuated total reflectance fourier transform infrared (ATR-FTIR) spectrometer equipped with a smart endurance diamond accessory (64 scans, 4 cm^{-1} resolution, wave number range 4000-550 cm^{-1}) was used to analyse neat chitosan (CS), glycolic acid grafted chitosan and glycolic acid grafted chitosan nanocomposite with hybrid Au/ Fe_3O_4 hybrid nanocrystals.

4.2.3.2 X-ray diffraction

XRD patterns of the samples were recorded on X-ray Diffractometer (WAXRD-Rigaku (Japan) with Cu-Kα radiation at a voltage of 50 KV. The scanning was 4 ^{0}/min and the scanning scope of 2θ was 2^0 to 80^0 at room temperature.

4.2.3.3 Atomic force microscopy

The surface morphology of nanocomposite film was studied by atomic force microscopy (AFM) (Model: Nanoscope IV) under contact mode.

4.2.3.4 Tensile strength testing

The tensile strength of the nanocomposite film was determined with Linkam TST 350 instrument. A dumb-bell strip was cut from each membrane and strained to break at a constant crosshead speed of 10 mm/min.

4.2.3.5 Dynamic mechanical analysis

Dynamic mechanical analysis (DMA) was investigated with a dynamic mechanical thermal analyser (DMTA RSA3, TA instrument) in tensile mode at a frequency of 1Hz with heating rate of 5 ^{0}C/min in the temperature range from -10 ^{0}C to 200 ^{0}C.

4.2.3.6 Water absorption measurement

According to ASTM D 570, the clean, dried film samples of known weights were immersed in distilled water at 25 ^{0}C for 24h (1 Day). The films were removed, blotted quickly with absorbent paper and weighed. The absorption percentage of these samples was calculated using the Eq. (1):

$$X\% = (W_1-W_0)/W_0 \quad (1)$$

where W_0 and W_1 are the weight of dry and swollen samples respectively.

4.2.3.7 Thermogravimetric analysis

Thermogravimetric analysis (TGA) of the sample was conducted with TGA Q5000 instrument. Temperature ranges from 50 ^{0}C to 900 ^{0}C with the heating rate of 10 ^{0}C/min under nitrogen condition with flow rate 20 ml/min.

4.2.4 RESULTS AND DISCUSSION

4.2.4.1 FTIR analysis

Fourier transform infrared (FT-IR) spectra were used to determine the structural information about pure chitosan (CS), glycolic acid grafted chitosan (CGAuF-1) and its nanocomposite with Au/Fe_3O_4 hybrid nanoparticle (CGAuF-2) (**Figure 4.2.1**). The

characteristic peaks in the FTIR spectrum of CS at 1633 cm^{-1} (-NH stretching) and 3500cm^{-1} (-OH stretching). In FTIR spectrum of CGAuF-1, a new peak appeared at 1733 cm^{-1} corresponds to υ_{co} stretching and shifting of peak (-NH stretching) towards the lower frequency region (1575 cm^{-1}) confirms the interaction of glycolic acid with NH_2 group of chitosan. These two peaks confirms the conversion of amine (NH_2) to amide (–NH-C=O). In the FTIR spectrum of CGAuF-2 include shift in peak to 1719 cm^{-1} (-C=O stretching) and 3390 cm^{-1} (-OH stretching) it may due to the interaction of Au/Fe_3O_4 hybrid nanoparticles with –C=O group of glycolic acid and –OH group of chitosan via metallic bond.

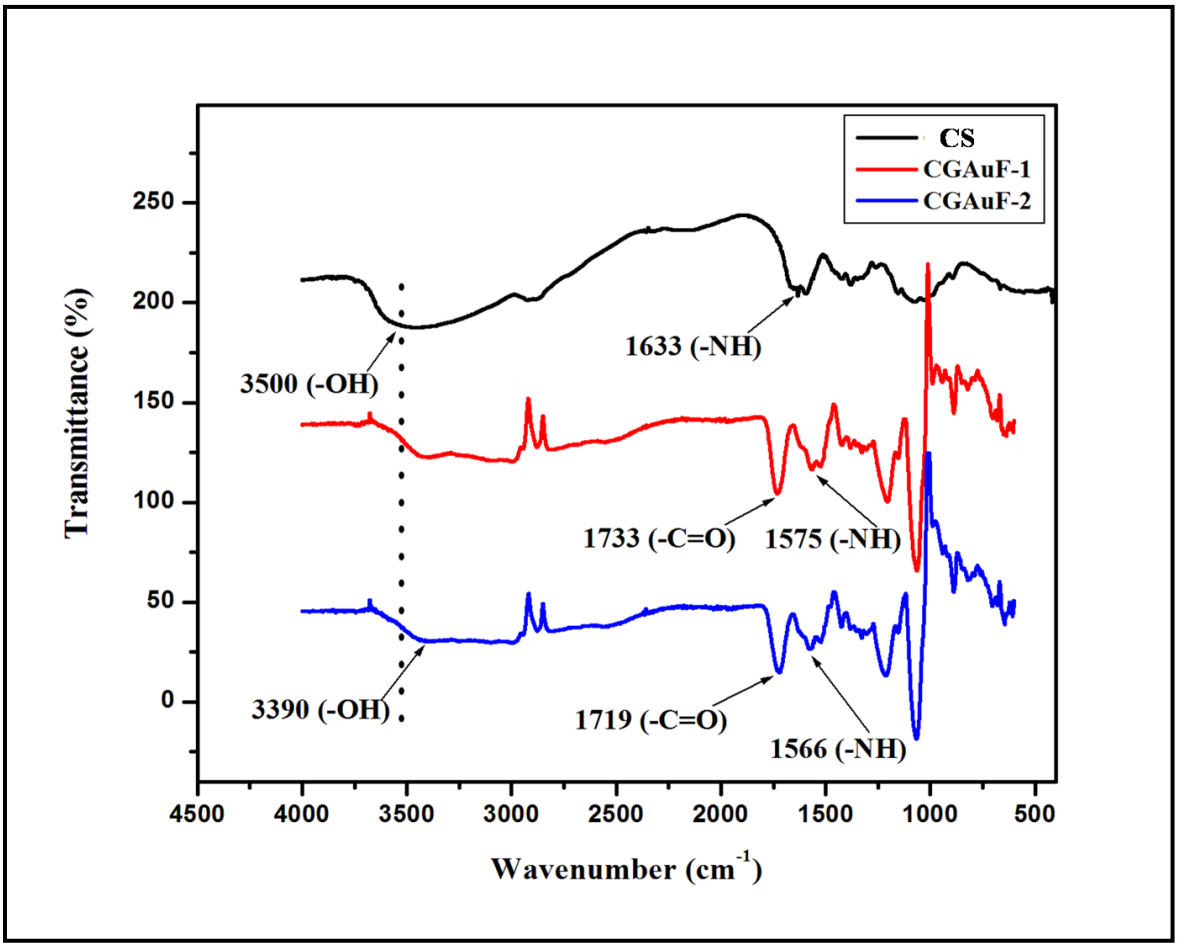

Figure 4.2.1 *FTIR spectra of neat chitosan (CS), grafted chitosan (CGAuF-1) and grafted chitosan-Au/Fe_3O_4 hybrid nanoparticle nanocomposite film (CGAuF-2).*

4.2.4.2 XRD analysis

Figure 4.2.2 shows XRD pattern of pure chitosan (CS), glycolic acid grafted chitosan (CGAuF-1) and CGAuF-1 with Au/Fe_3O_4 hybrid nanoparticle (CGAuF-2) nanocomposite films. The chitosan structure is strongly dependent on its processing treatment, such as dissolving, precipitation and drying, as well as its origin and characteristics, such as degree of deacetylation and molecular weight[27]**.** The neat chitosan film shows the peaks at $2\theta = 10.9^0$ and 19.8^0, corresponds to hydrated crystalline structure and an amorphous structure of chitosan, respectively[28, 29]. In grafted chitosan (CGAuF-1) film XRD peaks were shifted from 10.9^0 to 10.2^0 and 19.8^0 to 20.7^0 confirming the interaction of glycolic acid with chitosan. More shifts in CGAuF-2 nanocomposite film was observed that is, $2\theta = 10.2^0$ to 9.4^0 and 20.7^0 to 220.8^0. This is probably due to higher compatibility of the Au/Fe_3O_4 nanoparticle with the grafted chitosan matrix.

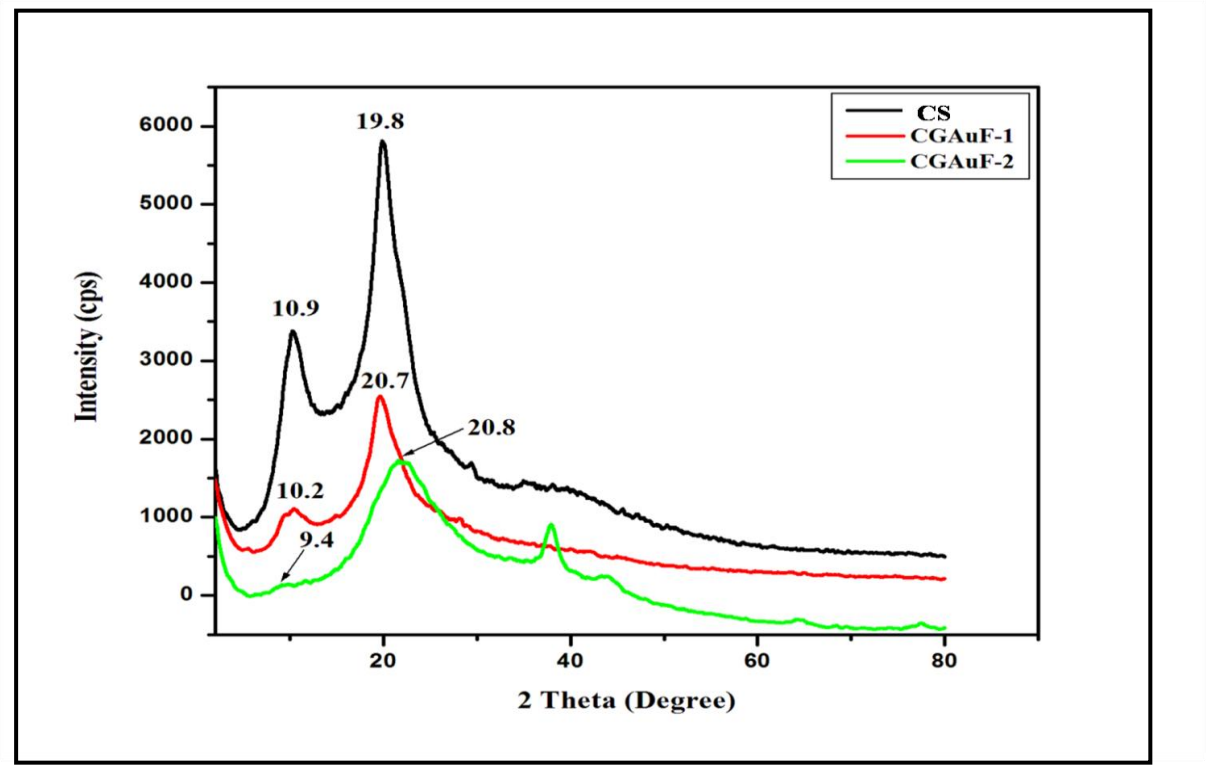

Figure 4.2.2 *X-ray diffraction spectra of neat chitosan, grafted chitosan and grafted chitosan/Au-Fe_3O_4 hybrid nanoparticle nanocomposite films.*

4.2.4.3 Morphological study

Atomic Force Microscopy (AFM) illustrates the surface topography of pure chitosan, grafted chitosan and nanocomposite film. **Figure 4.2.3** (a) shows the AFM image of chitosan film with smooth surface. Upon grafting the chitosan, roughness and height of the film surface were also increased (**Figure 4.2.3** (b)). The incorporation of Au/Fe_3O_4 composite nanoparticle in the matrix of chitosan film is shown in **Figure 4.2.3** (c, d).

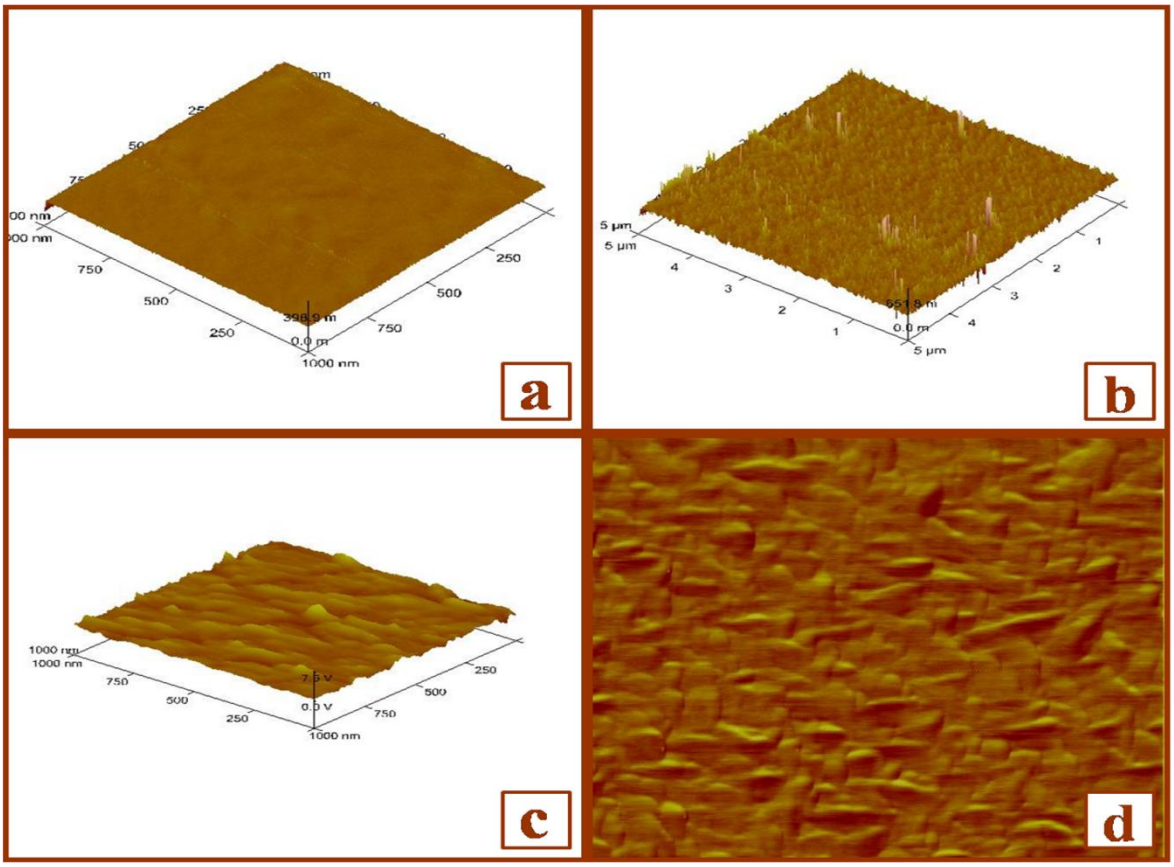

Figure 4.2.3 *(a) AFM image of pure chitosan film; (b) AFM image of grafted chitosan film. (c, d) AFM image of grafted chitosan/Au-Fe_3O_4 hybrid nanoparticle nanocomposite films.*

4.2.4.4 Tensile stress testing

Figure 4.2.4 (a, b) shows the tensile behavior of pure chitosan (CS), glycolic acid grafted chitosan (CGAuF-1) and CGAuF-1 with Au/Fe_3O_4 hybrid nanoparticle (CGAuF-2)

nanocomposite films. These membranes were semi-transparent and had uniform thickness of 0.19 mm. The tensile properties varied significantly with the crosshead speed. Crosshead speed used while testing is 10 mm/min at 27 ^{0}C. The elastic modulus of CS was observed to be 0.9855 MPa and it poses a break strain at 25- 26 %. In CGAuF-1 decrease in elastic modulus is observed. Incorporation of Au/Fe_3O_4 composite nanoparticle in polymer matrix (CGAuF-2) increases the elastic modulus and improves the tensile strength of the polymer film (**Table 4.2.2**).

Table 4.2.2 Tensile strength and testing of chitosan and nanocomposites

Sample Code	Elastic modulus (MPa)	Stress (%)	Strain (%)
CS	0.9855	47.97	25.83
CGAuF-1	0.9556	6.38	83.29
CGAuF-2	0.9727	5.64	126.82

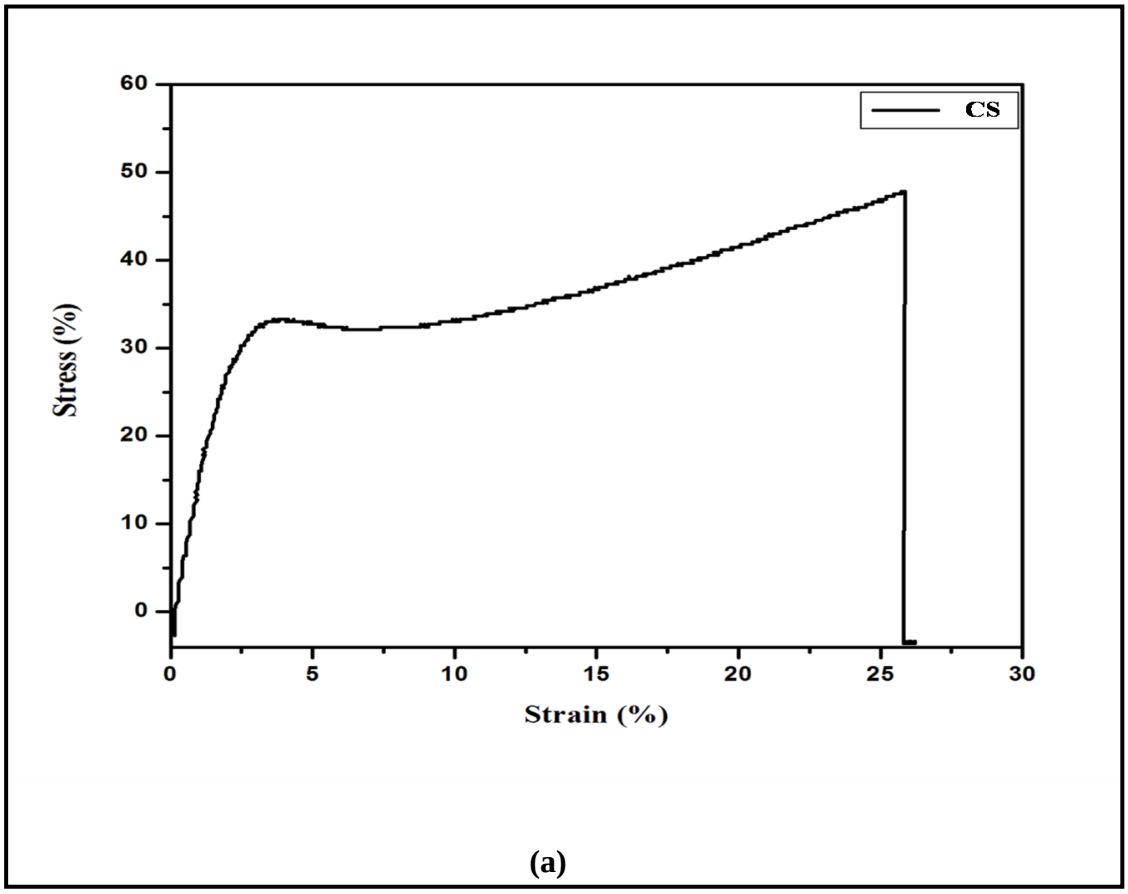

(a)

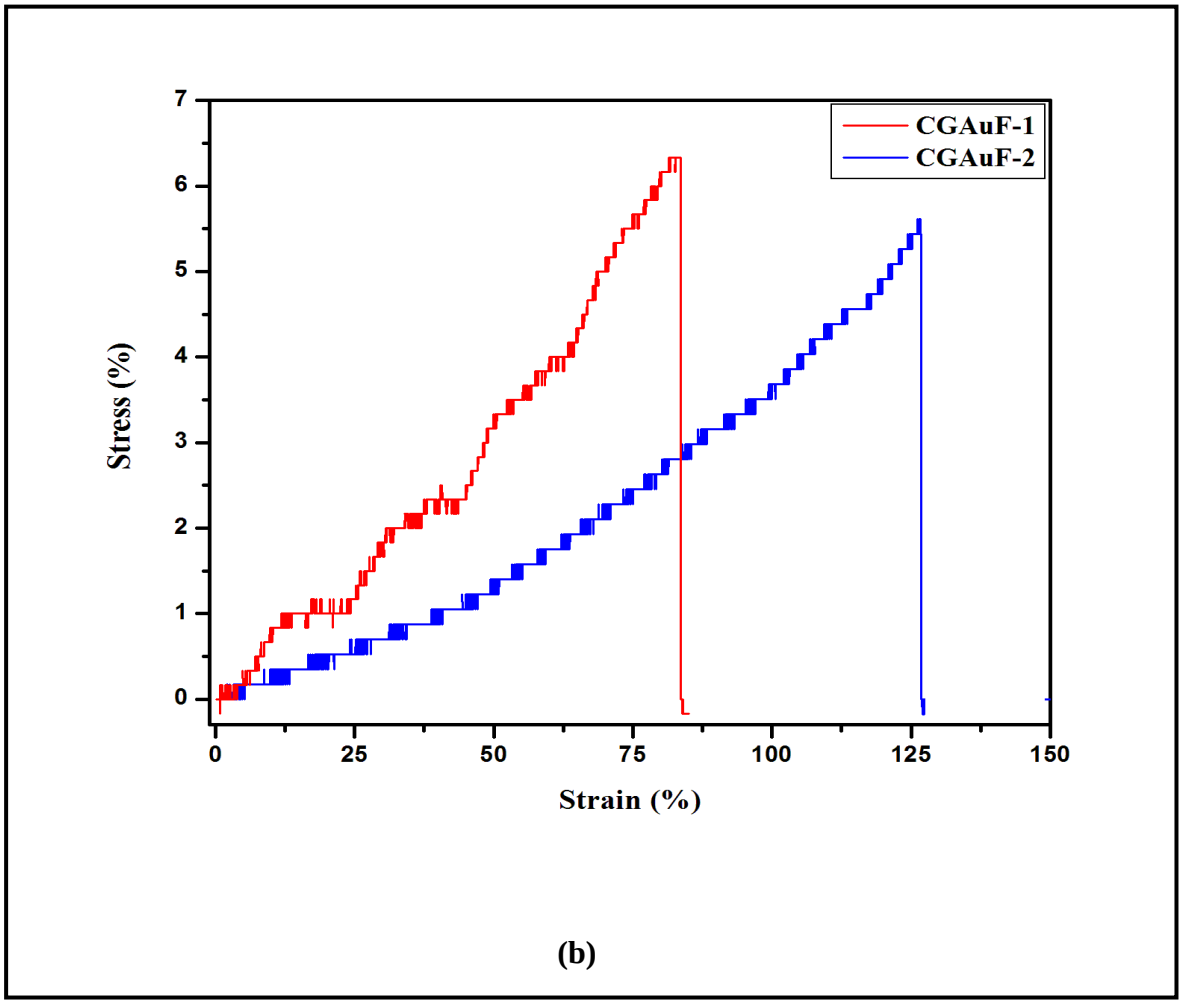

Figure 4.2.4 *(a) Stress strain behavior of pure chitosan membranes (b) Effect of grafting and nanoparticle stress strain behavior of grafted and nanocomposite chitosan membranes.*

4.2.4.5 Dynamic mechanical analysis

Figure 4.2.5 (a), (b), (c), (d) shows the variation in dynamic mechanical thermal property of pure chitosan (CS), glycolic acid grafted chitosan (CGAuF-1) and CGAuF-1 with Au/Fe_3O_4 hybrid nanoparticle (CGAuF-2) nanocomposite films, which has been determined by the change in viscoelastic property, glass transition temperature and stability of the polymer[30]. The storage modulus [E'] of CS film is 1.206×10^8 [Pa]. Upon grafting storage modulus decreases to 2.186×10^7 [Pa] and an increase in storage modulus [E'] of nanocomposite film is observed with the increase in nanoparticle content. The segmental

motion of the polymer increases upon increasing the temperature and there is a sharp increase in tanδ which corresponds to α relaxation temperature associated with the glass transition temperature T_g. The T_g of CS film was observed to be 153.86 ^{0}C, which decreases upon grafting, it is due to increase in the mobility of the polymer chains. The addition of Au/Fe_3O_4 hybrid nanoparticle restricts the mobility of the chains and causes the increase in the storage modulus and improves the mechanical strength of polymer film (**Table 4.2.3**).

Table 4.2.3 Viscoelastic properties of grafted chitosan- Au/Fe_3O_4 hybrid nanoparticle nanocomposites

Sample Code	Au/Fe_3O_4 (Wt %)	Storage modulus (Pa) at 121 ^{0}C	Tan delta (δ)
CS	0	1.206×10^8	0.42
CGAuF-1	0	2.186×10^7	0.59
CGAuF-2	40	1.373×10^6	0.50
CGAuF-3	80	5.040×10^6	0.58

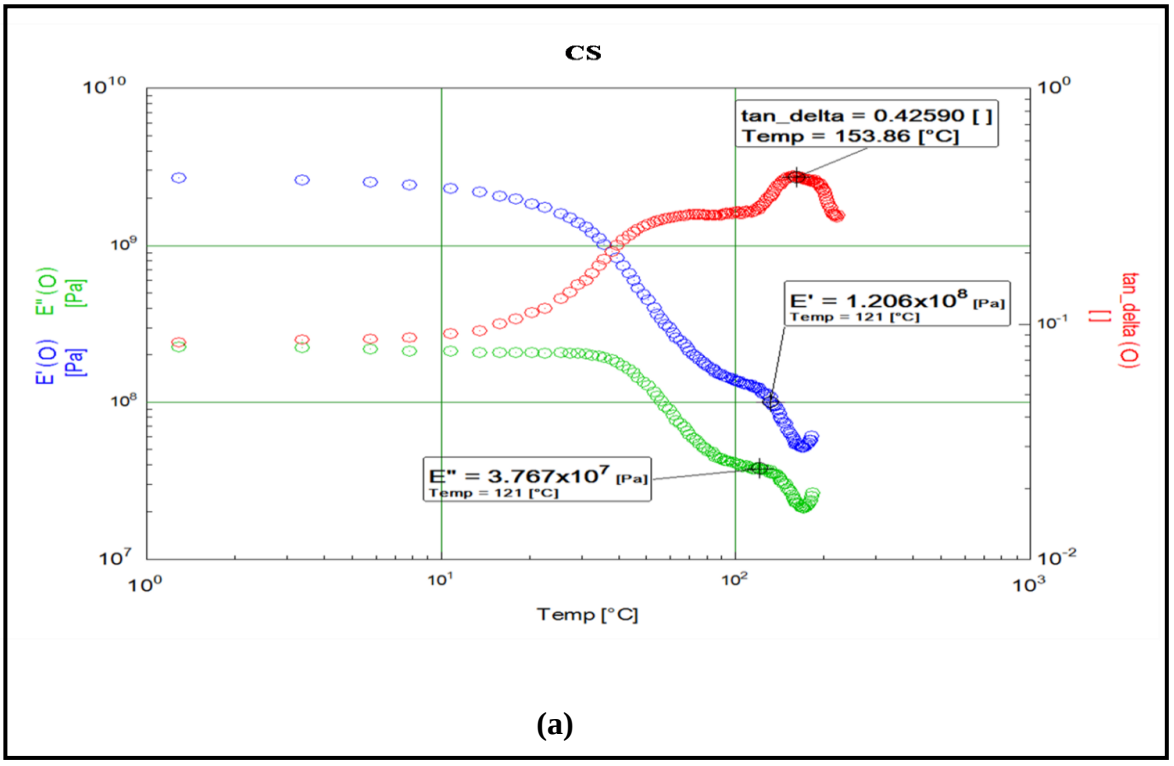

(a)

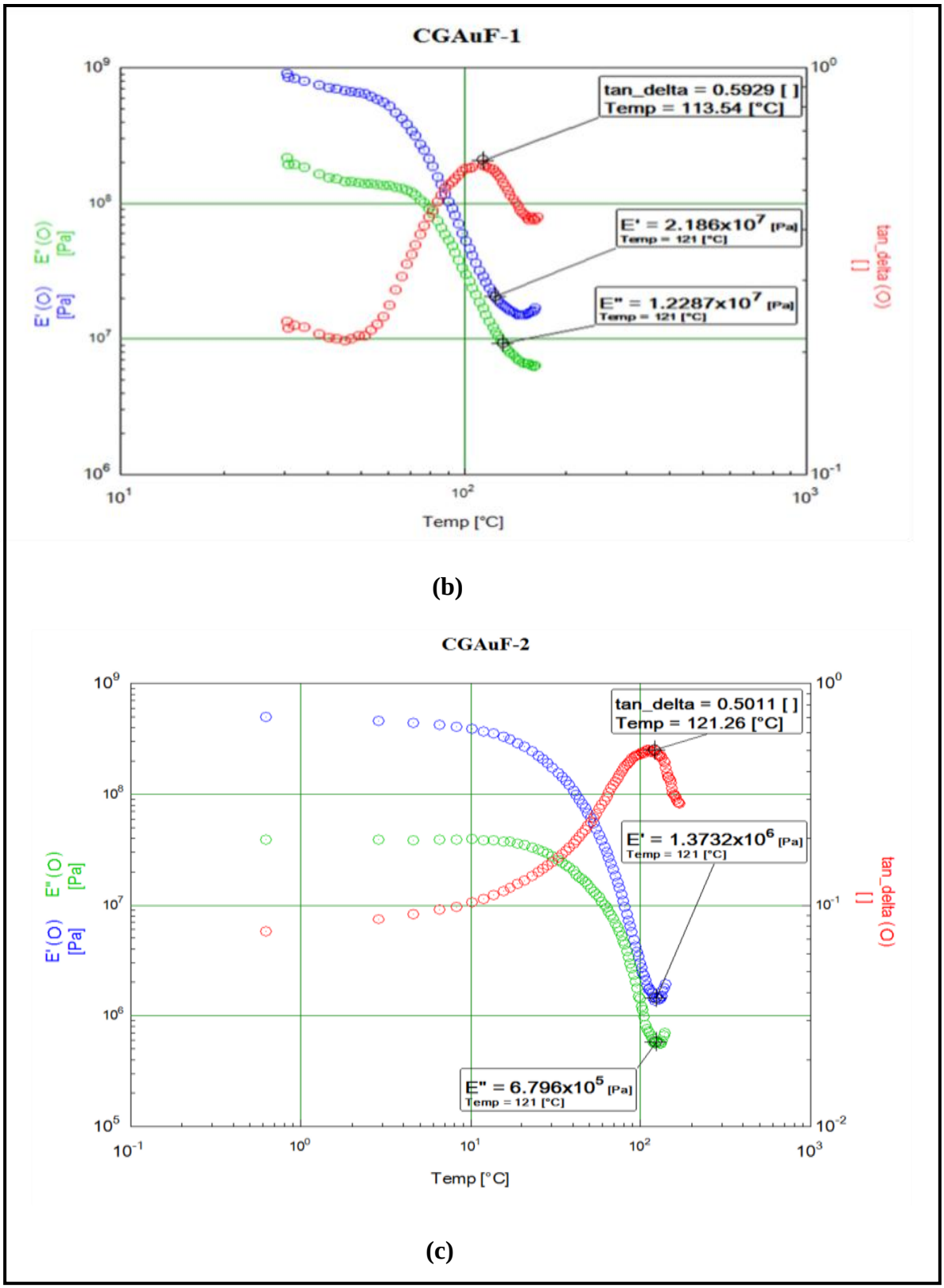

Figure 4.2.5 *Temperature variation of tanδ, glass transition temperature, storage modulus [E'] and loss modulus [E''] (a) Pure chitosan film (b)Grafted chitosan film (c) Grafted chitosan/Au-Fe_3O_4 hybrid nanoparticle nanocomposite films*

4.2.4.6 Thermogravimetric analysis

In TGA curve, two steps of non-oxidative degradation were observed (**Figure 4.2.6**). The weight loss at 70-150 ^{0}C is attributed to the water absorbed in chitosan. Whereas the weight loss in the temperature ranges of 200-350 ^{0}C corresponds to the degradation and deacetylation of chitosan[31]. Initially the thermal degradation temperature of CS decreases by 20-30 ^{0}C after grafting but upon addition of Au/Fe_3O_4 hybrid nanoparticles decrease in thermal degradation temperature reaches to 50-60 ^{0}C (**Table 4.2.4**). The thermal stability of chitosan decreases; this is due to the poor heat barrier properties of nanoparticle for polymer matrix during the formation of chars[32].

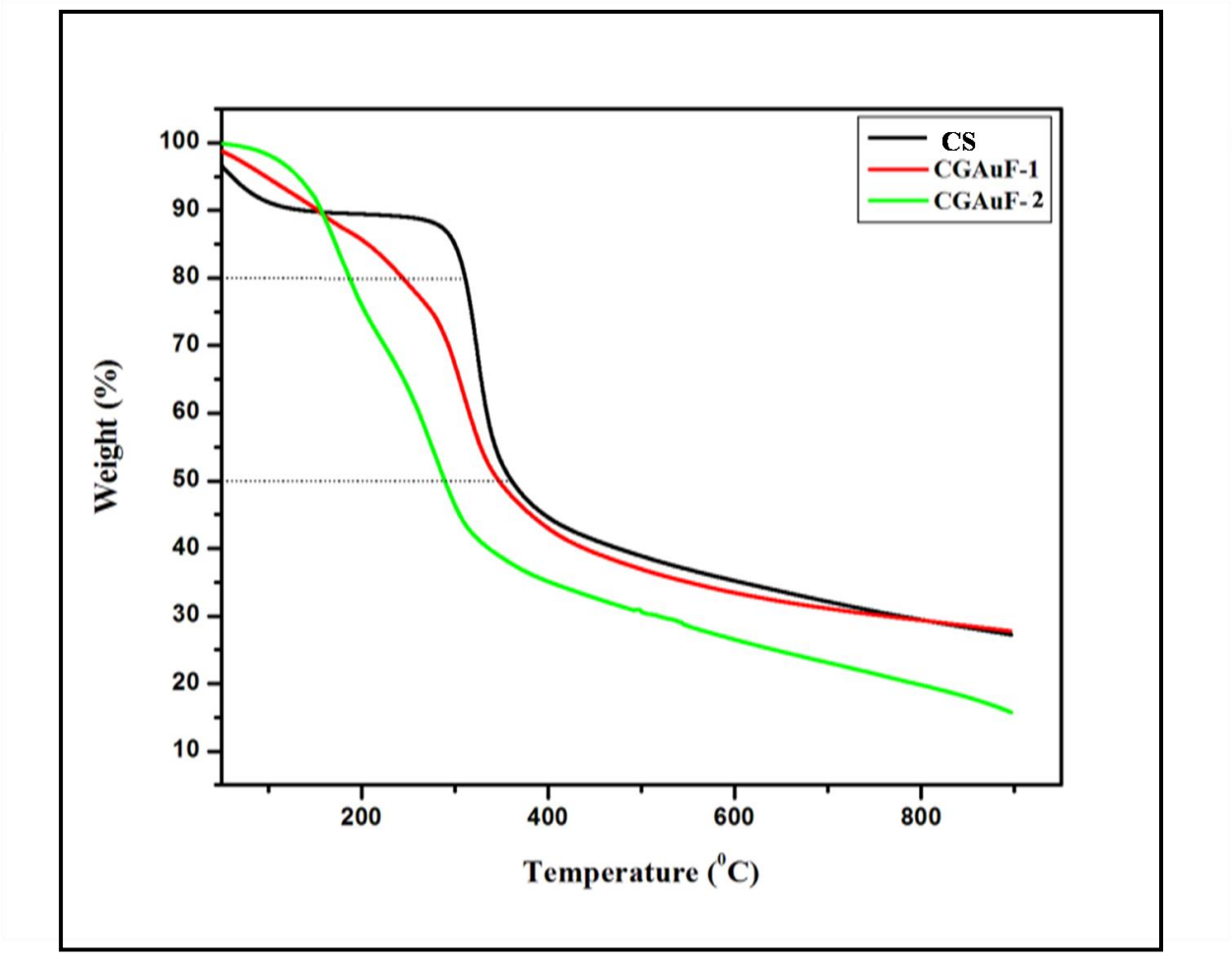

Figure 4.2.6 *Thermogravimetric curves of prepared nanocomposites.*

Table 4.2.4 TGA results for chitosan and its nanocomposites

Sample Code	Temperature at 20% loss (^{0}C)	Temperature at 50% loss (^{0}C)	char at 900 ^{0}C (wt %)
CS	310	360	27.1
CGAuF-1	246	347	27.7
CGAuF-2	187	286	15.57

4.2.4.7 Water absorption Behavior

The pure chitosan does not absorb water but it shows swelling behaivor, probably due to many OH and –NH groups in chitosan, which causes strong intermolecular and intramolecular hydrogen bonds. Upon grafting water absorption property of chitosan increases because the molecular structure integrity is broken in the grafted chitosan, which can expose more functional groups for water absorption (**Table 4.2.5**). This swelling extent will depend on the degree of ionization and grafting extent[33]. The water absorption of CGAu-2 film decreases with an increase of Au/Fe_3O_4 nanoparticle in grafted chitosan matrix. Since nanoparticle is hydrophobic, resulting nanocomposite were expected to be hydrophobic and also it is probably due to the formation of a barrier in the form of cross linking points, which prevents water permeation into chitosan.

Table 4.2.5 Sorption behavior of the nanocomposites

Sample Code	Water Absorption (%)
CS	54
CGAuF-1	77.7
CGAuF-2	55.14
CGAuF-3	52.76

4.2.5 CONCLUSIONS

The enhancement in the structural and functional properties was observed upon interaction of cationic chitosan with Au/Fe_3O_4 nanoparticles through metallic bond. The grafting of chitosan with glycolic acid imparts hydrophillicity and swelling behavior to the chitosan. The increasing content of nanoparticles decreases the water absorption, which imparts little branched crystalline structure in the film. Due to its swelling behavior and longer water retention it could be applied in the field of biomedical.

4.2.6 REFERENCES

1. A. S. Edelstein and R. C. Cammarata, *Nanomaterials: Synthesis, Properties and Application. Institute of Physics Publishing,* London, 1996.
2. C. Hayashi, R. Uyeda and A. Tasaki, *Ultra-fine particles: Exploratory Science and Technology. Noyes Publications,* Norwich, New York, 1997.
3. G. C. Hadjipanayis and G. A. Prinz, *Science and Technology of Nanostructured Magnetic Materials,* Plenum Press, New York, 1991.
4. W. Zhang, C. Wang and H. Lien, *Catal. Tod.,* **40,** 387 (1998).
5. W. Zhang and C. Wang, *Environ. Sci. Technol.*, **31,** 2154 (1997).
6. P. Poizot, S. Laruelle, S. Grugeon, L. Dupont and J. M. Tarascon, *Nat.* **407,** 496 (2000).
7. P. Go´mez-Romero and C. Sanchez, *Functional Hybrid Materials,* New York, Wiley, 2004.
8. H. Chen, X. Liu, H. Muthuraman, J. H. Zou, J. H. Wang, Q. Dai and Q. Huo, *Adv. Mat.,* **18,** 2876 (2006).
9. S. Dire, F. Babonneau, C. Sanchez and J. Livage, *J. Mater. Chem.,* **2,** 239 (1992).

10. S. S. Ozdemir, M. G. Buonomenna and E. Drioli, *Appl. Catal. a-General.* **307,** 167 (2006).
11. M. T. Sulak, O. Gokdogan, A. Gulce and H. Gulce, *Biosens. Bioelectro.* **21,** (2006) 1726.
12. H. Gu, Z. Yang, J. Gao, C. K. Chang and B. Xu, *J. Am. Chem. Soc.,* **127,** 34 (2005).
13. T. Teranishi, Y. Inoue, M. Nakaya, Y. Oumi and T. Sano, *J. Am. Chem. Soc.,* **126,** 9914 (2004).
14. H. W. Gu, R. K. Zheng, X. X. Zhang and B. Xu, *J. Am. Chem. Soc.*, 126, 5664 (2004).
15. Z. Hens, D. Vanmaekelbergh, E. Stoffels and H. van Kempen, *Phys. Rev. Lett.* 88 236803.1 (2002).
16. K. W. Kwon and M. Shim, *J. Am. Chem. Soc.*, **127,** 10269 (2005).
17. W. Shi, H. Zeng, Y. Sahoo, T. Y. Ohulchanskyy, Y. Ding, Z. L. Wang and P. N. Prasad, *Nano. Lett.,* **6,** 875 (2006).
18. H. Yu, M. Chen, P. M. Rice, S. X. Wang, R. L. White and S. Sun, *Nano. Lett.*, **5,** 379 (2005).
19. S. Kudera, L. Carbone, M. F. Casula, R. Cingolani, A. Falqui, E. Snoeck, W. J. Parak and L. Manna, *Nano. Lett.,* 5**,** 445 (2005).
20. K. T. Yong, Y. Sahoo, M. T. Swihart and P. N. Prasad, *Adv. Mater.,* 18 1978 (2006).
21. W. Wang and H. Cui, *J. Phys. Chem. C.* **112,** 10759 (2008).
22. J. Shan and H. Tenhu, *Chem. Commun.* **44,** 4580 (2007).
23. M. Xie, H. H. Liu, P. Chen, Z. L. Zhang, X. H. Wang, Z. X. Xie, Y. M. Du, B. Q. Pand and D. W. Pang, *Chem. Commun.*, **44,** 5518 (2005) -5520.
24. J. Xie, Q. Zhang, J. Y. Lee and D. I. C. Wang, *ACS Nano.,* **2,** 2473 (2008).

25. J. Rodriguez-Fernandez, J. Perez-Juste, F. J. G. Abajo and L. M. Liz- Marzan, Langmuir **22,** 7007 (2006).
26. T. D. Schladt, M. I. Shukoor, K. Schneider, M. N. Tahir and F. Natalio et al., *Angew. Chem.,* **49,** 3976 (2010).
27. M. Jaworska, K. Sakurai, P. Gaudon and E. Guibal, *Polym. Int.,* **2,** 198 (2003).
28. K. Ogawa, S. Hirano, T. Miyanishi, T. Yui and T. Watanabe, *Macromol.,* **17,** 973 (1984).
29. S. F. Wang, L. Shen, W. D. Zhang and Y. J. Tong, *Biomacromol.,* **6,** 3067 (2005).
30. F. Al-Sagheer and S. Muslim, *J. Nanomater.,* **2010,** 1(2009).
31. S. F. Wang, L. Chen and Y. J. Tong, *J. Polym. Sci. Part A Polym. Chem.,* **44,** 686 (2006).
32. S. F. Wang, L. Shen, Y. J. Tong, L. chen, I. Y. Phang and T. X. Liu, *Polym. Degrad. Stab.,* **90,** 123 (2005).
33. P. Seong, Y. Jin and P. Ham, *Biomater.,* **22,** 323 (2000).

CHAPTER 5

A: Preparation of Glycolic Acid-g-Chitosan-Pt-Fe_3O_4 Hybrid Nanoparticles Based Nanohybrid Scaffolds for Tissue Engineering and Drug Delivery Applications

5.1 INTRODUCTION

In the recent years, polymer-nanoparticle composites have attracted the interest of researcher due to their synergistic and hybrid properties derived from several components. These materials exhibit unique mechanical, electrical, optical[1] and thermal properties, which is due to the interaction of the polymer with the particle and state of dispersion[2-4]. Transition metal nanoparticles are one of the most studied systems due to their quantum size effects[5-7], novel electronic[8], optical[9], magnetic[10] and chemical properties. These metal nanostructure system play an important role in many different fields of science such as nano-electronics, catalysis[11-13] and recently, in biomedical application[14-16]. Recently, we have demonstrated that these hybrid materials can be used in the field of cell proliferation and controlled drug release systems, which is having major scientific application in the field of biomaterials[17].

Chitosan is selected in the present work because it easily forms stable film on the solid support, which has been used in the development of biosensors[18-21]. It has also been widely used in tissue repair, anti-microbial resistance, cell adhesion, food industry, for making biosensors[18] and drug delivery due to its biocompatibility, film forming properties[22] and polycationic nature. The grafting of side glycolic acid leads to marked changes in the chitosan structure[23, 24]. Chitosan has amino and hydroxyl functional group which act as potential site for altering the polymers functionality[25-27]. Chitosan is hydrophilic and compatible with nanoparticle and has better processability due to the presence of amino group in the chain.

Based on the above consideration, this study reports the biocompatibility and drug release behavior of nanohybrid based on chitosan-g-glycolic acid and Pt-Fe_3O_4 composite magnetic nanoparticles. The Pt-Fe_3O_4 hybrid magnetic nanoparticles have been dispersed into the matrix of grafted chitosan scaffolds by vacuum and freeze drying.

5.2 EXPERIMENTAL

5.2.1 Materials

Chitosan (MW=1.5×10^5, degree of deacetylation was 85%), glycolic acid (99% purity), oleic acid (OA), oleylamine (OAM), 1-octadecene iron (0) pentacarbonyl ($Fe(CO)_5$), 1, 2-tetradecanediol, cyclophosphamide (CPA) drug and chloroplatinic acid hexahydrate ($HPtCl_6.6H_2O$) was obtained from Sigma-Aldrich. Biphenyl ether, Tri phenyl phosphate (TPP), lithium chloride (LiCl), pyridine (Py) and N-methyl pyrilidone (NMP) was obtained from Sisco Research Laboratories. Ultra pure water was prepared by a Milli-Q system and used throughout the work.

5.2.2 Synthesis of platinum nanoparticles (PNP)

PNP were prepared by thermal decomposition of $H_2PtCl_6.6H_2O$ at high temperature. 1mmol $H_2PtCl_6.6H_2O$ and 9 mmol OAM were added to 20 ml biphenyl ether. It is followed by the addition of 4mmol of 1, 2-tetradecanediol. The reaction mixture was heated slowly upto 185 ^{0}C for 1.5 h under argon atmosphere. The reaction mixture was then cooled down to room temperature and precipitated with ethanol. After centrifugation, precipitate was dried and redispersed in 20 ml of hexane containing 10 mM OAM.

5.2.3 Synthesis of Pt-Fe_3O_4 hybrid nanoparticles (PFNP)

OA, OAM and 1-octadecene were heated 100 ^{0}C under argon atmosphere. Solution of PNP was injected at this temperature, followed by flushing with argon (to remove hexane) and then heated to 120 ^{0}C, at which $Fe(CO)_5$ was injected. The reaction mixture was slowly heated to reflux (1^0C min^{-1}) for 4.5 h. After cooling to room temperature, the reaction mixture was stirred for 1 h, followed by precipitation with acetone and then dried in air.

5.2.4 Preparation of nanohybrid scaffolds and drug loading

Glycolic acid grafted chitosan (1g) (Discussed in **chapter 3B. section 3.2.2.3**) was dispersed in deionised water (50 ml) and stirred for 1 h at room temperature. After 1 h, Pt-

Fe_3O_4 nanoparticles (50 mg) were added to the solution and stirred overnight at room temperature. The reaction mixture was heated upto 80 ^{0}C with continuous degassing for 40-45 min. Solution was cooled to room temperature after degassing, which is followed by drug (CPA, 10 mg) addition and the resulting reaction solution was stirred for 5 h, so that drug completely mixes with solution. After 5 h, solution was poured in tissue culture plates (20 mm × 20 mm diameter). The drug loaded solution was quenched in liquid nitrogen and freeze dried by lyophilisation under -100 ^{0}C temperature for 6 h. The formulations are shown in the **Table 5.1**.

In lyophilisation water molecules were removed by freezing and sublimation of ice crystals, which lead to the formation of pores. The polymer-rich phase forms the cell walls around the pores [27].

Table 5.1 Formulation of cyclophosphamide (CPA)-loaded nanohybrid of chitosan-g-glycolic acid and Pt-Fe_3O_4 composite nanoparticle

S.No	Grafted Chitosan (g)	Pt-Fe_3O_4 (mg)	CPA (%)	Drying Process	Sample code
1	1	_	_	Vacuum	CGPF-1
2	1	20	_	Vacuum	CGPF-2
3	1	40	10	Freeze	CGPF (S)

5.3 CHARACTERIZATION OF NANOHYBRID

5.3.1 Transmission Electron Microscopy

The morphology, particle size, Selected Area Diffraction pattern (SAED) and Energy Dispersive X-ray (EDAX) spectroscopy of Pt-Fe_3O_4 nanoparticles were analysed with High Resolution Transmission electron microscopy (HR-TEM model Technai TF30, 300KV FEG).

5.3.2 X-ray photoelectron spectroscopy

The formation of Pt-Fe_3O_4 hybrid nanoparticles were analysed with X-ray photoelectron spectroscopy (XPS) using an ESCA-3000 (VG Scientific Ltd., UK) with a base pressure of better than 1.0×10^{-9} Pa. Mg Kα radiation (1253.6 eV) was used as a X-ray source and operated at 150 W. All the binding energies were calibrated by using the contaminant carbon (C1s = 284.5 eV) as a reference[28].

5.3.3 Physical property measurement system

The formation of Pt-Fe_3O_4 hybrid magnetic nanoparticles were confirmed by measuring hysteresis loops of the synthesised nanoparticles using a physical property measuring system (PPMS) (quantum design Inc. San Diego, USA) equipped with 7T superconducting magnet and a vibrating sample magnetometer. The magnetic signal from the sample holder was negligible to affect our data accuracy.

5.3.4 Scanning Electron Microscopy

Surface morphology of the samples were analysed with Scanning electron microscopy (SEM) (Model, JOEL Stereoscan 440, Cambridge). Prior to the observation, specimens were fixed on the copper grid.

5.3.5 Attenuated total reflectances Fourier transform infrared spectroscopy (ATR-FTIR)

Fourier transform infrared spectra of neat chitosan (NCS), chitosan grafted glycolic acid (CGPF-1), nanohybrid scaffold (CGPF(S)) and drug (CPA) were investigated with attenuated total reflectance Fourier transform infrared (ATR-FTIR) Nicolet Nexus 870 FTIR spectrometer equipped with a smart Endurance diamond accessory (64 scans, 4 cm^{-1} resolution, wave number range 4000-550 cm^{-1}).

5.3.6 Swelling behavior

Shape retention of the porous scaffold was determined by measuring the change in the diameter as a function of time in the media. The swelling behavior of porous scaffold was determined by exposing them to media of different pH, 1N HCl, 1N NaOH and simulated body fluid (SBF) (pH 7.4) solutions.

5.3.7 In-vitro cell culture study

Cell viability study was performed on SP2/0 mouse myeloma cell line as direct contact test. These cells are derived from an immortalized mouse fibroblast cell line, are internationally recognized cells that are routinely used in in-vitro cytotoxicity assessments. The scaffold was sterilised by putting it in 6 well tissue culture plate containing isopropanol (5 ml) and exposed to UV radiation for 4 h. SP2/0 mouse myeloma cell were further seeded on nanohybrid scaffold placed in 6-well plate at a density of 5×10^3 cells/well and incubated at 37 °C, 5% CO_2 and 95% humidity incubation conditions. The tissue culture plate containing only cells were used as control. To study the cell proliferation on different substrates, cell proliferation was determined by the colorimetric MTT assay. MTT assay is based on the reduction of yellow 3-(4,5 dimethylthiazol-2-yl)-2,5-diphenyltetrazolium bromide (MTT) salt in MTT to form purple formazan by dehydrogenase enzymes secreted from the mitochondria of metabolically active cells. The amount of formazan formed is directly proportional to the number of viable cells. The relative cell growth was compared to control cell, which exhibit cell culture medium without chitosan. It was calculated by using the given eq. (1)

$$\% \text{ Live cell} = 100 - \left[\frac{(C - T)}{(C - B)} \times 100 \right] \qquad (1)$$

C = OD of control

T = OD of test sample

B = OD of blank

OD = Optical density

For this, after every fixed interval of time 100 µl of the cell culture was incubated for MTT assay and the absorbance is taken in spectrophotometer plate reader. All the in vitro tests were done in triplicate and results were reported as an average value.

5.3.8 In-vitro drug release

The drug loaded nanohybrid scaffold (CGPF (S)) were immersed in aliquots of 0.1 M sodium phosphate buffer (pH 7.4) and incubated at 37 ^{0}C. Aliquot 3ml from the specimen were withdrawn after specific intervals and immediately fresh medium is added to it. The "CPA" content in the aliquot was investigated by UV-vis spectrophotometer (UV-NIR- PL Lamda 950) at 180 nm. All the experiments were done in triplicate and mean value is reported.

5.4 RESULTS AND DISCUSSION

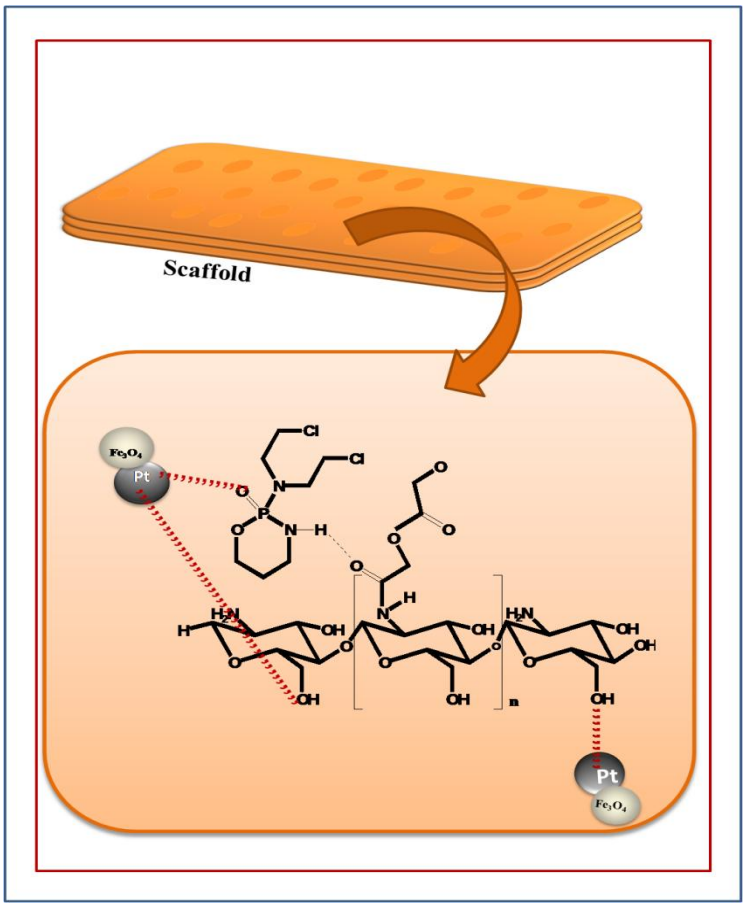

Scheme 5.1 *Schematic illustration of interactions between chitosan-g-glycolic acid, drug and Pt-Fe_3O_4 hybrid nanoparticles.*

5.4.1 TEM analysis of Pt-Fe_3O_4 hybrid nanoparticles

The Pt-Fe_3O_4 hybrid nanoparticles exhibit almost same particle size. The TEM image of these hybrid nanoparticles posses varying contrast, uniformly spherical or quasi spherical morphology (**Figure 5.1** (a)). The two lattices are commensurate. The distance between two adjacent lattice planes in Fe_3O_4 domains is 4.85 Å, which is close to the reference value of 4.88 Å for (1 1 1) planes and in Pt domain adjacent lattice planes are 2.27 Å apart and it is consistent with the reported value of 2.27 Å for (1 1 1) plane (**Figure 5.1** (b)). The SAED pattern shows the crystallinity of hybrid nanoparticles (**Figure 5.1** (c)). TEM-EDAX also confirms the formation of Pt-Fe_3O_4 hybrid nanoparticles (**Figure 5.1** (d)).

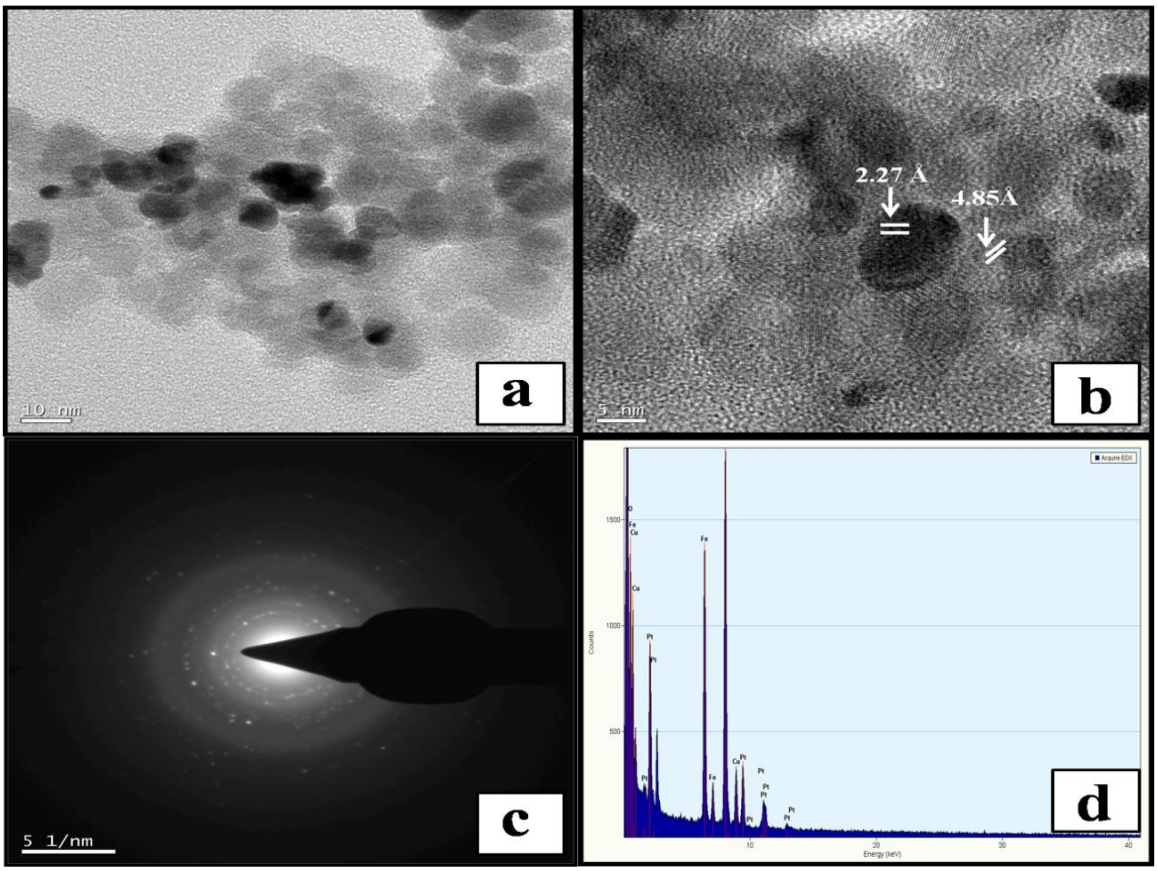

Figure 5.1 *(a) TEM image Pt/Fe_3O_4 hybrid nanoparticles; (b) HRTEM image of Pt-Fe_3O_4 hybrid nanoparticles (White line delineate distance between two lattice plane in Pt domain and Fe_3O_4 domain); (c) SAED pattern of Pt-Fe_3O_4 hybrid nanoparticles; (d) TEM-EDAX of Pt-Fe_3O_4 hybrid nanoparticles.*

5.4.2 XPS analysis

The electronic structure of Pt in Pt-Fe_3O_4 was qualitatively characterized by XPS measurement. **Figure 5.2** shows the electron binding energy of Pt_{4f} measured from XPS for 5nm PNP and 5-10nm PFNP. Pt-Fe_3O_4 hybrid nanoparticles have a ~2.197 eV decrease in electron binding energy. The change of binding energy is likely due to the electron transfer from Fe_3O_4 to Pt and may also be explained by the work function difference[29] in 5.93 eV[30] for Pt (111) and 5.52 eV[31] for Fe_3O_4 (111). Such observation of Pt chemical shift by XPS has also been reported in thin film studies of Pt/oxide interface, including both negative (receiving electrons)[32] and positive shift (losing electrons)[33].

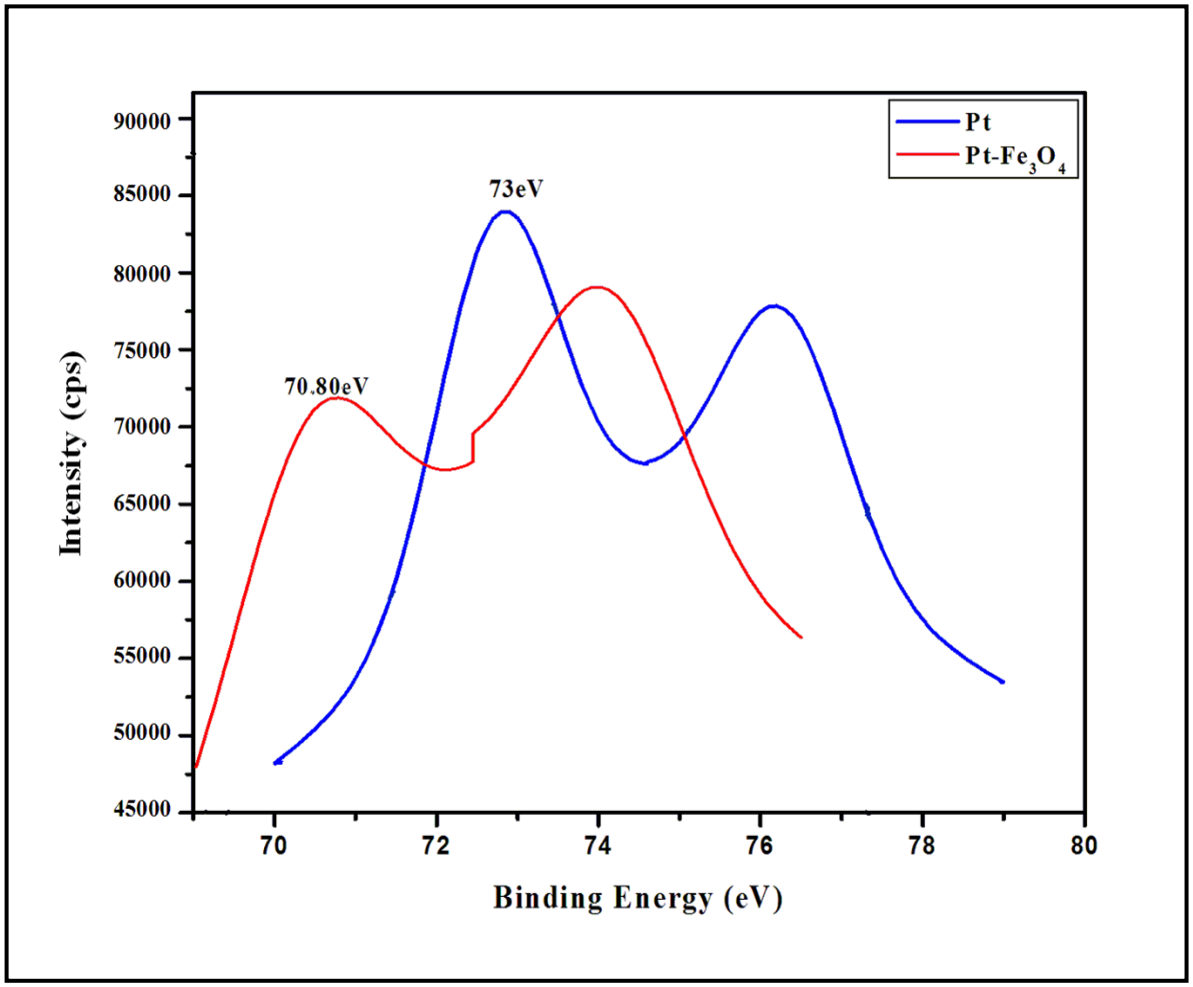

Figure 5.2 *Pt_{4f} XPS spectra of 5 nm Pt nanoparticles and 5-10 nm Pt-Fe_3O_4 nanoparticles.*

5.4.3 Physical property measurement system (PPMS) analysis

The magnetic properties of the hybrid nanoparticle were investigated to evaluate the influence of the diamagnetic Pt on the Fe_3O_4 domains. **Figure 5.3** shows magnetic hysteresis loops recorded at 300 k of Pt-Fe_3O_4 hybrid nanoparticle with Fe_3O_4 nanoparticle of size 5-10 nm. Hybrid nanoparticles are super paramagnetic; however the saturation magnetization decreases with Pt particles[34]. The decrease in the magnetization of Pt-Fe_3O_4 hybrid nanoparticle confirms the formation of Pt-Fe_3O_4 hybrid nanoparticle.

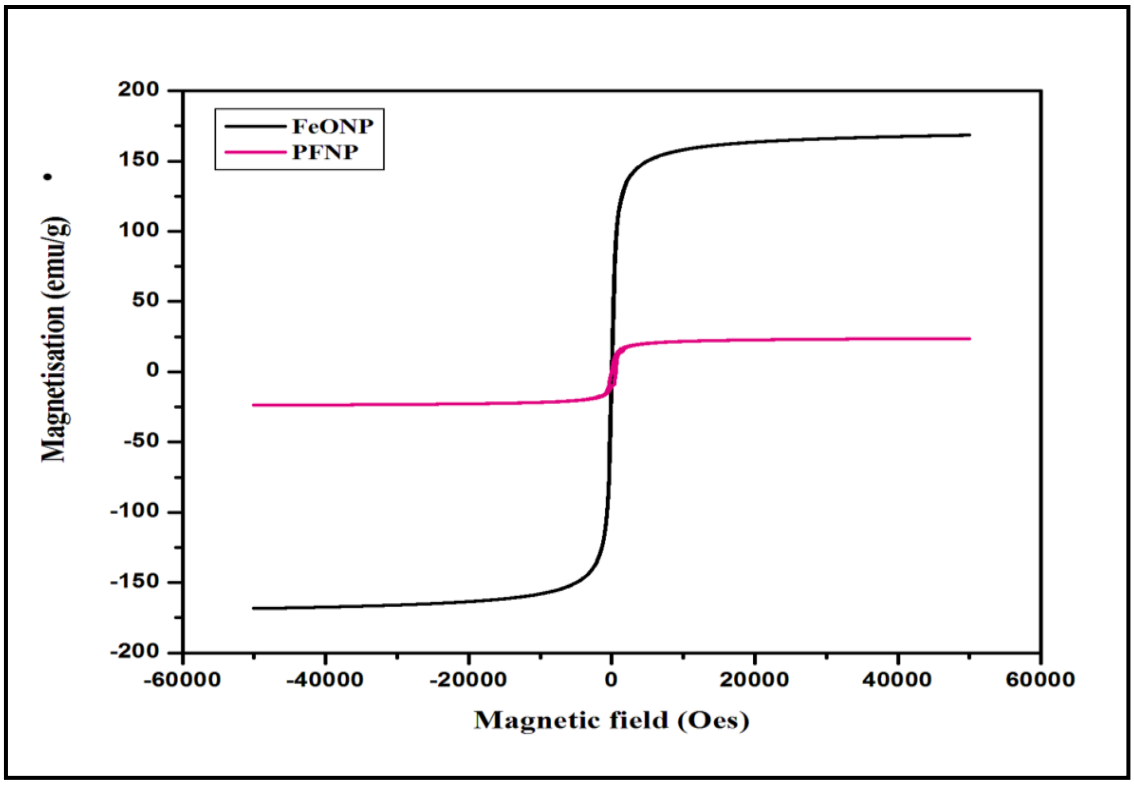

Figure 5.3 *Magnetic hysteresis curve recorded at 300k of Pt-Fe_3O_4 hybrid nanoparticle (PFNP) with Fe_3O_4 nanoparticles (FeONP).*

5.4.4 FT-IR analysis

Fourier transform infrared (FT-IR) spectra reveals information about the structure of neat chitosan (NCS), chitosan grafted glycolic acid (CGPF-1), nanohybrid scaffold (CGPF(S)) and drug (CPA) (**Figure 5.4**). The peak at 1630 cm^{-1} in the spectrum of neat chitosan is attributed to the –N-H bending vibration of amine (–NH_2) group in chitosan. The band at 3486 cm^{-1} is

corresponding to υ_{OH} stretching. The shift in peak of –N-H bending vibration of amine towards the lower frequency confirm the interaction of glycolic acid onto NH_3^+ group. In the spectrum of CGPF-1, a new peak appeared at 1730 cm^{-1} is attributed to the υ_{co} stretching. These peaks confirms the conversion of amine (NH_2) to amide (–NH-C=O). The drug (CPA) exhibit secondary amine in the molecule, which show –N-H bending at 1648 cm^{-1} and P=O group shows υ_{PO} stretching band at 1237 cm^{-1}. In the FT-IR spectrum of scaffold (CGPF (S)), P=O stretching band of drug and –OH stretching band of the grafted chitosan is shifted towards the lower frequency region confirming the interaction of Pt-Fe_3O_4 hybrid nanoparticles with drug molecule and chitosan chain through metallic bond. N-H bending vibration of the drug molecule as well υ_{co} stretching band is observed to be shifted towards lower frequency region, confirming the interaction of N-H group of drug with C=O group of glycolic acid through H-bonding.

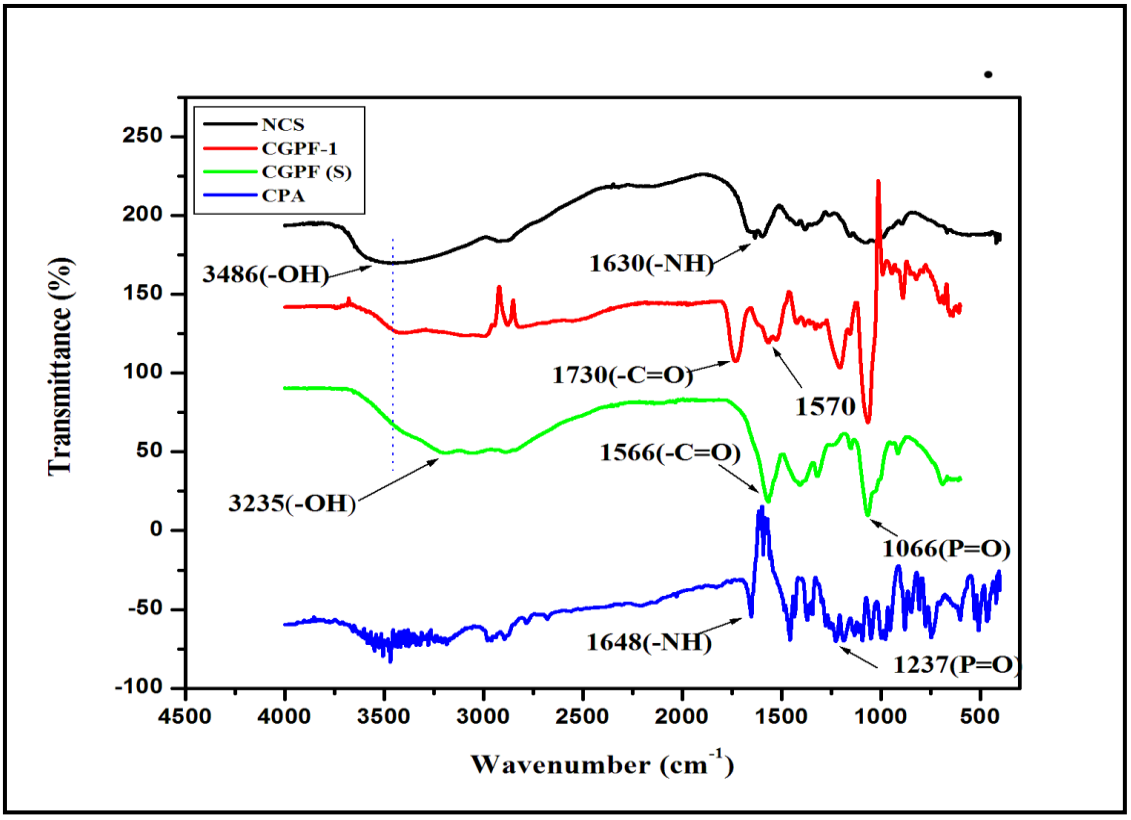

Figure 5.4 *FTIR spectra of neat chitosan (NCS), grafted chitosan (CGPF-1), grafted chitosan and Pt-Fe_3O_4 nanohybrid scaffold (CGPF (S)) and drug Cyclophosphamide (CPA).*

5.4.5 Scanning electron microscopy analysis of scaffolds

The SEM image (**Figure 5.5** (a, b)) reveals the morphology of nanohybrid scaffold before drug loading and after drug addition (**Figure 5.5** (c, d)). It is observed that pore size of scaffold before drug addition was ranging from 1.7 µm to 3.6 µm, but upon addition of drug pore size decreases and lies in the range of 1.2 µm to 2.2 µm. The decrease in the pore size may be due to the incorporation of drug molecule in the pores of scaffold. The SEM-EDAX of scaffold confirms the incorporation of Pt-Fe_3O_4 hybrid magnetic nanoparticles in it (**Figure 5.5** 5(e)).

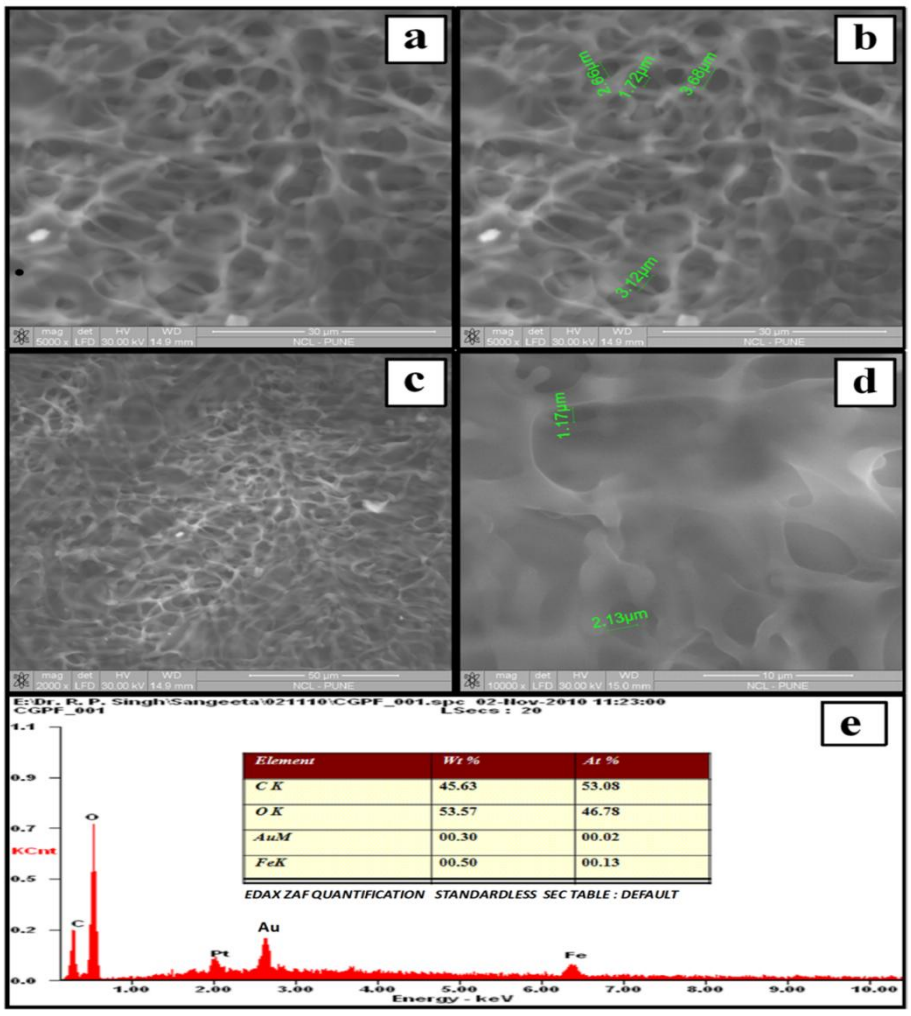

Figure 5.5 *(a, b) SEM image of grafted chitosan and Pt-Fe_3O_4 nanohybrid scaffold without drug; (c, d) SEM image of grafted chitosan and Pt-Fe_3O_4 nanohybrid scaffold with drug; (e) EDAX of nanohybrid scaffold(CGPF (S)).*

5.4.6 Swelling behavior

Shape retention of scaffold was investigated by measuring the change in the diameter as a function of immersion time in the media[35]. Swelling behavior of scaffold and its structural stability strongly depend upon the pH of the implantation site for their practical use in tissue engineering. Swelling behavior of scaffold was determined by exposing it to media at different pH, 1N HCl, 1N NaOH and simulated body fluid (SBF) (pH 7.4) solutions. Swelling of chitosan involves the protonation of amino/imine groups and the mechanical relaxation of coiled chitosan chain[36,37]. The in vitro cell culture studies indicate that initial swelling is desirable[38,39] but continuous swelling reduces the mechanical integrity and leads to the generation of compressive stress to the surrounding tissue. The scaffolds were subjected to SBF (pH 7.4), HCl (pH 1.2) and NaOH (pH 14) for 24h.

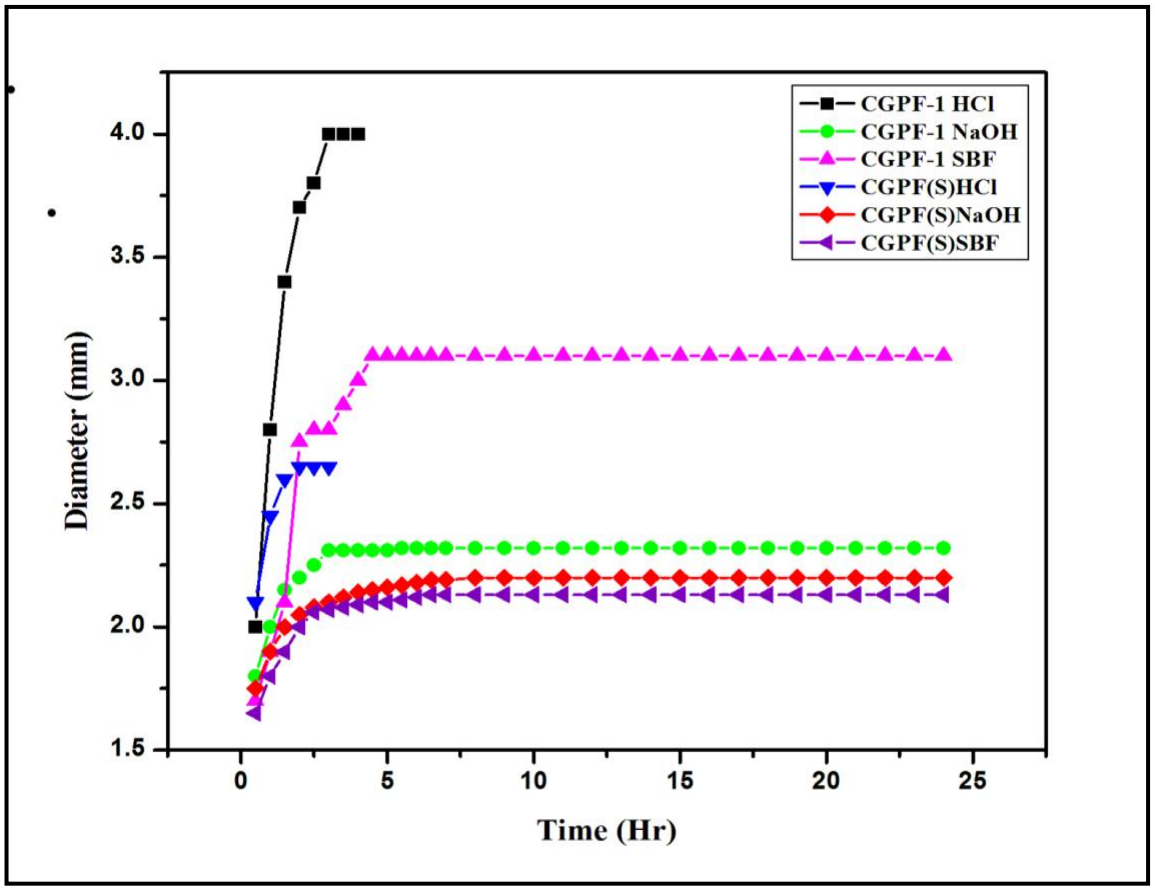

Figure 5.6 *Shape retention of scaffolds prepared from grafted chitosan and Pt-Fe_3O_4 nanohybrid.*

In the acidic medium, swelling of scaffold is higher than that of the SBF and NaOH. In acidic medium (HCl), scaffold (CGPF-1) dissolves completely within 3.5 h of immersion. It is observed that in basic medium (NaOH) rate of swelling is very low and reach the plateau level around 4 h of immersion but size of scaffold is found to increase within 4.5 h in SBF solution, whereas nanohybrid scaffold (CGPF (S)) dissolves completely in HCl within 2.5 h. Nanohybrid scaffold slight swelling was observed in NaOH and SBF within 3 h. These results reveal that the nanohybrid scaffold (CGPF (S)) is stable towards the SBF and higher pH solution (**Figure 5.6**).

5.4.7 In-vitro drug release

Figure 5.7 shows UV-VIS spectra of in vitro drug release study illustrating variation in the absorbance of the drug in the scaffold with respect to time. In vitro drug release was examined with SBF (pH 7.4) and release media was quantified by UV-visible spectral absorbance values. Initially the release of drug from freeze dried scaffold can be observed to be faster and higher and release of drug decreases with time. This is because the drug which is present on the surface of the scaffold is released much faster than the drug embedded deeply into the pores of scaffold. The incorporation of Pt-Fe_3O_4 hybrid nanoparticle effect can be significantly observed as reduced rate of release at initial stage of immersion (upto 200 min). The specimen is solvated initially, which facilitates the lateral diffusion of drug[40] after 250 min, The rate of release of drug decrease over the time, it may be due to the interaction of Pt-Fe_3O_4 hybrid nanoparticle and grafted glycolic acid chains with the loaded drug[41]. In FTIR spectra of CPA, the band at 3456 cm^{-1} corresponds to υ_{NH} stretching of drug molecule. In CGPF (S), shifting of υ_{co} stretching band towards the lower frequency region indicates the interaction of NH group of drug (Cyclophosphamide) with C=O group of amide via H-bonding. The interaction between drug (Cyclophosphamide) and scaffold surface via

(N-H----O=C-) H-bond is confirmed by the shifting of υ_{NH} stretching band of drug towards the lower frequency region in the CGPF (S) specimen (**Scheme 5.1**).

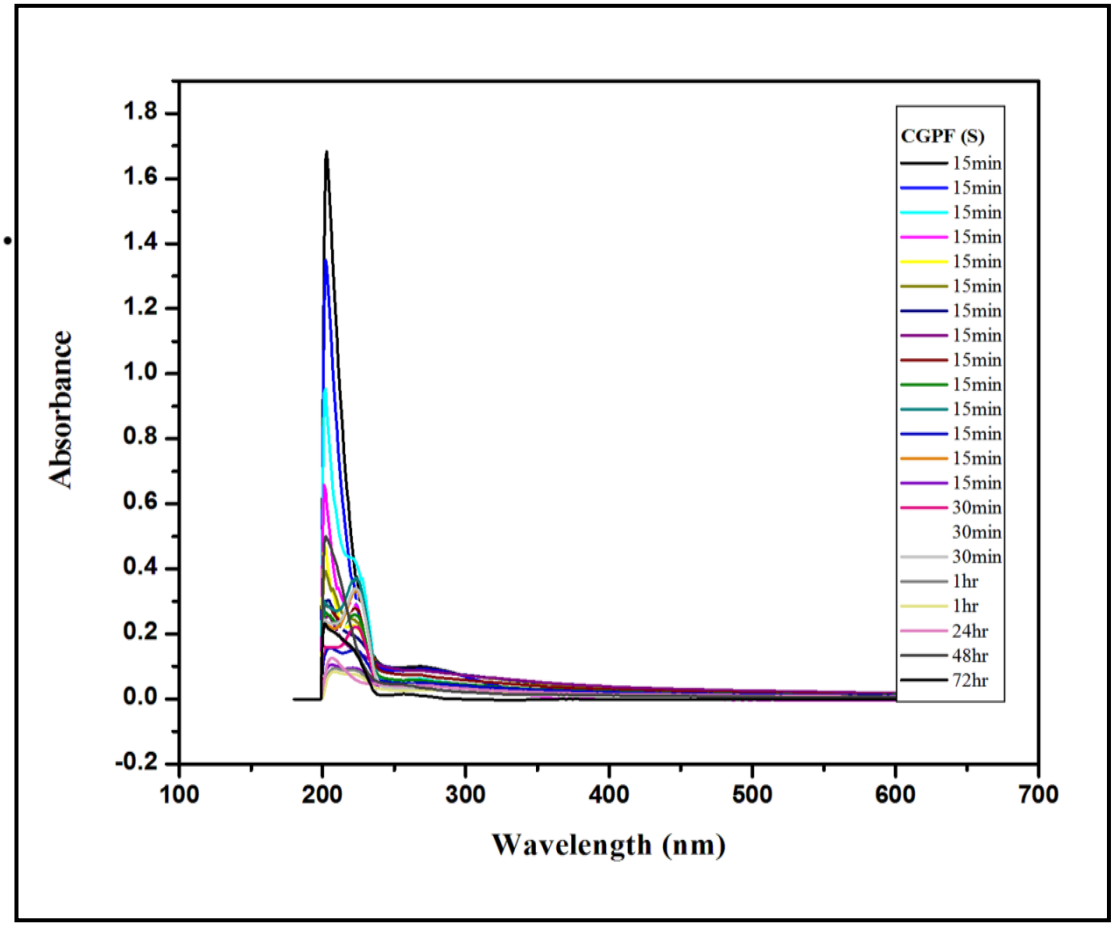

Figure 5.7 *Drug release profile from the prepared nanohybrid scaffold (CGPF (S)).*

5.4.8 Cell viability study

The cell viability was determined by using a 3-(4,5-dimethylthiazol-2-yl)-2,5-diphenyl tetrazolium bromide (MTT-formazan) method. The cell viability study is done with SP2/0 mouse myeloma cells to study, biocompatibility of the prepared scaffold (CGPF (S)). The growth of the cells cultured on the scaffold was higher during the first 2 h but slight decrease in the cell number was observed in next 4 h. This may be because during proliferation cells have occupied all the available spaces on the scaffold[41] (**Figure 5.8**). The present study implies that cell proliferation is not affected by the incorporation of Pt-Fe_3O_4 nanoparticles into glycolic acid grafted chitosan[42]. This may be due to the enhanced interaction between Pt-

Fe_3O_4 hybrid magnetic nanoparticles and growing cells on the biopolymer matrix. These Pt-Fe_3O_4 hybrid magnetic nanoparticles can act as adhesive between biopolymer and cells. The Pt-Fe_3O_4 hybrid magnetic nanoparticles may develop London- van der Waals forces with cells.

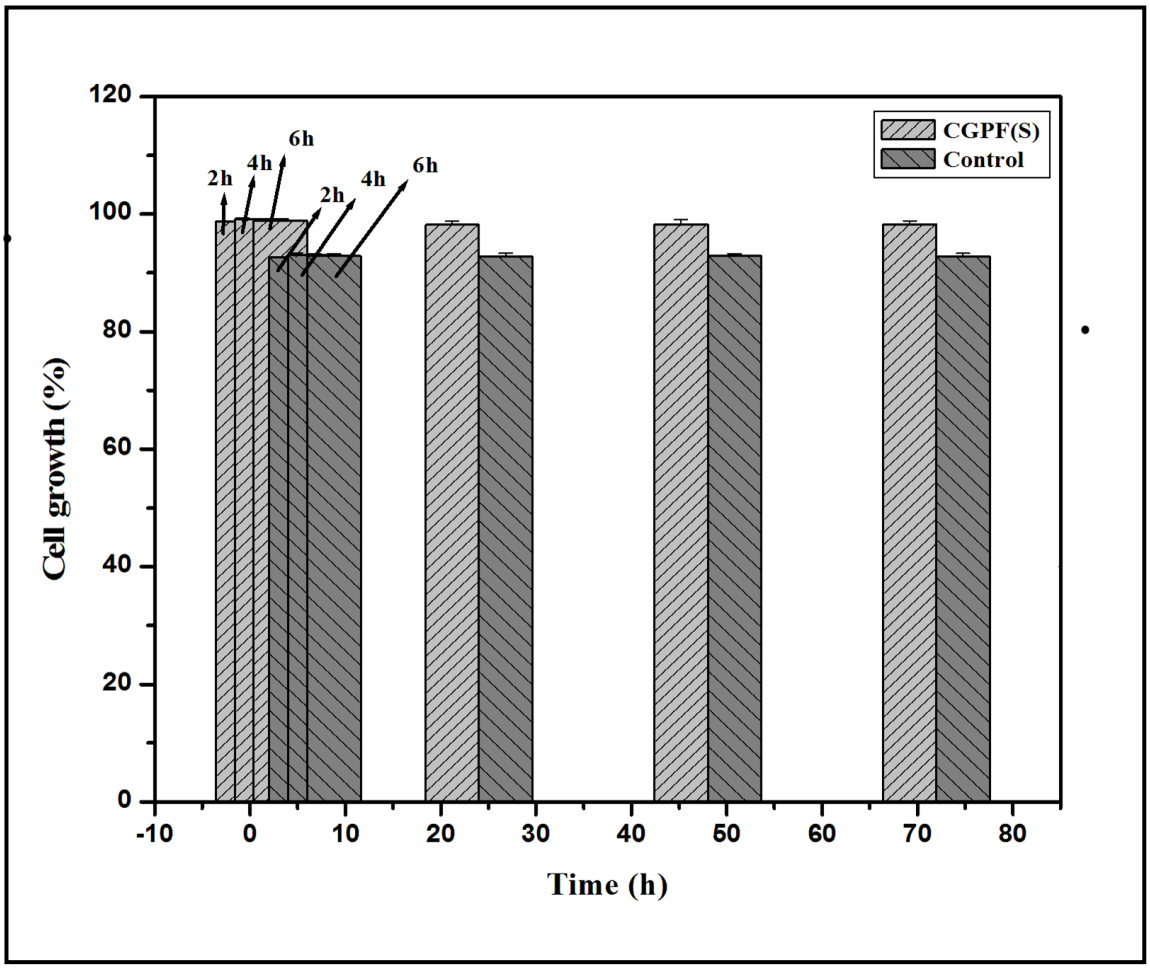

Figure 5.8 *Cell viability study done with MTT assay of cultured cells.*

5.5 CONCLUSIONS

This work reveals the potential use of novel nanohybrid based on chitosan-g-glycolic acid and Pt-Fe_3O_4 composite magnetic nanoparticles in biomedical applications. The prepared nanohybrid scaffolds posses porous morphology, which is attributed to the phase separation. The nanohybrid scaffolds are stable regardless of pH of the medium. The porous nanohybrid scaffolds have shown faster and higher drug release. From the results we concluded that, the

prepared nanohybrid scaffold are biocompatible and Pt-Fe_3O_4 magnetic nanoparticles are viable additive for formulating sustained drug delivery systems and could be applied in the field of biomaterials.

5.6 REFERENCES

1. R. Chapman and P. Mulvaney, Chem. Phys. Lett., **349,** 358 (2001).
2. R. Krishnamoorti and R. A. Vaia, *Polymer nanocomposites*, Washington DC, ACS, 2002.
3. G. Lagaly, *Appl. Clay Sci.*, **15,** 1 (1999).
4. P. F. Luckham and S. Rossi, *Adv. Coll. Interface Sci.*, **82,** 43 (1999).
5. R. Jin, *Nanoscale.*, **2,** 343 (2010).
6. M. M. Alvarez, J. T. Khoury, T. G. Schaaff, M. N. Shafi gullin, I. Vezmar and R. L. Whitten, *J. Phys. Chem. B.,* **101,** 3706 (1997).
7. M. Zhu, C. M. Aikens, F. J. Hollander, G. C. Schatz and R. Jin, *J. Am. Chem. Soc.*, 130, 5883 (2008).
8. T. Teranishi, Fabrication and electronic properties of gold nanoparticle superlattices, Comptes. Rendus Chimie. 6 (2003) 979-987.
9. I. Pastoriza-Santos, D. Gomez, J. Pérez-Juste, M. Luis, L. Marzán and P. Mulvaney, *Phys. Chem. Chem. Phys.*, **6,** 5056 (2004).
10. Y. Yamamoto, T. Miura, Y. Nakae, T. Teranishi, M. Miyake and H. Hori, *Physica B: Condensed Matter.*, **329,** 1183 (2003).
11. J. D. Aiken III and R. G. Finke, *J. Mol. Catal. A: Chem.*, **145,** 1(1999).
12. A. Roucoux, J. Schulz and H. Patin, *Chem. Rev.* **102,** 3757 (2002).
13. J. S. Bradley, G. Schmid and G. Schmid, in: (Ed.), *Nanoparticles, Wiley-VCH,* Weinheim, 2004.

14. S. Akiyama, T. Yoshimura and K. Esumi, *J. Jpn. Soc. Colour Mater.,* **78,** 112 (2005).

15. Y. Jiang, L. Zhang, D. Yang, L. Li, Y. Zhang, J. Li and Z. Jiang, *Ind. Eng. Chem. Res.,* **47,** 2495 (2008).

16. Y. Jiang, D. Yang, L. Zhang, Q. Sun, X. Sun, J. Li and Z. Jiang, *Adv. Funct. Mater.* **19,** 150 (2009).

17. K. C. Souza, Æ. J. D. Ardisson and Æ. E. M. B. Sousa, *J. Mater. Sci.*, **20,** 507 (2009).

18. W. Wang and H. Cui, *J. Phys. Chem. C.* **112,** 10759 (2008).

19. M. H. Xue, Q. Xu, M. Zhou and J. J. Zhu, *Electrochem. Commun.,* 8, 1468 (2006).

20. T. Tangkuaram, C. Ponchio, T. Kangkasomboon, P. Katikawong and W. Veerasai, *Biosens Bioelectron.,* **22,** 2071 (2007).

21. Y. Du, X. L. Luo, J. J. Xu and H. Y. Chen, *Bioeletrochem.,* **70,** 342 (2007).

22. J. Shan and H. Tenhu. *Chem. Commun.,* **44,** 4580- (2007).

23. M. Xie, H. H. Liu, P. Chen, Z. L. Zhang, X. H. Wang, Z. X. Xie, Y. M. Du, B. Q. Pand and D. W. Pang, *Chem. Commun.,* **44,** 5518 (2005).

24. J. Xie, Q. Zhang, J. Y. Lee and D. I. C. Wang, *ACS. Nano.* **2,** 2473 (2008).

25. J. D. S. Dos Santos, P. J. G. Goulet, N. P. W. Pieczonka, J. ONOliveira and R. F. Aroca, *Langmuir.,* **20,** 1027 (2004).

26. K. Kurita, *Prog. Polym. Sci.,* **26,** 1921 (2001).

27. R. L. Hong and J. Y. Yu, *J. Biomed. Mater: Appl. Biomater.,* **71B,** 52 (2004).

28. J. C. Riviere and S. Myhra. *Handbook of Surface and Interface Analysis: Methods for Problem-Solving; Marcel Dekker, Inc,* New York, 1998.

29. Z. H. Qin, M. Lewandowski, Y. N. Sun and S. Shaikhutdinov, H. J. J. Freund, *Phys. Chem. C.,* **112,** 10209 (2008).

30. R. C. Weast and M. J. Astle, *CRC Handbook of Chemistry and Physics, 63rd ed.; CRC Press*, Boca Rotan, FL, 1982.
31. W. Weiss and W. Ranke, *Prog. Surf. Sci.,* **70,** 1 (2002).
32. M. K. Bahl, S. C. Tsai and Y. W. Chung, *Phys. ReV. B.* **21,** 1344 (1980).
33. V. Murgai, S. Raaen, M. Strongin and R. F. Garrett, *Phys. ReV. B.,* **33,** 4345 (1986).
34. T. D. Schladt, M. I. Shukoor, K. Schneider, M. N. Tahir, F. Natalio, I. Ament, J. Becker, F. D. Jochum, S. Weber, O. Köhler, P. Theato, L. M. Schreiber, C. Sönnichsen, C. Schröder, W. E. G. Müller and W. Tremel, *Angew. Chem.* **49,** 3976 (2010).
35. S. Kumari and R. P. Singh, *Int. J. Bio. Macromol.* **50,** 878 (2012).
36. L. Vachoud, N. Zydowicz and A. Domard, *Carbohydrate Res.* **326,** 295 (2000).
37. S. Aiba, *Int. J. Biol. Macromol.,* **13,** 40 (1991).
38. L. M. Liz-Marzan, *Mat. Today.,* **7,** 26 (2004).
39. N. Shanmugasundram, P. Ravichandaran, P. N. Reddy, N. Ramamurth, S. Pal and K. P. Rao, *Biomat.* **22,** 1943 (2001).
40. T. Takahashi and M. Yamaguchi, *J. Colloid Interface Sci.,* **146,** 556 (1991).
41. S. I. Park and Y. Zhao, Incorporation of a high concentration of mineral or vitamin into chitosan-based films, J. Agric. Food Chem. **52,** 1933 (2004).
42. T. Takahashi and M. Yamaguchi, *J. Colloid Interface Sci.,* **146,** 556 (1991).

CHAPTER 5

B: Preparation and Characterization of Glycolic Acid-g-Chitosan-Pt-Fe_3O_4 Hybrid Nanoparticles Based Nanocomposite Films

5.2.1 INTRODUCTION

In the recent years, multifunctional hybrid materials[1] and polymer-nanoparticle composite are finding increasing interest in material science and biological system, due to their synergistic and hybrid properties derived from several components. These nanocomposites have the combined properties of organic polymers and inorganic nanoparticles such as flexibility, magnetic, mechanical[2], electrical[3], optical[4] and thermal properties[5]. This enhancement is induced by the physical presence of nanoparticle and by the interaction of polymer with nanoparticle and the state of dispersion[6, 7]. Efficient nanoparticle dispersion combined with polymer-particle. Magnetic nanoparticle polymer composites have been applied in biomedical research applications such as drug delivery[8-10] and hyperthermia treatment of cancer cells[11-13]. Multicomponent nanostructures can combine and enhance the chemical and physical properties of individual component. Several methods for the preparation of Multicomponent nanoparticles have been reported[14-22]. Here, we have described a procedure that allows the preparation of Pt-Fe_3O_4 hybrid nanoparticles differing in relative size and the number of iron oxide particle, which extends the original method of Sun et al.,[20] which is based on the thermal decomposition of $Fe(CO)_5$.

Chitosan is a well-known strong chelating agent for metals and protein[23], making it useful in sensor development[24]. It has better processability due to the presence of amino group (pKa 6.2). Chitosan is modified by chemical reaction, which involves the reactive hydroxyl and amino groups of the polymer chain. The grafting of glycolic acid on chitosan leads to marked changes in its structure[25, 26].

It is also expected that grafted chain may act as internal plasticizer to reduce the brittleness of the chitosan films to obtain more soft and elastic film. These nanocomposite films exhibit interesting structural, chemical, mechanical properties and could be used in the field of biomedical.

5.2.2 EXPERIMENTAL

5.2.2.1 Materials

Chitosan of low molecular weight (Mw=1.5×10^5, degree of deacetylation was 85%), glycolic acid with (99% purity), iron (0) pentacarbonyl ($Fe(CO)_5$), oleylamine (OAM), oleic acid (OA), 1-octadecene and chloroplatinic acid hexahydrate ($HPtCl_6.6H_2O$) was obtained from Sigma Aldrich. Phenyl ether was obtained from M/s Sisco Research Laboratories. Ultra pure water was prepared by a Milli-Q system and it was used throughout the study.

5.2.2.2 Preparation of chitosan-g-glycolic acid and Pt-Fe_3O_4 hybrid nanoparticle nanocomposite film

Chitosan-g-glycolic acid and Pt-Fe_3O_4 nanoparticle(Synthesis of Pt/ Fe_3O_4 nanoparticles is discussed in **chapter 4A**. **section 5.2.2**) nanocomposite film was prepared by dispersing chitosan in deionised water for 1h with constant stirring at room temperature. Glycolic acid was added to the solution after 1h, which is allowed to stir for 12 h. After 12 h, Pt-Fe_3O_4 hybrid nanoparticles were added to the resulting solution and stirred overnight at room temperature. The resulting solution was heated up to 80 ^{0}C with continuous degassing for 45 min. The solution was casted on a glass plate and dried at 60 ^{0}C for 8 h. To promote dehydration of grafted chitosan copolymer with formation of the corresponding amide linkages, again film was dried at 60 ^{0}C in vacuum oven for 8 h.

Table 5.2.1 The formulation of chitosan-g-glycolic acid and Pt-Fe_3O_4 nanoparticle

S. No	Chitosan (g)	Glycolic acid (g)	Pt-Fe_3O_4 (mg)	Sample code
1	1	0	0	CS
2	1	1	0	CGPF-1
3	1	1	20	CGPF-2
4	1	1	40	CGPF-3

To remove the oligomers of glycolic acid and unreacted glycolic acid, the samples were extracted with methanol in soxhlet apparatus for 48 h. The thickness of resulting films were measured and found to be about 0.17 mm. The formulation of chitosan and nanoparticle (Pt-Fe_3O_4) are given in **Table 5.2.1**.

5.2.3 CHARACTERIZATIONS OF NANOCOMPOSITE FILM

5.2.3.1 Fourier transform infrared spectroscopy

Fourier transform infrared spectra (FT-IR) of neat chitosan (CS), chitosan grafted glycolic acid (CS-g-GA) and CS-g-GA nanocomposite with Pt-Fe_3O_4 hybrid nanoparticle were acquired using a Nicolet Nexus 870 attenuated total reflectance fourier transform infrared (ATR-FTIR) spectrometer equipped with a smart endurance diamond accessory (64 scans, 4 cm^{-1} resolution, wave number range 4000-550 cm^{-1}).

5.2.3.2 X-ray diffraction pattern

X-ray Diffractometer (WAXRD – Rigaku, Japan) with Cu-kα radiation at a voltage of 50 KV records the XRD pattern of the samples. The scanning rate was 4^0/min and the scanning scope of 2θ was 2^0 to 80^0 at room temperature.

5.2.3.3 Atomic force microscopy

Surface morphology of nanohybrid was investigated by atomic force microscopy (AFM) (Model: Nanoscope IV) under contact mode.

5.2.3.4 Dynamic mechanical analysis

Dynamic mechanical analysis (DMA) was investigated with a dynamic mechanical thermal analyser (DMTA RSA3, TA instrument) in tensile mode at a frequency of 1Hz with heating rate of 5 ^{0}C/min in the temperature range from -10 ^{0}C to 200 ^{0}C.

5.2.3.5 Thermogravimetric analysis

TGA Q5000 instrument were used to conduct the thermogravimetric analysis (TGA) of the sample. Temperature ranges from 50 ^{0}C to 900 ^{0}C with the heating rate of 10 ^{0}C/min under nitrogen with flow rate 20 ml/min.

5.2.3.6 Tensile strength testing

Linkam TST 350 was used to conduct tensile stress testing of film. A dumb bell strip was cut from each membrane and strained to break at a constant crosshead speed of 10 mm/min. The break stress and strain was calculated with the associated software (Linkam).

5.2.3.7 Water absorption measurement

According to ASTM D 570, the clean, dried film samples of known weights were immersed in distilled water at 25 ^{0}C for 24h (1 Day). The films were removed, blotted quickly with absorbent paper and weighed. The absorption percentage of these samples was calculated using the Eq. (1):

$$X\% = (W_1-W_0)/W_0 \quad (1)$$

where W_0 and W_1 are the weight of dry and swollen samples, respectively.

5.2.4 RESULTS AND DISCUSSION

5.2.4.1 FTIR analysis

Figure 5.2.1 shows the FTIR spectra of CS, CGPF-1 and CGPF-2. The characteristic peaks in the FTIR spectrum of CS include 1633 cm^{-1} (-NH stretching) and 3500cm^{-1} (-OH stretching). In FTIR spectrum of CGPF-1, presence of extra peak at 1738 cm^{-1} (-C=O stretching) and shifting of peak (-NH stretching) towards the lower frequency region (1574 cm^{-1}) confirms the interaction of glycolic acid with NH_2 group of chitosan. The grafting of glycolic acid on chitosan was confirmed by the formation of amide (–NH-C=O) linkage between amine (-NH_2) group of chitosan and –C=O group of glycolic acid. In the FTIR

spectrum of CGPF-2 include shift in peak 1722 cm^{-1} (-C=O stretching) and 3417 cm^{-1} (-OH stretching) it may due to the interaction of Pt-Fe_3O_4 hybrid nanoparticles with –C=O group of glycolic acid and –OH group of chitosan via metallic bond.

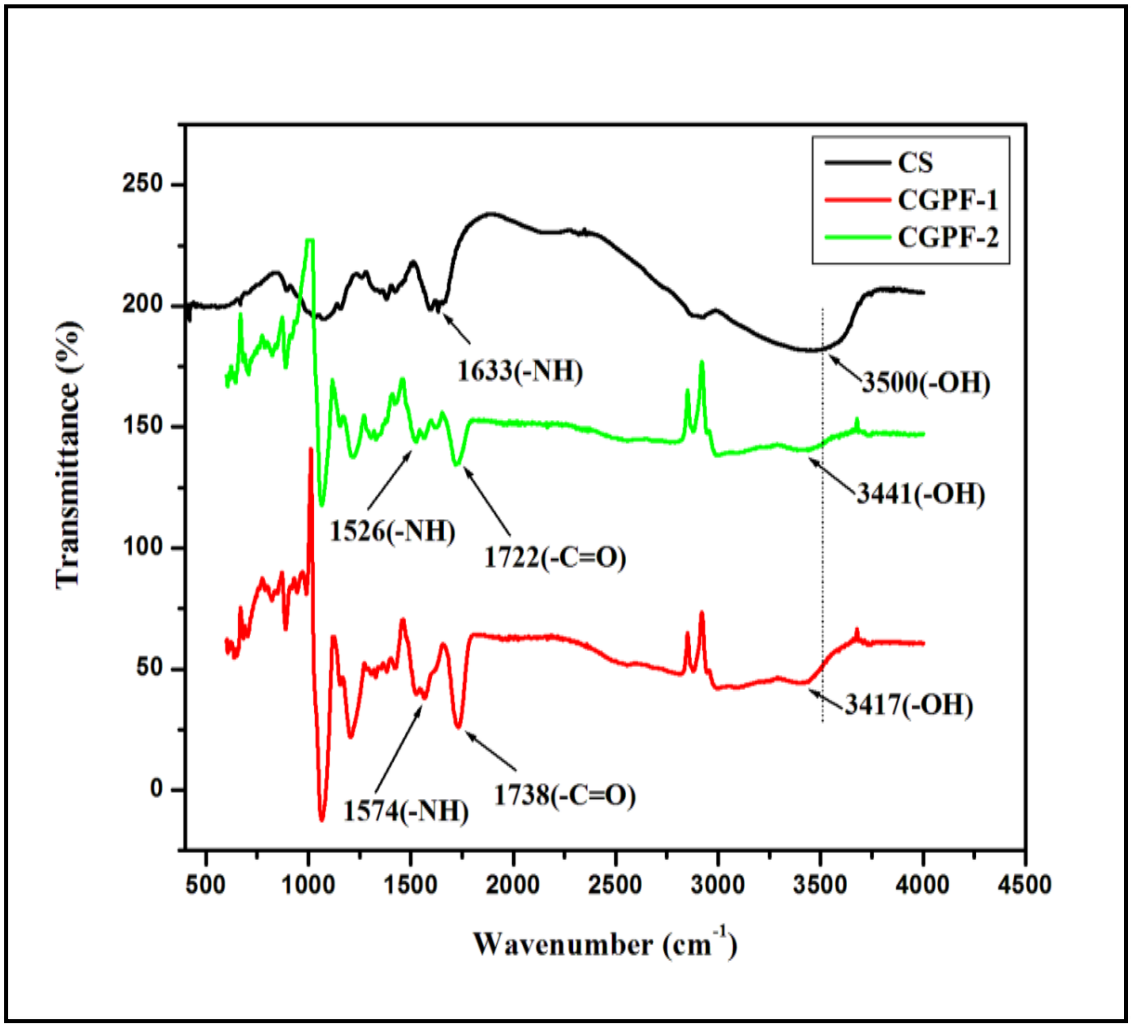

Figure 5.2.1 *FTIR spectra of neat chitosan (CS), grafted chitosan (CGPF-1) and grafted chitosan-Pt-Fe_3O_4 hybrid nanoparticle nanocomposite film.*

5.2.4.2 XRD analysis

Figure 5.2.2 shows XRD pattern of pure chitosan (CS), glycolic acid grafted chitosan (CGPF-1) and CS-g-GA/Pt-Fe_3O_4 hybrid nanoparticle nanocomposite (CGPF-2) films. Chitosan powder showed characteristic peaks at $2\theta = 10.5^0$ and 20.1^0, corresponds to hydrated crystalline structure and an amorphous structure of chitosan, respectively[30, 31]. The

structure of chitosan is strongly dependent on its processing treatment, such as dissolving, precipitation and drying, as well as its origin and characteristics, such as degree of deacetylation and molecular weight[32]**.** In grafted chitosan (CGPF-1) film XRD peaks were shifted from 10.5^0 to 10.1^0 and 20.1^0 to 19.2^0 confirming the interaction of glycolic acid with chitosan. XRD pattern of CS-g-GA/Pt-Fe_3O_4 nanocomposite (CGPF-2) film showed shift in the peaks from $2\theta = 10.1^0$ to 15.5^0 and 19.2^0 to 21.9^0. More shifts in CS-g-GA/Pt-Fe_3O_4 nanocomposite film are probably due to higher compatibility of the Pt-Fe_3O_4 nanoparticle with the grafted chitosan matrix.

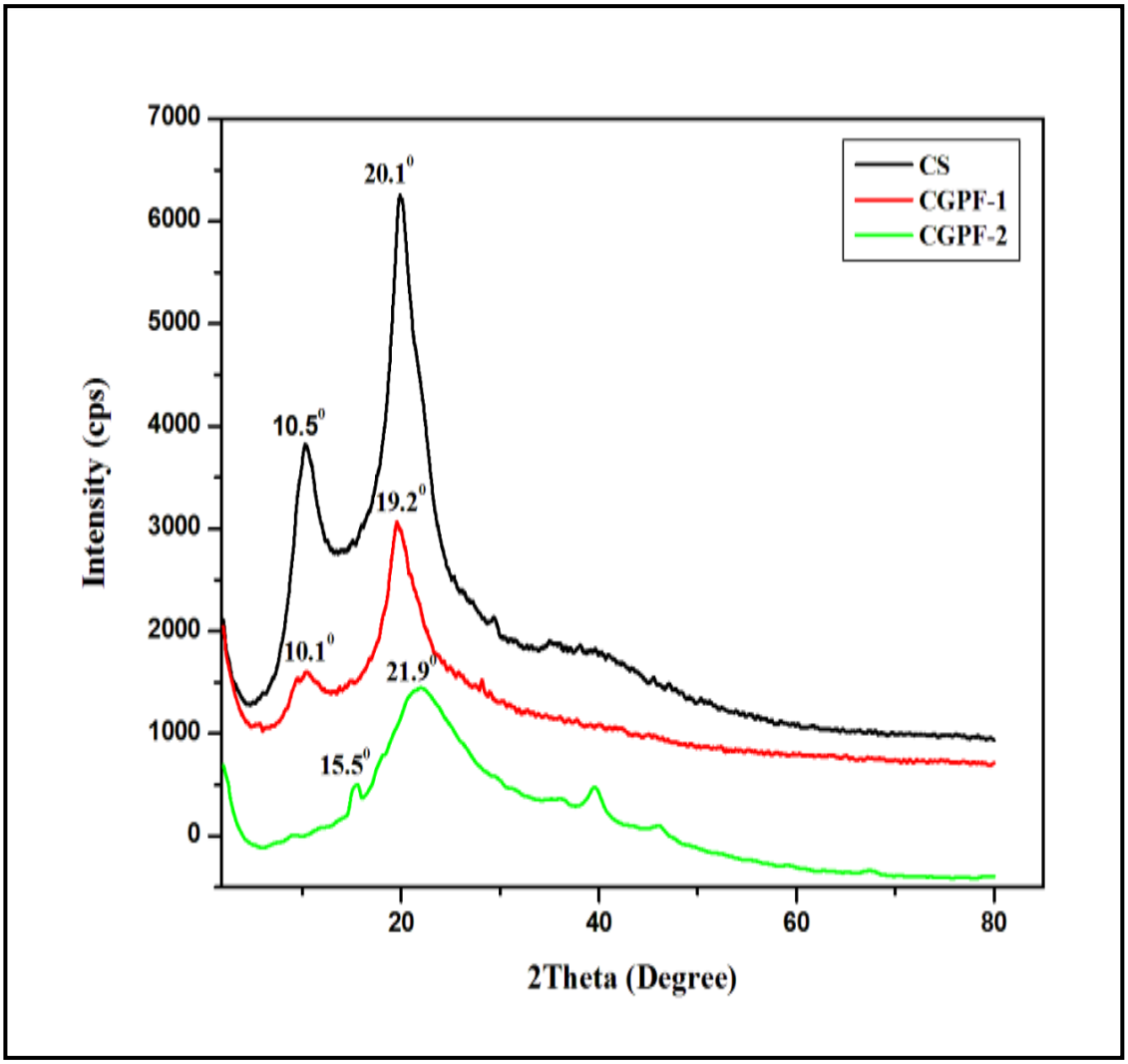

Figure 5.2.2 *X-ray diffraction spectra of neat chitosan, grafted chitosan and grafted chitosan/Pt-Fe_3O_4 hybrid nanoparticle nanocomposite films.*

5.2.4.3 Morphological studies

Surface topography of pure chitosan, grafted chitosan and CS-g-GA/Pt-Fe_3O_4 nanocomposite film is illustrated with AFM; the image size was 5 μm × 5 μm. **Figure 5.2.3** (a) shows the AFM image of chitosan film with smooth surface. Upon grafting the chitosan, roughness and height of the film surface were also increased (**Figure 5.2.3** (b)). AFM image of CS-g-GA/Pt-Fe_3O_4 nanocomposite film shows the incorporation of nanoparticle in the matrix chitosan film (**Figure 5.2.3** (c), (d)).

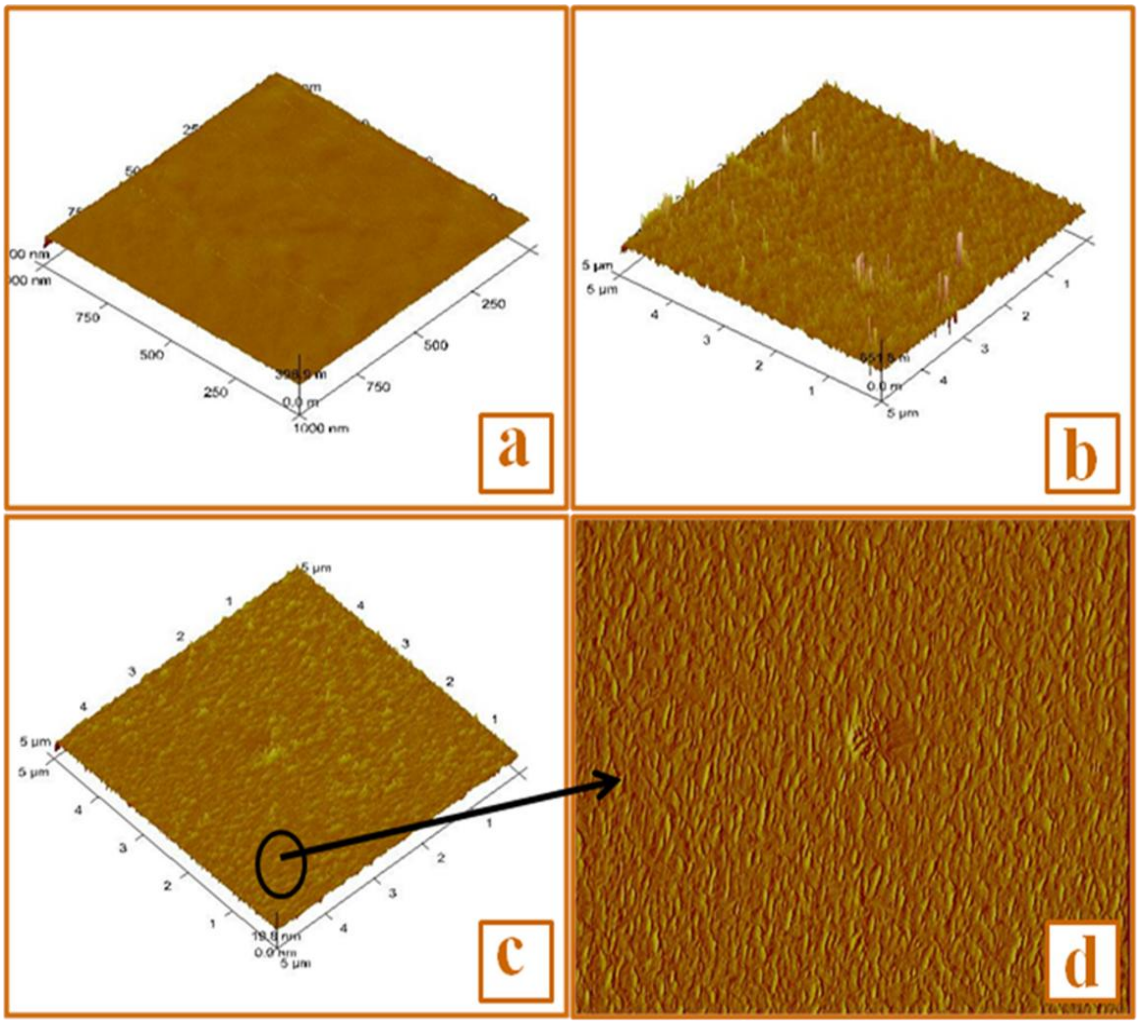

Figure 5.2.3 *(a) AFM image of pure chitosan film; (b) AFM image of grafted chitosan film. (c, d) AFM image of grafted chitosan/Pt-Fe_3O_4 hybrid nanoparticle nanocomposite films.*

5.2.4.4 Dynamic mechanical analysis

The variation in dynamic mechanical thermal property of CS-g-GA/Pt-Fe_3O_4 hybrid nanoparticle nanocomposite has been determined by the change in viscoelastic property, stability and glass transition temperature of the polymer **(Figure 5.2.4** (a), (b), (c), (d)**)**[33]. The storage modulus [E'] of pure chitosan film is $1.226x10^8$ [Pa] and it decreases to $3.1052x10^7$ [Pa] for grafted polymer film. Increase in storage modulus [E'] of nanocomposite film is observed with the increase in nanoparticle content. The segmental motion of the polymer increases upon increasing the temperature and there is a sharp increase in tanδ which corresponds to α relaxation temperature associated with the glass transition temperature T_g. Pure chitosan film exhibit T_g =153.86^{0}C, decrease in T_g of grafted film is observed due to increase in the mobility of the polymer chains. The addition of Pt-Fe_3O_4 hybrid nanoparticle restricts the mobility of the chains, which increases the storage modulus and improves the mechanical strength of polymer film **Table 5.2.2**.

Table 5.2.2 Viscoelastic properties of grafted chitosan-Pt-Fe_3O_4 hybrid nanoparticle nanocomposites

Sample Code	Pt-Fe_3O_4 (Wt %)	Storage modulus (Pa) at 110 ^{0}C	Tg (^{0}C)	Tan delta (δ)
CS	0	1.22×10^8	153.86	0.42
CGPF-1	0	3.1052×10^7	113.54	0.59
CGPF-2	20	1.1906×10^7	119.84	0.47
CGPF-3	40	4.4006×10^7	117.93	0.42

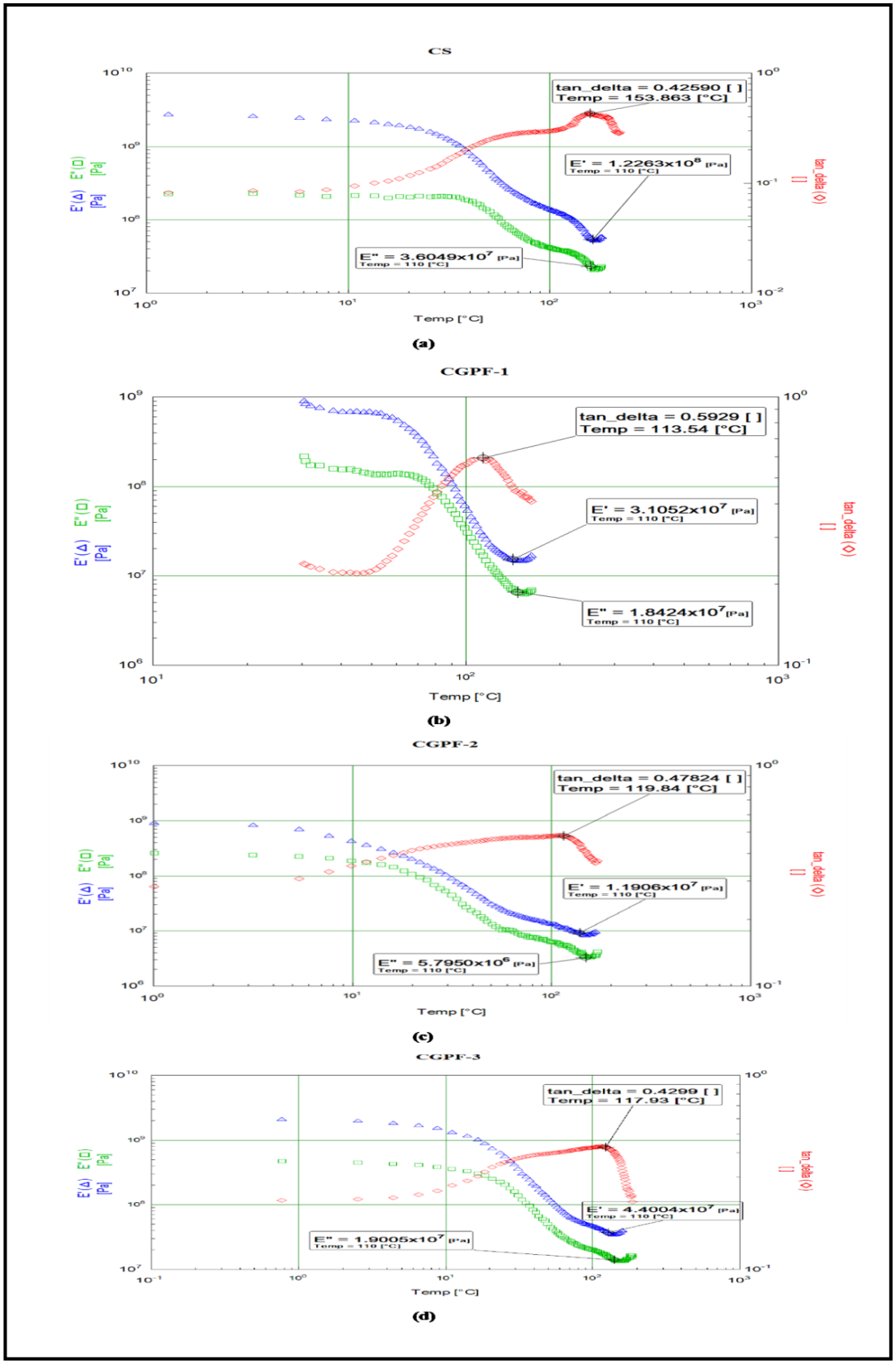

Figure 5.2.4 *Temperature variation of tanδ, glass transition temperature, storage modulus [E'] and loss modulus [E''] (a) Pure chitosan film (b) Grafted chitosan film (c) Grafted chitosan/Pt-Fe_3O_4 hybrid nanoparticle nanocomposite films (d) Grafted chitosan/Pt-Fe_3O_4 hybrid nanoparticle nanocomposite films*

5.2.4.5 Water absorption Behavior

The pure chitosan is hydrophilic but it does not absorb much water, probably due to many –OH and –NH groups in chitosan, which causes strong intermolecular and intramolecular hydrogen bonds; thus, the infiltration and diffusion of water is restrained. The water absorption property of the glycolic acid grafted chitosan is higher than that of the pure chitosan. Fact attributed to it is that the molecular structure integrity is broken in the grafted chitosan, which can expose more functional groups for water absorption. This swelling extent will depend on the osmotic pressure and charge repulsion, the degree of ionization and grafting extent[34]. The water absorption of chitosan-g-GA/Pt-Fe_3O_4 nanocomposites film decreases with an increase of Pt-Fe_3O_4 nanoparticle with grafted chitosan matrix. This is probably due to the formation of a barrier in the form of cross linking points, which prevents water permeation into chitosan. In comparison of grafted chitosan, nanocomposite films show lower water absorption and deceases with the increasing content of nanoparticles. It can be attributed to the interaction between nanoparticle and copolymer. Since nanoparticle is hydrophobic, resulting nanocomposite were expected to be hydrophobic. The formation of nanocomposite occurs through the metallic bond formation between Pt-Fe_3O_4 nanoparticle and copolymer, resulting in the decrease in the water absorption. Increasing content of nanoparticle reduces the exposure of more functional group towards the water, thus the hydrophobicity of the nanocomposite film increases. The behavior of water absorption of chitosan-g-GA/Pt-Fe_3O_4 nanocomposites was investigated, and results were shown in **Table 5.2.3**.

The nanocomposite films are allowed to upto their equilibrium, which was reached after 24h. After complete swelling, film was dried under vaccume at 65^0C to evaluate the moisture retention capacity of the nanocomposite films. It is observed that the film could hold the moisture for a long time. Grafted chitosan shows high water retention capacity. On increasing

the nanoparticle content, the water absorption decreases and the time of drying up to constant weight increases that is they hold the moisture for longer time. Therefore, nanoparticle acts as a physical barrier for the moisture to exude out from the films.

Table 5.2.3 Sorption behavior of the nanocomposites

Sample Code	Water Absorption (%)
CS	54
CGPF-1	77.7
CGPF-2	62.98
CGPF-3	33.2

5.2.4.6 Tensile stress testing

The mechanical properties of chitosan are inconsistent and lack clarity in the mode of analysis such as crosshead speed or molecular weight[35-37]. Therefore, the tensile properties of chitosan were analysed first (**Figure 5.2.5** (a)). All the membranes had uniform thickness of 0.17mm and were semi-transparent. The pure chitosan film exhibits a break stress as 25- 26 %. The elastic modulus of pure chitosan film was observed to be 0.9855 MPa. Crosshead speed used while testing is 10mm/min at 27 ^{0}C. The tensile properties varied significantly with the crosshead speed. Grafted chitosan exhibited a decrease in elastic modulus. Incorporation of nanoparticle increases the elastic modulus of polymer matrix (**Table 5.2.4**) and improves the tensile strength of the polymer film (**Figure 5.2.5** (b)).

Table 5.2.4 Tensile strength and testing of chitosan and nanocomposites

Sample Code	Elastic modulus (MPa)	Stress (%)	Strain (%)
CS	0.9855	47.97	25.83
CGPF-1	0.9556	6.38	83.29
CGPF-2	0.9726	4.99	89.76
CGPF-3	0.9737	4.50	109.20

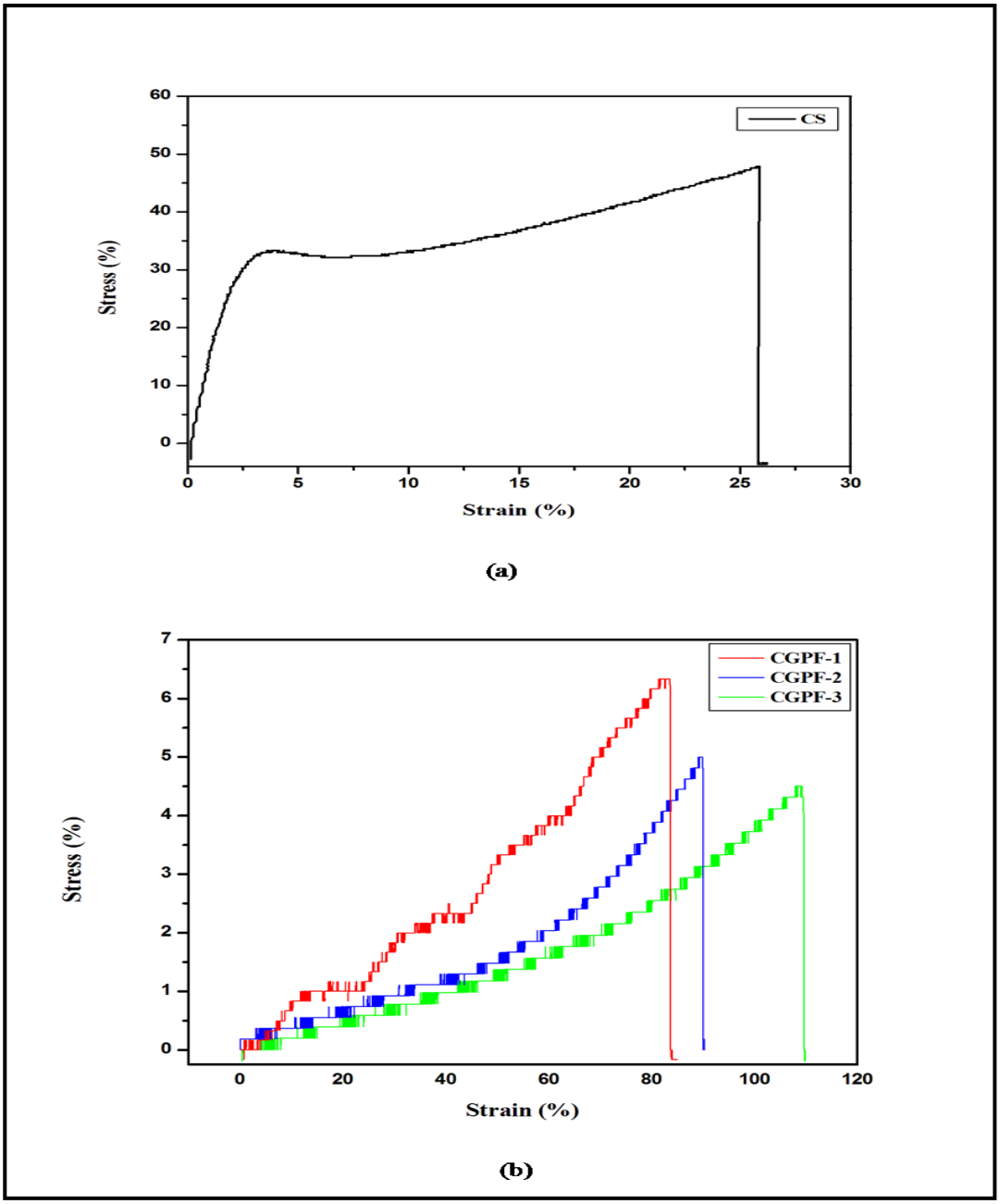

Figure 5.2.5 *(a) Stress strain behavior of pure chitosan membranes (b) Effect of grafting and nanoparticle stress strain behavior of grafted and nanocomposite chitosan membranes.*

5.2.4.7 Thermogravimetric analysis

The thermal degradation of chitosan and nanocomposite with various components under nitrogen flow are shown in **Figure 5.2.6.** In TGA curve, three parameters were measured: temperature of thermal degradation at 20% weight loss, the temperature at 50% weight loss

and the yield of charred residue under nitrogen flow. Two steps of non-oxidative degradation were observed. The weight loss at 50-150 ^{0}C is attributed to the water absorbed in chitosan. Secondly, the weight loss in the temperature range of 200-350 ^{0}C corresponds to the degradation and deacetylation of chitosan[38]. Thermal degradation temperature of chitosan decreases by 20-30 ^{0}C after grafting, however, decrease of 50-60 ^{0}C was observed upon addition of nanoparticles to polymer matrix (**Table 5.2.5**).

Table 5.2.5 TGA results for chitosan and its nanocomposites

Sample Code	Temperature at 20% loss (^{0}C)	Temperature at 50% loss (^{0}C)	char at 900 ^{0}C (wt %)
CS	310	360	27.1
CGPF-1	246	347	27.7
CGPF-2	188	305	2.91
CGPF-3	197	300	11.14

The highest char residues (27.7% at 900 ^{0}C) are observed for grafted chitosan matrix. Increase in char residue is observed upon increasing the nanoparticles wt %. This result indicates the significant effect of combination of glycolic acid and nanoparticles on the thermal properties of chitosan. The thermal stability of chitosan decreases; this is due to the poor heat barrier properties of nanoparticle for polymer matrix during the formation of chars[39]. The amount of weight loss at this temperature range decreases with the increasing content of nanoparticles in samples. This implies that due the grafted chitosan-Co_3O_4-Fe_3O_4 nanoparticles bonding water absorbability that is hydrophillicity of the films decreases. This was also confirmed in water swelling behavior section.

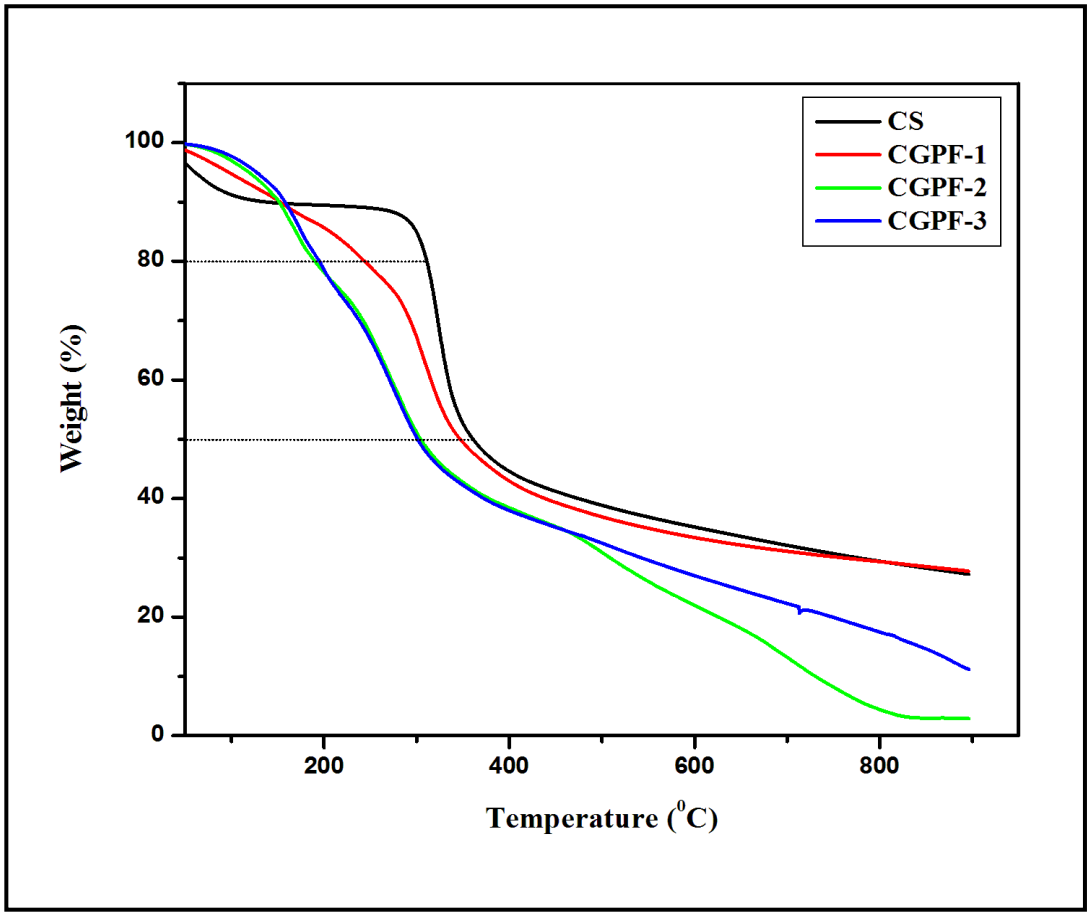

Figure 5.2.6 *Thermogravimetric curves of prepared nanocomposites.*

5.2.5 CONCLUSIONS

In this study, novel inorganic-organic hybrids were prepared from biopolymer and hybrid nanoparticles. The interaction of cationic chitosan with Pt-Fe_3O_4 nanoparticles is through metallic bond, which results in enhancement in structural and functional properties. The grafting of chitosan with glycolic acid imparts hydrophillicity and swelling behavior to the chitosan. The grafted glycolic acid chains were acting as plasticizer to give flexible films. The increasing content of nanoparticles decreases the water absorption, which imparts little branched crystalline structure in the film. The longer water retention and swelling behavior properties were discussed, which could be applied in the field of biomedical.

5.2.6 REFERENCES

1. P. Go´mez-Romero and Sanchez C, *Functional Hybrid Materials, Wiley,* New York, 2004.
2. R. Kishnamoorti and RA. Vaia, *Polymer nanocomposites,* ACS, Washington DC, 2002.
3. R. Chapman and P. Mulvaney, *Chem. Phys. Lett.,* **349,** 358 (2001).
4. O. Wilson, G. J. Wilson and P. Mulvaney, *Adv. Mater.,* **14,** 1000 (2002).
5. P. J. Yoon, T. D. Fornes and D. R. Paul, *Polym.,* **43,** 6727 (2002).
6. G. Lagaly, *Appl. Clay Sci.,* **15,** 1 (1999).
7. P. F. Luckham and S. Rossi, *Adv. Coll. Interface Sci.,* **82,** 43 (1999).
8. J. Dobson, *Drug. Dev. Res.,* **67,** 55 (2006).
9. N. J. Francüois, S. Allo, S. E. Jacobo and M. E. Daraio, *J. Appl. Polym. Sci.,* **105,** 647 (2007).
10. R. Jurgons, C. Seliger, A. Hilpert, L. Trahms, S. Odenbach and C. Alexiou, *J. Phy. Condens. Matter.,* **18,** S2893 (2006).
11. D. L. Zhao, H. L. Zhang, X. W. Zeng, Q. S. Xia and J. T. Tang, *Biomed. Mater.,* **1,** 198 (2006).
12. Q. A. Pankhurst, J. Connolly, S. K. Jones and J. Dobson, J. Phys. D. *Appl. Phys.,* **36,** R167 (2003).
13. R. Hergt, S. Dutz, R. Mu¨ller and M. Zeisberger, *J. Phys. Condens. Matter.,* **18,** S2919 (2006).
14. H. Gu, Z. Yang, J. Gao, CK. Chang and B. Xu, *J. Am. Chem. Soc.,* **127,** 34 (2005).
15. T. Teranishi, Y. Inoue, M. Nakaya, Y. Oumi and T. Sano, *J. Am. Chem. Soc.,* **126,** 9914 (2004).

16. H. W. Gu, R. K. Zheng, X. X. Zhang and B. Xu, *J. Am. Chem. Soc.*, **126,** 5664 (2004).
17. Z. Hens, D. Vanmaekelbergh, E. Stoffels and H. van Kempen, *Phys. Rev. Lett.*, **88,** 236803.1 (2002).
18. K. W. Kwon and M. Shim, *J. Am. Chem. Soc.*, **127,** 10269 (2005).
19. W. Shi, H. Zeng, Y. Sahoo, T. Y. Ohulchanskyy, Y. Ding, Z. L. Wang and P. N. Prasad, *Nano. Lett.*, **6,** 875 (2006).
20. H. Yu, M. Chen, P. M. Rice, S. X. Wang, R. L. White and S. Sun, *Nano. Lett.*, **5,** 379 (2005).
21. S. Kudera, L. Carbone, M. F. Casula, R. Cingolani, A. Falqui, E. Snoeck, W. J. Parak and L. Manna, *Nano. Lett.*, **5,** 445 (2005).
22. K. T. Yong, Y. Sahoo, M. T. Swihart and P.N. Prasad, *Adv. Mater.*, **18,** 1978 (2006).
23. C. L. Schauer, M. S. Chen, M. Chatterley, K. Eisemann, E. R. Welsh, R. R. Price, P. E. Schoen and F. S. Ligler, *Thin Solid Films.*, **434,** 250 (2003).
24. D. S. Dos Santos, A. Jr. Riul, R. R. Malmegrin, F. J. Fonseca, O. N. Jr. Oliveira and L. H. C. Mattoso, *Macromol. Biosci.*, **3,** 591 (2003).
25. M. Xie, H. H. Liu, P. Chen, Z. L. Zhang, X. H. Wang, Z. X. Xie, Y. M. Du, B. Q. Pand and D. W. Pang, *Chem. Commun.*, **44,** 5518 **(**2005).
26. J. Xie, Q. Zhang, J. Y. Lee and D. I. C. Wang, *ACS. Nano.*, **2,** 2473 (2008) .
27. J. Rodriguez-Fernandez, J. Perez-Juste, F. J. G. Abajo and L. M. Liz- Marzan, *Langm.*, **22,** 7007 (2006).
28. H. Yu, M. Chen, P. M. Rice, S. X. Wang, R. L. White and S. Sun, *Nano. Lett.*, **5,** 379 (2005).
29. T. D. Schladt, M. I. Shukoor, K. Schneider, M. N. Tahir and F. Natalio et al., *Angew. Chem.*, **49,** 3976 (2010).

30. K. Ogawa, S. Hirano, T. Miyanishi, T. Yui and T. Watanabe, *Macromol.,* **17,** 973 (1984).

31. S. F. Wang, L. Shen, W. D. Zhang and Y. J. Tong. *Biomacromol.,* **6,** 3067 (2005).

32. M. Jaworska, K. Sakurai, P. Gaudon and E. I. Guibal, *Polym. Int.,* **2,** 198 (2003).

33. F. Al-Sagheer and S. Muslim, *J. Nanomater.,* **2010,** 1 (2009).

34. P. Seong, Y. Jin and P. Ham, *Biomater.,* **22,** (2000) 323–330.

35. M. Cheng, J. Deng, F. Yang, Y. Gong, N. Zhao and X. Zhang, *Biomater.,* **24,** (2003) 2871–80.

36. R. Chen and H. Hwa, *Carbohyd. Polym.,* **29,** 353 (1996).

37. M. Qurashi, H. Blair and S. Allen, *J. Appl. Polym. Sci.,* 46, 255 (1992).

38. S. F. Wang, L. Chen and Y. J. Tong, *J. Polym. Sci. Part A. Polym.,* Chem. **44,** 686 (2006).

39. S. F. Wang, L. Shen, Y. J. Tong, L. chen, I. Y. Phang and T. X. Liu, *Polym. Degrad. Stab.,* **90,** 123 (2005).

40. J. H. Han and J. M. Krochta, *Trans. ASAE.,* **42,** 1375 (1999).

CHAPTER 6

A: Preparation and Characterization of Glycolic Acid-g-Chitosan-Co_3O_4 Nanoparticles Based Nanohybrid Scaffolds for Drug-Delivery and Tissue Engineering Applications

6.1 INTRODUCTION

In the field of nanotechnology, polymer matrix based nanocomposites have become a prominent area of current research and development. These materials exhibit unique optical[1], thermal, electrical and mechanical properties due to the interaction of the polymer with the particle and state of dispersion[2-4]. Transition metal nanoparticles are one of the most–studied systems due to their quantum size effects[5], novel electronic[8], optical[9], magnetic[10] and chemical properties. These metal nanostructure system play an important role in many different fields of science such as nano-electronics, catalysis[11-13] and recently, in biomedical application[14-16]. Cobalt oxide nanoparticles are currently attracting enormous interest owing to their unique size- and shape dependent properties and potential applications for example, pigments, catalysis, sensors, electrochemistry, magnetism, energy storage, etc[17]. Here, we have demonstrated that these Cobalt oxide nanoparticles based materials can be used in the field of controlled drug release and cell proliferation systems, which is having major scientific application in the field of biomaterials[18].

A wide range of materials have been employed as drug carriers such as lipids, surfactant, dendrimers and natural or synthetic polymers[19-22]. Chitosan has prompted the continuous movement for the development of safe and effective drug delivery systems because of its unique physicochemical and biological characteristics. This polycationic biopolymer is generally obtained by alkaline deacetylation of chitin, which is the main component of the exo-skeleton of crustaceans[23]. Chitosan is hydrophilic and compatible with nanoparticle and has better processability due to the presence of amino group (pKa value is 6.2) in the chain. Chemical modification of chitosan is useful for the association of bioactive molecules to polymer and controlling the drug release profile. The grafting of side glycolic acid leads to marked changes in the chitosan structure[24, 25]. Chitosan has amino and hydroxyl functional groupS which act as potential site for altering the polymers functionality[26-28].

6.2 EXPERIMENTAL

6.2.1 Materials

Deionised water was used throughout, which is prepared by Milli-Q-system. Chitosan of low molecular weight (Mw =1.5×10^5, degree of deacetylation was 85%), glycolic acid (99% purity), cobalt acetate ($Co(OAc)_2$), citric acid ($C_6H_8O_7$) was obtained from sigma Aldrich. lithium chloride (LiCl), Tri phenyl phosphate (TPP), pyridine (Py), sodium hydroxide (NaOH) was obtained from M/s Sisco Research Laboratories, Mumbai.

6.2.2 Preparation of Co_3O_4 nanoparticles

Co_3O_4 nanoparticles **(**CoNP) were prepared by hydrothermal method. Cobalt acetate (2g), citric acid (2g) and NaOH (4g) was taken in stainless steel teflon lined hydrothermal bomb. To the reaction mixture, 110 mL of deionised water was added. The hydrothermal bomb was screw tight and heated at 120 ^{0}C for 40 h. After 40 h hydrothermal bomb was cooled to room temperature. The formed black precipitate was centrifuged and calcinated at 350 ^{0}C for 24 h (**Scheme 6.2.1**).

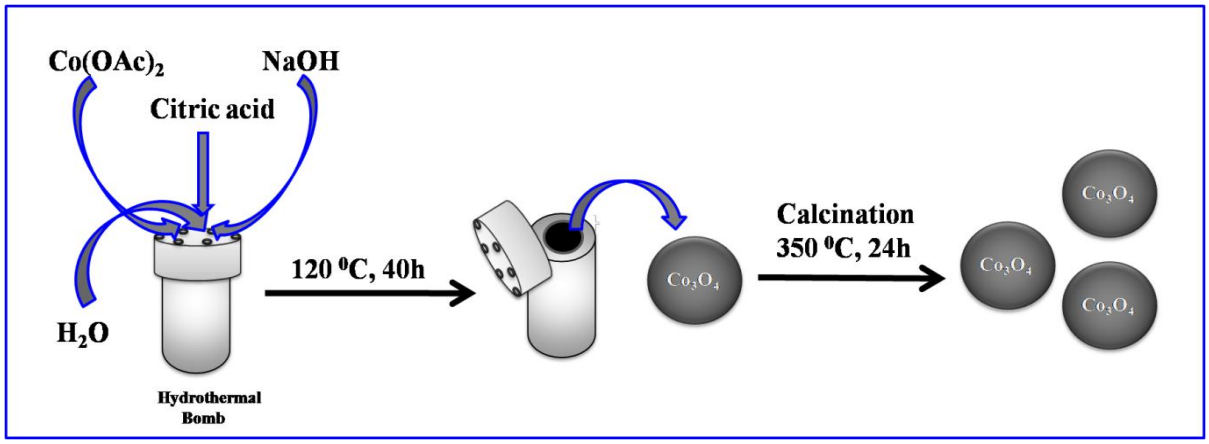

Scheme 6.1 *Schematic illustration of synthesis of Co_3O_4 hybrid nanoparticles.*

6.2.3 Preparation of nanohybrid scaffolds and drug loading

Glycolic acid grafted chitosan (1g) (Discussed in **chapter 3B. section 3.2.2.3**) was dispersed in deionised water (50 mL) and stirred for 1 h at room temperature. After 1h, Co_3O_4

nanoparticles (50 mg) were added to the solution and stirred overnight at room temperature. The resulting solution was heated up to 80 ^{0}C with continuous degassing for 30 min. The resulting solution was cooled to room temperature after degassing. The drug (CPA) (10 mg) was added to the resulting solution and stirred for 5 h, so that drug completely mixes with the solution. The drug loaded solution was poured in tissue culture plates (20×20 mm diameter) and quenched in liquid nitrogen. The quenched sample was freeze dried by lyophilisation under -100 ^{0}C temperature for 6 h. In lyophilisation water molecules were removed by freezing and sublimation of ice crystals, which lead to the formation of pores. The formulations are shown in the **Table 6.1**.

Table 6.1 Formulation of Cyclophosphamide (CPA)-loaded nanohybrid of chitosan-g-glycolic acid and Co_3O_4 nanoparticles

S.No	Grafted Chitosan (g)	Co_3O_4 (mg)	CPA (%)	Drying Process	Sample Code
1	1	_	_	Vacuum	CGCo-1
2	1	50	_	Vacuum	CGCo-2
3	1	50	_	Freeze	CGCo (D)
4	1	50	10	Freeze	CGCo (S)

6.3 CHARACTERIZATION OF NANOHYBRID

6.3.1 Transmission Electron Microscopy (TEM)

High Resolution Transmission Electron Microscopy (HR-TEM model Technai TF30, 300KV FEG) was used to analyse the particle size, morphology and Selected Area Diffraction pattern (SAED) of Co_3O_4 nanoparticles.

6.3.2 X-ray photoelectron spectroscopy (XPS)

The formation of Co_3O_4 nanoparticles was analysed with X-ray photoelectron spectroscopy (XPS) using an ESCA-3000 (VG Scientific Ltd., UK) with a base pressure of better than 1.0×10^{-9} Pa. Mg Kα radiation (1253.6 eV) was used as a X-ray source and operated at 150 W. All the binding energies were calibrated by using the contaminant carbon (C1s = 284.5 eV) as a reference[29].

6.3.3 Fourier transform infrared spectroscopy

Attenuated total reflectance Fourier transform infrared (ATR-FTIR) Nicolet Nexus 870 FTIR spectrometer equipped with a smart Endurance diamond accessory (64 scans, 4 cm^{-1} resolution, wave number range 4000-550 cm^{-1}) was used to analyse fourier transform infrared spectra of neat chitosan (CS), chitosan grafted glycolic acid (CGCo-1), nanohybrid scaffold (CGCo (S)) and drug (CPA).

6.3.4 Scanning Electron Microscpy (SEM)

Scanning Electron Microscpy (SEM) (Model, JOEL Stereoscan 440, Cambridge) was used to investigate the surface morphology of the porous scaffolds. Prior to the observation, specimens were fixed on the copper grid.

6.3.5 In vitro drug release

The drug loaded nanohybrid scaffold (CGCo-(S)) were immersed in 10 ml of aliquots of 0.1 M phosphate buffer (pH 7.4) and incubated at 37 ^{0}C. After specific interval, 3 ml aliquot of the specimen were withdrawn and immediately fresh medium is added to it. Drug content in each aliquot was quantitatively analysed by UV-vis spectrophotometer (UV-NIR- PL Lamda 950) at 180 nm.

6.3.6 Swelling behavior

The swelling behavior of porous scaffold was determined by exposing them to media of different pH, 1N HCl, 1N NaOH and simulated body fluid (SBF) (pH 7.4) solutions. The

shape retention of porous scaffold was determined by measuring the change in its diameter of scaffold as a function of time in the media.

6.3.7 Cell viability study

In vitro cell culture was carried out using L929 cell. These cells are derived from an immortalized mouse fibroblast cell line and are internationally recognized cells that are routinely used in *in-vitro* cytotoxicity assessments. The scaffold was sterilised by putting it in 6 well tissue culture plate containing isopropanol (5 mL) and exposed to UV radiation for 4 h. L929 cells were further seeded on nanohybrid scaffold placed in 6-well plate at a density of 5×10^3 cells/well and incubated at 37 °C, 5% CO_2 and 95% humidity incubation conditions. The tissue culture plate containing only cells were used as control. To study the cell proliferation on different substrates, cell proliferation was determined by the colorimetric MTT assay. MTT assay is based on the reduction of yellow 3-(4, 5 dimethylthiazol-2-yl)-2, 5-diphenyltetrazolium bromide (MTT) salt in MTT to form purple formazan by dehydrogenase enzymes secreted from the mitochondria of metabolically active cells. The amount of formazan formed is directly proportional to the number of viable cells. After 2 h, 4 h, 6 h, 24 h, 48 h, 72 h, the cells solution (100 µl) was transferred to an ELISA micro-plate and optical density (OD) was measured at 540 nm using the spectroscopic method[30]. The relative cell growth was compared to control cell, which exhibit cell culture medium without chitosan. It was calculated by using the given eq. (1)

$$\% \text{ Live cell} = 100 - \left[\frac{(C - T)}{(C - B)} \times 100 \right] \qquad (1)$$

C = OD of control

T = OD of test sample

B = OD of blank

OD = Optical density

All the in vitro tests were done in triplicate and results were reported as an average value.

6.4 RESULTS AND DISCUSSION

Scheme 6.2 *Schematic illustration of interactions between chitosan-g-glycolic acid, drug and* Co_3O_4 *hybrid nanoparticles in nanohybrid porous scaffold.*

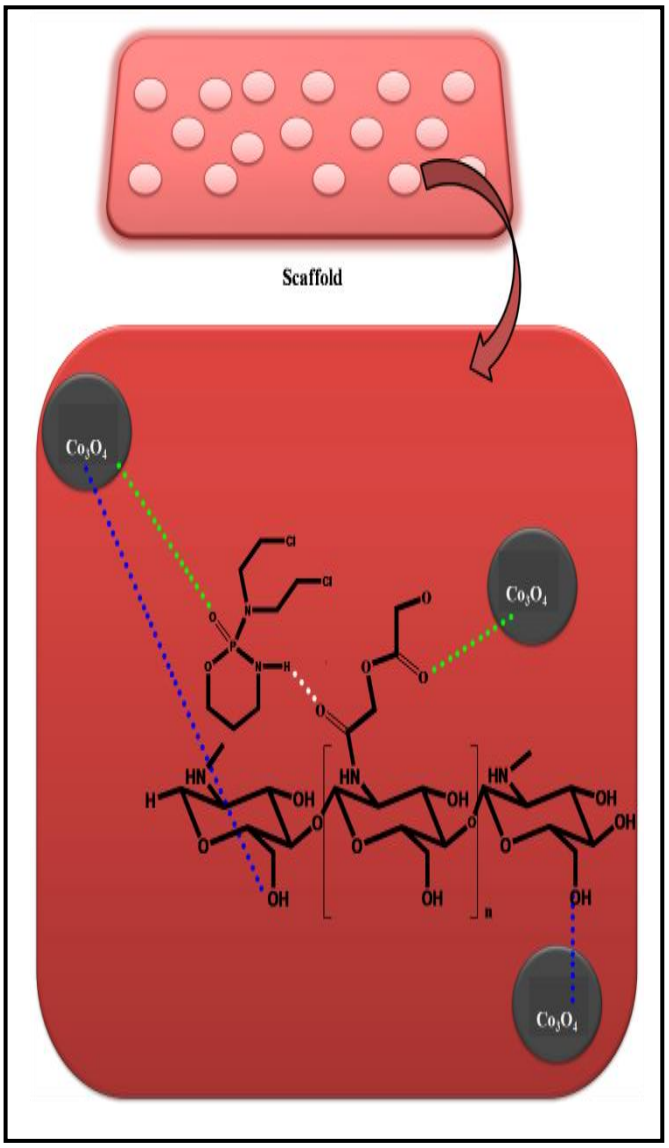

6.4.1 TEM analysis

The TEM image of Co_3O_4 nanoparticles (**Figure 6.1** (a)) exhibit uniformly spherical morphology almost same overall size. **Figure 6.1** (b) shows the high resolution TEM image of Co_3O_4 nanoparticles, which are crystalline as shown in selected area diffraction (SAED)

pattern **Figure 6.1** (c). The electron diffraction pattern can be determined by face centred cubic (FCC) structure of Co_3O_4 with (1 1 1), (2 2 0) and (3 1 1) planes. The distance between the two adjacent lattice planes in Co_3O_4 domain is consistent with the reported value.

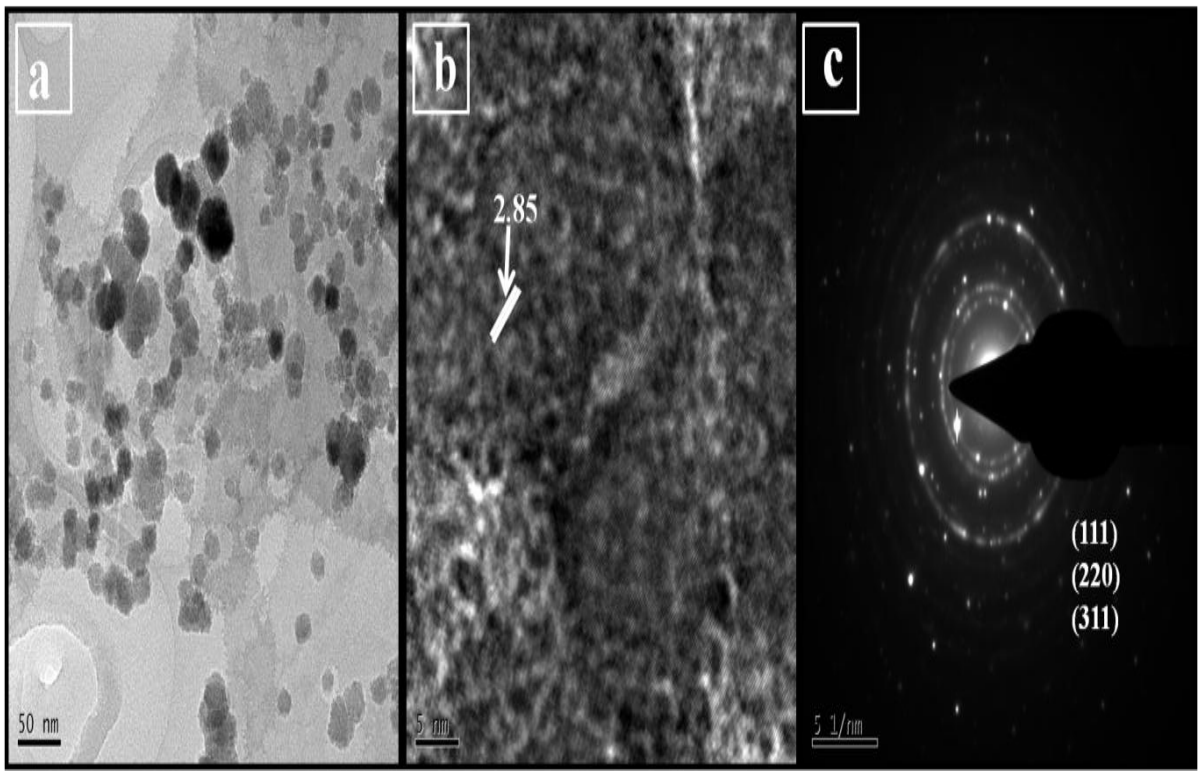

Figure 6.1 *(a) TEM image of Co_3O_4 nanoparticles, (b) HRTEM image of Co_3O_4 nanoparticles, (c) SAED Pattern of Co_3O_4 nanoparticles.*

6.4.2 XPS analysis

The formation of Co_3O_4 nanoparticles were confirmed with X-ray photoelectron spectroscopy (XPS) measurements, which were carried out in the region of 0-1300 eV. **Figure 6.2** shows Co $2p_{3/2}$ and $2p_{1/2}$ core-level signals with binding energy at 780.2 and 795.2 eV, respectively. These binding energies as well as their difference (spin–orbit splitting) were very close to those reported for the mixed valence $Co^{II}Co_2^{III}O_4$ compound having similar electronic configuration[29]. The results demonstrate that the formed nanostructures were composed of Co_3O_4.

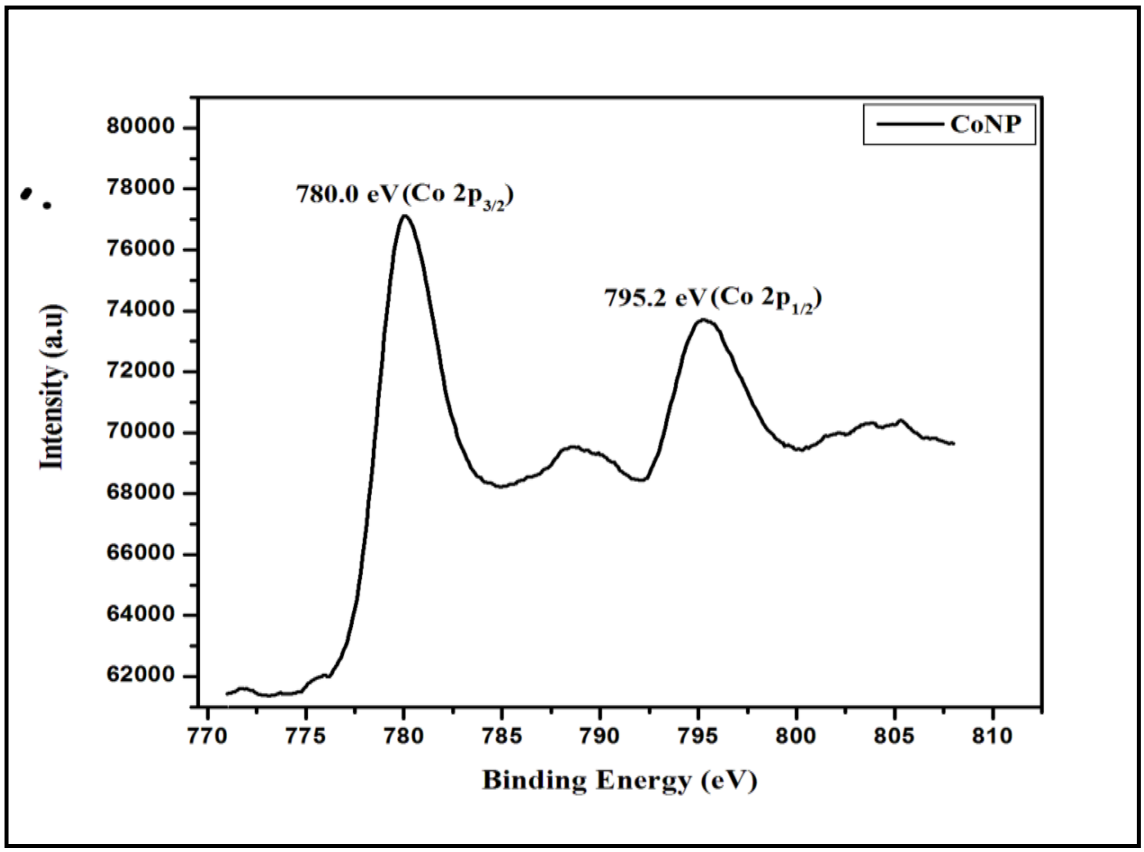

Figure 6.2 XPS *core spectrum for Co 2p in Co_3O_4 nanoparticles.*

6.4.3 FTIR analysis

Fourier transform infrared (FT-IR) spectra reveals information about the structure of neat chitosan (CS), chitosan grafted glycolic acid (CGCo-1), nanohybrid scaffold (CGCo (S)) and drug (CPA) (**Figure 6.3**). The characteristic peaks in the FTIR spectrum of CS include 1633 cm^{-1} (-NH stretching) and 3500cm^{-1} (-OH stretching). The presence of extra peak at 1728 cm^{-1} (-C=O stretching) and shifting of peak (-NH stretching) towards the lower frequency region (1567 cm^{-1}) confirms the interaction of glycolic acid with NH_2 group of chitosan. The grafting of glycolic acid on chitosan was confirmed by the formation of amide (–NH-C=O) linkage between amine (-NH_2) group of chitosan and –C=O group of glycolic acid. In the FTIR spectrum of CPA include peak at 1237 cm^{-1} (-P=O stretching) and 1648 cm^{-1} (-NH stretching). The FTIR spectrum of CGAF-(D) include shift in peak 1069 cm^{-1} (-P=O stretching) and 3194 cm^{-1} (-OH stretching) it may due to the interaction of Co_3O_4

nanoparticles with –P=O group of drug molecule and –OH group of chitosan via metallic bond. The peak at 1567 cm^{-1} in CGCo-(S) is attributed to shift in –C=O stretching towards lower frequency region, it may be due to the interaction of CPA with –C=O group of grafted glycolic acid via H- bonding (**Scheme 6.1**).

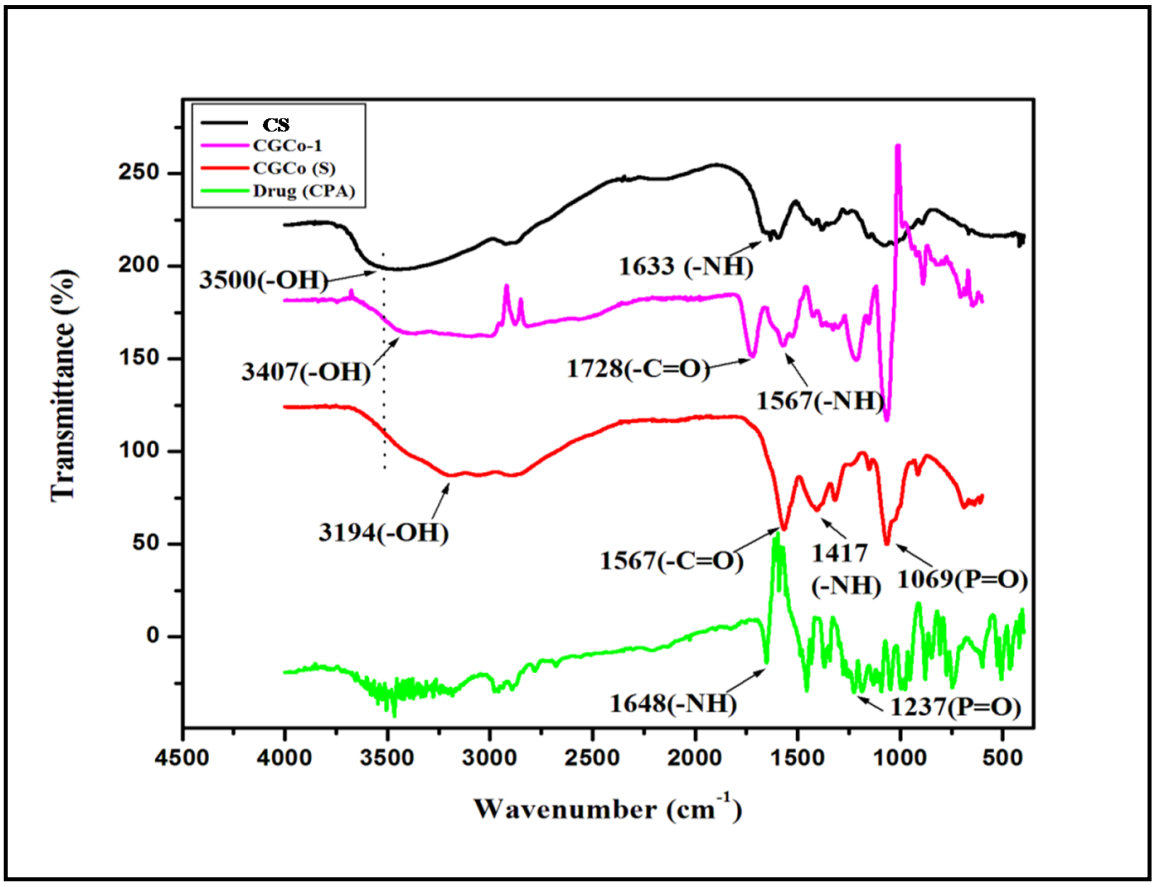

Figure 6.3 *FTIR spectra of neat chitosan (CS), grafted chitosan (CGCo-1), grafted chitosan and Co_3O_4 nanohybrid scaffold (CGCo (S)) and Cyclophosphamide (CPA) drug.*

6.4.4 Morphological study

The SEM image (**Figure 6.4** (a, b)) reveals the morphology of nanohybrid scaffold before and after drug loading (**Figure 6.4** (c, d)). It is observed that pore size of scaffold before drug addition was ranging from 10.84µm to 12.62 µm, but upon addition of drug pore size decreases and lies in the range of 9.20 µm to 11.07 µm. The decrease in the pore size may be

due to the incorporation of drug molecule in the pores of scaffold. The SEM-EDAX of scaffold confirms the incorporation of Co_3O_4 nanoparticles in it (**Figure 6.4** (e))

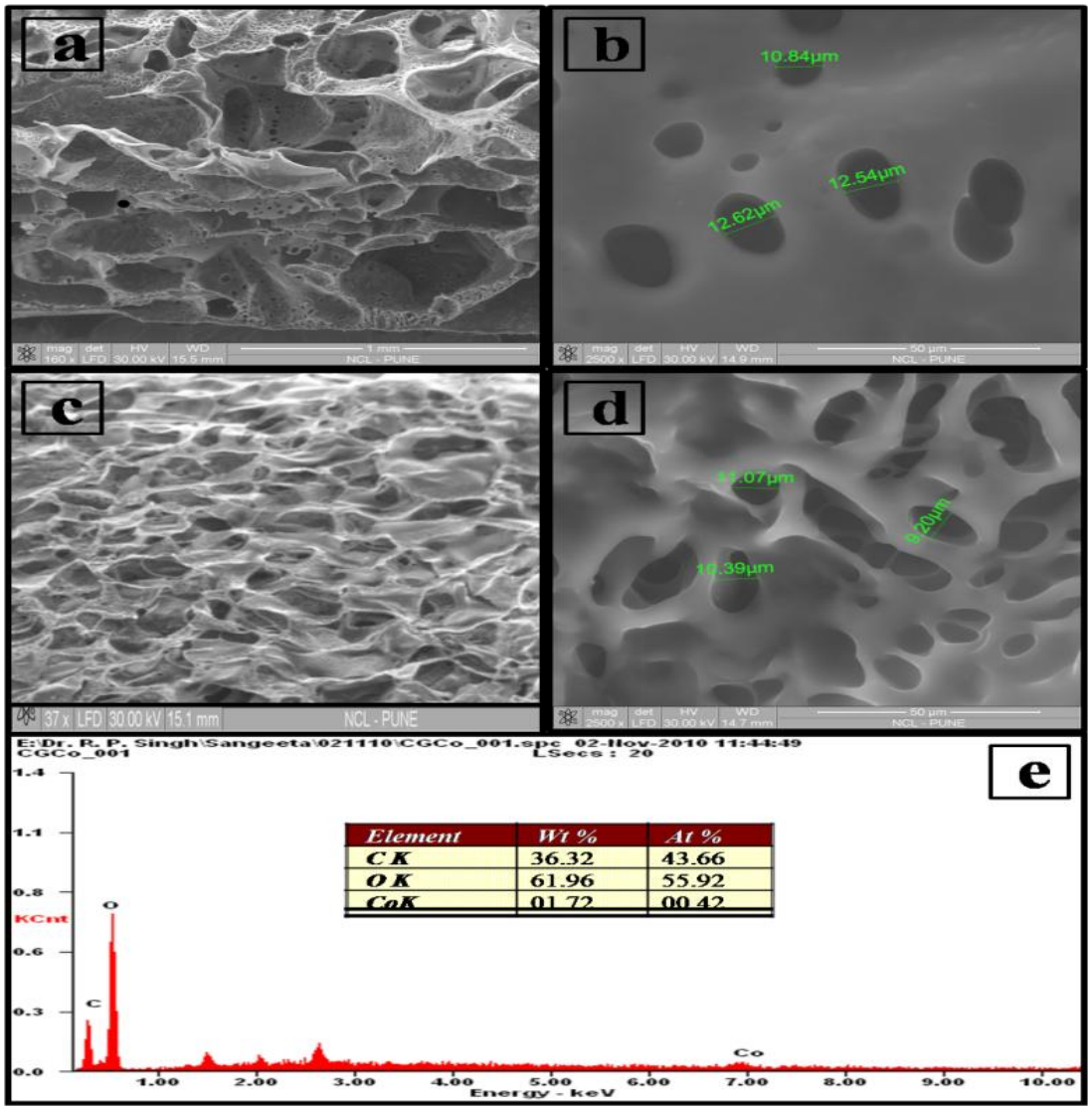

Figure 6.4 *(a, b) SEM image of grafted chitosan and Co_3O_4 nanohybrid scaffold without drug; (c, d) SEM image of grafted chitosan and Co_3O_4 nanohybrid scaffold with drug; (e) EDAX of nanohybrid scaffold (CGCo (S)).*

6.4.5 In vitro drug release

Figure 6.5 shows UV-vis spectra of in vitro drug release study illustrating variations in the absorbance of the drug in the scaffold with respect to time. In vitro drug release was examined with SBF (pH 7.4) and release media was quantified by UV-visible spectral

absorbance values. It is observed that initially the release of drug was high and it decreases with the time because the drug which is at the surface of scaffold is released much faster than the drug incorporated deeply into the pores of the scaffold. The effect of incorporation of Co_3O_4 nanoparticle can be significantly observed as reduced rate of release at initial stage of immersion (upto 200 min). Initially specimen is solvated, which facilitates the lateral diffusion of drug after 250 min[31]. The rate of release of drug decrease over the time, it may be due to the interaction of Co_3O_4 nanoparticle and grafted glycolic acid chains with the loaded drug[30].

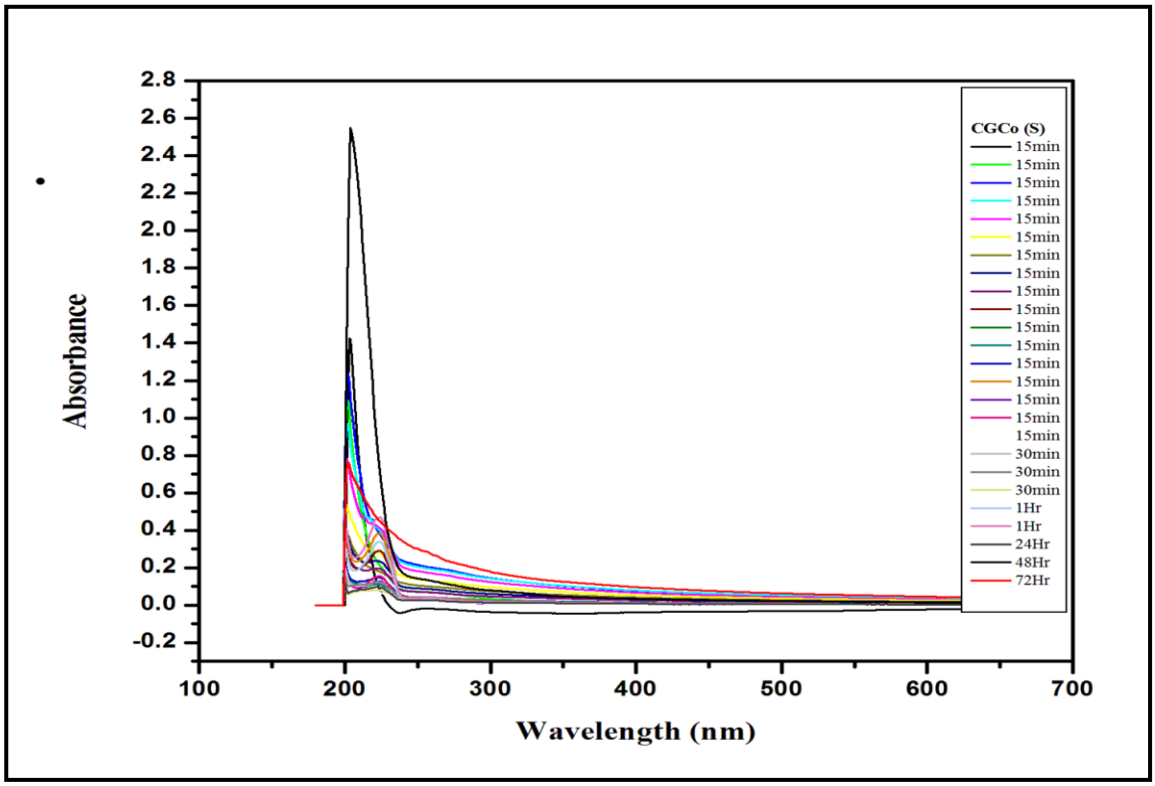

Figure 6.5 *Drug release study of prepared nanohybrid scaffold (CGCo (S)).*

6.4.6 Shape retention study

In general, swelling of chitosan involves the protonation of amino/imine groups and the mechanical relaxation of coiled chitosan chain[32,33]. Shape retention was studied by measuring the change in the diameter as a function of immersion time in the media[34]. Swelling behavior

of scaffold strongly depends upon the pH of the implantation site for their practical use in tissue engineering. It was investigated by exposing it to media at different pH, 1N HCl (pH 1.2), 1N NaOH (pH 14) and simulated body fluid (SBF) (pH 7.4) solutions for 24 h. The in vitro cell culture studies indicate that initial swelling is desirable[35,36], but continuous swelling reduces the mechanical integrity and leads to the generation of compressive stress to the surrounding tissue. It is observed that scaffold CGCo (D) dissolve completely in the HCl solution within 2.5 h of immersion, whereas, rate of swelling is very low in NaOH and reached the plateau level around 3 h of immersion but increase in size of scaffold is observed within 6 h in SBF solution. In the case of scaffold CGCo (S), its complete dissolution was observed in HCl solution within 2.5 h of immersion, whereas slight swelling was observed in SBF within 3.5 h. These results showed that nanohybrid scaffold is stable towards the SBF and higher pH solution (**Figure 6.6**).

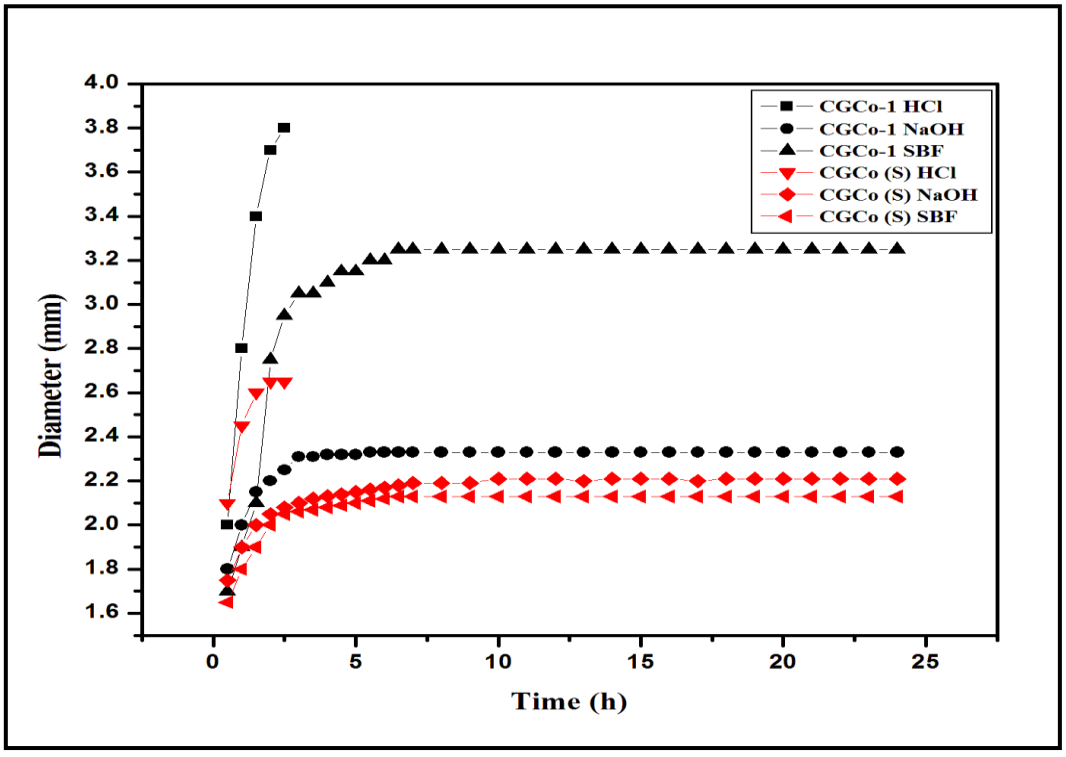

Figure 6.6 *Shape retention of scaffolds prepared from grafted chitosan and* Co_3O_4 *nanohybrid.*

6.4.7 Cell viability study

MTT assay was carried out to evaluate the proliferation of L929 on (CGCo-(S)). Growth of the cells cultured on the scaffold was higher during the first 2 h but slight decrease in the cell number was observed in next 4 h. It may be because during proliferation, cells have occupied all the available spaces on the scaffold[37]. Present study implies that the cell proliferation is not affected by the incorporation of Co_3O_4 nanoparticle into glycolic acid grafted chitosan[38]. This may be due to the enhanced interaction between Co_3O_4 hybrid nanoparticles and growing cells on the biopolymer matrix (**Figure 6.7**). These results of improved cell proliferation and cell adherence on scaffold was mainly due to the presence of reactive groups on the polymer surface and improved hydrophillicity after hydrolysis, similar to those reported by other researchers[39]. The Co_3O_4 nanoparticles may develop London- van der Waals forces with cells. These Co_3O_4 nanoparticles can act as adhesive between biopolymer and cells.

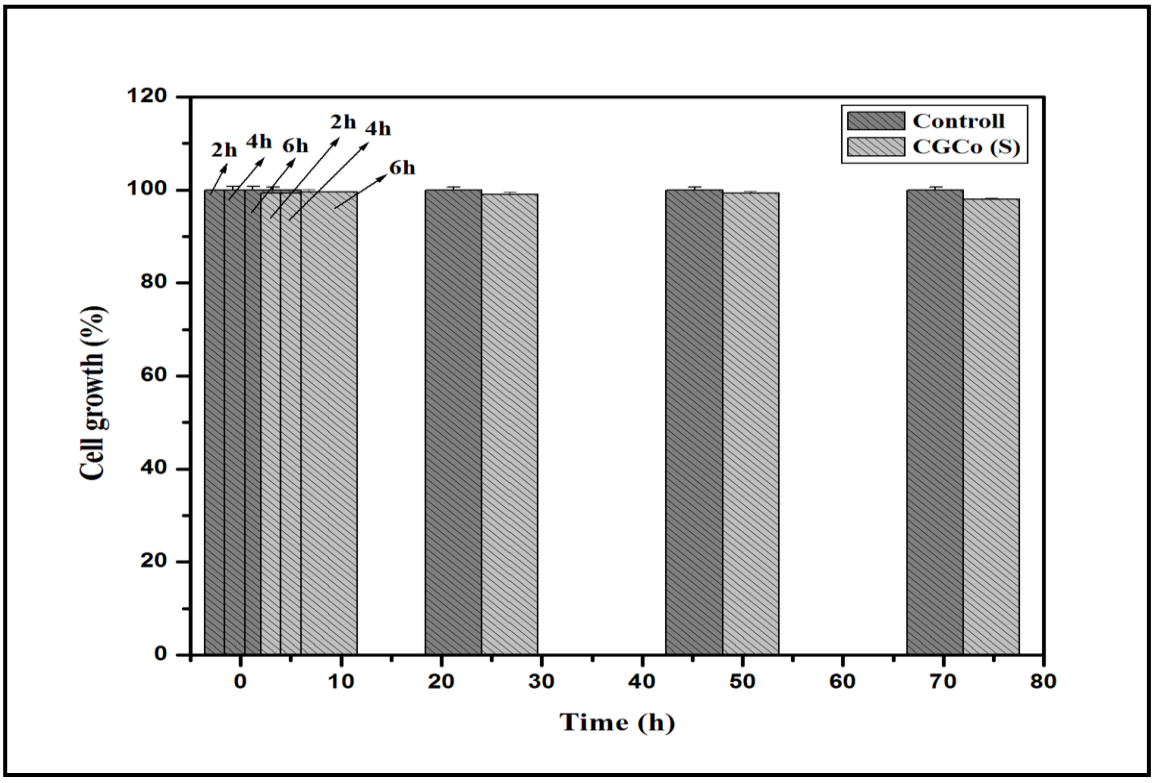

Figure 6.7 *Cell viability study done with MTT assay of cultured cells.*

6.5 Conclusion

The present study examined the potential use of hybrids of chitosan-g-glycolic acid and Co_3O_4 nanoparticles as biomaterial. The FTIR confirmed the interaction of cationic chitosan with Co_3O_4 nanoparticles via metallic bond and linkage of drug with the polymer matrix via H-bond. The nanohybrid scaffolds are stable regardless of pH of the medium. The nanohybrid scaffold posses porous morphology. The porous nanohybrid scaffolds have shown faster and higher drug release. The incorporation of Co_3O_4 nanoparticles was observed to control the initial release of drug. The results show that the prepared nanohybrid scaffold is biocompatible. It also concludes that Co_3O_4 nanoparticles are viable additive for formulating sustained drug delivery systems and could be applied in the field of biomaterials.

6.6 REFERENCES

1. R. Chapman and P. Mulvaney, *Chem. Phys. Lett.,* **349,** 358 (2001).
2. R. Krishnamoorti and R. A. Vaia, *Polymer nanocomposites,* Washington DC, ACS **2002**.
3. G. Lagaly, *Appl. Clay Sci.,* **15,** 1(1999).
4. P. F. Luckham and S. Rossi, *Adv. Coll. Interface Sci.,* **82,** 43 (1999).
5. R. Jin, *Nanoscale.,* **2,** 343 (2010).
6. M. M. Alvarez, J. T. Khoury, T. G. Schaaff, M. N. S. gullin, I. Vezmar and R. L. Whitten, *J. Phys. Chem. B.,* **101,** 3706 (1997).
7. M. Zhu, C. M. Aikens, F. J. Hollander, G. C. Schatz and R. Jin, *J. Am. Chem. Soc.,* **130,** 5883 (2008).
8. T. Teranishi, *Comptes. Rendus. Chimie.* **6,** 979 (2003).
9. I. Pastoriza-Santos, D. Gomez, J. Pérez-Juste, M. Luis, L. Marzán and P. Mulvaney, *Phys. Chem. Chem. Phys.,* 6, 5056 (2004).

10. Y. Yamamoto, T. Miura, Y. Nakae, T. Teranishi, M. Miyake and H. Hori, *Phys. B:Condensed Matter.,* **329,** 1183 (2003).
11. J. D. Aiken and R. G. Finke, *J. Mol. Catal. A: Chem.* **145,** 1(1999).
12. A. Roucoux, J. Schulz and H. Patin, *Chem. Rev.,* **102,** 3757 (2002).
13. J. S. Bradley and G. Schmid, *Nanoparticles*, Wiley-VCH, Weinheim, **2004**.
14. S. Akiyama, T. Yoshimura and K. Esumi, *J. Jpn. Soc. Colour Mater.,* **78,** 112 (2005).
15. Y. Jiang, L. Zhang, D. Yang, L. Li, Y. Zhang, J. Li and Z. Jiang, *Ind. Eng. Chem. Res.* **47,** 2495 (2008).
16. Y. Jiang, D. Yang, L. Zhang, Q. Sun, X. Sun, J. Li and Z. Jiang, *Adv. Funct. Mater.,* **19,** 150 (2009).
17. X. Liu, G. Qiu and X. Li, *Nanotechnology*., **16,** 3035 (2005).
18. K. C. Souza, Æ. J. D. Ardisson and Æ. E. M. B. Sousa, *J. Mater Sci.,* **20,** 507 (2009).
19. R. Duncan, *Nat. Rev. Drug Discov.* **2,** 347 (2003).
20. R. Duncan, *J. Drug Target.*, **14,** 333 (2006).
21. V. Torchilin, *Drug Deliv.* **5,** 1003 (2008).
22. S.G. Sampathkumar and K. J. Yarema, Chem. Biol. **12,** 5 (2005).
23. T. N. Van, C. H. Ng, K. N. Aye, T. S. Trang and W. F. Stevens, *J. Chem. Tech. Biotech.,* **81,** 1113 (2006).
24. M. Xie, H. H. Liu, P. Chen, Z. L. Zhang, X. H. Wang, Z. X. Xie, Y. M. Du, B. Q. Pand and D. W. Pang, *Chem. Commun.*, **44,** 5518 (2005).
25. J. Xie, Q. Zhang, J. Y. Lee and D. I. C. Wang, *ACS Nano.* **2,** 2473 (2008).
26. J. D. S. Dos Santos, P. J. G. Goulet, N. P. W. Pieczonka, J. ONOliveira and R. F. Aroca, *Langmuir.* **20,** 1027 (2004).
27. K. Kurita, *Prog. Polym. Sci.,* **26,** 1921 (2001).
28. R. L. Hong and J. Y. Yu, *J. Biomed. Mater: Appl. Biomater.,* **71B,** 52 (2004).

29. B. Varghese, T. C. Hoong, Z. Yanwu, , M. V. Reddy, B. V. R. Chowdari, A. T. S. Wee, T. B. C. Vincent, C. T. Lim and C. H. Sow, *Adv. Funct. Mater.*, **17,** 1932 (2007).
30. T. Takahashi and M. Yamaguchi, *J. Colloid Interface Sci.*, **146,** 556 (1991).
31. S. Liu, H. Hu, J. Zhou and L. Zhang, *Cellulose.*, **18,** 1273 (2011).
32. S.I Park and Y. Zhao, *J. Agric. Food Chem.*, **52,** 1933 (2004).
33. L. Vachoud, N. Zydowicz and A. Domard, *Carbohydrate Res.*, **326,** 295 (2000).
34. S. Aiba, *Int. J. Biol. Macromol.*, **13,** 40 (1991).
35. S. Kumari and R.P. Singh, *Int. J. bio. Macromol.*, **50,** 883 (2012).
36. L. M. Liz-Marzan, *Mater Today.*, 7, 26 (2004).
37. N. Shanmugasundram, P. Ravichandaran, P.N. Reddy, N. Ramamurth, S. Pal and K.P. Rao *Biomaterials***., 22,** 1943 (2001).
38. S.I Park and Y. Zhao, *J. Agric. Food Chem.*, **52,** 1933 (2004).
39. F. Chen, C. N. Lee and S. H. Teo, *Mater. Sci. Eng.C.*, **27,** 325 (2007).

CHAPTER 6

B: Preparation and Characterization of Glycolic acid-g-Chitosan-Co_3O_4 Nanoparticles Based nanocomposite Films

6.2.1 INTRODUCTION

In recent years, nanoparticles have received special attention because of their unique optical, electronic, magnetic, chemical and mechanical properties[1]. These properties vary as a function of the nanoscale domain size. The metal-containing nanoparticles including those stabilized in polymer matrices is stimulated by the ever increasing interest in nanotechnology and materials research[2-7] because of their wide area of applications as micromechanical device[8], optical device[9], catalytic membrane[10], and biosensors[11]. The nanoparticles are the most attractive for the fabrication of metal-containing polymer-matrix nanocomposites because they possess a number of unique characteristics, which is missing in bulk materials[12-16]. The organic/inorganic nanocomposite materials are fast growing area of research. Different approaches have been developed for the synthesis of nanocomposites such as incorporation of premade nanoparticles into the polymer matrix. This can be achieved with the reduction of metal salt dispersed in polymer matrix using an external reducing agent[17]. The metal nanoparticle embedded polymer film can show enhanced electrical[18-20], mechanical and thermo-mechanical properties of polymers[21, 22]. The polymer-matrix nanocomposites are of great importance because such nanosystems offer unique combination of chemical, physical and mechanical properties. Therefore, attempts have been made to synthesize metal nanoparticles embedded chitosan films. The presence of reactive functional groups in chitosan offers great opportunity for chemical modification. The grafting of glycolic acid on chitosan leads to marked changes in its structure[23, 24].

6.2.2 EXPERIMENTAL

6.2.2.1 Materials

Chitosan of low molecular weight (Mv =1.5×10^5, degree of deacetylation was 85%), glycolic acid with (99% purity), cobalt acetate ($Co(OAc)_2$), citric acid ($C_6H_8O_7$) was obtained from

sigma Aldrich. Sodium hydroxide (NaOH) was obtained from M/s Sisco Research Laboratories, Mumbai. Deionised water was used throughout, which is prepared by Milli-Q-system.

6.2.2.2 Preparation of chitosan-g-glycolic acid-Co_3O_4 hybrid nanoparticle nanocomposite films

The grafted chitosan (1g) (Discussed in **chapter 3B. section 3.2.2.3**) was dispersed in deionised water for 1 h with constant stirring at room temperature. After 1 h, Co_3O_4 nanoparticles nanoparticle (synthesis of Co_3O_4 nanoparticles is discussed in **chapter 5A**. **section 6.2.3**) was added to the resulting solution and stirred overnight at room temperature. The resulting solution was heated up to 80 ^{0}C with continuous degassing for 45 min. The solution was casted on a glass plate and dried at 60 ^{0}C in vacuum for 8 h. To remove the oligomers of glycolic acid and unreacted glycolic acid, the samples were extracted with methanol in soxhlet apparatus for 48 h. The formulation of chitosan and nanoparticle (Co_3O_4) are given in **Table 6.2.1**.

Table 6.2.1 The formulation of chitosan-g-glycolic acid and Co_3O_4 nanoparticles

S. No	Chitosan (g)	Glycolic acid (g)	Co_3O_4 (mg)	Sample code
1	1	0	0	CS
2	1	1	0	CGCo-1
3	1	1	50	CGCo-2
4	1	1	100	CGCo-3

6.2.3 CHARACTERIZATION OF NANOCOMPOSITE FILM

6.2.3.1 Fourier transform infrared spectroscopy (FT-IR)

The Nicolet Nexus 870 attenuated total reflectance Fourier transform infrared (ATR-FTIR) spectrometer equipped with a smart endurance diamond accessory (64 scans, 4 cm^{-1} resolution, wave number range 4000-550 cm^{-1}) were used to analyse Fourier transform infrared spectra (FT-IR) of neat chitosan (CS), chitosan grafted glycolic acid (CGCo-1) and grafted chitosan nanocomposite with Co_3O_4-Fe_3O_4 hybrid nanoparticles (CGCo-2).

6.2.3.2 X-ray diffraction (XRD)

XRD pattern of the nanoparticle as well as nanocomposites were recorded by using X-ray Diffractometer (WAXRD – Rigaku, Japan) with Cu-Kα radiation at a voltage of 50 KV. The scanning rate was 4^0/min and the scanning scope of 2θ was from 2^0 to 80^0 at room temperature.

6.2.3.3 Atomic force microscopy (AFM)

The surface morphology of nanohybrid film were investigated by atomic force microscopy (AFM) (Model: Nanoscope IV) under contact mode.

6.2.3.4 Water absorption measurement

The water absorption measurement was investigated by ASTM D 570 method, according to which, the clean, dried film samples of known weights were immersed in distilled water at 25 ^{0}C for 24h (1 Day), The films were removed, blotted quickly with absorbent paper and weighed. The absorption percentage of prepared samples was calculated using the Eq. (1):

$$X\% = (W_1-W_0)/W_0 \quad (1)$$

where W_0 and W_1 are the weight of dry and swollen samples, respectively.

6.2.3.5 Dynamic mechanical analysis (DMA)

Dynamic mechanical analysis (DMA) was investigated with a dynamic mechanical thermal analyser (DMTA RSA3, TA instrument) in tensile mode at a frequency of 1Hz with heating rate of 5 ^{0}C/min in the temperature range from -10 ^{0}C to 200 ^{0}C.

6.2.3.6 Tensile strength testing (TST)

Linkam TST 350 was used to conduct tensile stress testing of film. A dumb bell strip was cut from each membrane and strained to break at a constant crosshead speed of 10 mm/min. The break stress and strain was calculated with the associated software (Linkam).

6.2.3.7 Thermogravimetric analysis (TGA)

TGA Q5000 instrument were used to conduct the thermogravimetric analysis (TGA) of the sample. Temperature ranges from 50 ^{0}C to 900 ^{0}C with the heating rate of 10 ^{0}C/min under nitrogen with flow rate 20 ml/min.

6.2.4 RESULTS AND DISCUSSION

***Scheme* 6.2.1** *Schematic illustration of preparation of Co_3O_4 nanoparticles and its interactions with chitosan-g-glycolic acid*

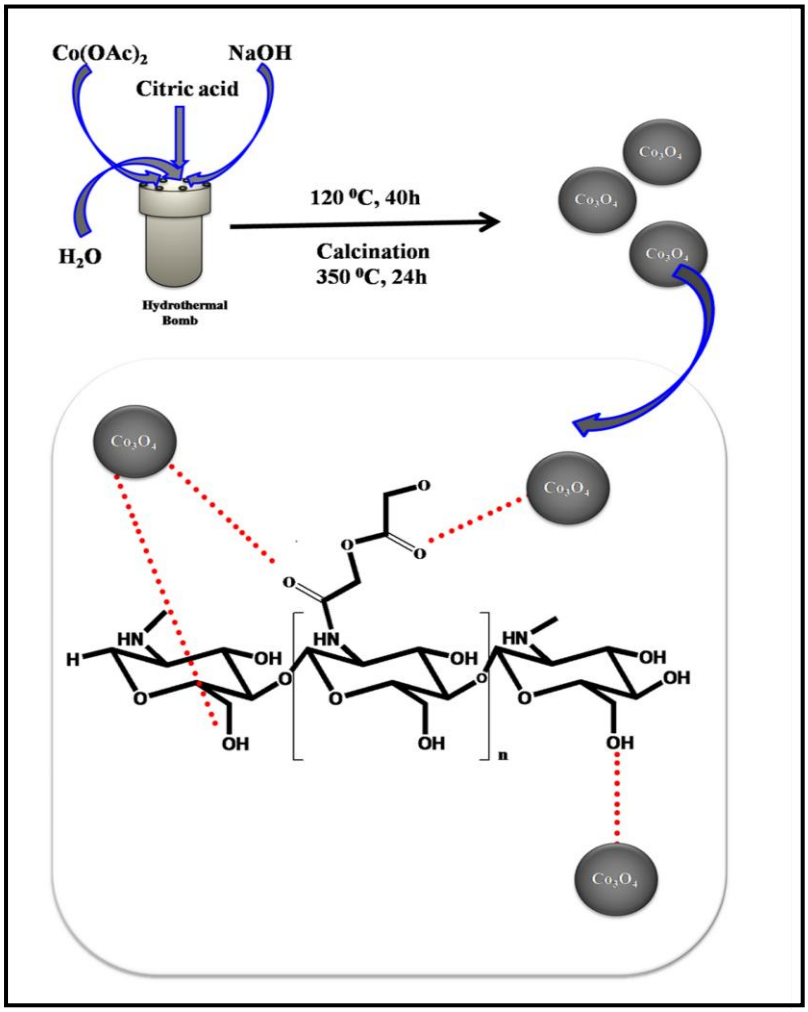

6.2.4.1 FTIR analysis

Figure 6.2.1 shows the FTIR spectra of CS, CGCo-1 and CGCo-2. The characteristic peaks in the FTIR spectrum of CS include 1633 cm^{-1} (-NH stretching) and 3500 cm^{-1} (-OH stretching). In FTIR spectrum of CGCo-1, presence of extra peak at 1730 cm^{-1} (-C=O stretching) and shifting of peak (-NH stretching) towards the lower frequency region (1570 cm^{-1}) confirms the interaction of glycolic acid with NH_2 group of chitosan. The grafting of glycolic acid on chitosan was confirmed by the formation of amide (–NH-C=O) linkage between amine ($-NH_2$) group of chitosan and –C=O group of glycolic acid. In the FTIR spectrum of CGCo-2 include shift in peak 1716 cm^{-1} (-C=O stretching) and 3405 cm^{-1} (-OH stretching), it may due to the interaction of Co_3O_4 nanoparticles with –C=O group of glycolic acid and –OH group of chitosan via metallic bond (**Scheme 6.2.1**).

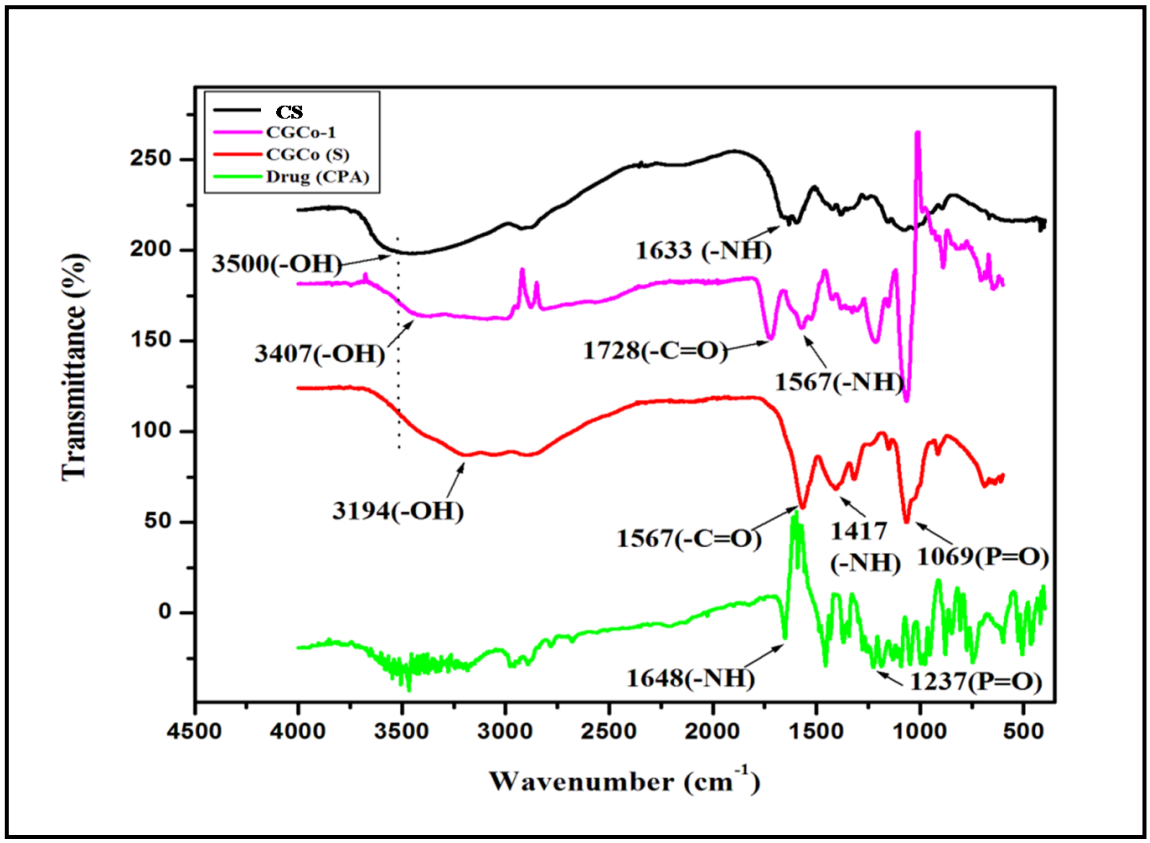

Figure 6.2.1 *FTIR spectra of neat chitosan (CS), grafted chitosan (CGCo-1) and grafted chitosan-Co_3O_4 nanoparticles nanocomposite (CGCo-2) film.*

6.2.4.2 XRD analysis

The crystalline structure of Co_3O_4 nanoparticles were characterized by XRD measurements. The typical XRD pattern is shown in **Figure 6.2.2** (a). The positions of all the diffraction peaks are in accordance with those of the standard bulk Co_3O_4 pattern. **Figure 6.2.2** (b) illustrates the X- ray diffraction pattern of neat chitosan (CS), glycolic acid grafted chitosan (CGCo-1) and grafted chitosan-Co_3O_4 nanoparticles nanocomposite (CGCo-2) films. It was observed that neat chitosan (CS) shows the characteristic peak at 10.9^o and 19.8^o, which correspond to a hydrated crystalline structure and an amorphous structure of chitosan, respectively.[25,26]

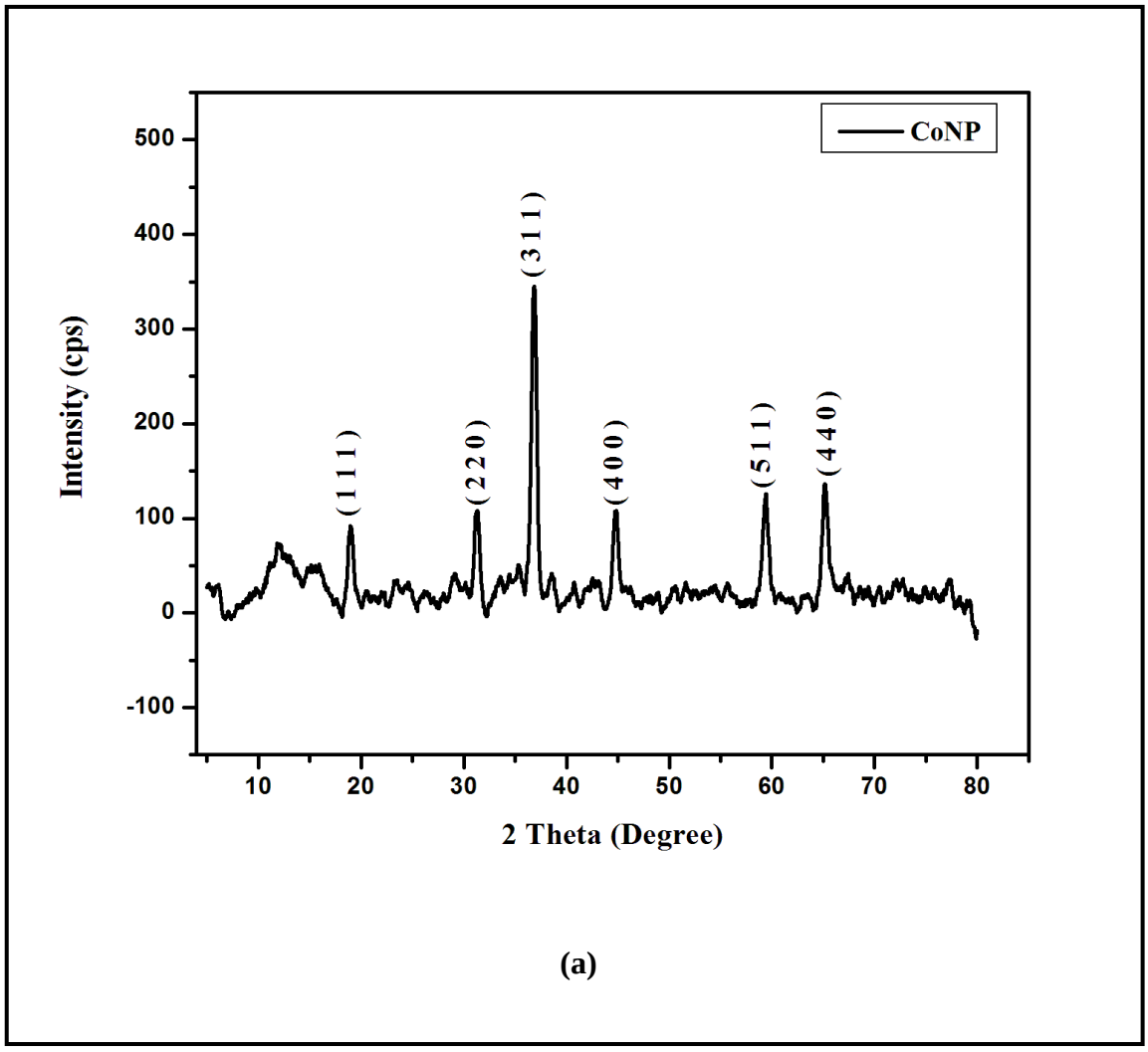

(a)

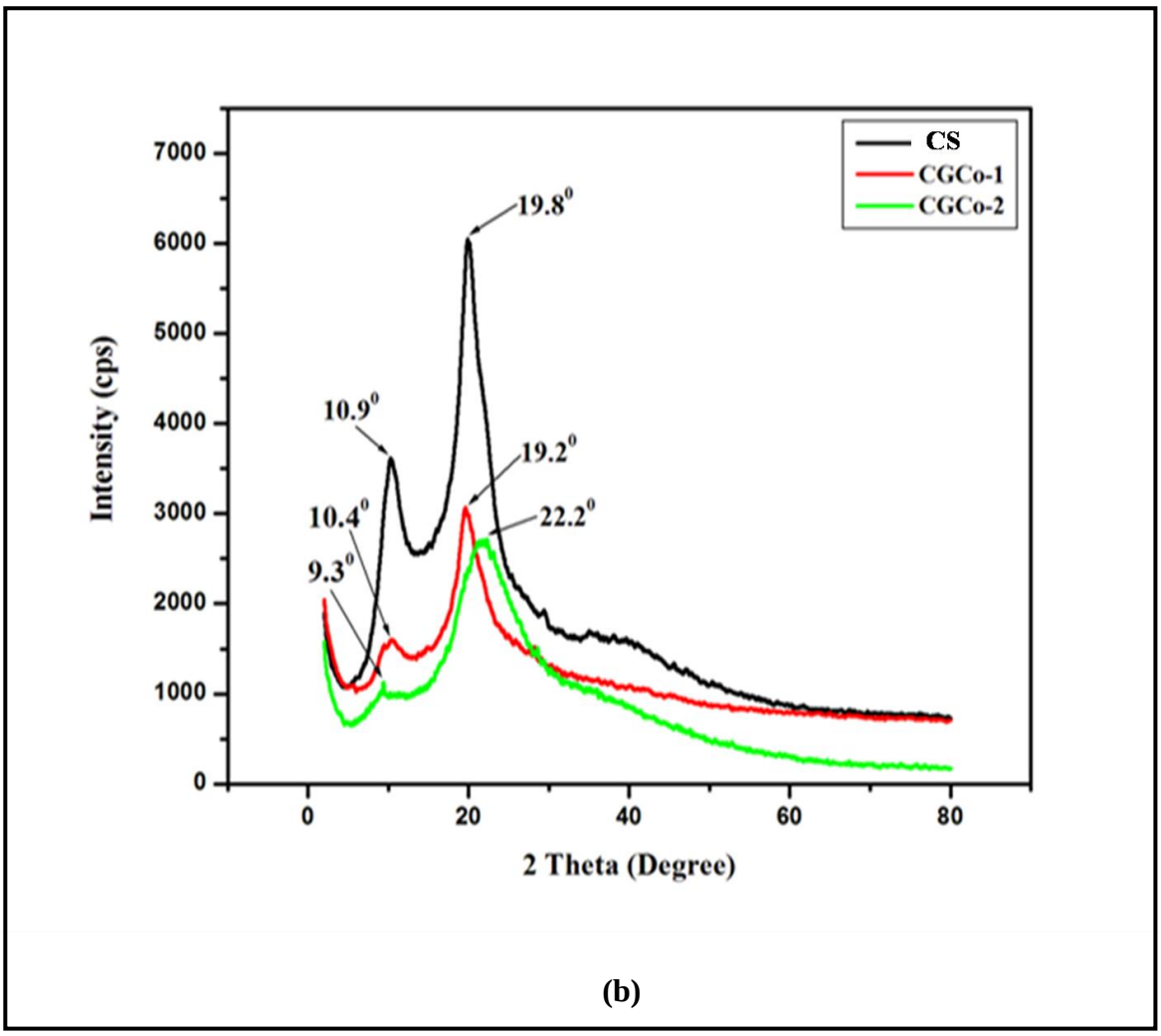

Figure 6.2.2 *(a) X-ray diffraction spectra of Co_3O_4 nanoparticles (b) X-ray diffraction spectra of neat chitosan, grafted chitosan and grafted chitosan/Co_3O_4 nanoparticles nanocomposite film.*

Grafting of chitosan with glycolic acid (CGCo-1) resulted in a shift of peak from 10.9^o to 10.4^o and 19.8^o to 19.2^o which confirms the interaction of chitosan with glycolic acid. These peaks were shifted from 10.4^o to 9.3^o and 19.2^o to 22.2^o, showing the interaction of Co_3O_4 nanoparticles with the grafted chitosan (CGCo-2). More shift in nanocomposite film is probably due to higher compatibility of the Co_3O_4 nanoparticle with the grafted chitosan matrix.

6.2.4.3 Morphological studies

The surface topography of pure chitosan, grafted chitosan and grafted chitosan-Co_3O_4 nanoparticles nanocomposite film is illustrated with AFM; the image size was 5 μm × 5 μm. **Figure 6.2.3** (a) shows the AFM image of chitosan film with smooth surface. Upon grafting the chitosan, roughness and height of the film surface were also increased (**Figure 6.2.3** (b)). AFM image of grafted chitosan-Co_3O_4 nanoparticles nanocomposite film shows the incorporation of nanoparticle in the matrix of grafted chitosan film (**Figure 6.2.3** (c, d)).

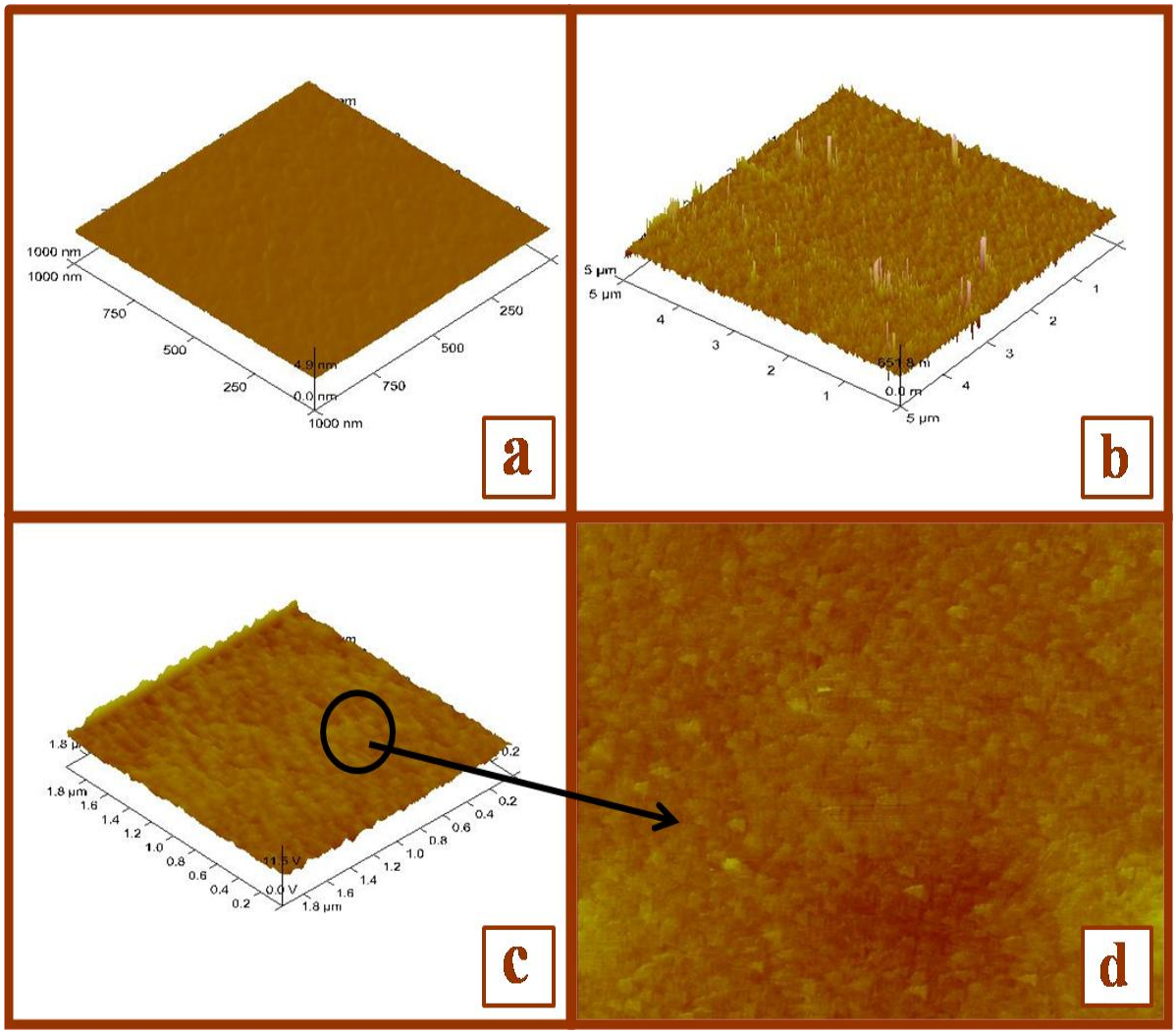

Figure 6.2.3 *(a) AFM image of pure chitosan film (b) AFM image of grafted chitosan film (c, d) AFM image of grafted chitosan/Co_3O_4 nanoparticles nanocomposite film.*

6.2.4.4 Water absorption Behavior

The pure chitosan is hydrophilic but it does not absorb much water, probably due to many –OH and –NH groups in chitosan, which causes strong intermolecular and intramolecular hydrogen bonds; thus, the infiltration and diffusion of water is restrained. The water absorption property of the glycolic acid grafted chitosan is higher than that of the pure chitosan. Fact attributed to it is that the molecular structure integrity is broken in the grafted chitosan, which can expose more functional groups for water absorption. This swelling extent will depend on the osmotic pressure, charge repulsion, the degree of ionization and grafting extent[27]. The water absorption of chitosan-g-glycolic acid/Co_3O_4 nanoparticle nanocomposite films decreases with an increase of Co_3O_4 nanoparticle in grafted chitosan matrix. This is probably due to the formation of a barrier in the form of cross linking points, which prevents water permeation into chitosan. In comparison of grafted chitosan, nanocomposite films show lower water absorption and deceases with the increasing content of nanoparticles. It can be attributed to the interaction between nanoparticle and copolymer. Since nanoparticle is hydrophobic, resulting nanocomposite were expected to be hydrophobic. The formation of nanocomposite occurs through the metallic bond formation between Co_3O_4 nanoparticle and copolymer, which results in the decreased water absorption. Increasing content of nanoparticle reduces the exposure of more functional group towards the water, thus the hydrophobicity of the nanocomposite film increases. The behaviors of water absorption nanocomposite films were shown in **Table 6.2.2**.

The nanocomposite films are allowed to reach upto their equilibrium, which was achieved after 24 h. After complete swelling, film was dried under vaccume at 65 ^{0}C to evaluate the moisture retention capacity of the nanocomposite films. It is observed that the film could hold the moisture for a long time. Grafted chitosan shows high water retention capacity. On increasing the nanoparticle content, the water absorption decreases and the time of drying up

to constant weight increases that is they hold the moisture for longer time. Therefore, nanoparticle acts as a physical barrier for the moisture to exude out from the films.

Table 6.2.2 Sorption behavior of the nanocomposites

Sample Code	Water Absorption (%)
CS	54
CGCo-1	77.7
CGCo-2	62.98
CGCo-3	33.2

6.2.4.5 Dynamic mechanical analysis

Figure 6.2.4 (a, b, c and d) shows the variation in dynamic mechanical thermal property of chitosan-g-glycolic acid/ Co_3O_4 nanoparticles nanocomposite, which has been determined by change in viscoelastic property, glass transition temperature and stability of the polymer[29]. The storage modulus [E'] of pure chitosan film was observed to be $1.178x10^8$ [Pa] at 149 ^{0}C. The storage modulus of grafted chitosan film decrease to 1.503×10^7 [Pa]. An increase in storage modulus [E'] of nanocomposite film is observed with the increase in nanoparticle content. There is a sharp increase in tanδ which corresponds to α relaxation temperature associated with the glass transition temperature T_g. The increase in tanδ value is due to the increase in the segmental motion of the polymer with temperature. Pure chitosan film exhibit T_g=153.86 ^{0}C, which decreases upon grafting, it is due to increase in the mobility of the polymer chains. The addition of Co_3O_4 nanoparticles restrict the mobility of the chain and cause the increase in the storage modulus and improve the mechanical strength of polymer film (**Table 6.2.3**).

Table 6.2.3 Viscoelastic properties of grafted chitosan-Co_3O_4 hybrid nanoparticle nanocomposites

Sample Code	Co_3O_4 (Wt %)	Storage modulus (Pa) at 149 ^{0}C	Tg (^{0}C)	Tan delta (δ)
CS	0	1.178×10^8	153.86	0.42
CGCo-1	0	1.503×10^7	113.54	0.59
CGCo-2	50	3.424×10^6	87.23	0.61
CGCo-3	100	1.359×10^7	110.58	0.60

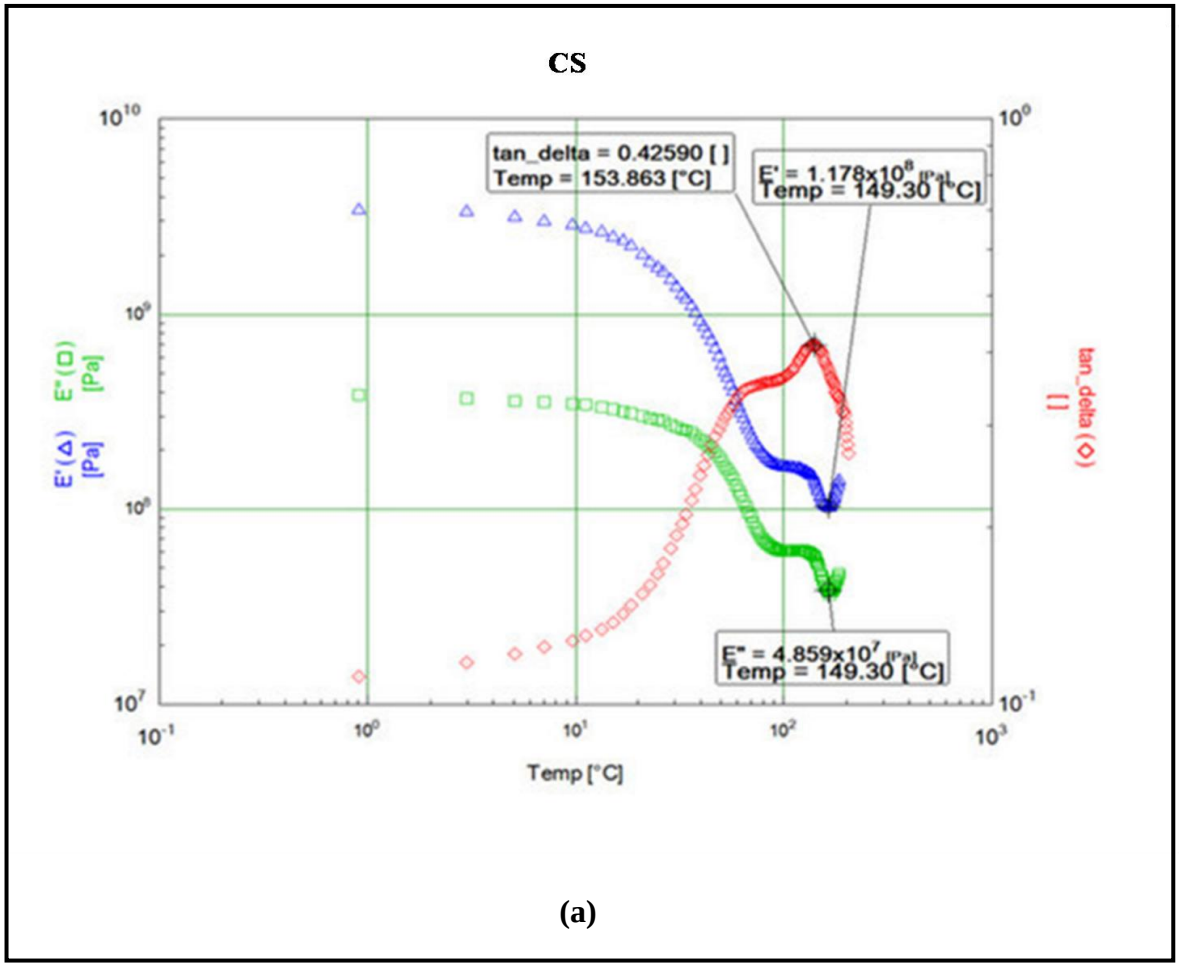

(a)

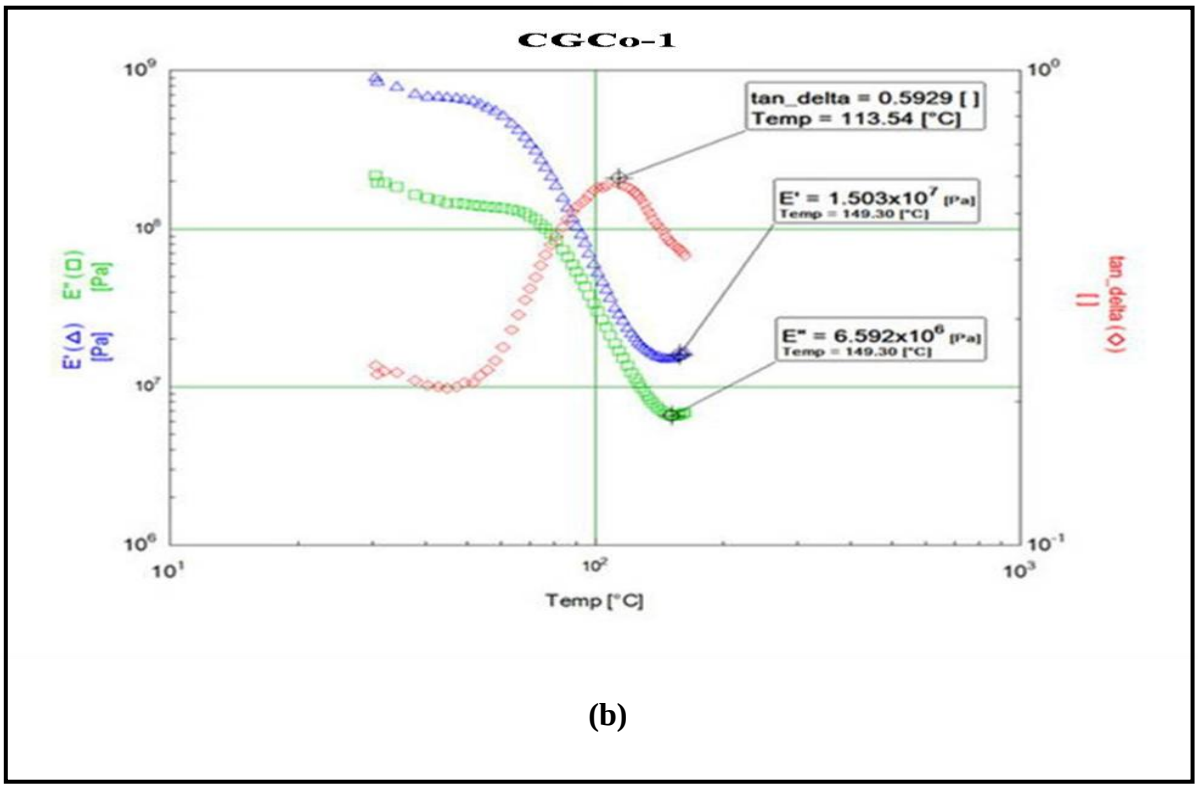

(b)

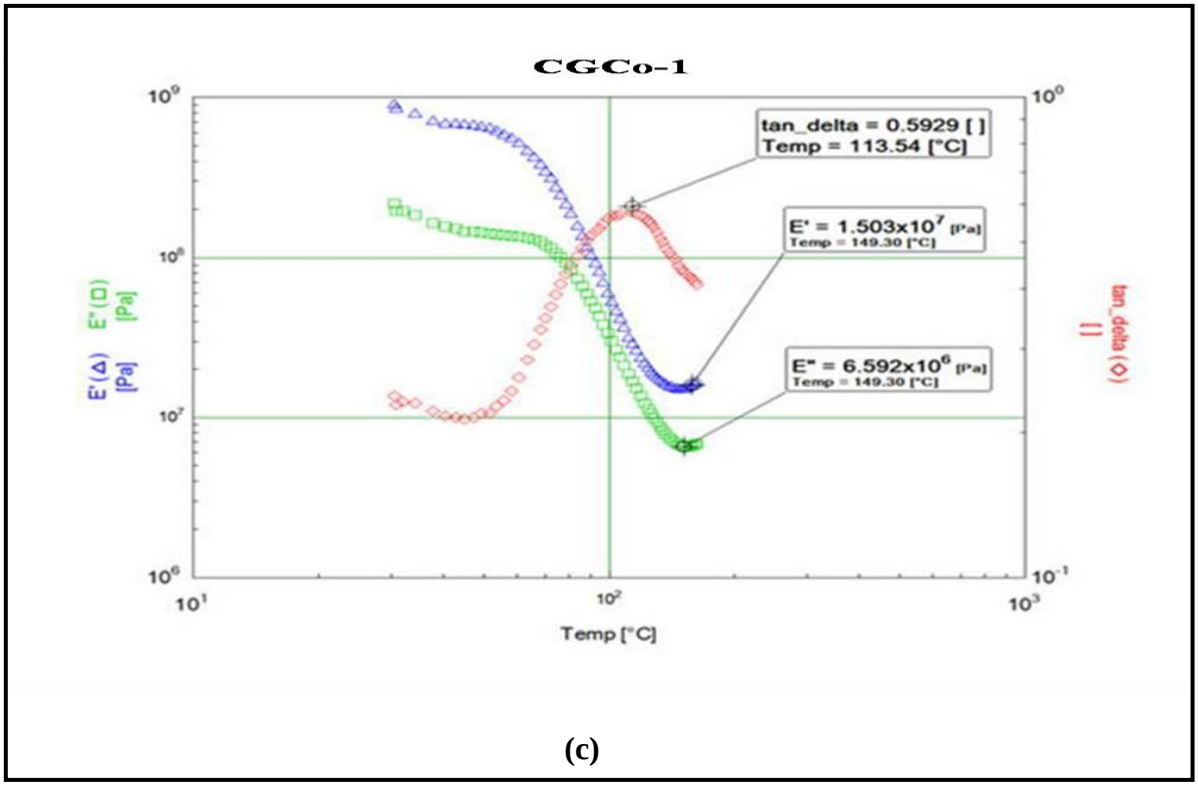

(c)

Figure 6.2.4 *Temperature variation of tanδ, glass transition temperature, storage modulus [E'] and loss modulus [E''] (a) Pure chitosan film (b) Grafted chitosan film (c) Grafted chitosan/Co_3O_4 nanoparticle nanocomposite films (d) Grafted chitosan/ Co_3O_4 nanoparticle nanocomposite films.*

6.2.4.6 Tensile behavior

The mechanical properties of pure chitosan film are inconsistent and lack clarity in the mode of analysis such as crosshead speed or molecular weight[30-32]. The crosshead speed used while testing is 10 mm/min at 27 ^{0}C. The tensile properties varied significantly with the crosshead speed. All the membranes had uniform thickness of 0.22 mm and were semi-transparent. The pure chitosan film exhibits a break stress of 0.9855 MPa (**Figure 6.2.5** (a)). The grafted chitosan film posses relatively decrease in elastic modulus. The incorporation of nanoparticles in grafted chitosan matrix increases elastic modulus (**Table 6.2.4**) and improves the tensile strength of the nanocomposite film (**Figure 6.2.5** (b)).

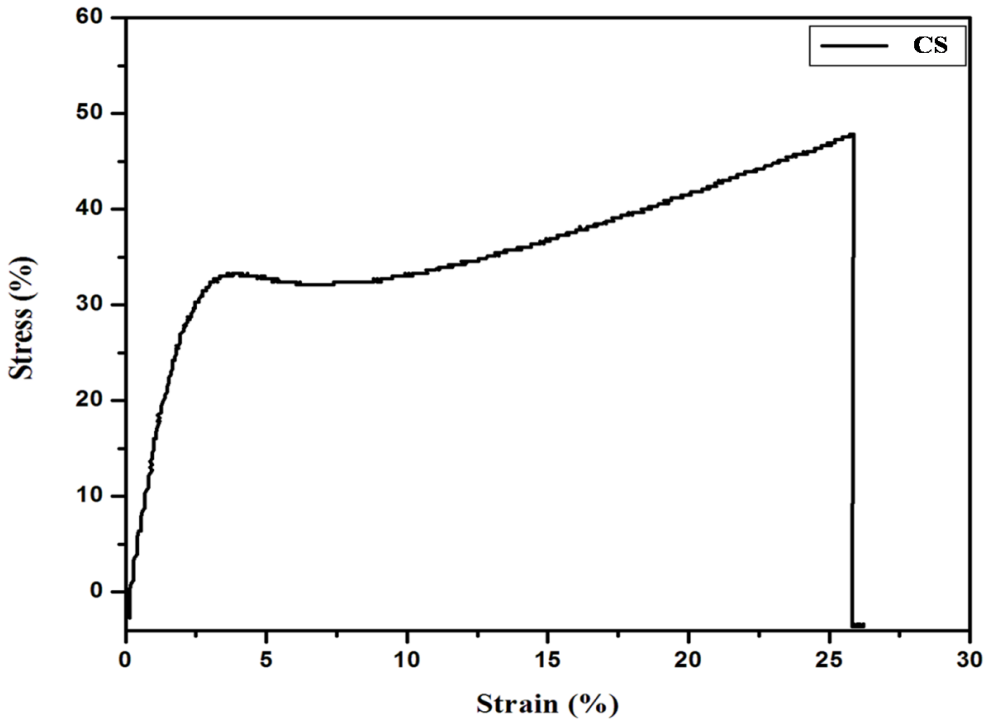

(a)

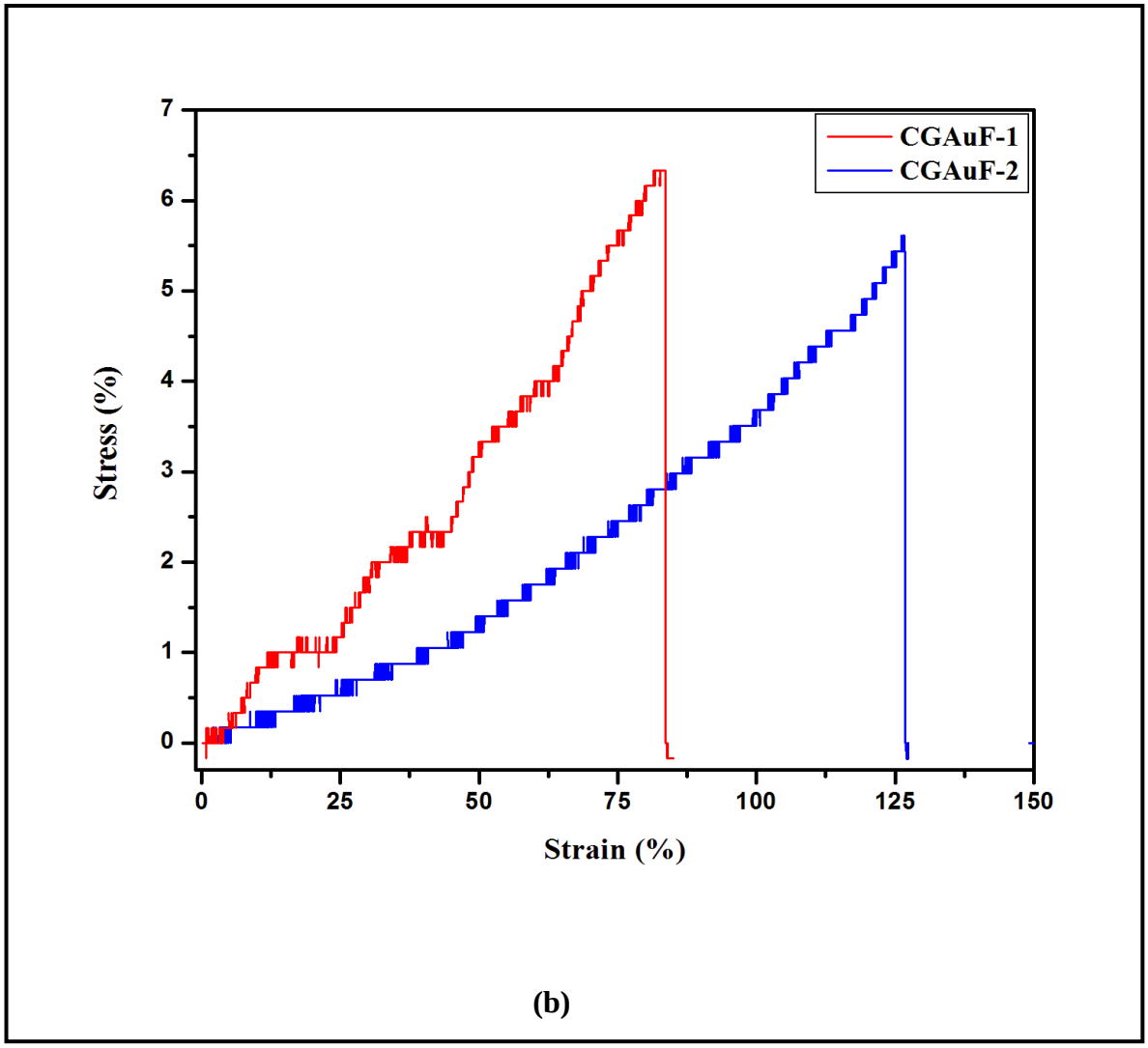

Figure 6.2.5 *(a) Stress strain behavior of pure chitosan membranes (b) Effect of grafting and nanoparticle to stress strain behavior of grafted and nanocomposite chitosan membranes.*

Table 6.2.4 Tensile strength and testing of chitosan-Co_3O_4 nanocomposites

Sample Code	Elastic modulus (MPa)	Stress (%)	Strain (%)
CS	0.9855	47.97	25.83
CGCo-1	0.9556	6.38	83.57
CGCo-2	0.9619	6.66	92.19
CGCo-3	0.9807	6.83	83.00

6.2.4.7 Thermogravimetric analysis

Figure 6.2.6 shows the thermal degradation of pure chitosan and nanocomposite films. The weight loss at 50-150 ^{0}C is attributed to the water in the chitosan film. Further the weight loss in the temperature range of 200-350 ^{0}C was attributed to the deacetylation and degradation of chitosan[33]. The thermal degradation temperature of chitosan film decreases by 10-20 ^{0}C after grafting. The decrease of 55-60 ^{0}C was observed upon addition of Co_3O_4 nanoparticles to grafted chitosan matrix. The char residue of pure chitosan film as well as grafted chitosan film was observed to be 27.7% at 900 ^{0}C (**Table 6.2.5**). The percentage of char residue increases upon increasing the percentage of Co_3O_4 nanoparticles. These results indicate that addition of Co_3O_4 nanoparticles to grafted chitosan enhances the thermal property of chitosan. The amount of weight loss at this temperature range decreases with the increasing content of nanoparticles in samples. This implies that due the grafted chitosan-Co_3O_4 nanoparticles bonding water absorbability that is hydrophillicity of the films decreases. This was also confirmed in water swelling behavior section.

Table 6.2.5 TGA results for chitosan and Co_3O_4 nanocomposites

Sample Code	Temperature at 20% loss (^{0}C)	Temperature at 50% loss (^{0}C)	char at 900 ^{0}C (wt %)
CS	310	360	27.1
CGCo-1	246	347	27.7
CGCo-2	185	292	19.2
CGCo-3	192	286	21.1

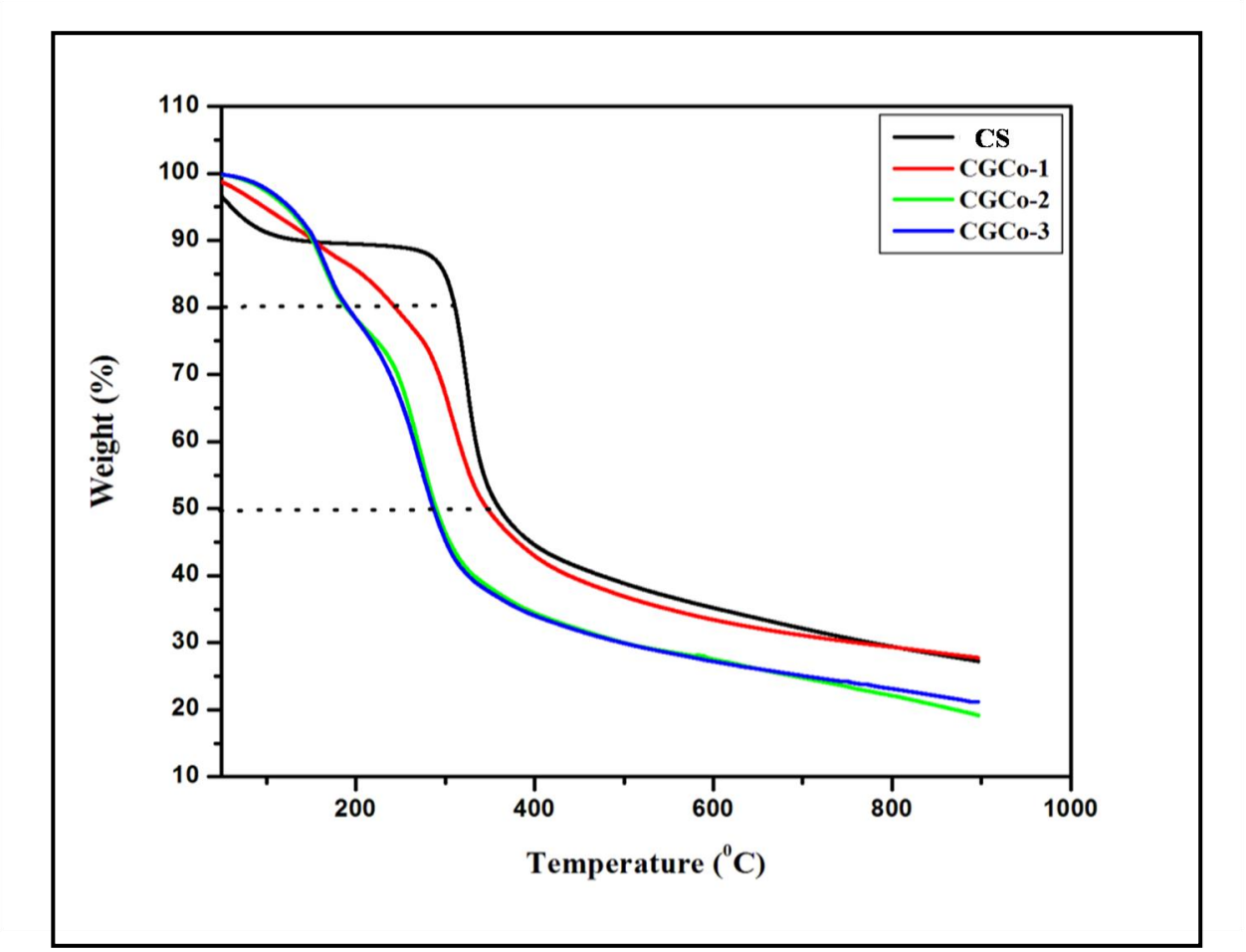

Figure 6.2.6 *Thermogravimetric curves of prepared nanocomposites.*

6.2.5 CONCLUSIONS

The glycolic acid grafted chitosan-Co_3O_4 nanoparticles based nanocomposites were prepared by film casting method. The interaction of cationic chitosan with Co_3O_4 nanoparticles is through metallic bond, which results in enhancement in physical properties of nanocomposites. The dynamic mechanical thermal analysis (DMTA) measure the shift in the glass transition temperature (Tg) of the composites from the maxima of the α transition curves. The glass transition temperature and the storage modulus show an increase with increasing nanoparticles content. The tensile strength of nanocomposite increases with increasing content of nanoparticles. An enhancement in mechanical and tensile properties of nanocomposites than pure chitosan was observed. The grafting of chitosan with glycolic acid

imparts hydrophillicity to the film. The results showed that increasing content of nanoparticles reduces hydrophillicity, which imparts little branched crystalline structure to the nanocomposite film. The longer water retention and swelling behavior properties were discussed which could be applied in the field of biomedical and cell adhesion study is under progress.

6.2.6 REFERENCES

1. P. Poizot, S. Laruelle, S. Grugeon, L. Dupont and J. M. Tarascon, *Nat.*, **407**, 496(2000).
2. B. A. Trofimov, B. G. Sukhov, G. P. Aleksandrova, S. A. Medvedeva, L. A. Grishchenko, A. G. Mal'kina, L. P. Feoktistova, A. N. Sapozhnikov, V. I. Dubrovina and E. F. Martynovich.et al., *Chemistry and materials sci.,* **393**, 287(2003).
3. S. P. Gubin, Yu. A. Koksharov, G. B. Khomutov and G. Yu. Yurkov. *Usp Khim.,* **74**, 539(2005).
4. S. P. Gubin, G. Yu. Yurkov and I. D. Kosobudsky, *Int . J. Mater. Prod. Technol.,* **23**, 2(2005).
5. R. Scomski, *J. Phys: Condens. Mat.,* **15**, 841 (2003).
6. T. Hyeon, *Chem. Comm.,* **8**, 927 (2003).
7. X. M. Lin and A.C.S. Samia, *J. Magn. Magn. Mat.,* **305**, 100 (2006).
8. H. Chen, X .Liu, H. Muthuraman, J. H. Zou, J. H. Wang, Q. Dai and Q. Huo, *Adv. Mat.,* **18**, 2876 (2006).
9. S. Dire, F. Babonneau, C. Sanchez and J. Livage, *Mater Chem.,* **2**, 239 (1992).
10. S. S. Ozdemir, M. G. Buonomenna and E. Drioli, *Appl. Catal a-General.,* **307**, 167(2006).
11. M. T. Sulak, O. Gokdogan, A. Gulce and H. Gulce, *Bioelectro.,* **21**, 1719 (2006).

12. M. Kawasumi, N. Hasegawa and M. Kato, et al., *Macromol.*, **30**, 6333 (1997).

13. Y. Wang and N. Herron, *J. Phys. Chem.*, **95**, 525 (1991).

14. R. W. Siegel, *Nanostruct. Mater.*, **3**, 1 (1993).

15. H. Gleiter, J. Weissmuller, O. Wollersheim and R. Wurschum, *Acta. Mat.*, **49**, 737 (2001).

16. S. P. Gubin, Yu. I. Spichkin and Yu. A. Koksharov, et al., *J. Magn. Magn. Mat.*, **265**, 234 (2003).

17. J. H. Park, Y. T. Lim, O. O. Park, J. K. Kim, J. W. Yu and Y. C. Kim, *Chem. Mat.*, **16**, 688 (2004).

18. K. T. Chung, A. Sabo and A. P. Pica, *J. Appl. Phys.*, **53,** 6867 (1982).

19. X. W. Zhang, Y. Pan and Q. Zheng, et al., *J. Polym. Sci. Part B: Polym. Phys.*, **38**, 2739 (2000).

20. J. I. Hong, P. Winberg, L. S. Schadler and R. W. Siegel, *Mater Lett.*, **59**, 473 (2005).

21. X. Xia, S. Cai and C. Xie, *Mater Chem. Phys.*, **95**, 122 (2006).

22. C. B. Ng, B. J. Ash, L. S. Schadler and R. W. Siegel, *Adv. Compos. Lett.*, **10**, 101 (2001).

23. M. Xie, H. H. Liu, P. Chen, Z. L. Zhang, X. H. Wang, Z. X. Xie, Y. M. Du and B. Q. Pand, D. W. Pang, *Chem. Comm.*, **44**, 5518 (2005).

24. J. Xie, Q. Zhang, J. Y. Lee and D. I. C Wang, *ACS. Nano.*, **2**, 2473 (2008).

25. K. Ogawa, S. Hirano, T. Miyanishi, T. Yui and T. Watanabe, *Macromol.*, **17**, 973 (1984).

26. S. F. Wang, L. Shen, W. D. Zhang and Y. J. Tong, *Biomacromol.*, **6**, 3067 (2005).

27. P. Seong, Y. Jin and P. Ham, *Biomater.*, **22**, 323 (2000).

28. J. H. Han and J. M. Krochta, *Trans. ASAE.*, **42**, 1375 (1999).

29. F. Al-Sagheer and S. Muslim, *J. Nanomater.*, **2010**, 1 (2009).

30. M. Cheng, J. Deng, F. Yang, Y. Gong, N. Zhao and X. Zhang, *Biomater.*, **24**, 2871 (2003).
31. R. Chen and H. Hwa, *Carbohyd. Polym.*, **29**, 353 (1996).
32. M. Qurashi, H. Blair and S. Allen, *J. Appl. Polym. Sci.*, **46**, 255 (1992).
33. S. F. Wang, L. Chen and Y. J. Tong, *J. Polym. Sci. Part A Polym. Chem.*, **44**, 686 (2006).

CHAPTER 7

A: Preparation of Glycolic Acid-g-Chitosan-Co_3O_4-Fe_3O_4 Hybrid Nanoparticles Based Nanohybrid Scaffolds for Drug-Delivery and Tissue Engineering

7.1 INTRODUCTION

In the field of nanotechnology, polymer matrix based nanocomposites have become a prominent area of current research and development. These materials exhibit unique optical[1], thermal, electrical and mechanical properties due to the interaction of the polymer with the particle and state of dispersion[2-4]. Transition metal nanoparticles are one of the most–studied system due to their quantum size effects[5-7], novel electronic[8], optical[9], magnetic[10] and chemical properties. These metal nanoparticles play an important role in many different fields of science such as nano-electronics, catalysis[11-13] and recently, in biomedical application[14-16]. Cobalt oxide and Fe_3O_4 nanoparticles are currently attracting enormous interest owing to their unique size- and shape dependent properties and potential applications in the field of catalysis, sensors, electrochemistry, magnetism, energy storage, etc[17]. Here, we have demonstrated Co_3O_4-Fe_3O_4 composite magnetic nanoparticles based materials can be use in the field of controlled drug release and cell proliferation systems, which is having major scientific application in the field of biomaterials[18].

A wide range of materials have been employed as drug carriers such as lipids, surfactant, dendrimers and natural or synthetic polymers[19-22]. Chitosan has prompted the continuous movement for the development of safe and effective drug delivery systems because of its unique physicochemical and biological characteristics. It is polycationic biopolymer[23]. Chitosan is hydrophilic and compatible with nanoparticle and has better processability due to the presence of amino group (pKa value is 6.2) in the chain. Chemical modification of chitosan is useful for the association of bioactive molecules to polymer and controlling the drug release profile. The grafting of side glycolic acid leads to marked changes in the chitosan structure[24, 25].

7.2 EXPERIMENTAL

7.2.1 Materials

Chitosan of low molecular weight (Mw =1.5×10^5, degree of deacetylation was 85%), glycolic acid (99% pure), iron (0) pentacarbonyl ($Fe(CO)_5$), cobalt acetate ($Co(OAc)_2$), citric acid ($C_6H_8O_7$) was obtained from sigma Aldrich. lithium chloride (LiCl), Tri phenyl phosphate (TPP), pyridine (Py), Sodium hydroxide (NaOH) and phenyl ether was obtained from M/s Sisco Research Laboratories, Mumbai. Deionised water was used throughout the work, which is prepared by Milli-Q-system.

7.2.2 Synthesis of Co_3O_4-Fe_3O_4 hybrid nanoparticles (CFNP)

Cobalt oxide nanoparticles (CoNP, synthesis is given in **chapter 6 section 6.2.3**), 1-octadecene, OAM and OA were heated to 120 ^{0}C under argon atmosphere. At the temperature of 120 ^{0}C, $Fe(CO)_5$ was injected to the reaction mixture. The reaction mixture was slowly heated to reflux (1 ^{0}C min^{-1}) for 4.5 h. After completion of reaction, it is cooled to room temperature and stirred for 1 h, followed by precipitation with acetone. The precipitate was then dried in air (**Scheme 7.1**).

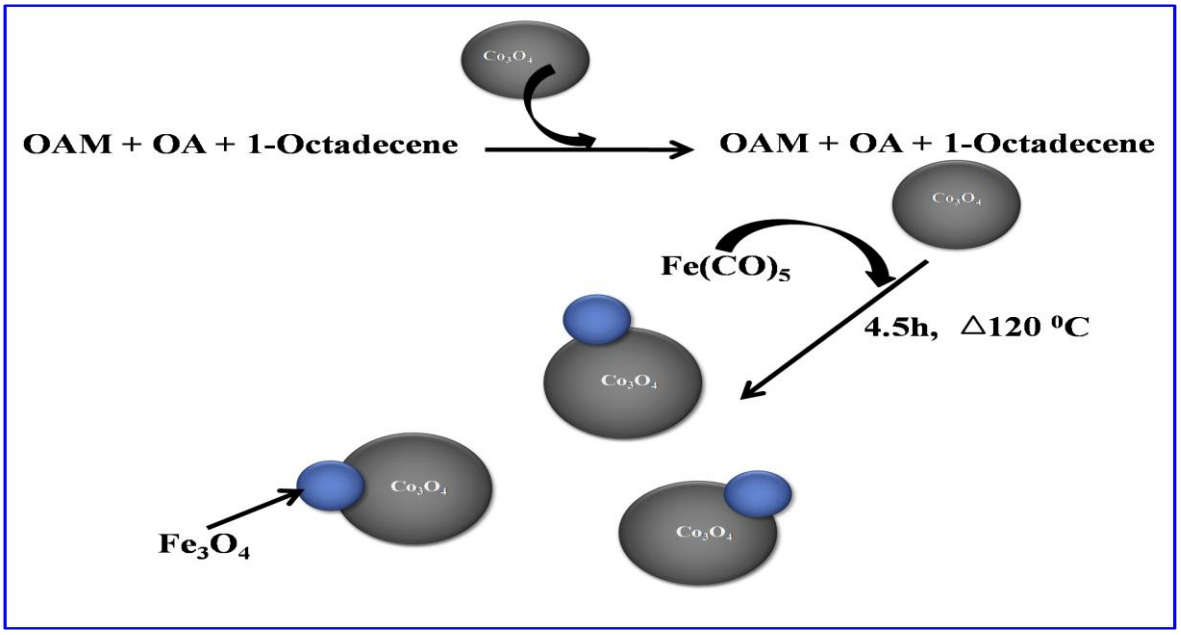

Scheme 7.1 *Schematic illustration of synthesis of Co_3O_4/Fe_3O_4 hybrid nanoparticles*

7.2.3 Preparation of nanohybrid scaffolds and drug loading

Glycolic acid grafted chitosan (1g) (Discussed in **chapter 3B. section 3.2.2.3**) was dispersed in deionised water (50 ml) and stirred for 1 h at room temperature. After 1 h, Co_3O_4-Fe_3O_4 composite magnetic nanoparticles (50 mg) was added to the solution and stirred overnight at room temperature. The resulting solution was heated up to 80 ^{0}C with continuous degassing for 30 min. The resulting solution was cooled to room temperature after degassing. The drug (CPA) (10 mg) was added to the resulting solution and stirred for 5 h, so that drug completely mixes with the solution. The drug loaded solution was poured in tissue culture plates (20×20 mm diameter) and quenched in liquid nitrogen. The quenched sample was freeze dried by lyophilisation under -100 ^{0}C temperature for 6 h. In lyophilisation water molecules were removed by freezing and sublimation of ice crystals, which lead to the formation of pores. The formulation is shown in the **Table 7.1**.

Table 7.1 Formulation of Cyclophosphamide (CPA)-loaded nanohybrid of chitosan-g-glycolic acid and Co_3O_4-Fe_3O_4 hybrid magnetic nanoparticles

S.No	Grafted Chitosan (g)	Co_3O_4-Fe_3O_4 (mg)	CPA (%)	Drying Process	Sample code
1	1	_	_	Vacuum	CGCF-1
2	1	50	_	Vacuum	CGCF-2
3	1	50	_	Freeze	CGCF (S)
4	1	50	10	Freeze	CGCF (D)

7.3 CHARACTERIZATIONS OF NANOHYBRID

7.3.1 Transmission Electron Microscopy (TEM)

High Resolution Transmission Electron Microscopy (HR-TEM model Technai TF30, 300KV FEG) was used to analyse the particle size, morphology and Selected Area Diffraction pattern (SAED) of Co_3O_4-Fe_3O_4 hybrid magnetic nanoparticles.

7.3.2 Physical property measuring system (PPMS)

The formation of Co_3O_4-Fe_3O_4 hybrid nanoparticle was confirmed by measuring hysteresis loops of the synthesised nanoparticles using a physical property measuring system (PPMS) (quantum design Inc. San Diego, USA) equipped with 7T superconducting magnet and a vibrating sample magnetometer [26].

7.3.3 Fourier transform infrared spectroscopy

Attenuated total reflectance Fourier transform infrared (ATR-FTIR) Nicolet Nexus 870 FTIR spectrometer equipped with a smart Endurance diamond accessory (64 scans, 4 cm^{-1} resolution, wave number range 4000-550 cm^{-1}) was used to analyse fourier transform infrared spectra of neat chitosan (CTS), chitosan grafted glycolic acid (CGCF-1), nanohybrid scaffold (CGCF (D)) and drug (CPA).

7.3.4 X-ray photoelectron spectroscopy (XPS)

XRD patterns of the samples were recorded on X-ray Diffractometer (WAXRD – Rigaku (Japan)) with Cu-kα radiation at a voltage of 50 KV. The scanning rate was 4^0/min and the scanning scope of 2θ was from 2^0 to 80^0 at room temperature.

7.3.5 Scanning Electron Microscpy (SEM)

Scanning Electron Microscpy (SEM) (Model, JOEL Stereoscan 440, Cambridge) was used to investigate the surface morphology of the porous scaffolds. Prior to the observation, specimens were fixed on the copper grid.

7.3.6 Swelling behavior

The swelling behavior of porous scaffold was determined by exposing them to media of different pH, 1N HCl, 1N NaOH and simulated body fluid (SBF) (pH 7.4) solutions. The shape retention of porous scaffold was determined by measuring the change in its diameter of scaffold as a function of time in the media. The drug "CPA" content in the aliquot was investigated by UV-vis spectrophotometer (UV-NIR- PL Lamda 950) at 180 nm.

7.3.7 Cell viability study

In vitro cell culture was carried out using L929 cell. These cells are derived from an immortalized mouse fibroblast cell line, are internationally recognized cells that are routinely used in *in-vitro* cytotoxicity assessments. The scaffold was sterilised by putting it in 6 well tissue culture plate containing isopropanol (5 mL) and exposed to UV radiation for 4 h. L929 cells were further seeded on nanohybrid scaffold placed in 6-well plate at a density of 5×10^3 cells/well and incubated at 37 °C, 5% CO_2 and 95% humidity incubation conditions. The tissue culture plate containing only cells were used as control. To study the cell proliferation on different substrates, cell proliferation was determined by the colorimetric MTT assay. MTT assay is based on the reduction of yellow 3-(4,5 dimethylthiazol-2-yl)-2,5-diphenyltetrazolium bromide (MTT) salt in MTT to form purple formazan by dehydrogenase enzymes secreted from the mitochondria of metabolically active cells. The amount of formazan formed is directly proportional to the number of viable cells. After 2 h, 4 h, 6 h, 24 h, 48 h, 72 h, the cells solution (100 µl) was transferred to an ELISA micro-plate and optical density (OD) was measured at 540 nm using the spectroscopic method.[27] The relative cell growth was compared to control cell, which exhibit cell culture medium without chitosan. It was calculated by using the given eq. (1)

$$\% \text{ Live cell} = 100 - \left[\frac{(C - T)}{(C - B)} \times 100 \right] \qquad (1)$$

C = OD of control

T = OD of test sample

B = OD of blank

OD = Optical density

All the in vitro tests were done in triplicate and results were reported as an average value.

7.4 RESULTS AND DISCUSSION

Scheme 7.2 *Grafting of glycolic acid on chitosan, formation of Chitosan-g-glycolic acid and Co_3O_4-Fe_3O_4 hybrid nanoparticles based nanohybrid scaffold and interaction between chitosan-g-glycolic acid, drug and Co_3O_4-Fe_3O_4 hybrid nanoparticles.*

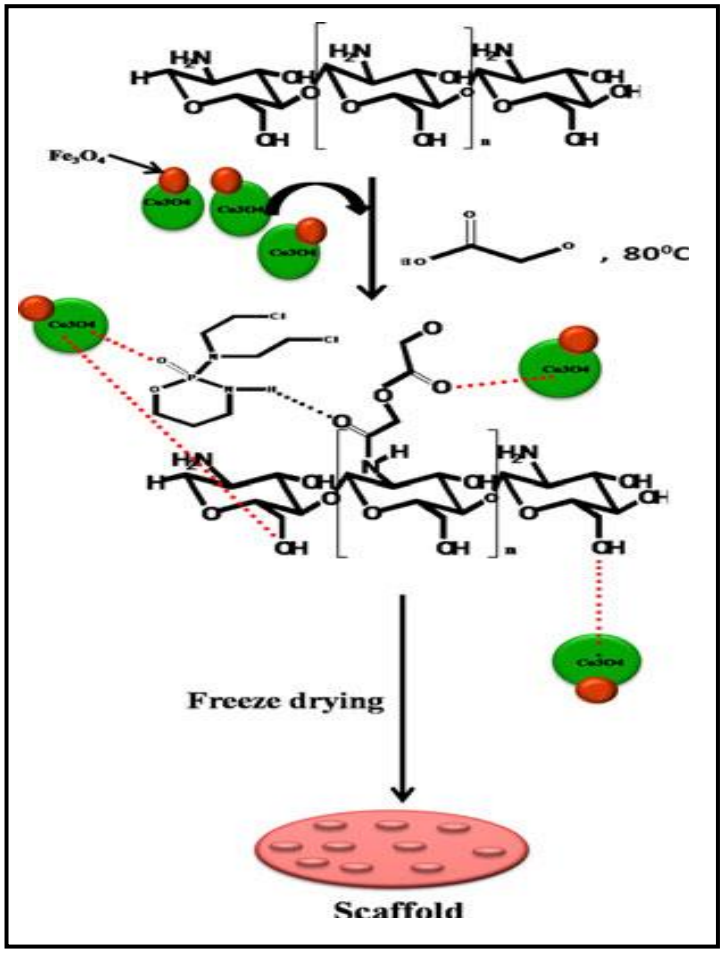

7.4 .1 TEM analysis

The TEM image of Co_3O_4-Fe_3O_4 composite magnetic nanoparticles (**Figure 7.1** (a)) exhibit uniformly spherical morphology almost same overall size. **Figure 7.1** (b) shows the high

resolution TEM image of these composite magnetic nanoparticles, which are crystalline as shown in selected area diffraction (SAED) pattern **Figure 7.1** (c). The distance between the two adjacent lattice planes in Co_3O_4 domain is 2.31Å, close with the reported value of 2.33 Å for (2 2 2) plane[28] and that in Fe_3O_4 domains 4.85Å, close to the literature value of 4.88 Å for (1 1 1) plane. TEM-EDAX also confirms the formation of Co_3O_4-Fe_3O_4 hybrid nanoparticles (**Figure 7.1** (d)).

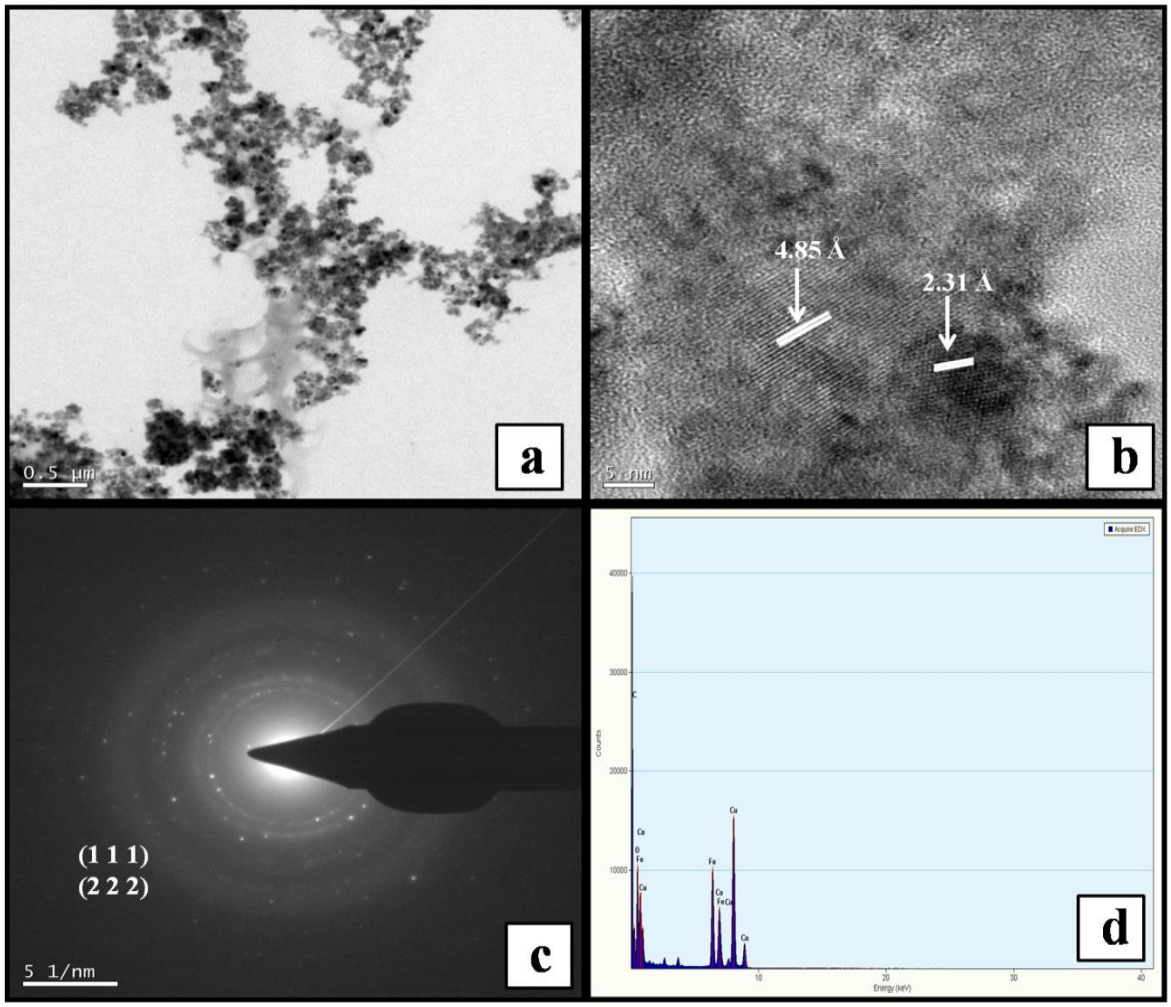

Figure 7.1 *(a) TEM image Co_3O_4-Fe_3O_4 hybrid nanoparticles; (b) HRTEM image of Co_3O_4-Fe_3O_4 hybrid nanoparticles (White line delineate distance between two lattice plane in Co_3O_4 domain and Fe_3O_4 domain); (c) SAED pattern of Co_3O_4-Fe_3O_4 hybrid nanoparticles; (d) TEM-EDAX of Co_3O_4-Fe_3O_4 hybrid nanoparticles.*

7.4.2 Magnetization study

The magnetic properties of the hybrid nanoparticle were investigated to evaluate the influence of the diamagnetic Co_3O_4 on the Fe_3O_4 domains. **Figure 7.2** shows magnetic hysteresis loops recorded at 300 k of Co_3O_4-Fe_3O_4 hybrid nanoparticle with Fe_3O_4 nanoparticle of size 5-10nm. Hybrid nanoparticles are super paramagnetic, however the saturation magnetization increases with Co_3O_4 particles.[29] The decrease in the magnetization of Co_3O_4-Fe_3O_4 hybrid nanoparticle confirms the formation of Co_3O_4-Fe_3O_4 hybrid nanoparticles.

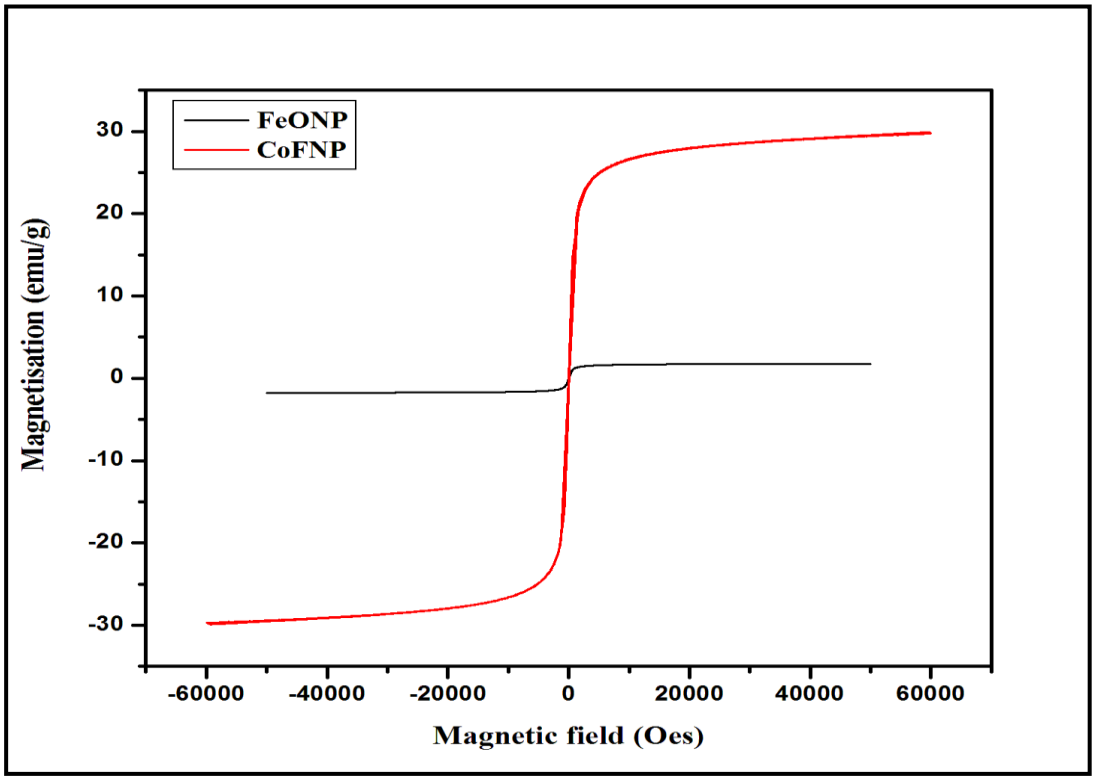

Figure 7.2 *Magnetic hysteresis curve recorded at 300 k of Co_3O_4-Fe_3O_4 hybrid nanoparticle (CoFNP) with Fe_3O_4 nanoparticles (FeONP).*

7.4.3 X-ray photoelectron spectroscopic (XPS) analysis

Figure 7.3 shows the electron binding energy of Co_{2p} measured from XPS for 10nm CoNP and 10-15 nm CoFNP. Co^{3+} in CoNP exhibit binding energy at 779.8eV[25]. Whereas, Co_3O_4-

Fe_3O_4 hybrid nanoparticles exhibit ~5.4 eV increase in binding energy. The change in binding energy is likely due to the transfer of electron from Fe_3O_4 to Co^{3+} of Co_3O_4 nanoparticle. The shift in the peak of binding energy indicates the formation of Co_3O_4-Fe_3O_4 hybrid nanoparticles.

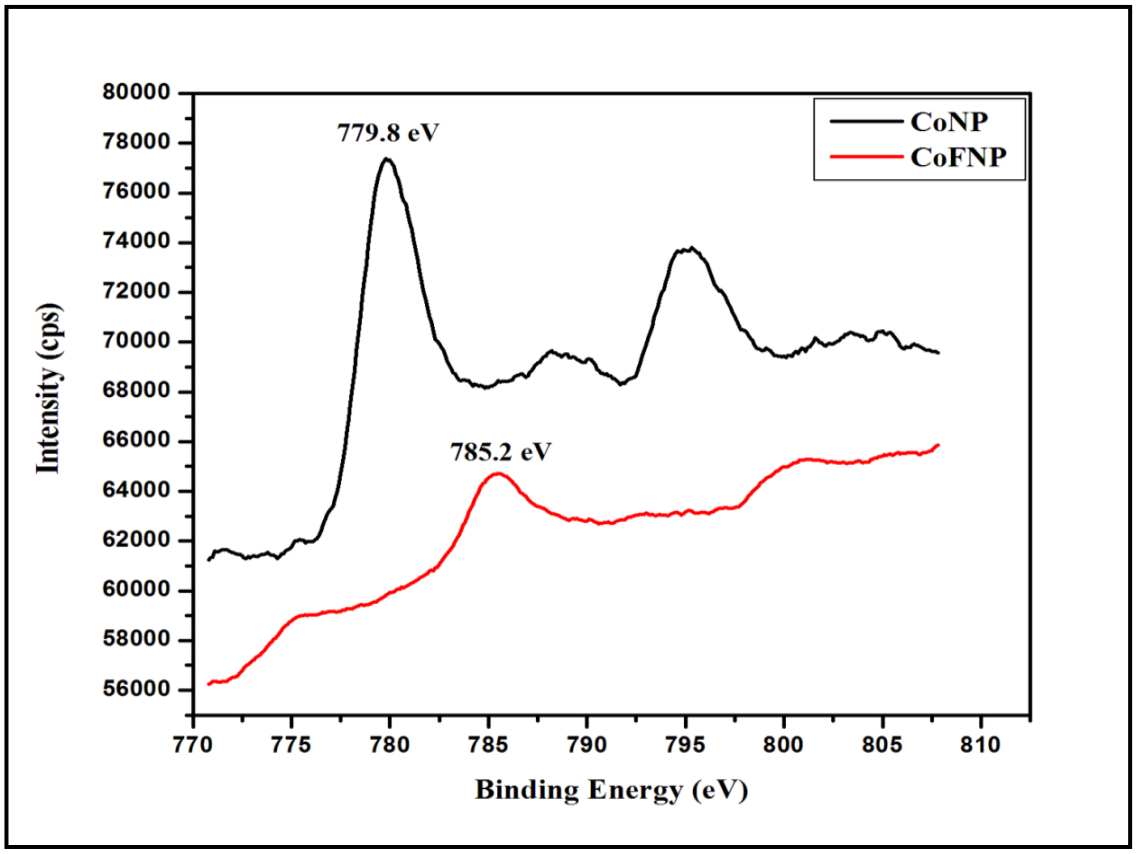

Figure 7.3 *XPS spectra of 5nm Co_3O_4 nanoparticles and 5-10nm Co_3O_4-Fe_3O_4 hybrid nanoparticles.*

7.4.4 FTIR analysis

Fourier transform infrared (FT-IR) spectra reveals information about the structure of neat chitosan (CTS), chitosan grafted glycolic acid (CGCF-1), nanohybrid scaffold (CGCF (D)) and drug (CPA) (**Figure 7.4**). The characteristic peaks in the FTIR spectrum of CTS include 1633 cm^{-1} (-NH stretching) and 3500cm^{-1} (-OH stretching). The presence of extra peak at 1730 cm^{-1} (-C=O stretching) and shifting of peak (-NH stretching) towards the lower

frequency region (1568 cm^{-1}) confirms the interaction of glycolic acid with NH_2 group of chitosan. The grafting of glycolic acid on chitosan was confirmed by the formation of amide (–NH-C=O) linkage between amine (-NH_2) group of chitosan and –C=O group of glycolic acid. In the FTIR spectrum of CPA include peak at 1237 cm^{-1} (-P=O stretching) and 1652 cm^{-1} (-NH stretching). The FTIR spectrum of CGCF-(D) include shift in peak 1067 cm^{-1} (-P=O stretching) and 3214 cm^{-1} (-OH stretching) it may due to the interaction of Co_3O_4-Fe_3O_4 hybrid nanoparticles with –P=O group of drug molecule and –OH group of chitosan via metallic bond. The peak at 1568 cm^{-1} in CGCF-(D) is attributed to shift in –C=O stretching towards lower frequency region, it may be due to the interaction of CPA with –C=O group of grafted glycolic acid via H- bonding (**Scheme 7.1**).

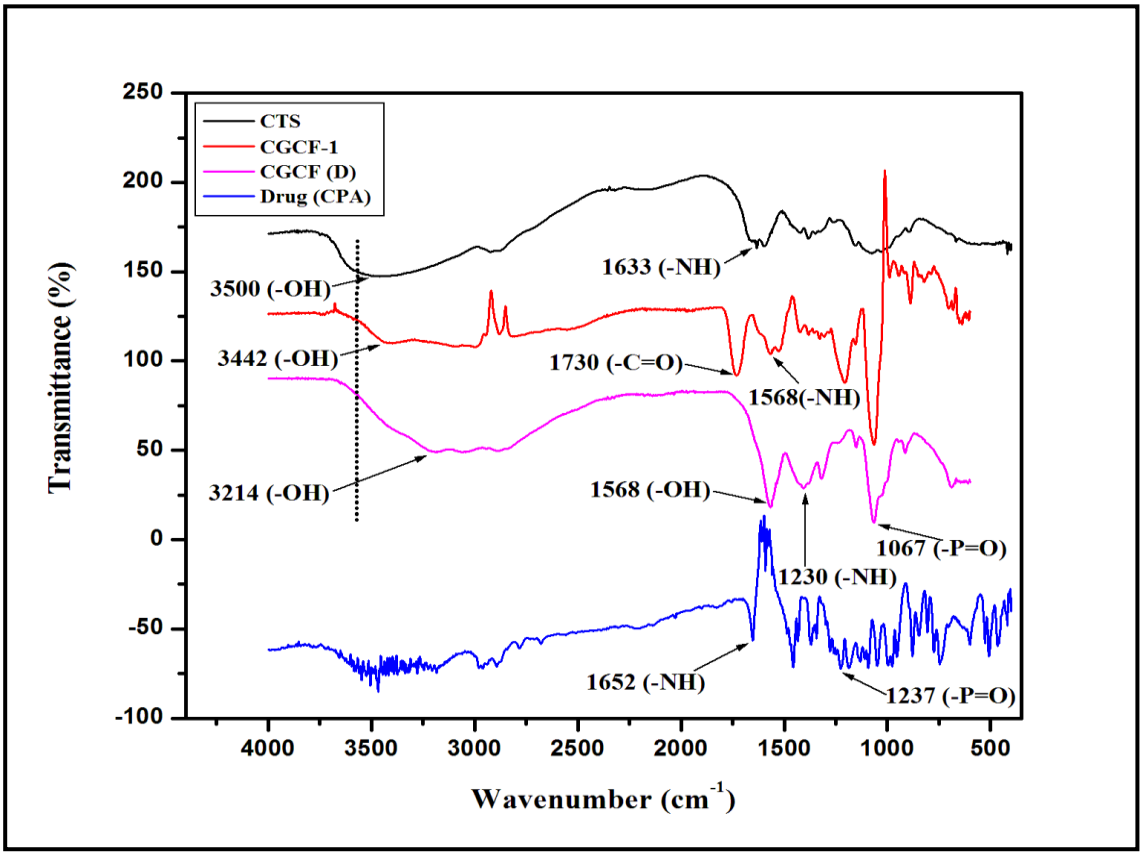

Figure 7.4 *FTIR spectra of neat chitosan (CTS), grafted chitosan (CGCF-1), grafted chitosan and Co_3O_4-Fe_3O_4 hybrid nanoparticles based nanohybrid scaffold (CGCF (D)) and drug cyclophosphamide (CPA).*

7.4.5 XRD analysis

Figure 7.5. (a) Illustrates the X- ray diffraction pattern of neat chitosan (CTS) and glycolic acid grafted chitosan (CGCF-1). It was observed that neat chitosan (CTS) shows the characteristic peak at 10.9^{o} and 19.8^{o}, which correspond to a hydrated crystalline structure and an amorphous structure of chitosan, respectively.[29-31] Grafting of chitosan with glycolic acid (CGCF-1) resulted in a shift of peak from 10.9^{o} to 10.1^{o} and 19.8^{o} to 20.6^{o} which confirms the interaction of chitosan with glycolic acid. These peaks were shifted from 10.1^{o} to 8.1^{o} and 20.6^{o} to 22.5^{o}, showing the interaction of Co_3O_4-Fe_3O_4 hybrid nanoparticles with the grafted chitosan (CGCF-2) as shown in **Figure 7.5.** (b).

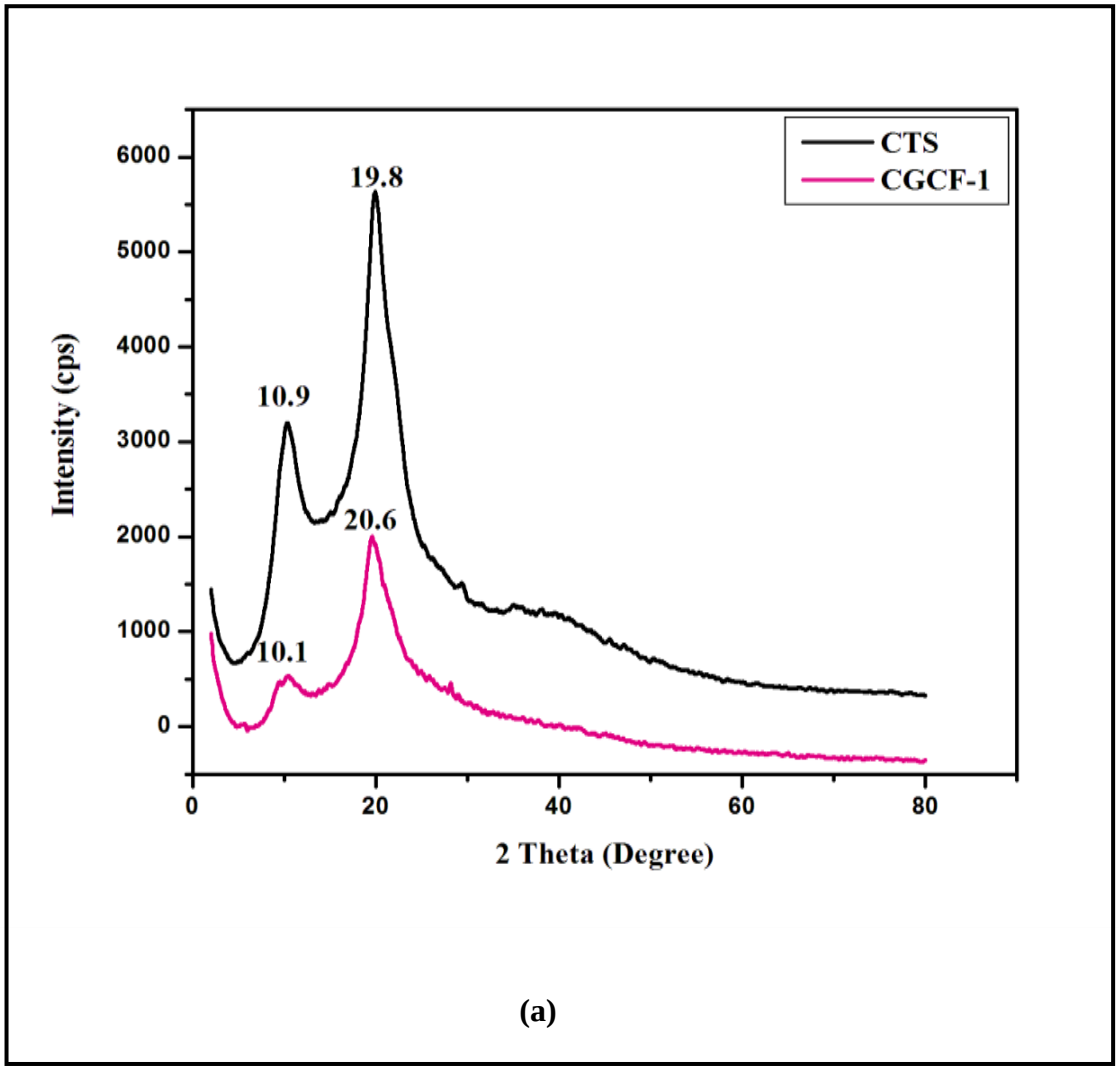

(a)

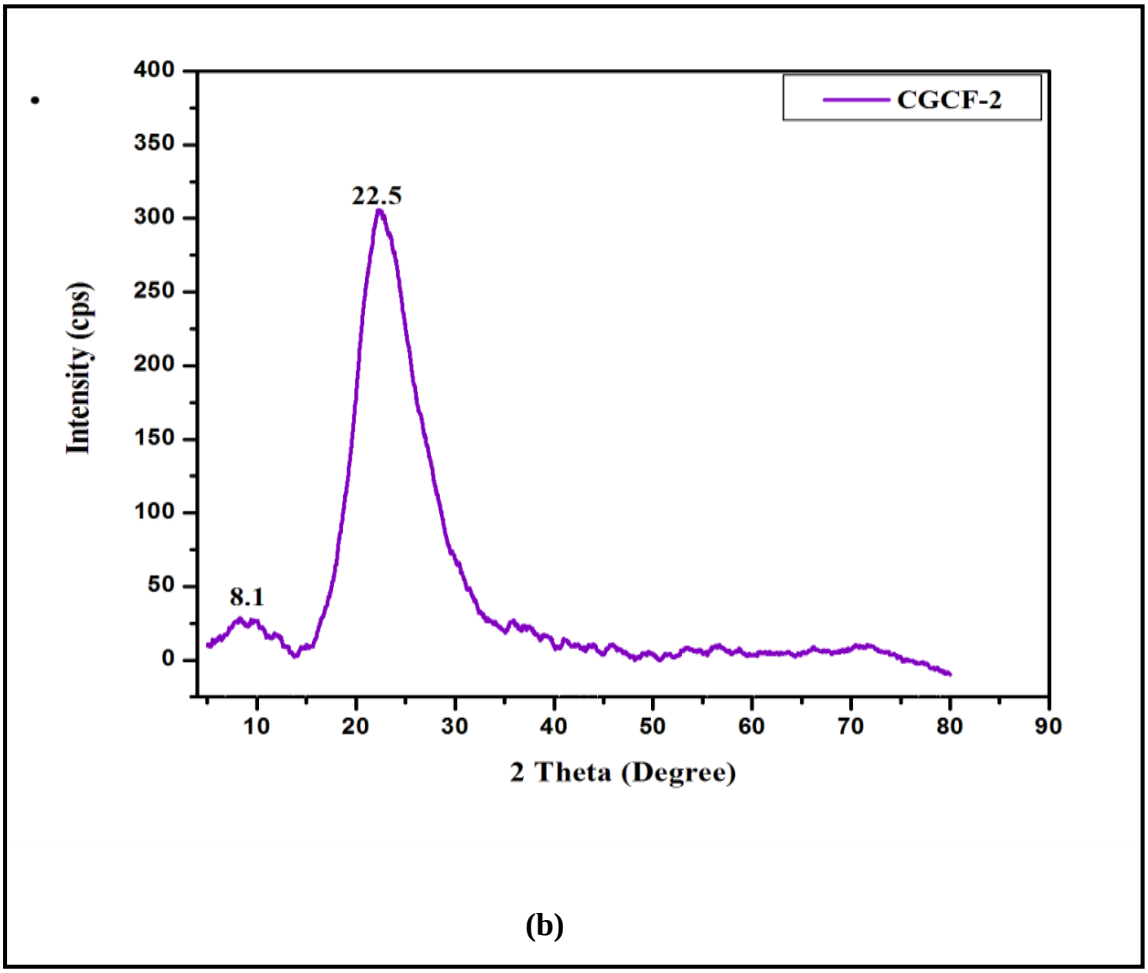

Figure 7.5 *(a) X-ray diffraction spectra of neat chitosan and grafted chitosan. (b) X-ray diffraction spectra of CS-g-glycolic acid and* Co_3O_4-Fe_3O_4 *hybrid nanoparticles based nanohybrid scaffold.*

7.4.6 Morphological study

The SEM image (**Figure 7.6** (a, b)) reveals the morphology of nanohybrid scaffold before drug loading and after drug addition (**Figure 7.6** (c, d)). It is observed that pore size of scaffold before drug addition was ranging from 30.10 µm to 40.10 µm, but upon addition of drug pore size decreases and lies in the range of 12.87 µm to 11.07 µm. The decrease in the pore size may be due to the incorporation of drug molecule in the pores of scaffold. The SEM-EDAX of scaffold confirms the incorporation of Co_3O_4-Fe_3O_4 hybrid nanoparticles in it (**Figure 7.6** (e)).

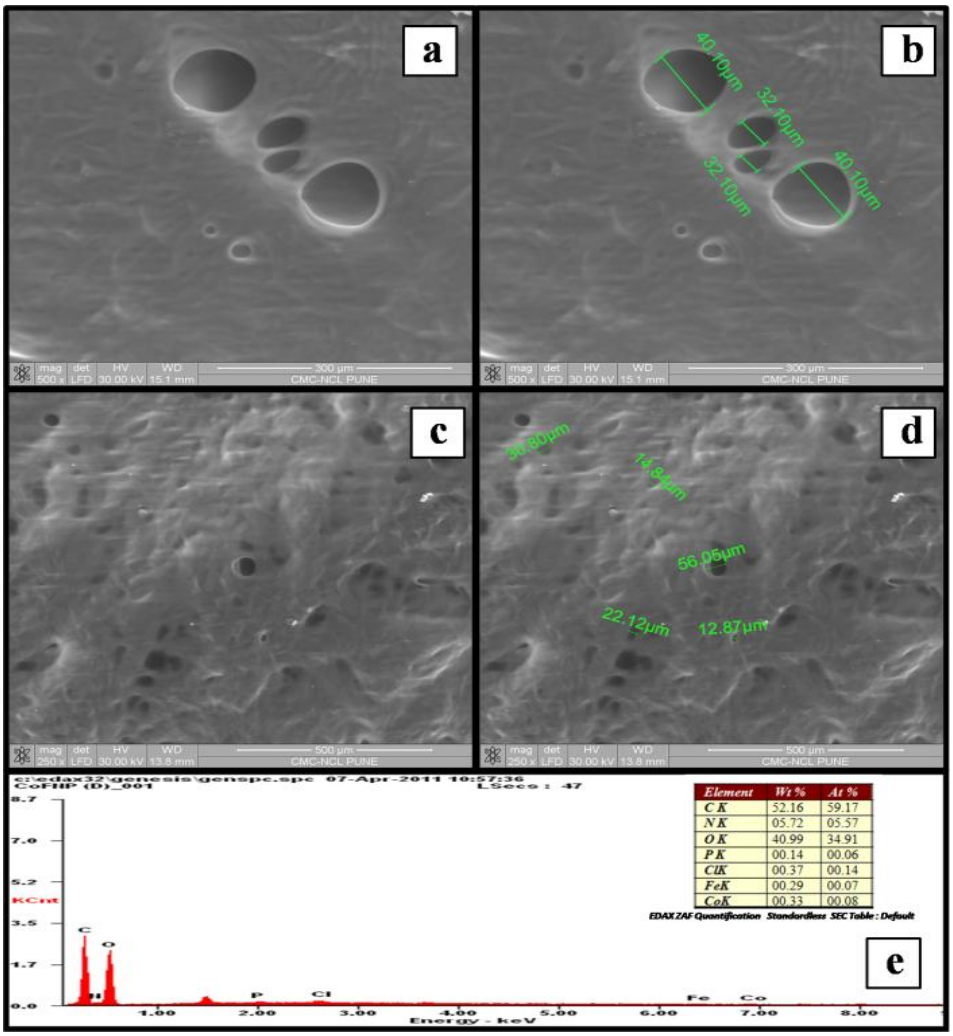

Figure 7.6 (*a, b) SEM image of grafted chitosan and Co_3O_4-Fe_3O_4 nanohybrid scaffold without drug; (c, d) SEM image of grafted chitosan and Co_3O_4-Fe_3O_4 nanohybrid scaffold with drug; (e) EDAX of nanohybrid scaffold(CGCF (D)).*

7.4.6 In vitro drug release

Figure 7.7 shows UV-vis spectra of in vitro drug release study illustrating variation in the absorbance of the drug in the scaffold with respect to time. In vitro drug release was examined with SBF (pH 7.4) and release media was quantified by UV-visible spectral absorbance values. It is observed that initially the release of drug was high and it decreases with the time because the drug which is at the surface of scaffold is released much faster than the drug incorporated deeply into the pores of the scaffold. The effect of incorporation of

Co_3O_4-Fe_3O_4 hybrid nanoparticles can be significantly observed as reduced rate of release at initial stage of immersion (upto 200 min). Initially specimen is solvated, which facilitates the lateral diffusion of drug after 250 min[32]. The rate of release of drug decrease over the time, it may be due to the interaction of Co_3O_4-Fe_3O_4 composite nanoparticles and grafted glycolic acid chains with the loaded drug[31].

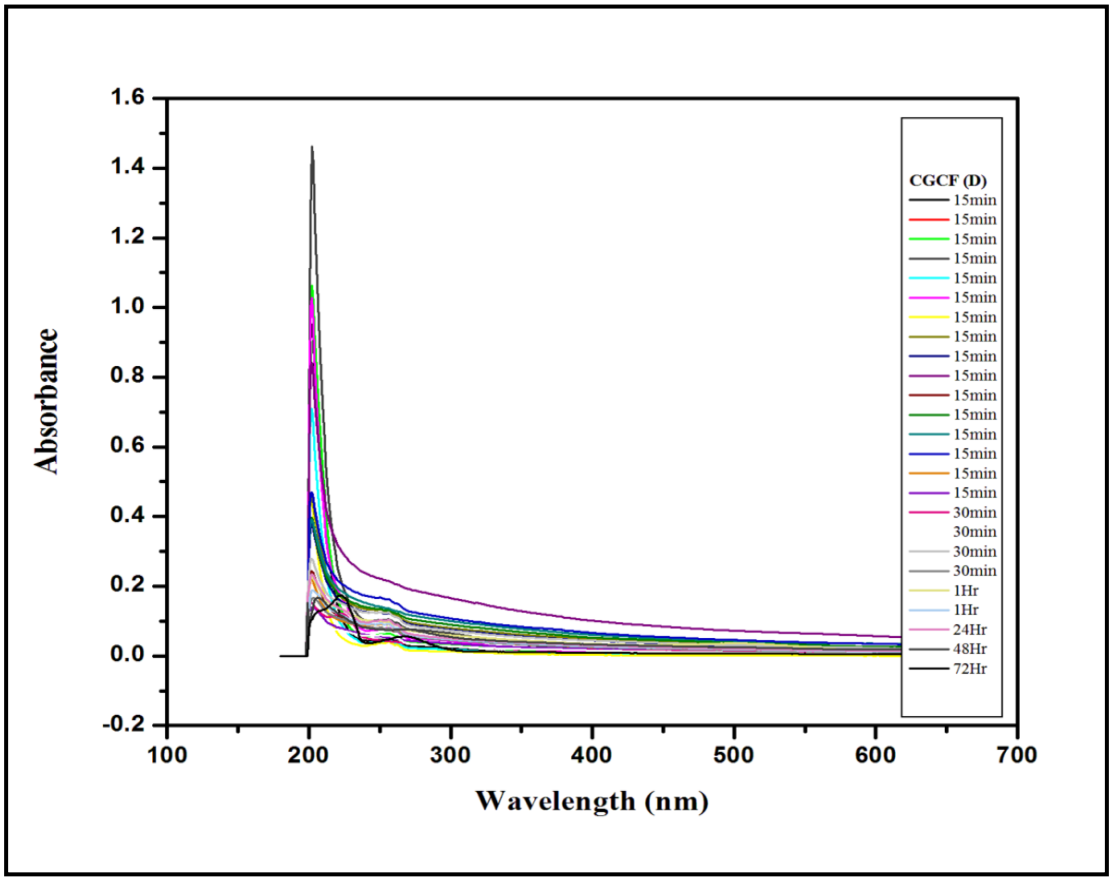

Figure 7.7 *Drug release profile from the prepared nanohybrid scaffold (CGCF (D)).*

7.4.8 Shape retention study

In general, swelling of chitosan involves the protonation of amino/imine groups and the mechanical relaxation of coiled chitosan chain[33, 34]. Shape retention was studied by measuring the change in the diameter as a function of immersion time in the media[35]. Swelling behavior of scaffold strongly depends upon the pH of the implantation site for their practical use in tissue engineering. It was investigated by exposing it to media at different pH, 1N HCl (pH

1.2), 1N NaOH (pH 14) and simulated body fluid (SBF) (pH 7.4) solutions for 24 h. The in vitro cell culture studies indicate that initial swelling is desirable[36, 37], but continuous swelling reduces the mechanical integrity and leads to the generation of compressive stress to the surrounding tissue. It is observed that scaffold CGCF (S) dissolve completely in the HCl solution within 2.5 h of immersion, whereas, rate of swelling is very low in NaOH and reached the plateau level around 3 h of immersion but increase in size of scaffold is observed within 6 h in SBF solution. In the case of scaffold CGCF (D), its complete dissolution was observed in HCl solution within 2.5 h of immersion, whereas slight swelling was observed in SBF within 3.5 h. These results showed that nanohybrid scaffold is stable towards the SBF and higher pH solution (**Figure 7.8**).

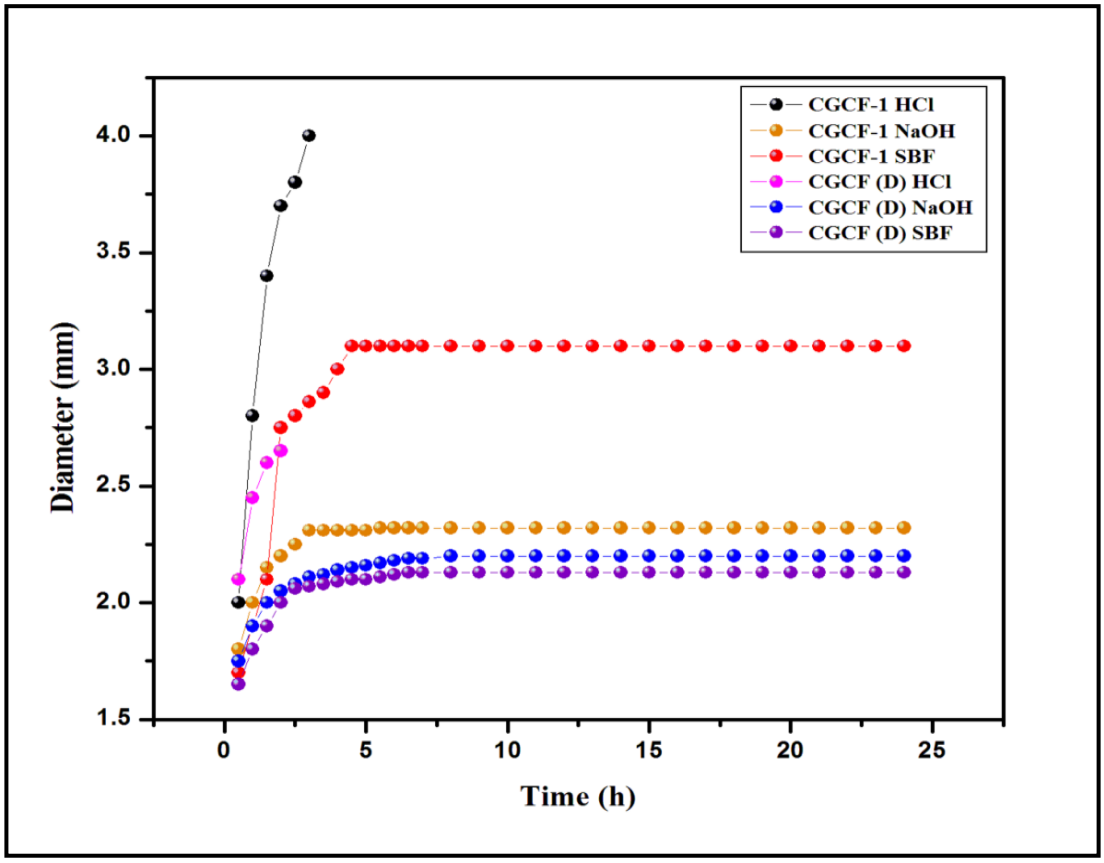

Figure 7.8 *Shape retention of scaffolds prepared from grafted chitosan and Co_3O_4-Fe_3O_4 nanohybrid.*

7.4.9 Cell viability study

MTT assay was carried out to evaluate the proliferation of L929 on (CGCF-(D)). Growth of the cells cultured on the scaffold was higher during the first 2 h but slight decrease in the cell number was observed in next 4 h. It may be because during proliferation cells have occupied all the available spaces on the scaffold[38]. Present study implies that the cell proliferation is not affected by the incorporation of Co_3O_4-Fe_3O_4 composite nanoparticles into glycolic acid grafted chitosan[34]. This may be due to the enhanced interaction between Co_3O_4-Fe_3O_4 composite nanoparticles and growing cells on the biopolymer matrix (**Figure 7.9.**). These results of improved cell proliferation and cell adherence on scaffold was mainly due to the presence of reactive groups on the polymer surface and improved hydrophillicity after hydrolysis, similar to those reported by other researchers[39]. The Co_3O_4-Fe_3O_4 composite nanoparticles may develop London- van der Waals forces with cells. These Co_3O_4-Fe_3O_4 composite magnetic nanoparticles can act as adhesive between biopolymer and cells.

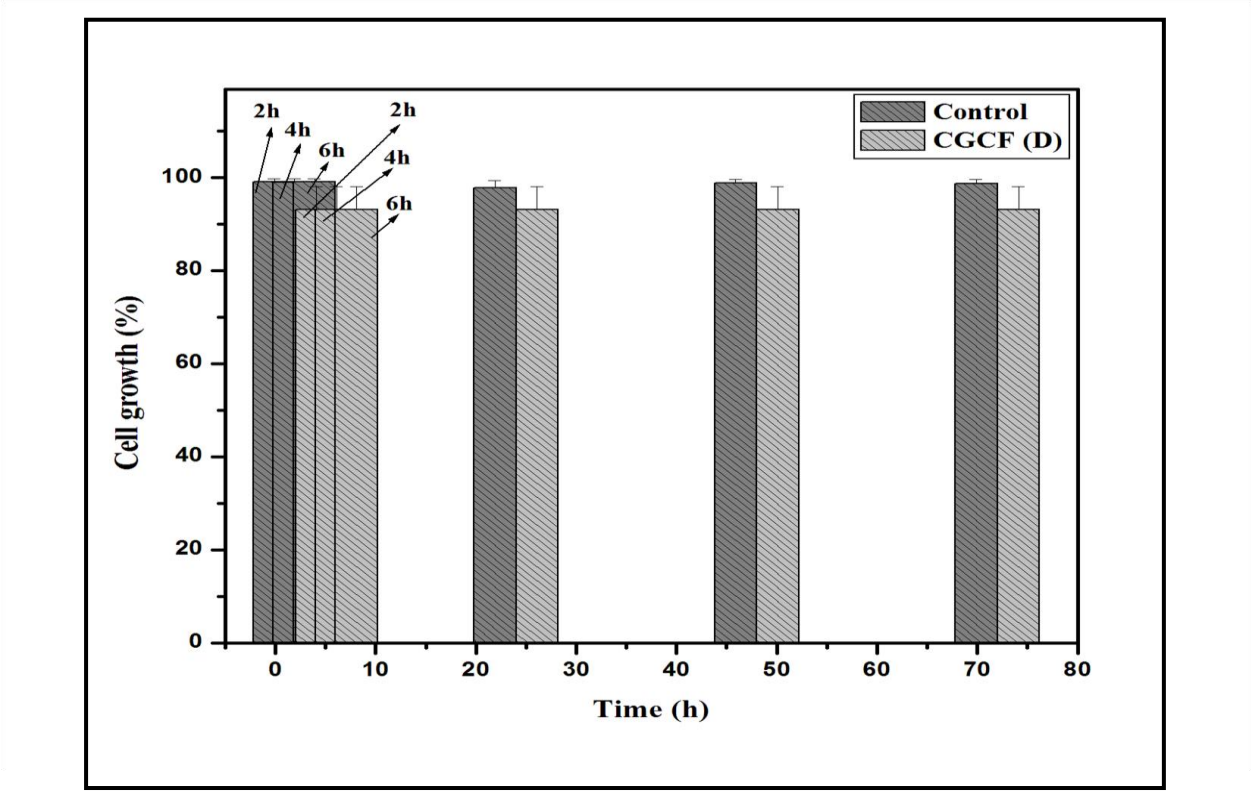

Figure 7.9. *Cell viability study done with MTT assay of cultured cells.*

7.5 CONCLUSIONS

The present study examined the potential use of hybrids of chitosan-g-glycolic acid and Co_3O_4-Fe_3O_4 composite magnetic nanoparticles as biomaterial. The FTIR confirmed the interaction of cationic chitosan with Co_3O_4-Fe_3O_4 composite nanoparticles via metallic bond and linkage of drug with the polymer matrix via H-bond. The nanohybrid scaffolds are stable regardless of pH of the medium. The nanohybrid scaffold posses porous morphology. The porous nanohybrid scaffolds have shown faster and higher drug release. The incorporation of Co_3O_4-Fe_3O_4 composite nanoparticles was observed to control the initial release of drug. From the results we conclude that, the prepared nanohybrid scaffold is biocompatible and also Co_3O_4-Fe_3O_4 composite magnetic nanoparticles are viable additive for formulating sustained drug delivery systems and could be applied in the field of biomaterials.

7.6 REFERENCES

1. R. Chapman, P. Mulvaney. *Chem. Phys. Lett.,* **349**, 358 (2001).
2. R. Krishnamoorti, R. A. Vaia. *Washington DC*, ACS, 2002.
3. G. Lagaly. *Appl. Clay. Sci.*, **15**, 1(1999).
4. P. F. Luckham, S. Rossi. *Adv. Coll. Interface Sci.,* **82**, 43(1999).
5. R. Jin. *Nanoscale.*, **2**, 343 (2010).
6. M. M. Alvarez, J. T. Khoury, T. G. Schaaff, M. N. Shafi gullin, I. Vezmar, R. L. Whitten. *J. Phys. Chem. B.,* **101**, 3706 (1997).
7. M. Zhu, C. M. Aikens, F. J. Hollander, G. C. Schatz, R. Jin. *J. Am. Chem. Soc.,* **130**, 5883 (2008).
8. T. Teranishi, *Comptes. Rendus. Chimie.*, **6**, 979 (2003).

9. I. Pastoriza-Santos, D. Gomez, J. Pérez-Juste, M. Luis, L. M. Liz-Marzán, P. Mulvaney. *Phys. Chem. Chem. Phys.*, **6**, 5056 (2004).
10. Y. Yamamoto, T. Miura, Y. Nakae, T. Teranishi, M. Miyake, H. Hori. *Phys. B: Condensed. Matter.*, **329**, 1183 (2003).
11. J. D. Aiken III, R. G. Finke. *J. Mol. Catal. A: Chem.*, **145**, 1 (1999).
12. A. Roucoux, J. Schulz, H. Patin. *Chem. Rev.* 2002, **102**, 3757-3778.
13. J. S. Bradley, G. Schmid, Schmid in: G. *Nanoparticles, Wiley-VCH*, Weinheim, 2004.
14. S. Akiyama, T. Yoshimura, K. Esumi. *J. Jpn. Soc. Colour. Mater.*, **78**, 112 (2005).
15. Y. Jiang, L. Zhang, D. Yang, L. Li, Y. Zhang, J. Li, Z. Jiang. *Ind. Eng. Chem. Res.*, **47**, 2495 (2008).
16. Y. Jiang, D. Yang, L. Zhang, Q. Sun, X. Sun, J. Li, Z. Jiang. *Adv. Funct. Mater.*, **19**, 150 (2009).
17. X. Liu, G. Qiu, X. Li. *Nanotechnology.*, **16**, 3035 (2005).
18. K. C. Souza, Æ. J. D. Ardisson. *J. Mater. Sci.*, **20**, 507 (2009).
19. R. Duncan. *Nat. Rev. Drug. Discov.*,**2**, 347 (2003).
20. R. Duncan. *J. Drug. Target.*, **14**, 333 (2006).
21. V. Torchilin. *Drug. Deliv.*, **5**, 1003 (2008).
22. S. G. Sampathkumar, K. Yarema. *J. Chem. Biol.*, **12**, 5 (2005).
23. T. N. Van, C. H. Ng, K. N. Aye, T. S. Trang, W. F. Stevens. *Chem. Tech. Biotech.*, **81**, 1113 (2006).
24. M. Xie, H. H. Liu, P. Chen, Z. L. Zhang, X. H. Wang, Z. X. Xie, Y. M. Du, B. Q. Pand, D. W. Pang. *Chem. Commun.*, **44**, 5518 (2005).
25. J. Xie, Q. Zhang, J. Y. Lee, D. I. C. Wang. *ACS Nano.*, **2**, 2473 (2008).

26. T. D. Schladt, M. I. Shukoor, K. Schneider, M. N. Tahir, F. Natalio, I. Ament, J. Becker, F. D. Jochum, S. Weber, O. Köhler, P. Theato, L. M. Schreiber, C. Sönnichsen, C. Schröder, W. E. G. Müller, W. Tremel. *Angew. Chem.*, **49**, 3976 (2010).

27. T. Takahashi, M. Yamaguchi. *J. Colloid Interface Sci.,* **146**, 556 (1991).

28. R. L. Hong, J. Y. Yu. *J. Biomed. Mater: Appl. Biomater.,* **71B**, 52 (2004).

29. J. W. Rhim, I. N. Hong Seok, H. M. Park, K. W. N. G. Perry. *J. Agric. Food. Chem.,* **54**, 5814 (2006).

30. Y. Mei, Y. Zhao. *J. Agric. Food Chem.,* **51**, 1914 (2003).

31. S. I. Park, Y. Zhao. *J. Agric. Food Chem.,* **52**, 1933 (2004).

32. L. Shilin, H. Haoze, Z. Jinping, Z. Lina. *Cellulose.,* **18**, 1273 (2011).

33. S. I. Park, Y. Zhao. *J. Agric. Food Chem.,* **52**, 1933 (2004).

34. L.Vachoud, N. Zydowicz, A. Domard. *Carbohyd. Res.,* **326**, 295 (2000).

35. S. Aiba. *Int. J. Biol. Macromol.* 1991, **13**, 40-44.

36. S. Kumari, R. P. Singh. *Inter. J. of Bio. Macromol.*, **50,** 878 (2012).

37. L. M. Liz-Marzan. *Mat. Today.*, **7**, 26 (2004).

38. N. Shanmugasundram, P. Ravichandaran, P. N. Reddy, N. Ramamurth, S. Pal, K. P. Rao. *Biomater.,* **22**, 1943 (2001).

39. F. Chen, C. N. Lee, S. H. Teoh. *Mater. Sci. Eng. C.,* **27**, 325 (2007).

CHAPTER 7

B: Preparation and Characterization of Chitosan-g-Glycolic Acid-Co_3O_4-Fe_3O_4 Hybrid Nanoparticles Based Nanocomposite Film

7.2.1 INTRODUCTION

The nanotechnology field is one of the interesting areas for current research and development in all technical discipline. In this field the investigation cover a broad range of topics, this obviously includes polymer science and technology. Other areas include polymer based biomaterials, layer by layer self assembled polymer films, imprint lithography, electro-spun nanofiber, nanocomposites, fuel cell electrode polymer bound catalysts and nanoparticle drug delivery. The nanocomposites of inorganic materials in polymer matrices have attracted a great deal of attention because of their wide area of applications as micromechanical devices[1], optical device[2], catalytic membrane[3] and biosensors[4]. The field of nanocomposites include composites rein-enforcement, electro-optical properties, barrier properties and cosmetic applications. Different approaches have been developed for the synthesis of nanocomposites such as incorporation of premade nanoparticles into the polymer matrix. This can be achieved with the use of a common blending solvent or by reduction of metal salt dispersed in polymer matrix using an external reducing agent[5]. Various methods are known for the embedment of nanoparticles in polymer matrices such as physical and chemical vapour deposition, ion implantation and sol-gel synthesis[6-8]. The Metallic and metal oxide nanoparticles have become an area of growing interest of fundamental studies and technological applications, due to their unique mechanical, electronic, chemical, magnetic and optical properties[9-14]. The metal nanoparticle embedded polymer film can show enhanced mechanical properties. Therefore, attempts have been made to synthesize metal nanoparticles embedded chitosan films.

Chitosan is used to prepare a variety of forms such as powders, hydrogels, membranes, fibers, porous scaffolds and films that have been tested in many medical and biological applications[15-18].

7.2.2 EXPERIMENTAL

7.2.2.1 Materials

Chitosan of low molecular weight (Mv 1.5×10^5, degree of deacetylation was 85%), glycolic acid with (99% purity), iron (0) pentacarbonyl ($Fe(CO)_5$), oleylamine (OAM), oleic acid (OA), 1-octadecene, cobalt acetate ($Co(OAc)_2$) and citric acid ($C_6H_8O_7$) was obtained from sigma Aldrich. Sodium hydroxide and phenyl ether was obtained from Sisco Research Laboratories. Deionised water was used throughout, which is prepared by Milli-Q-system.

7.2.2.2 Preparation of nanocomposite film

Chitosan-g-glycolic acid and Co_3O_4-Fe_3O_4 nanoparticle (**synthesis of nanoparticles has been given in chapter 7A, section 7.2.2**) nanocomposite film was prepared by dispersing chitosan in deionised water for 1 h with constant stirring at room temperature. Glycolic acid was added to the solution after 1 h, which is allowed to stirred for 12 h. After 12 h, Co_3O_4-Fe_3O_4 hybrid nanoparticles were added to the resulting solution and stirred overnight at room temperature. Degassing of resulting solution was done at 80 ^{0}C for 25- 30 min. The solution was casted on a glass plate and dried at 60 ^{0}C for 8 h under vacuum to promote the dehydration of grafted chitosan copolymer with formation of the amide linkage. The thickness of the prepared film were measured and found to be 0.18 mm. The formulation of chitosan and nanoparticles are given in **Table 7.2.1**. The unreacted glycolic acid and the oligomers of glycolic acid were extracted with methanol in soxhlet apparatus for 48 h.

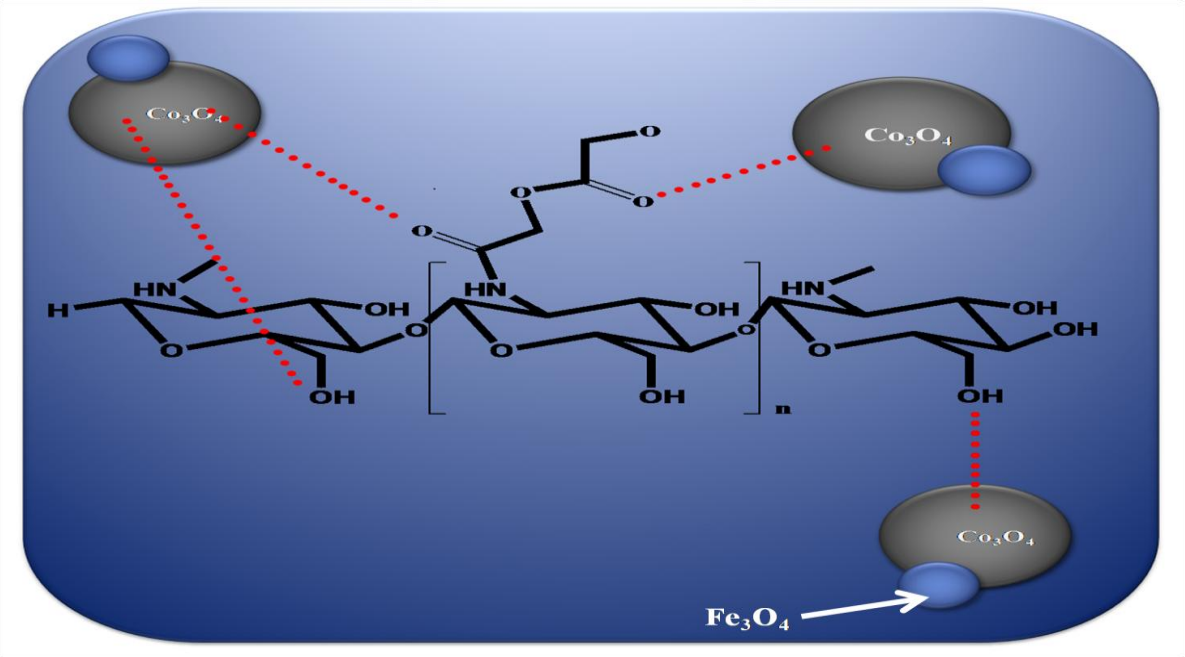

Scheme 7.2.1 *Schematic illustration of interactions between glycolic acid grafted chitosan and Co_3O_4/Fe_3O_4 hybrid nanoparticles.*

Table 7.2.1 The formulation of chitosan-g-glycolic acid and Co_3O_4-Fe_3O_4 nanoparticle

S. No	Chitosan (g)	Glycolic acid (g)	Co_3O_4 -Fe_3O_4 (mg)	Sample code
1	1	0	0	CS
2	1	1	0	CGCoF-1
3	1	1	40	CGCoF-2
4	1	1	80	CGCoF-3

7.2.3 CHARACTERIZATION OF NANOCOMPOSITE FILM

7.2.3.1 Attenuated total reflectance Fourier transform infrared (ATR-FTIR)

The Nicolet Nexus 870 attenuated total reflectance Fourier transform infrared (ATR-FTIR) spectrometer equipped with a smart Endurance diamond accessory (64 scans, 4 cm^{-1} resolution, wave number range 4000-550 cm^{-1}) were used to analyse Fourier transform

infrared spectra (FT-IR) of neat chitosan (CS), chitosan grafted glycolic acid (CGCoF-1) and grafted chitosan nanocomposite with Co_3O_4-Fe_3O_4 hybrid nanoparticles (CGCoF-2).

7.2.3.2 X-ray diffraction (XRD)

XRD pattern of the samples were recorded by using X-ray Diffractometer (WAXRD – Rigaku, Japan) with Cu-kα radiation at a voltage of 50 KV. The scanning rate was 4^0/min and the scanning scope of 2θ was from 2^0 to 80^0 at room temperature.

7.2.3.3 Atomic force microscopy (AFM)

The surface morphology of nanohybrid film were investigated by atomic force microscopy (AFM) (Model: Nanoscope IV) under contact mode.

7.2.3.4 Water absorption measurement

The water absorption measurement was investigated by ASTM D 570 method, according to which, the clean, dried film samples of known weights were immersed in distilled water at 25 ^{0}C for 24h (1 Day), The films were removed, blotted quickly with absorbent paper and weighed. The absorption percentage of prepared samples was calculated using the Eq. (1):

$$X\% = (W_1-W_0)/W_0 \quad (1)$$

where W_0 and W_1 are the weight of dry and swollen samples, respectively.

7.2.3.5 Dynamic mechanical analysis (DMA)

The mechanical strength of prepared nanohybrid films were investigated with dynamic mechanical thermal analyser (DMTA RSA3, TA instrument) in tensile mode at a frequency of 1Hz with heating rate of 5 ^{0}C/min in the temperature range from -10 ^{0}C to 200 ^{0}C.

7.2.3.6 Tensile strength testing (TST)

The tensile stress testing of the nanohybrid film was determined with Linkam TST 350. The break stress and strain was calculated with the associated software (Linkam). A dumb bell strip was cut from each membrane and strained to break at a constant crosshead speed of 10 mm/min.

7.2.3.7 Thermogravimetric analysis (TGA)

TGA Q5000 instrument were used to conduct the thermogravimetric analysis (TGA) of the sample. Temperature ranges from 50 ^{0}C to 900 ^{0}C with the heating rate of 10 ^{0}C/min under nitrogen with flow rate 20

7.2.4 RESULT AND DISCUSSION

7.2.4.1 FTIR analysis

The structural information about pure chitosan (CS), glycolic acid grafted chitosan (CGCoF-1) and its nanocomposite with Co_3O_4-Fe_3O_4 composite nanoparticles (CGCoF-2) were investigated by Fourier transform infrared (FT-IR) spectra (**Figure 7.2.1**). In pure chitosan spectrum, peak at 1634 cm^{-1} is attributed to the –N-H bending vibration of amine (–NH_2) group in chitosan. In glycolic acid grafted chitosan (CGCoF-1) spectrum, the peak attributed to the –N-H bending vibration is shifted towards the lower frequency region confirming the interaction of glycolic acid onto NH_3^+ group. In CGCoF-1 a new peak appeared at 1734 cm^{-1} corresponds to υ_{co} stretching. These two peaks confirms the conversion of amine (NH_2) to amide (–NH-C=O). The band at 3437 cm^{-1} is corresponding to υ_{NH} stretching. The N-H bending of the molecule as well υ_{co} stretching band is observed to be shifted towards lower frequency region, indicating the interaction of Co_3O_4-Fe_3O_4 with N-H group of chitosan and C=O group of glycolic acid through metallic-bond, in FTIR spectrum of CGCoF-2 (**Scheme 7.2.3**).

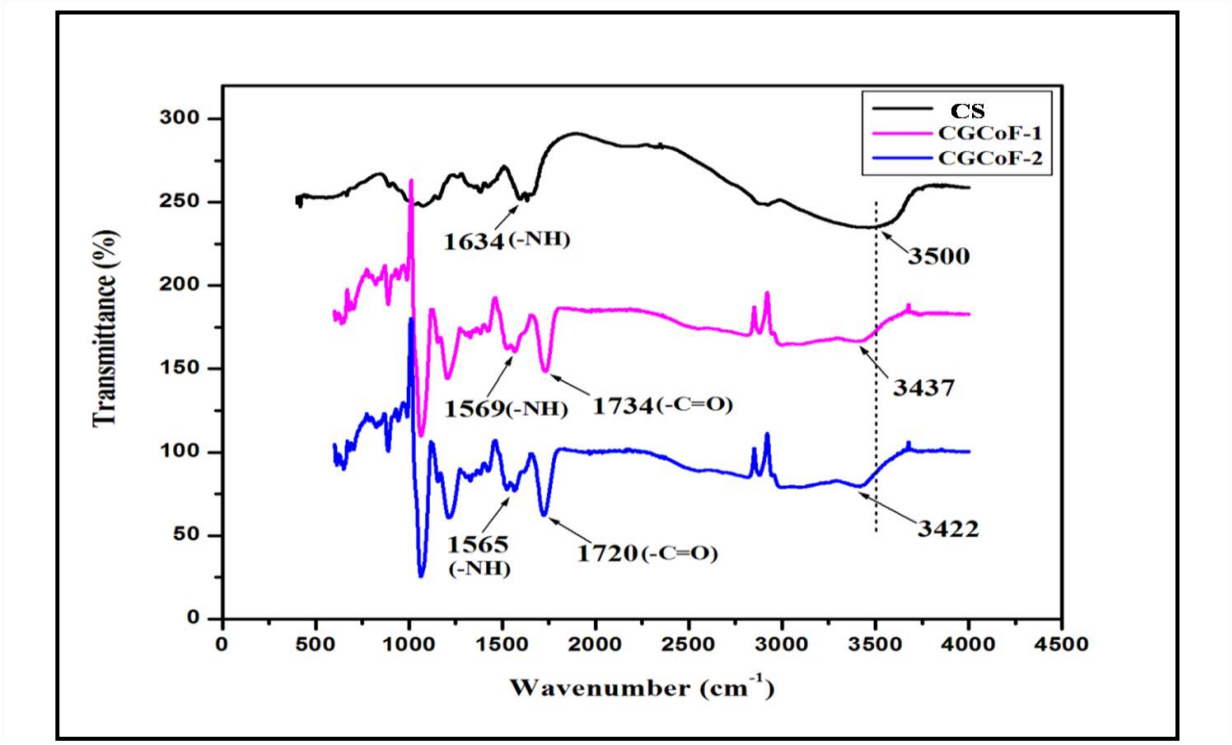

Figure 7.2.1 *FTIR spectra of neat chitosan (CS), grafted chitosan (CGCoF-1) and grafted chitosan/Co_3O_4-Fe_3O_4 hybrid nanoparticle nanocomposite film (CGCoF-2).*

7.2.4.2 XRD analysis

The XRD pattern of neat chitosan (CS), chitosan grafted with glycolic acid (CGCoF-1) and nanocomposite of grafted chitosan with Co_3O_4-Fe_3O_4 composite nanoparticles (CGCoF-2) was shown in **Figure 7.2.2** (a, b). The chitosan structure is strongly dependent on its processing treatment, such as dissolving, precipitation and drying, as well as its origin and characteristics, such as degree of deacetylation and molecular weight[19]**.** The neat chitosan film shows the peaks at $2\theta = 10.3^0$ and 20.1^0, corresponds to hydrated crystalline structure and an amorphous structure of chitosan, respectively[20-21]. The XRD peaks were shifted from 10.3^0 to 9.6^0 and 20.1^0 to 19.6^0 confirming the interaction of glycolic acid with chitosan in CGCoF-1 sample film. More shifts in CGCoF-2 nanocomposite film was observed that is, $2\theta = 9.6^0$ to 9.0^0 and 19.6^0 to 21.5^0. This is probably due to higher compatibility of the Co_3O_4-Fe_3O_4 nanoparticle with the grafted chitosan matrix.

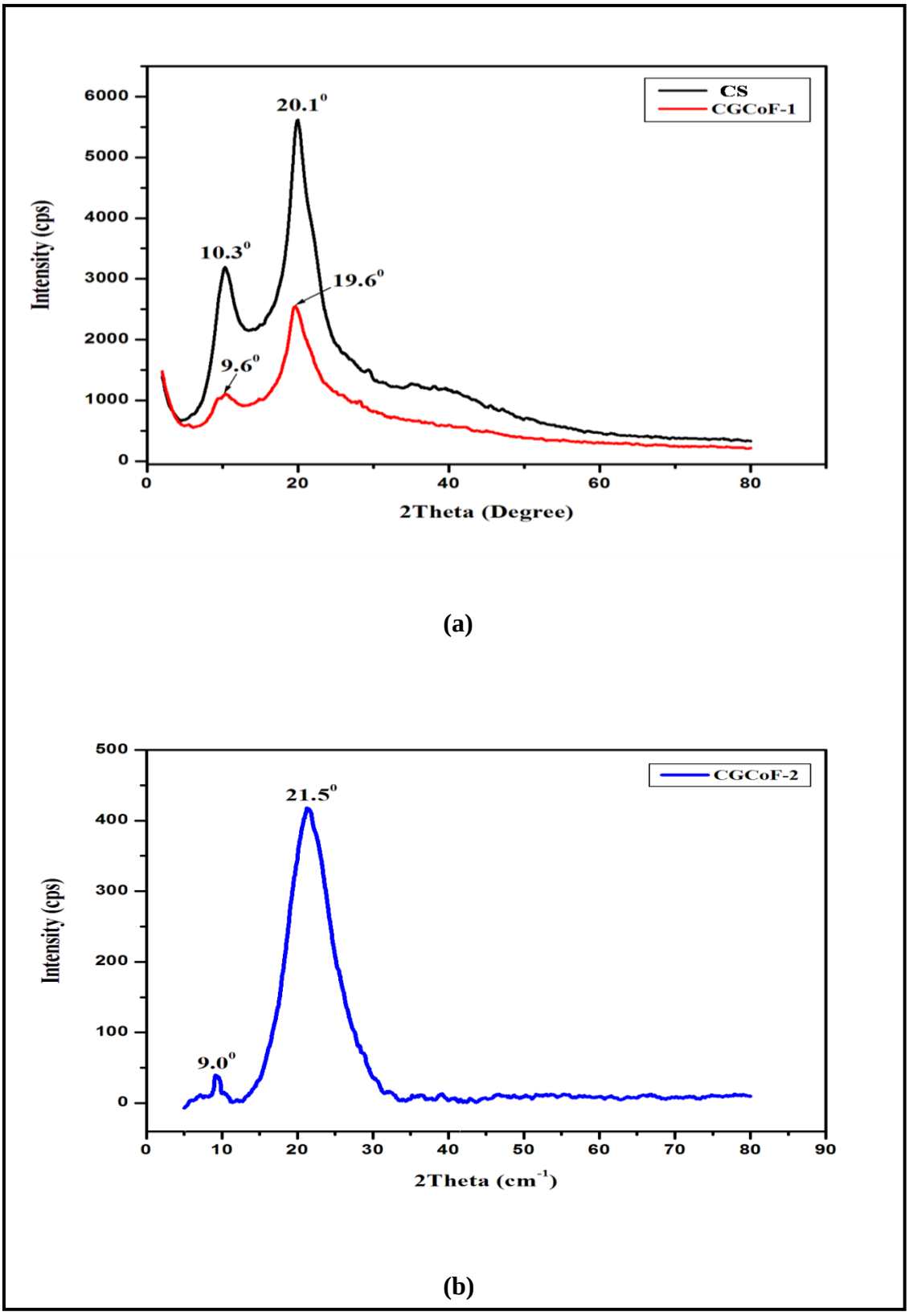

Figure 7.2.2 *(a) X-ray diffraction spectra of neat chitosan (CS) and grafted chitosan (CGCoF-1). (b) X-ray diffraction spectra of grafted chitosan/Co_3O_4-Fe_3O_4 hybrid nanoparticle nanocomposite films.*

7.2.4.3 Morphological studies

Atomic Force Microscopy (AFM) illustrates the surface topography of pure chitosan, grafted chitosan and nanocomposite film. **Figure 7.2.3** (a) shows the AFM image of neat chitosan film, which is observed to exhibit smooth surface. The image size was 5 μm × 5 μm. Grafting of chitosan with glycolic acid increases the roughness and height of the surface (**Figure 7.2.3** (b)). The incorporation of Co_3O_4-Fe_3O_4 composite nanoparticle in the matrix of chitosan film is shown in **Figure 7.2.3** (c, d).

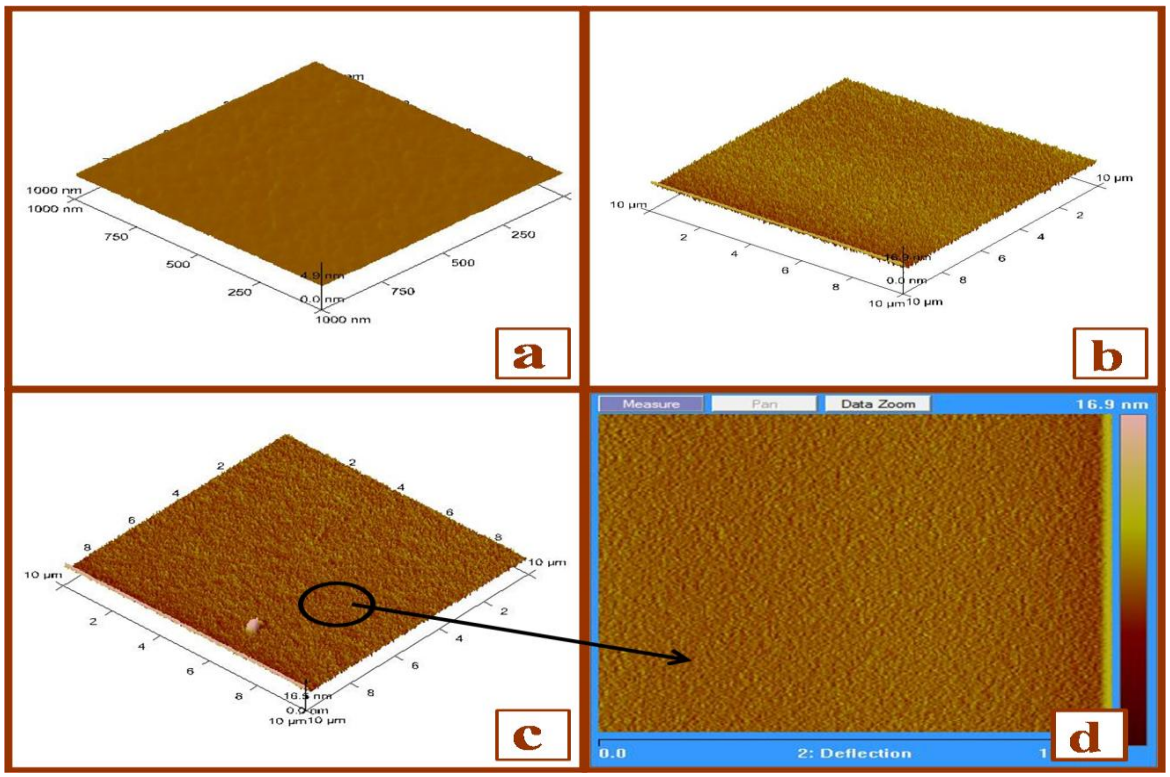

Figure 7.2.3 *(a) AFM image of pure chitosan film; (b) AFM image of grafted chitosan film. (c, d) AFM image of grafted chitosan/Co_3O_4-Fe_3O_4 hybrid nanoparticle nanocomposite films.*

7.2.4.4 Water absorption Behavior

The water absorption property of the glycolic acid grafted chitosan is higher than that of the pure chitosan. The pure chitosan is hydrophilic but it does not absorb much water, probably due to many –OH and –NH groups in chitosan, which causes strong intermolecular

and intramolecular hydrogen bonds. The higher water absorption in grafted chitosan is probably because the molecular structure integrity is broken in the grafted chitosan, which can expose more functional groups for water absorption. This swelling extent will depend on the osmotic pressure and charge repulsion, the degree of ionization and grafting extent. In comparison of grafted chitosan, nanocomposite films show lower water absorption and deceases with the increasing content of nanoparticles. This is probably due to the formation of a barrier in the form of cross linking points, which prevents water permeation into chitosan. Since nanoparticle is hydrophobic, resulting nanocomposite were expected to be hydrophobic. It can be attributed to the interaction between nanoparticle and copolymer. Upon increasing content of nanoparticle reduces the exposure of more functional group towards the water, thus the hydrophobicity of the nanocomposite film increases. The formation of nanocomposite occurs through the metallic bond formation between Co_3O_4-Fe_3O_4 composite nanoparticle and copolymer, which decreases the water absorption (**Table 7.2.2**). The nanocomposite films were kept in water for 24 h till the equilibrium is reached. After complete swelling, film was dried under vaccume at 65 ^{0}C to evaluate the moisture retention capacity of the nanocomposite films. Grafted chitosan shows high water retention capacity. Nanoparticles act as a physical barrier for the moisture to exude out from the films this is because on increasing the nanoparticle content, the water absorption decreases.

Table 7.2.2 Sorption behavior of the nanocomposites

Sample Code	Water Absorption (%)
CS	54
CGCoF-1	70.7
CGCoF-2	52.98
CGCoF-3	33.2

7.2.4.5 Dynamic mechanical analysis

The change in viscoelastic property, stability and glass transition temperature of polymer determines the variation in dynamic mechanical thermal property of glycolic acid grafted Co_3O_4-Fe_3O_4 hybrid nanoparticle nanocomposites. The storage modulus [E'] of pure chitosan film at 77.92 ^{0}C is observed to be 1.766×10^8 [Pa] (**Figure 7.2.4** (a)). The storage modulus [E'] increases to 2.502×10^8 [Pa] for grafted polymer film (**Figure 7.2.4** (b)). Storage modulus [E'] of nanocomposite film increases with the increase in Co_3O_4-Fe_3O_4 hybrid nanoparticle content (**Figure 7.2.4** (c, d)). The loss factor (tanδ), which is the ratio of the loss modulus to the storage modulus decreases with the increase in glass transition temperature. The neat chitosan film exhibit T_g =153.63^{0}C. Decrease in T_g of grafted film is observed due to increase in the mobility of the polymer chains. The addition of Co_3O_4-Fe_3O_4 hybrid nanoparticle restricts the mobility of the chains, thus the storage modulus increases and improves the mechanical strength of polymer film **Table 7.2.3**.

Table 7.2.3 Viscoelastic properties of grafted chitosan- Co_3O_4 -Fe_3O_4 hybrid nanoparticle nanocomposites

Sample Code	Co_3O_4-Fe_3O_4 (Wt %)	Storage modulus (Pa) at 77.92 ^{0}C	Tg (^{0}C)	Tan delta (δ)
CS	0	1.766×10^8	153.86	0.43
CGCoF-1	0	2.507×10^8	113.54	0.59
CGCoF-2	40	4.133×10^6	24.62	0.55
CGCoF-3	80	2.306×10^7	38.02	0.43

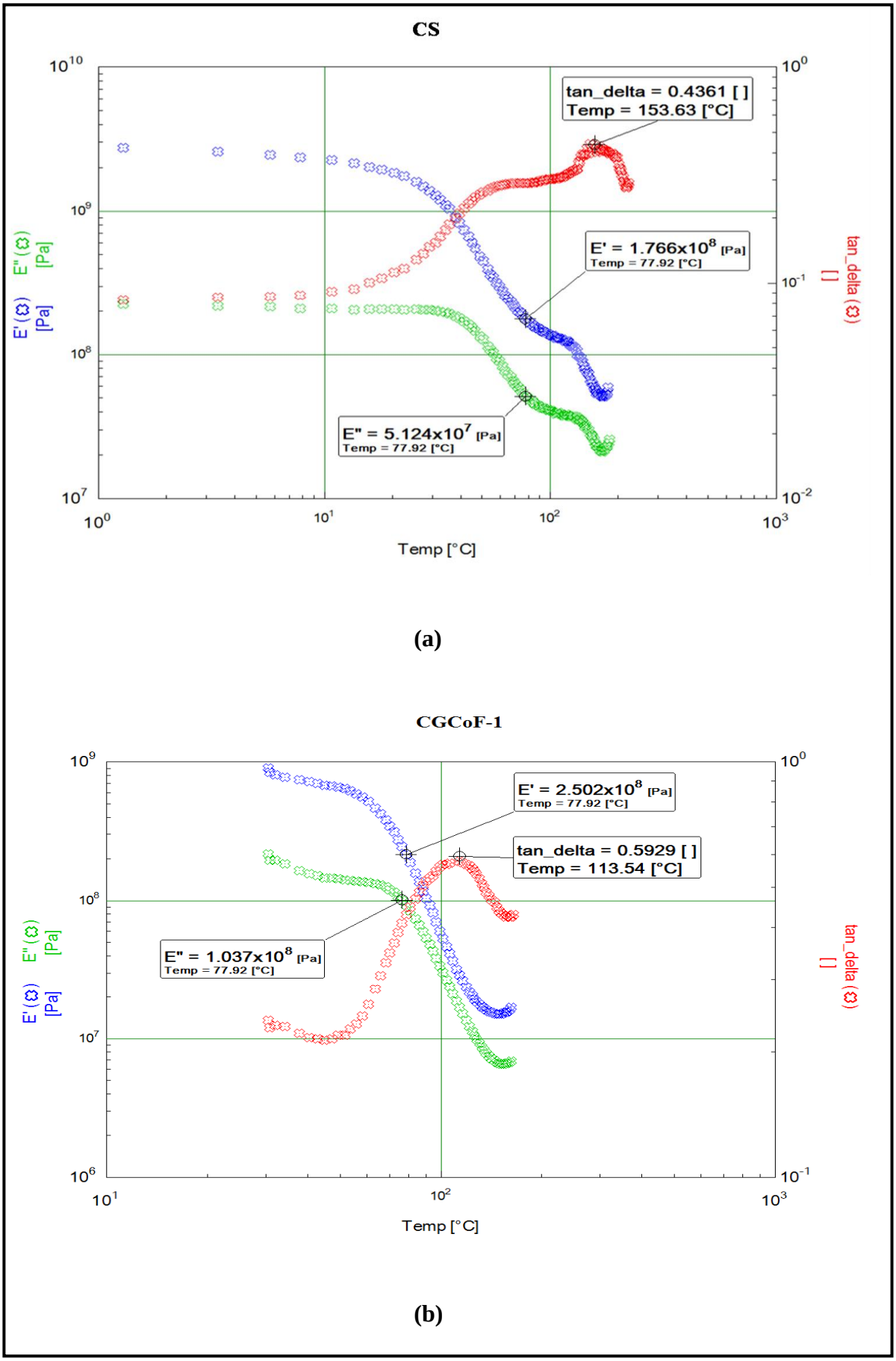
CS
tan_delta = 0.4361 [ ]
Temp = 153.63 [°C]
E' = 1.766x10^8 [Pa]
Temp = 77.92 [°C]
E" = 5.124x10^7 [Pa]
Temp = 77.92 [°C]
E'(ω) E"(ω) [Pa]
tan_delta (ω) [ ]
Temp [°C]
(a)
CGCoF-1
E' = 2.502x10^8 [Pa]
Temp = 77.92 [°C]
tan_delta = 0.5929 [ ]
Temp = 113.54 [°C]
E" = 1.037x10^8 [Pa]
Temp = 77.92 [°C]
E'(ω) E"(ω) [Pa]
tan_delta (ω) [ ]
Temp [°C]
(b)

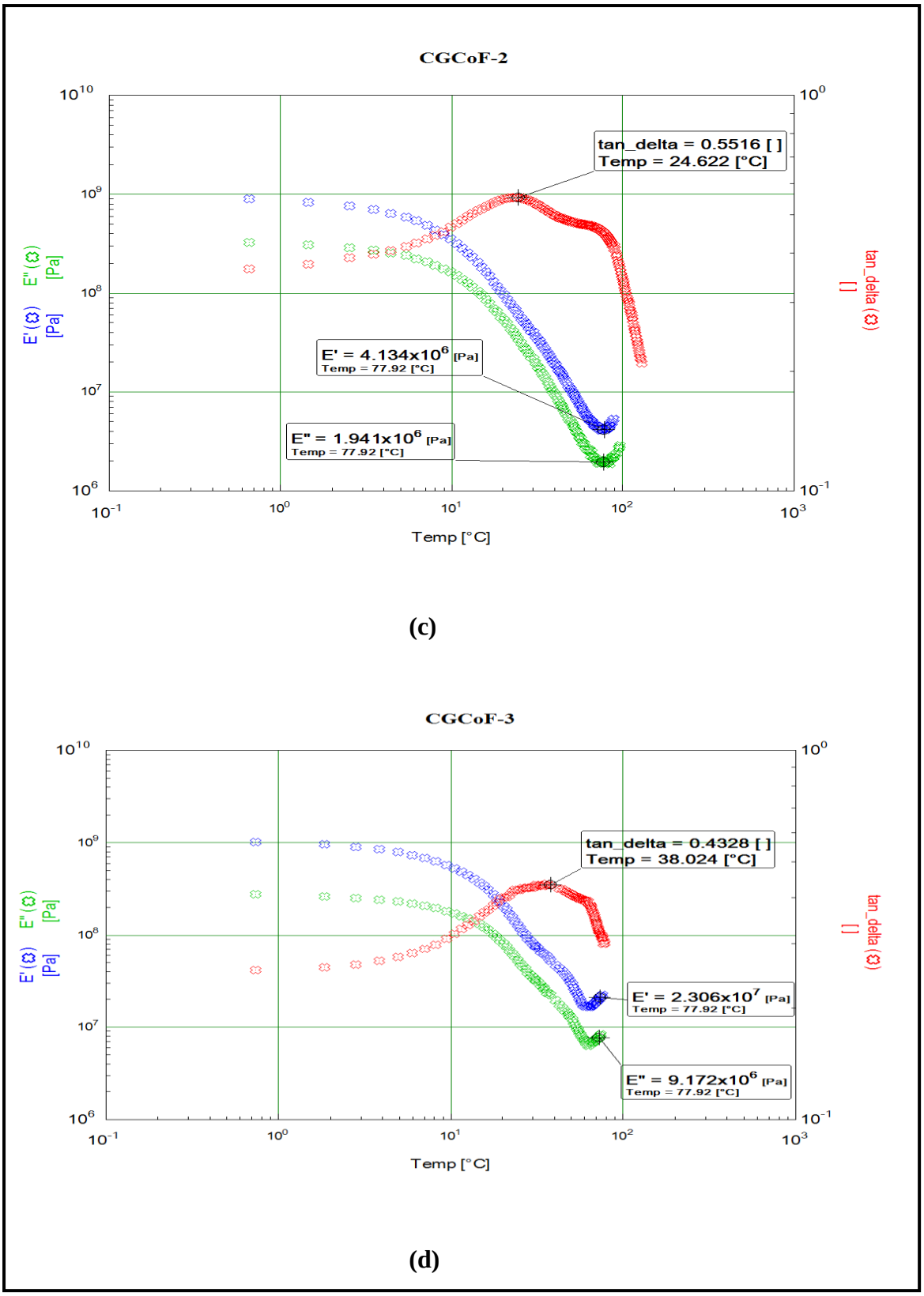

Figure 7.2.4 *Temperature variation of tanδ, glass transition temperature, storage modulus [E'], and loss modulus [E''] (a) Pure chitosan film (CS); (b) Grafted chitosan film (CGCoF-1); (c) Grafted chitosan/Co_3O_4-Fe_3O_4 hybrid nanoparticle nanocomposite films (CGCoF-2); (d) Grafted chitosan/ Co_3O_4-Fe_3O_4 hybrid nanoparticle nanocomposite films (CGCoF-3).*

7.2.4.6 Tensile stress testing

All the membranes had uniform thickness of 0.17mm and were semi-transparent. The mechanical properties of chitosan are inconsistent and lack clarity in the mode of analysis such as crosshead speed or molecular weight[22-24]. Therefore, the tensile properties of chitosan were analysed first (**Figure 7.2.5** (a)). The tensile properties varied significantly with the crosshead speed. Crosshead speed used while testing is 10mm/min at 27 ^{0}C.The neat chitosan film exhibits break strain as 25-26%. The elastic modulus of neat chitosan film was observed to be 0.9855 MPa. The grafted chitosan exhibits relatively decrease in elastic modulus. Addition of Co_3O_4-Fe_3O_4 hybrid nanoparticle improves the tensile strength of the polymer (**Figure 7.2.5** (b)).

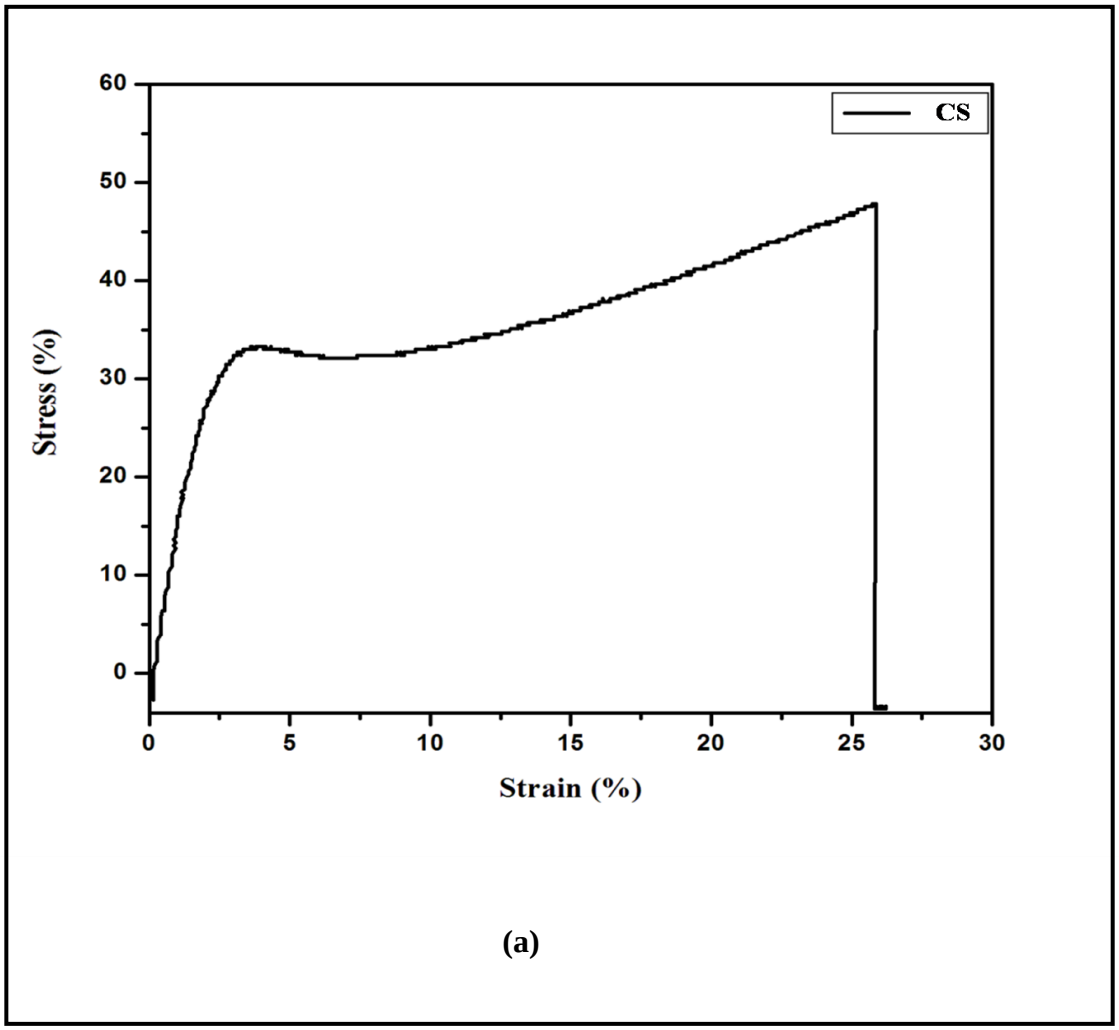

(a)

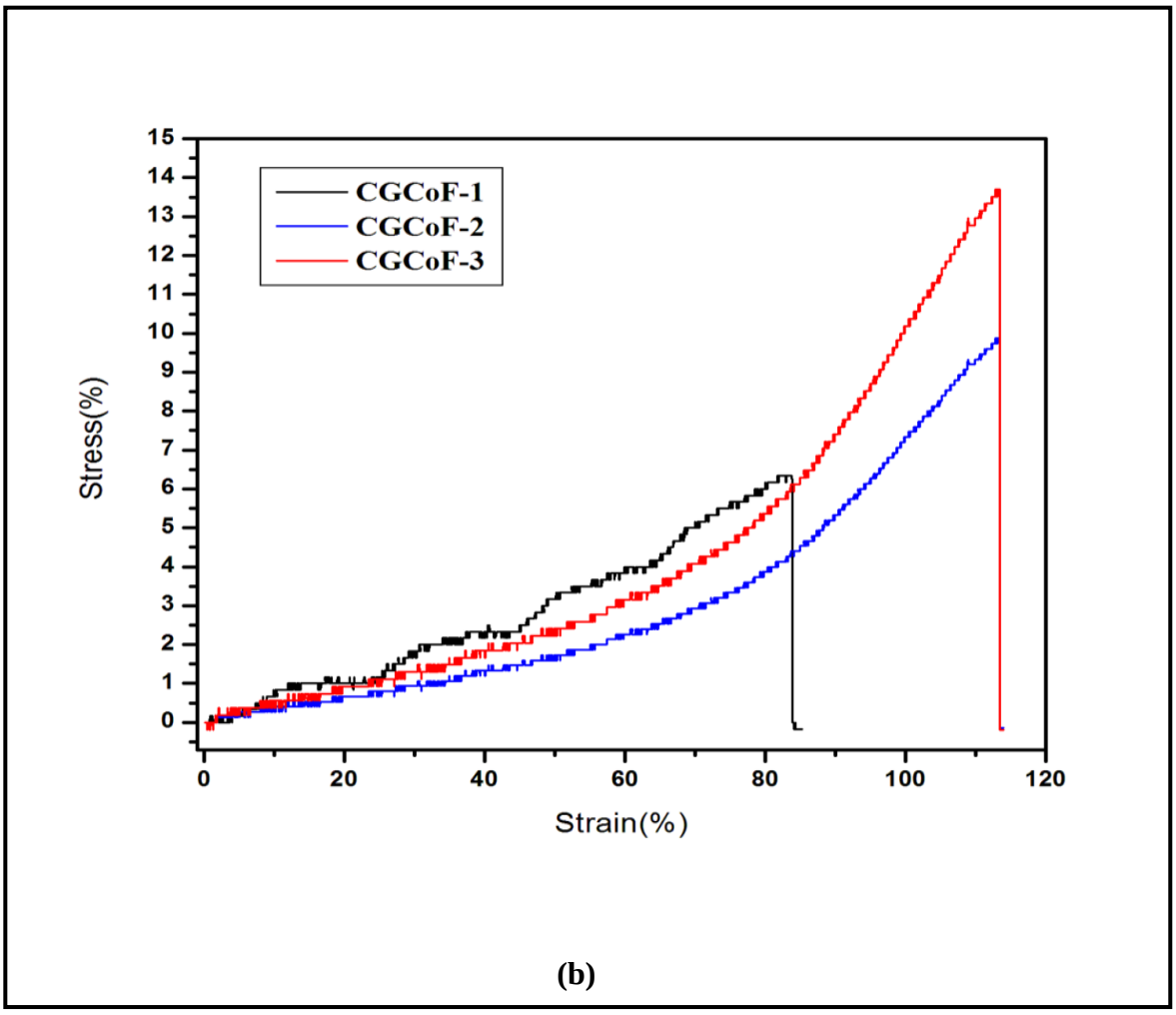

(b)

Figure 7.2.5 *(a) Stress strain behavior of pure chitosan membranes (CS); (b) Effect of grafting and nanoparticle stress strain behavior of grafted and nanocomposite chitosan membranes.*

Table 7.2.4 Tensile strength and testing of chitosan and nanocomposites

Sample Code	Elastic modulus (MPa)	Stress (%)	Strain (%)
CS	0.9855	47.97	25.83
CGCoF-1	0.9556	6.38	83.29
CGCoF-2	0.9829	9.98	113.4
CGCoF-3	0.9838	13.71	113.3

7.2.4.7 Thermogravimetric analysis

Figure 7.2.6 shows thermal degradation of neat chitosan, grafted chitosan and its nanocomposite with various ratio of Co_3O_4-Fe_3O_4 nanoparticles under nitrogen flow. Two steps of non-oxidative degradation were observed. The weight loss at 50-150 ^{0}C is attributed to the water absorbed in chitosan. Whereas, the weight loss in the temperature range of 200-350 ^{0}C corresponds to the degradation and deacetylation of chitosan[21, 25]. In TGA curve, three parameters were measured: temperature of thermal degradation at 20% weight loss, the temperature at 50% weight loss and the yield of charred residue under nitrogen flow. Upon grafting thermal degradation temperature of chitosan decreases by 20-30 ^{0}C. The thermal stability of chitosan is decreased. This is probably due to the poor heat barrier properties of nanoparticle for polymer matrix during the formation of chars[21]. The grafted chitosan matrix have highest char residue ((27.7% at 900 ^{0}C). The char residue is increased upon increasing the nanoparticles wt %. However decrease of 75-80 ^{0}C was observed upon addition of Co_3O_4-Fe_3O_4 nanoparticles (**Table 7.2.5**). The amount of weight loss at this temperature range decreases with the increasing content of nanoparticles in samples. This implies that due the grafted chitosan-Co_3O_4-Fe_3O_4 nanoparticles bonding water absorbability, that is hydrophillicity of the films decreases. This was also confirmed in water swelling behavior section.

Table 7.2.5 TGA results for chitosan and its nanocomposites

Sample Code	Temperature at 20% loss (^{0}C)	Temperature at 50% loss (^{0}C)	char at 900 ^{0}C (wt %)
CS	310	360	27.1
CGCoF-1	246	347	27.7
CGCoF-2	168	272	18.9
CGCoF-3	172	280	21.0

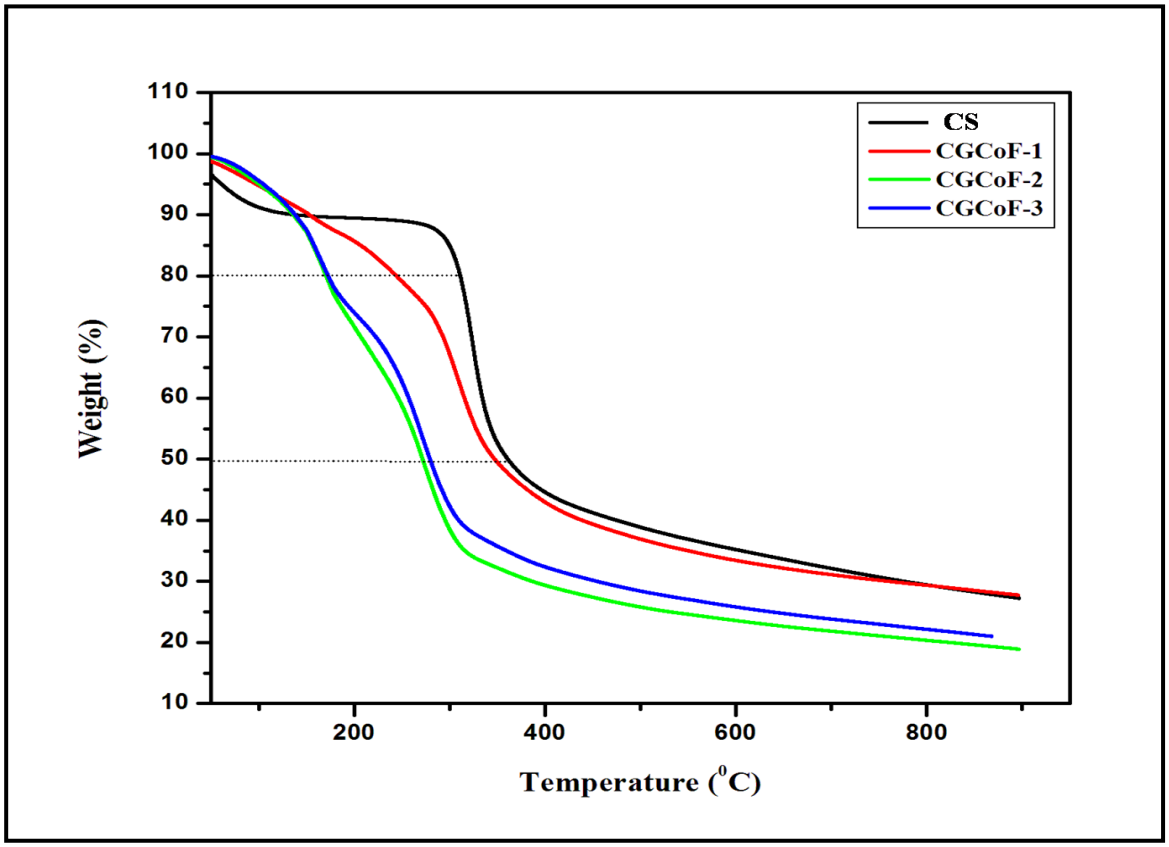

Figure 7.2.6 *Thermogravimetric curves of prepared nanocomposites*

7.2.5 CONCLUSION

In summary, novel nanocomposite film of chitosan-g-glycolic acid and Co_3O_4-Fe_3O_4 hybrid nanoparticles was prepared. The interaction of cationic chitosan with Co_3O_4-Fe_3O_4 nanoparticles is through metallic bond, which results in enhancement in structural and functional properties. The chemical modification of chitosan with glycolic acid and nanoparticles increases its mechanical as well as tensile strength. The grafting of chitosan with glycolic acid imparts hydrophillicity to the film. The results showed that increasing content of nanoparticles reduces hydrophillicity of the nanocomposite film. The longer water retention and swelling behavior properties were discussed, which could be applied in the field of biomedical. AFM showed the morphological study of nanocomposite film.

7.2.6 REFERENCES

1. H. Chen, X. Liu, H. Muthuraman, J.H. Zou, J.H. Wang, Q. Dai, Q. Huo, *Adv. Mater.*, **18,** 2876 (2006).
2. S. Dire, F. Babonneau, C. Sanchez, J. Livage, *J. Mater. Chem.*, **2,** 239 (1992).
3. S.S. Ozdemir , M.G. Buonomenna, E. Drioli, *Appl. Catal. a-General.*, **307,** 167 (2006).
4. M.T. Sulak, O. Gokdogan, A. Gulce, H. Gulce, *Biosens, Bioelectro.*, **21,** 1719 (2006).
5. J.H. Park, Y.T. Lim, O.O. Park, J.K. Kim, J.W. Yu, Y.C. Kim. *Chem. Mater.*, **16,** 688 (2004).
6. K.S. Giesfeldt, R.M. Connatser, M.A. De Jesus, N.V. Lavrik, P. Dutta, M.J. Sepaniak, *Appl. Spectr.*, **57,** 1346 (2003).
7. E.W. Kreutz, H. Frerichs, J. Stricker, D.A. Wesner, *Nuclear Instruments & Methods in Physics Research Section B-Beam Interactions with Materials and Atoms.* **105,** 245 (1995).
8. I. Yoshinaga, N. Yamada, S. Katayama, *J. Sol–Gel Sci. Technol.*, **35,** 21(2005).
9. A.S. Edelstein, R.C. Cammarata, *Nanomaterials: Synthesis, Properties and Application;*

   Institute of Physics Publishing: London, 1996.
10. C. Hayashi, R. Uyeda, A. Tasaki, *Ultra-fine particles: Exploratory Science and Technology, Noyes Publications: Norwich,* NY, 1997.
11. G.C. Hadjipanayis, G.A. Prinz, *Science and Technology of Nanostructured Magnetic Materials, Plenum Press:* New York, 1991.
12. W. Zhang, C. Wang, H. Lien, *Catal. Today.*, **40,** 387 (1998).
13. W. Zhang, C. Wang, *Sci. Technol.* **31,** 2154 (1997).
14. P. Poizot, S. Laruelle, S. Grugeon, L. Dupont, J.M. Tarascon, *Nat.,* **407,** 496 (2000).

15. H. Tamura, H. Nagahama, S. Tokura, *Cellulo.,* **13,** 357 (2006).

16. S.V. Madihally, H.W.T. Mattew, *Biomater.,* **20,** 1133 (1999).

17. N. Nwe, W.F. Stevens, *Production of chitin and chitosan and their applications in the medical and biological sector, In Recent Research in Biomedical Aspects of Chitin and Chitosan; Research Signpost:* India, 2008.

18. N. Nwe, W.F. Stevens, *Preparation and characteristics of chitosan scaffolds for tissue Engineering, In Recent Research in Biomedical Aspects of Chitin and Chitosan; Research Signpost:* India, 2008.

19. M. Jaworska, K. Sakurai, P. Gaudon, E. Guibal, *Poly. Internat.*, **2,** 198 (2003).

20. K. Ogawa, S. Hirano, T. Miyanishi, T. Yui, T. Watanabe, *Macromol.*, **17,** 973 (1984).

21. S.F. Wang, L. Shen, W.D. Zhang, Y.J. Tong, *Biomacromol.,* **6,** 3067 (2005).

22. M. Cheng, J. Deng, F. Yang, Y. Gong, N. Zhao, X. Zhang, *Biomater.*, **24,** 2871 (2003).

23. R. Chen, H. Hwa, *Carbohy. Poly.,* **29,** 353 (1996).

24. M. Qurashi, H. Blair, S. Allen, *J. App. Poly. Sci.,* **46,** 255 (1992).

25. S.F. Wang, L. Chen, Y.J. Tong, *J. Poly. Sci. Part A: Polymer Chemistry.,* **44,** 686 (2006).

CHAPTER 8

Conclusions

8.1 SUMMARY AND CONCLUSIONS

The present study focuses upon the objective of preparation of chitosan and metal/metal oxide nanoparticles based nanocomposites. Further chitosan surface is modified by chemical modification method like grafting. Although there are several reports on grafting of chitosan with synthetic polymers, but our study focused on the grafting of chitosan with glycolic acid by polycondensation method. The influence of intercalation of grafted chitosan with metal/metal oxide nanoparticles on the properties was deduced from their physiomorphic analysis, cell-viability and controlled drug release experiments.

Chapter 1 portrays the literature background and main motivation for this study, and

Chapter 2 describes the objectives and approaches focused in the present study.

Chapter 3 Examined the potential use of 'hybrids' of chitosan-g-glycolic acid and gold nanoflower as biomaterial. The scaffolds of nanohybrid are stable towards the simulated body fluid (SBF) and alkaline pH value of the solution over time. In vitro drug release study of this nanohybrid scaffold is performed; it is observed that initially there is higher and faster release of drug, which decreases with time. The incorporation of gold nanoparticle was observed to control the initial release of drug. In the next part of this chapter, glycolic acid grafted chitosan-Au nanoparticles based nanocomposites were prepared by film casting method. The grafted glycolic acid chains were acting as plasticizer to give flexible films. The interaction of cationic chitosan with Au nanoparticles is through metallic bond, which results in enhancement in structural and functional properties. The increasing content of nanoparticles decreases the water absorption. The results showed that increasing content of nanoparticles reduces hydrophillicity of the nanocomposite film.

Chapter 4 glycolic acid functionalised chitosan- Au-Fe_3O_4 hybrid nanoparticle based novel nanohybrid scaffold was prepared. The nanohybrid scaffold poses porous morphology. The nanohybrid scaffolds are stable regardless of pH of the medium. The porous nanohybrid scaffolds have shown faster and higher drug release. In the next part of this chapter, an enhancement in the structural and functional properties was observed upon interaction of cationic chitosan with Au/Fe_3O_4 nanoparticles through metallic bond. The grafting of chitosan with glycolic acid imparts hydrophillicity and swelling behavior to the chitosan. The increasing content of nanoparticles decreases the water absorption. Due to its swelling behavior and longer water retention it could be applied in the field of biomedical.

Chapter 5 Reveals the potential use of nanohybrid based on chitosan-g-glycolic acid and Pt-Fe_3O_4 composite magnetic nanoparticles in biomedical applications. The porous nanohybrid scaffolds have shown faster and higher drug release. The prepared nanohybrid scaffolds posses porous morphology. From the results it has been concluded that, the prepared nanohybrid scaffold are biocompatible and Pt-Fe_3O_4 magnetic nanoparticles are viable additive for formulating sustained drug delivery systems and could be applied in the field of biomaterials. In the next part of this chapter, an enhancement in the structural and functional properties was observed upon interaction of cationic chitosan with Pt/Fe_3O_4 nanoparticles through metallic bond. The grafting of chitosan with glycolic acid imparts hydrophillicity and swelling behavior to the chitosan. The increasing content of nanoparticles decreases the water absorption, which imparts little branched crystalline structure in the film.

Chapter 6 Examined the potential use of hybrids of chitosan-g-glycolic acid and Co_3O_4 nanoparticles as biomaterial. The nanohybrid scaffolds are stable regardless of pH of the medium. The porous nanohybrid scaffolds have shown faster and higher drug release. The incorporation of Co_3O_4 nanoparticles was observed to control the initial release of drug. In

the next part of this chapter, glycolic acid grafted chitosan-Co_3O_4 nanoparticles based nanocomposites were prepared by film casting method. The interaction of cationic chitosan with Co_3O_4 nanoparticles is through metallic bond, which results in enhancement in physical properties of nanocomposites. An enhancement in mechanical and tensile properties of nanocomposites than pure chitosan was observed. The longer water retention and swelling behavior properties were discussed which could be applied in the field of biomedical and cell adhesion study is under progress.

Chapter 7 Examined the potential use of hybrids of chitosan-g-glycolic acid and Co_3O_4-Fe_3O_4 composite magnetic nanoparticles as biomaterial. The porous nanohybrid scaffolds have shown faster and higher drug release. The incorporation of Co_3O_4-Fe_3O_4 composite nanoparticles was observed to control the initial release of drug. The prepared nanohybrid scaffold is biocompatible and also Co_3O_4-Fe_3O_4 composite magnetic nanoparticles are viable additive for formulating sustained drug delivery systems and could be applied in the field of biomaterials. In the next part of this chapter, nanocomposite film of chitosan-g-glycolic acid and Co_3O_4-Fe_3O_4 hybrid nanoparticles was prepared. The interaction of cationic chitosan with Co_3O_4-Fe_3O_4 nanoparticles is through metallic bond, which results in enhancement in structural and functional properties. The grafting of chitosan with glycolic acid imparts hydrophillicity to the film. The longer water retention and swelling behavior properties were discussed, which could be applied in the field of biomedical. The chemical modification of chitosan with glycolic acid and nanoparticles increases its mechanical as well as tensile strength.

8.2 FUTURE PERSPECTIVES:

On the basis of the above results of the present investigation, the further research can be extended to study the following aspects;

1. Preparation and Characterization of Glycolic Acid-g-Chitosan-Gold Nanoflower Based Nanocomposite Films for Drug Delivery and Tissue Engineering Applications
2. Preparation and Characterization of Glycolic Acid-g-Chitosan- Au-Fe_3O_4 Hybrid Nanoparticles Based Nanocomposite Films for Drug Delivery and Tissue Engineering Applications
3. Preparation of Glycolic Acid-g-Chitosan-Pt-Fe_3O_4 Hybrid Nanoparticles Based Nanohybrid Films for Tissue Engineering and Drug Delivery Applications
4. Preparation and Characterization of Glycolic Acid-g-Chitosan-Co_3O_4 Nanoparticles Based Nanohybrid Films for Drug-Delivery and Tissue Engineering Applications
5. Preparation of Glycolic Acid-g-Chitosan-Co_3O_4-Fe_3O_4 Hybrid Nanoparticles Based Nanohybrid Films for Drug-Delivery and Tissue Engineering

PUBLICATIONS

RESEARCH ARTICLES

1. **Sangeeta Kumari**, Rajpal Singh**.** Glycolic acid-g-chitosan-gold nanoflower nanocomposite scaffolds for drug delivery and tissue engineering. ***International Journal of Biological Macromolecules.*** **2012; 50: 878– 883.**
2. **Sangeeta Kumari**, Raj Pal Singh. Glycolic acid-g-chitosan–Pt–Fe3O4 nanoparticles nanohybrid scaffold for tissue engineering and drug delivery. ***International Journal of Biological Macromolecules.*** **2012; 51: 76– 82.**
3. **Sangeeta Kumari**, Rajpal Singh. Glycolic acid-Grafted chitosan–Co_3O_4–Fe_3O_4 hybrid magnetic nanoparticles- based nanohybrid scaffolds for drug-delivery and tissue engineering. ***Journal Of Material Science.*** **2013; 48: 1524-1532.**
4. **Sangeeta Kumari**, Rajpal Singh. Glycolic acid functionalised chitosan- Au-Fe_3O_4 hybrid nanoparticle based novel nanohybrid scaffolds for drug delivery and tissue engineering application, ***International Journal of Biological Macromolecules*** **2013; 54: 244–249.**
5. **Sangeeta Kumari**, Nayaku Chavan, Raj pal Singh. Mechanical and Thermal Behavior of Glycolic acid Functionalised Chitosan-Co_3O_4 Nanoparticle Based Nanohybrid Films, ***Materials characterization*** **(Under Minor Revision).**
6. **Sangeeta Kumari**, Rajpal Singh. Preparation and characterization of novel hybrid of chitosan-g-glycolic acid and Pt-Fe_3O_4 hybrid nanoparticle. ***Composites Part B: Engineering*** **(Under Minor Revision).**
7. **Sangeeta Kumari**, Rajpal Singh. Preparation and characterization of novel hybrid of chitosan-g-glycolic acid and Au/Fe_3O_4 hybrid nanoparticles, ***Polymer Engineering & Science*** **(Under revision).**

8. **Sangeeta Kumari**, Rajpal Singh. Mechanical behavior of glycolic acid functionalised chitosan-Co_3O_4-Fe_3O_4 nanoparticle based novel nanohybrid, **(Communicated).**
9. **Sangeeta Kumari**, Rajpal Singh. Glycolic acid Grafted Chitosan-Co_3O_4 nanoparticles Based Nanohybrid Scaffolds for Drug-Delivery and Tissue Engineering, **(communicated).**
10. **Sangeeta Kumari**, Raj pal Singh. Preparation and characterization of glycolic acid functionalised chitosan-gold nanoparticle based nanohybrid films, **(Communicated).**

CONFERENCES/ SYMPOSIA

1. Sunil. P. Lonkar, **Sangeeta Kumari** and R. P. Singh, Preparation and crystallization behavior of PP/LDH nanocomposite. Poster Presentation in International Conference on Polymers- **MACRO 2009** at **Indian Institute of Technology Chennai on** 9-11th Mar 2009.
2. **Sangeeta Kumari** and R. P. Singh, Novel synthesis and characterization of chitosan-g-glycolic acid and gold nanoflower nanocomposites and their drug delivery application. Oral presentation in international conference **RAPT 2009** at **Jalgaon University** on 29-30th Dec 2009.
3. **Sangeeta Kumari** and R. P. Singh, Gold nanoflower and its Embedment in Glycolic Acid Grafted Chitosan nanocomposite: Synthesis and Imaging. Poster presentation in international conference **MACRO 2010** at **Indian Institute of Technology Delhi** on 15-17th Dec 2010.
4. **Sangeeta Kumari**, Rajpal Singh. Glycolic acid-g-chitosan-Pt-Fe_3O_4 nanoparticles nanohybrid scaffold for tissue engineering and drug delivery. Poster presentation in international conference **POLY TECH 2012** at **Bharti Vidyapeeth University Pune** on 15-17 December 2012.

5. **Sangeeta Kumari**, Nayaku Chavan, Rajpal Singh. Glycolic Acid-Grafted-Chitosan-Au-Fe_3O_4 Hybrid Nanoparticle Based Nanohybrid Scaffold for Drug Delivery and Tissue Engineering Applications. Poster presentation in International conference 3rd Polymer Congress and **MACRO 2013** at **Indian Institute of Science Bangalore** on 15-18th May 2013**.**